



**HAL**  
open science

# Characterization of the Dystrophin-Associated Protein Complex and its role in the regulation of the K2P potassium channel TWK-28 in *C. elegans* muscle

Nora Zariohi

► **To cite this version:**

Nora Zariohi. Characterization of the Dystrophin-Associated Protein Complex and its role in the regulation of the K2P potassium channel TWK-28 in *C. elegans* muscle. Neurobiology. Université de Lyon, 2020. English. NNT : 2020LYSE1155 . tel-03934563

**HAL Id: tel-03934563**

**<https://theses.hal.science/tel-03934563v1>**

Submitted on 11 Jan 2023

**HAL** is a multi-disciplinary open access archive for the deposit and dissemination of scientific research documents, whether they are published or not. The documents may come from teaching and research institutions in France or abroad, or from public or private research centers.

L'archive ouverte pluridisciplinaire **HAL**, est destinée au dépôt et à la diffusion de documents scientifiques de niveau recherche, publiés ou non, émanant des établissements d'enseignement et de recherche français ou étrangers, des laboratoires publics ou privés.



N°d'ordre NNT : 2020LYSE1155

**THESE de DOCTORAT DE L'UNIVERSITE DE LYON**  
opérée au sein de  
**l'Université Claude Bernard Lyon 1**

**École Doctorale N° 340**  
**École Doctorale de Biologie Moléculaire, Intégrative et**  
**Cellulaire (BMIC)**

**Spécialité de doctorat :**  
Neurobiologie et Génétique

Soutenue publiquement le 18/09/2020, par :

**Nora Zariohi**

---

**Characterization of the Dystrophin-Associated Protein Complex and its role in the regulation of the K2P potassium channel TWK-28 in *C. elegans* muscle**

---

Devant le jury composé de :

Mme. Gieseler, Kathrin	PU	UCBL/INMG	Présidente
M. Bertrand, Vincent	CR	AMU/IBDM	Rapporteur
M. Schnorrer, Frank	DR	AMU/IBDM	Rapporteur
Mme. Gally, Christelle	MCU	UNISTRA/IGBMC	Examinatrice
M. Boulin, Thomas	CR	UCBL/INMG	Directeur de thèse



# **Université Claude Bernard – LYON 1**

Administrateur provisoire de l'Université	M. Frédéric FLEURY
Président du Conseil Académique	M. Hamda BEN HADID
Vice-Président du Conseil d'Administration	M. Didier REVEL
Vice-Président du Conseil des Etudes et de la Vie Universitaire	M. Philippe CHEVALLIER
Vice-Président de la Commission de Recherche	M. Jean-François MORNEX
Directeur Général des Services	M. Pierre ROLLAND

## **COMPOSANTES SANTE**

Département de Formation et Centre de Recherche en Biologie Humaine	Directrice : Mme Anne-Marie SCHOTT
Faculté d'Odontologie	Doyenne : Mme Dominique SEUX
Faculté de Médecine et Maïeutique Lyon Sud - Charles Mérieux	Doyenne : Mme Carole BURILLON
Faculté de Médecine Lyon-Est	Doyen : M. Gilles RODE
Institut des Sciences et Techniques de la Réadaptation (ISTR)	Directeur : M. Xavier PERROT
Institut des Sciences Pharmaceutiques et Biologiques (ISBP)	Directrice : Mme Christine VINCIGUERRA

## **COMPOSANTES & DEPARTEMENTS DE SCIENCES & TECHNOLOGIE**

Département Génie Electrique et des Procédés (GEP)	Directrice : Mme Rosaria FERRIGNO
Département Informatique	Directeur : M. Behzad SHARIAT
Département Mécanique	Directeur M. Marc BUFFAT
Ecole Supérieure de Chimie, Physique, Electronique (CPE Lyon)	Directeur : Gérard PIGNAULT
Institut de Science Financière et d'Assurances (ISFA)	Directeur : M. Nicolas LEBOSNE
Institut National du Professorat et de l'Education	Administrateur Provisoire : M. Pierre CHAREYRON
Institut Universitaire de Technologie de Lyon 1	Directeur : M. Christophe VITON
Observatoire de Lyon	Directrice : Mme Isabelle DANIEL
Polytechnique Lyon	Directeur : Emmanuel PERRIN
UFR Biosciences	Administratrice provisoire : Mme Kathrin GIESELER
UFR des Sciences et Techniques des Activités Physiques et Sportives (STAPS)	Directeur : M. Yannick VANPOULLE
UFR Faculté des Sciences	Directeur : M. Bruno ANDRIOLETTI

<b><u>ACKNOWLEDGEMENTS/REMERCIEMENTS</u></b> .....	<b><u>7</u></b>
<b><u>ABSTRACT</u></b> .....	<b><u>9</u></b>
<b><u>LIST OF ABBREVIATIONS</u></b> .....	<b><u>10</u></b>
<b><u>LIST OF FIGURES</u></b> .....	<b><u>11</u></b>
<b><u>INTRODUCTION</u></b> .....	<b><u>14</u></b>
<b><u>CHAPTER 1. TWO-PORE DOMAIN (K2P) POTASSIUM CHANNELS</u></b> .....	<b><u>15</u></b>
<b>I. Structure and function of K2P channels</b> .....	<b>16</b>
<b>II. Mechanisms that regulate K2P channel density at the cell surface</b> .....	<b>20</b>
A. $\beta$ -spectrin localizes TREK-1 at intercalated discs in the heart.....	20
B. P11 is required for TASK-1 cellular trafficking .....	23
C. UNC-44/Ankyrin is involved in the trafficking of the K2P channel UNC-58 in <i>C. elegans</i> .....	26
<b>III. In vivo expression and localization of K2P channels in <i>C. elegans</i></b> .....	<b>27</b>
A. Distribution of K2P channels in body wall muscle .....	27
<b>IV. Identification of regulatory mechanisms – principle of <i>gain-of-function</i>     genetic screens</b> .....	<b>30</b>
A. SUP-9 likely forms a complex with the regulator subunits SUP-10 and UNC-93.....	30
B. TWK-18 first characterization.....	31
<b>V. Building new K2P <i>gain-of-function</i> mutants</b> .....	<b>32</b>
A. EMS forward genetic screen on TWK-28.....	33
<b><u>CHAPTER 2 BODY WALL MUSCLE OF <i>C. ELEGANS</i></u></b> .....	<b><u>37</u></b>
<b>I. Organization and structure of striated muscle tissue in <i>C. elegans</i></b> .....	<b>38</b>
A. Body wall muscle organization and development.....	38
B. Muscle cells attachments allow the force transduction .....	41
C. Innervation through muscle arms projections .....	43
<b>II. Ion channels and regulation of <i>C. elegans</i> muscle excitability</b> .....	<b>45</b>
A. TWK-18, the first TWK channel characterized .....	45
B. SUP-9 is also involved in muscle excitability.....	46
C. SLO-1, a BK potassium channels in <i>C. elegans</i> .....	47

**CHAPTER 3 DYSTROPHIN-ASSOCIATED PROTEIN COMPLEX (DAPC).. 50**

**I. The dystrophin-associated proteins complex and its conservation in *C. elegans*.....51**

A. General overview..... 51

B. Molecular composition of the DAPC in vertebrates’ muscle: differences and commonalities with *C. elegans*..... 51

**II. Dystrophin as a structural linker in muscle .....55**

A. Evidence in vertebrates ..... 55

B. DMD diseases..... 58

C. Dystrophin/*dys-1* in *C. elegans*: consequences of different mutations..... 58

**III. Dystroglycan in vertebrates .....64**

A. Biosynthesis and functions..... 64

B. Interaction with DAPC ..... 64

C. Interaction with ECM ..... 66

**IV. Everything we know about DG in worms .....68**

A. Dystroglycan structure and conservation in *C. elegans*..... 68

B. Dystroglycan expression in worm muscle ..... 70

C. DGN-1 functions and mutations consequences..... 72

**V. Sarcoglycans as organizers of the DAPC? .....73**

A. Expression and localization..... 73

B. Regulation of surface expression..... 73

C. Absence of SG..... 75

D. Interaction with extracellular and intracellular factors ..... 76

**VI. All we know about SG in *C. elegans*.....78**

A. Conservation, expression and localization in muscle ..... 78

B. Sarcoglycans mutants ..... 81

**VII. Syntrophin and dystrobrevin are associated to dystrophin in the DAPC 82**

A. Dystrobrevin structure and expression in muscle..... 82

B. Syntrophin structure and expression in muscle ..... 84

C. Characterizing syntrophin and dystrobrevin in *C. elegans* ..... 86

**VIII. Most of the DAPC proteins are interdependent .....92**

A. Dystrophin, dystrobrevin and syntrophin interactions in vertebrates..... 92

B. Dystrophin, dystrobrevin and syntrophin interactions in *C. elegans* ..... 95

C. Dystroglycans are strongly reduced in <i>mdx</i> mice.....	96
D. Loss of one of the sarcoglycan complex subunits destabilizes the whole sub-complex.....	97
<b><u>CHAPTER 4 DYSTROPHIN-ASSOCIATED PROTEINS COMPLEX AND ION CHANNELS.....</u></b>	
<b><u>99</u></b>	
<b>I. An additional role of the DAPC: interaction with ion channel in vertebrates .....</b>	<b>100</b>
A. Dystrophin complex interacts with voltage-dependent sodium channels (Na <sub>v</sub> ) in skeletal and cardiac muscle .....	100
B. A PDZ domain-dependent interaction of syntrophin and the potassium channel K <sub>ir</sub> 4.1 in mice .....	104
C. TRPC1, a non-selective permeant calcium channel, binds to the PDZ domain of syntrophin.....	105
<b>II. Implication of the DAPC in the regulation of SLO-1, a muscular BK channel in <i>C. elegans</i> .....</b>	<b>108</b>
<b><u>RESULTS.....</u></b>	<b><u>111</u></b>
<b><u>PART I: DAPC AND PCP PATHWAYS ORGANIZE ASYMMETRIC MEMBRANE DOMAINS OF <i>C. ELEGANS</i> MUSCLES.....</u></b>	
<b><u>112</u></b>	
<b><u>PART II: MUTATION OF A SINGLE RESIDUE PROMOTES GATING OF VERTEBRATE AND INVERTEBRATE TWO-PORE DOMAIN POTASSIUM CHANNELS.....</u></b>	
<b><u>141</u></b>	
<b><u>PART III: RELIABLE CRISPR/Cas9 GENOME ENGINEERING IN CAENORHABDITIS ELEGANS USING A SINGLE EFFICIENT SGRNA AND AN EASILY RECOGNIZABLE PHENOTYPE .....</u></b>	
<b><u>169</u></b>	
<b><u>DISCUSSION AND PERSPECTIVES.....</u></b>	<b><u>193</u></b>
<b><u>K2P POTASSIUM CHANNELS IN <i>C. ELEGANS</i> MUSCLE .....</u></b>	
<b><u>194</u></b>	
1. Why K2P channels are asymmetrically localized in muscle cells? .....	194
2. Why so many K2P channels in a single cell? .....	196
3. Potassium channels are present in different sub-complexes in body wall muscle .....	198

NOVEL GENETIC ASSOCIATION BETWEEN DAPC AND K2P CHANNELS

..... 201

1. Discovery of new regulatory factors of TWK-28..... 201
2. Specificity of Dystrophin in the regulation of TWK-28. Could different DSY-1/Dystrophin isoforms have separate functions? ..... 201
3. Is the syntrophin PDZ domain implicated in the regulation of TWK-28?  
203
4. Dystroglycan/DGN-1 in body wall muscle of *C. elegans*. Which role does it play? ..... 205
5. Do sarcoglycans in *C. elegans* function as in vertebrates? ..... 207

GENERAL CONCLUSIONS..... 210

REFERENCES ..... 212

# Acknowledgements/Remerciements

Avant de commencer, je voudrais remercier les membres de mon jury de thèse. Merci à **Vincent Bertrand** et **Frank Schnorrer** d'avoir accepté de rapporter ce manuscrit. Merci à **Kathrin Gieseler** et **Christelle Gally** pour votre disponibilité et envie de faire partie de cette petite communauté.

Je tiens à remercier **Vincent Mirouse** et **Laurent Schaeffer**, membres de mon comité de suivi de thèse, pour le temps qu'ils m'ont consacré ainsi que pour leurs précieux conseils et leurs nouvelles perspectives. Grâce notamment aux longues discussions avec Vincent, nous avons pu explorer de nouvelles hypothèses.

Mes plus grands remerciements vont à **Thomas Boulin**, mon directeur de thèse et mon encadreur depuis notre premier entretien en 2014. Je te remercie de m'avoir permis de faire partie de ton équipe. Je te remercie avant tout pour ta patience, ta présence, ton engagement et ton dynamisme. Ton exigence m'a fait évoluer professionnellement et personnellement et c'est grâce à cela que j'ai pu arriver ici. Je te remercie de m'avoir fait confiance.

Merci à **Marie Gendrel**, sans ton aide, je n'aurais probablement pas pu réussir à obtenir ma bourse de thèse. Merci d'être ma " partenaire de crible " et pour tous tes conseils et moments partagés.

Merci à **Caroline**, ma partenaire hispanophone. Tu es extraordinaire ! Merci pour tes conseils, pour les longues discussions, pour les soirées et la musique. Tu étais toujours là quand j'avais besoin de toi. Grâce à des gens comme toi, je reviendrai toujours sur Lyon. Merci à **Philippe**, mon consultant privé en informatique lorsque je rencontrais des problèmes sur Fiji. Merci pour ton enthousiasme et ta positivité et pour tes conseils pour traverser cette étape et en tirer profit.

Merci à **Alice Rouse**, toute expression française authentique que je connais aujourd'hui, c'est à toi que je la dois. Merci pour ta patience pour toutes les fois où je t'ai demandé quelle était la température pour induire des mâles. Merci pour toutes les rigolades et les soirées.

Merci à **Olga** d'être toujours là quand j'ai vraiment besoin de soutien. Merci d'avoir été la première à lire ce manuscrit.

Merci à **Estèle**, tu m'as beaucoup appris en très peu de temps. Merci pour tes blagues et tes rires contagieux. Ce fut un plaisir de t'avoir dans l'équipe.

Enfin, merci à **Alice P...** Je ne sais vraiment pas comment te remercier pour tout ce que tu as fait. Quand Thomas m'a dit que j'allais avoir un stagiaire M2, j'ai eu peur, mais

maintenant je sais que ça a été la meilleure expérience qui pouvait m'arriver. Travailler avec toi est extrêmement facile et agréable. Tu es toujours motivée et bienveillante, en plus avec un sourire qui fait le bonheur tout le monde autour de toi. Tu as toujours veillé à mes intérêts personnels et professionnels, merci. Plus qu'une collègue, je pars maintenant avec une grande amie et je t'en remercie. Tu es incroyable.

Merci à l'équipe voisine, « les Bessereau », en particulier à **Camille, Marine, Océane, Melissa, Charline, Laure, Florence**. Vous m'avez donné beaucoup de bons moments et j'espère continuer à les partager avec vous. Camille, une pensée particulière pour toi, ma partenaire de rédaction.

Merci à Maïté pour avoir toujours eu le temps de m'écouter et de m'aider.

Finalement, merci à ma famille pour avoir toujours veillé à mon éducation et m'avoir inculqué la valeur de l'effort, pour son soutien inconditionnel et constant ; en bref, c'est à vous quatre que je dois d'être arrivée jusqu'ici, je ne pourrai jamais vous remercier suffisamment. *Por cierto, os lo iba a escribir en español... pero como me entendéis casi todos, así se queda!*

En résumé, je tiens à remercier le soutien, la compréhension, la patience et l'affection de tous ceux que j'aurais pu oublier et qui ont été à mes côtés au cours de ce parcours personnel et professionnel.

# Abstract

**Two-pore domain (K2P) potassium channels** belong to a large family of ion channels implicated in determining and maintaining the resting cell membrane potential. K2P channels are proteins extensively conserved throughout evolution, being present in almost all animal cells. In the nematode *Caenorhabditis elegans*, 47 genes code K2P channels sub-units, but only three of them have been characterized and reported in the literature. By tagging a certain number of them with fluorescent proteins (CRISPR/Cas9), we have found that nine channels are co-expressed in body wall muscle, showing a highly specific sub-cellular distribution. The most fascinating distribution was the one of TWK-28, which exhibits a polarized comet-like pattern that occupy only the anterior tip of each body wall muscle cell.

In order to elucidate the cellular mechanisms underlying this particular distribution, we performed a genetic screen on the novel TWK-28 *gain-of-function* strain. We revealed that genes belonging to **Dystrophin-Associated Protein Complex (DAPC)** are involved in determining the amount of this channel at the muscle cell surface. DAPC is composed of at least 10 intra and extracellular proteins and plays a key role in physically connecting the extracellular matrix to the actin cytoskeleton. Interestingly, when tagging multiple components of DAPC with fluorescent proteins by CRISPR/Cas9 gene editing, we found that most of the dystrophin-associated proteins, such as syntrophin/STN-1, dystrobrevin/DYB-1 or even sarcoglycans (SGCA-1 and SGCB-1), show a particularly asymmetric distribution in muscle. We also revealed the, to date excluded, presence of dystroglycan/DGN-1 in body wall muscle of *C. elegans*.

Finally, the asymmetric distribution of TWK-28 along the antero-posterior axis on a cellular and tissue scale, suggests that the **Planar Cell Polarity** pathways might be implicated. By gene candidate approach of the WNT pathway, we showed that proteins such as Disheveled, ROR/CAM-1 or WNT ligand/EGL-20 can modify the localization of TWK-28 by driving it into a new posterior sub-complex in the muscle cells.

**Key words:** Dystrophin-Associated Proteins Complex, Muscular K2P Potassium Channels, Compartmentalized Protein Distribution, Planar Cell Polarity, WNT, *C. elegans*.



# List of abbreviations

---

AA	Arachidonic acid
aa	Amino acid
Ach	Acetylcholine
AchR	Acetylcholine receptor
AP	Action potentiel
BK	Big potassium channel
BMD	Becker muscular dystrophy
BWM	Body wall muscle
CC	Coiled coil
CH	Calponin homology
COS	CV-1 Origin SV40
DAPC	Dystrophin-associated proteins complex
DB	Dystrobrevin
DG	Dystroglycan
DMD	Duchenne muscular dystrophy
DNA	Deoxyribonucleic acid
ECM	Extracellular matrix
EMS	Ethyl methanesulfonate
ePSC	excitatory postsynaptic current
ER	endoplasmic reticulum
GABA	Gamma aminobutyric acid
gof	Gain-of-function
ID	Intercalated discs
K2P	Two-pore domain potassium channels
Kir	Inward rectifier potassium channels
Kv	Voltage-gated potassium channels
LGMD	Limb girdle muscular dystrophies
LGMD2D	Limb girdle muscular dystrophies type 2
LM	Lateral membrane
lof	Loss-of-function
MHC	Myosin heavy chain
NMJ	Nueomuscular junction
p11	Calpactin I or annexin II light chain
PDZ	Acronym of the first three PDZ-containing proteins identified: <u>P</u> SD-95/ <u>S</u> AP90, <u>D</u> iscs-large, and <u>Z</u> O-1.
PDZ-BD	PDZ-binding domain
PDZ-DM	PDZ-binding motif
PH	Pleckstrin homology
RNA	Ribonucleic acid
RT-PCR	Reverse transcription polymerase chain reaction
SG	Sarcoglycan
TASK-1	TWIK-related acid-sensitive K <sup>+</sup> channel
TREK-1	TWIK-related K <sup>+</sup> channel
TWIK	Tandem of Pore domains in a Weak Inwardly rectifying K <sup>+</sup> channel
Y2H	Yeast two-hybrid

---

# List of figures

<b>Figure 1</b> K2P potassium channels structure. ....	17
<b>Figure 2</b> K2P potassium channels regulation. ....	18
<b>Figure 3</b> $\beta$ IV-spectrin is involved in the regulation of TREK-1 localization and function in mice heart. ....	22
<b>Figure 4</b> TASK-1 requires p11 to reach the cell membrane. ....	25
<b>Figure 5</b> UNC44/Ankyrin regulates the K2P channel UNC-58. ....	26
<b>Figure 6</b> Numerous potassium channels coexist in muscle cells, exhibiting different distributions. ....	28
<b>Figure 7</b> SUP-9 interacts and co-localizes with the regulatory proteins SUP-10 and UNC-93 in body wall muscle. ....	30
<b>Figure 8</b> <i>twk-18</i> is expressed in body wall muscle. ....	31
<b>Figure 9</b> The K2P channels TM2.6 residue is highly conserved in evolution. ....	32
<b>Figure 10</b> TWK-28 has a particular localization in body wall muscle. ....	35
<b>Figure 11</b> <i>C. elegans</i> striated muscle corresponds to body wall muscle and is arranged in four quadrants. ....	40
<b>Figure 12</b> The body wall muscle functional unit, the sarcomere, is conserved. ....	42
<b>Figure 13</b> In <i>C. elegans</i> , the muscle project muscle arms toward axons, where muscle can be excited (Ach) or inhibited (GABA). ....	44
<b>Figure 14</b> TWK-18 is a K2P potassium channel that controls body wall muscle excitability. ....	45
<b>Figure 15</b> SUP-9 is a K2P channel which is expressed in <i>C. elegans</i> body wall muscle. ....	46
<b>Figure 16</b> SLO-1 is a BK channels in <i>C. elegans</i> , involved in muscle excitability, through repolarization regulation. ....	48
<b>Figure 17</b> Dystrophin-Associated Protein Complex (DAPC) in skeletal muscle. ....	53
<b>Figure 18</b> Dystrophin gene and protein structure. ....	57
<b>Figure 19</b> Dystrophin/dys-1 in <i>C. elegans</i> is highly conserved and is expressed in muscle tissues. ....	60
<b>Figure 20</b> <i>dys-1</i> mutants in <i>C. elegans</i> present a "head-bending" phenotype but not muscular degeneration, unless combined with <i>h1h-1</i> mutants. ....	63
<b>Figure 21</b> A single precursor give rise to $\alpha$ and $\beta$ -dystroglycan. ....	66
<b>Figure 22</b> Dystroglycan/DGN-1 in <i>C. elegans</i> is conserved. ....	69

<b>Figure 23</b> DGN-1 is expressed in body wall muscle of <i>C. elegans</i> , unlike previously reported.....	71
<b>Figure 24</b> Four subunits compose the sarcoglycan sub-complex. ....	74
<b>Figure 25</b> Sarcoglycans are conserved in <i>C. elegans</i> and found in muscle.....	79
<b>Figure 26</b> Four dystrobrevin isoforms are products of two genes: $\alpha$ and $\beta$ dystrobrevin. ....	83
<b>Figure 27</b> Syntrophins present functional domains that are conserved.....	85
<b>Figure 28</b> Syntrophin/STN-1 is conserved in <i>C. elegans</i> muscle. ....	88
<b>Figure 29</b> A highly conserved dystrobrevin is expressed in worms' muscle and neurons. ....	90
<b>Figure 30</b> Dystrophin, dystrobrevin and syntrophin interact with each other in muscle. ....	94
<b>Figure 31</b> Dystroglycan is reduced in <i>mdx</i> mice.....	96
<b>Figure 32</b> Mutations in one sarcoglycan subunit lead to the total loss of the SG complex and other DAPC proteins. ....	98
<b>Figure 33</b> Muscular $\text{Na}_v$ channels localization and function depend on DAPC.....	103
<b>Figure 34</b> $\text{K}_{ir}4.1$ channels are associated to dystrophin and syntrophin in the DAPC. ....	105
<b>Figure 35</b> TRPC ion channels are associated with dystrophin and altered in <i>mdx</i> mice. ....	106
<b>Figure 36</b> SLO-1, a BK channel in <i>C. elegans</i> , interact with DAPC proteins for its localization and function. ....	109
<b>Figure 37</b> <i>Caenorhabditis elegans</i> sinusoidal locomotion <b>Error! Bookmark not defined.</b>	
<b>Figure 38</b> Principal tissues expressing K2P channels in <i>C.elegans</i> <b>Error! Bookmark not defined.</b>	
<b>Figure 39</b> K2P channels distribution pattern in muscle. LEV-10 and MADD-4 are required for the AchRs clustering. .... <b>Error! Bookmark not defined.</b>	
<b>Figure 40</b> <i>dys-1</i> isoforms and genetic screen alleles..... <b>Error! Bookmark not defined.</b>	
<b>Figure 41</b> Dystrophin and dystroglycan conservation in <i>C. elegans</i> <b>Error! Bookmark not defined.</b>	



# INTRODUCTION

## Chapter 1. Two-pore domain (K2P) potassium channels

The cytoplasmic membrane is a barrier that separates two aqueous mediums with different composition. The movement of ions across cell membranes is the basis for many fundamental physiological processes such as cell excitability or the maintenance of ionic homeostasis, being the ion channels the key elements in both processes. Potassium channels, which are transmembrane proteins that form selective pores for  $K^+$ , play a central role in establishing and maintaining resting potential. There are three main classes of potassium channels, which are classified according to their structural organization and biophysical properties: (1) voltage-gated channels ( $K_v$ ), (2) inward rectifier channels ( $K_{ir}$ ) and (3) two-pore domain channels (K2P). Among the three classes mentioned, the K2P channels remain open regardless of the membrane potential. In our laboratory, one of the major topics we are interested in, is the regulation of K2P channels in *C. elegans*. Concretely, we aim to identify and understand the molecular and cellular mechanisms that control the number of channels present on the surface of a cell as well as their subcellular distribution.

## I. Structure and function of K2P channels

- Structure and characteristics of K2P potassium channels

Among all the potassium channels, the family of potassium channels with two-pore domain (K2P) is the latest to have been discovered ([Lesage et al., 1996](#)). K2P potassium channels are proteins extensively conserved throughout evolution, being found in the genome of mammals (15 members) and other organisms, such as the fruit fly *Drosophila melanogaster* (11 sub-units), in the nematode *Caenorhabditis elegans* (47 sub-units), as well as in yeasts and plants.

In K2P channels, each subunit is composed of four transmembrane domains and the main characteristic, as its name suggests, is the presence of two-pore-forming domains, P1 and P2 ([Figure 1 A](#)). Likewise, to make an operational channel, unlike other potassium channels, K2P channels require the dimerization of two subunits, which involve the extra-cellular loop ([Figure 1 A](#)) located between the first transmembrane segment M1 and the first pore-forming domain P1 of each subunit ([Lesage and Lazdunski, 2000](#)). They also contain a short N-terminus (NH<sub>2</sub>) and a long C-terminus (COOH) domains, both of which being cytoplasmic. Despite the fact that the central region of these channels is very conserved (segments TM1 to TM4), there is considerable diversity in the intracellular C- and N-terminus ends.

Interestingly, in K2P channels the sequence G(Y/F)G is conserved in the first pore ([Figure 1 B](#)), although in the second pore it is replaced by the sequence G(F/L)G. This sequence is crucial for the channel selectivity. Thus, in the pore we find the following regions: 1) Inner helices: consist of two  $\alpha$ -helices that form the inner wall of the pore. They correspond to the transmembrane segments M2 and M4 of each subunit. 2) P-loop: including a particularly long region on the K2P channels. This region also contains the channel selectivity filter. 3) And finally, outer helices, corresponding to segments M1 and M3.

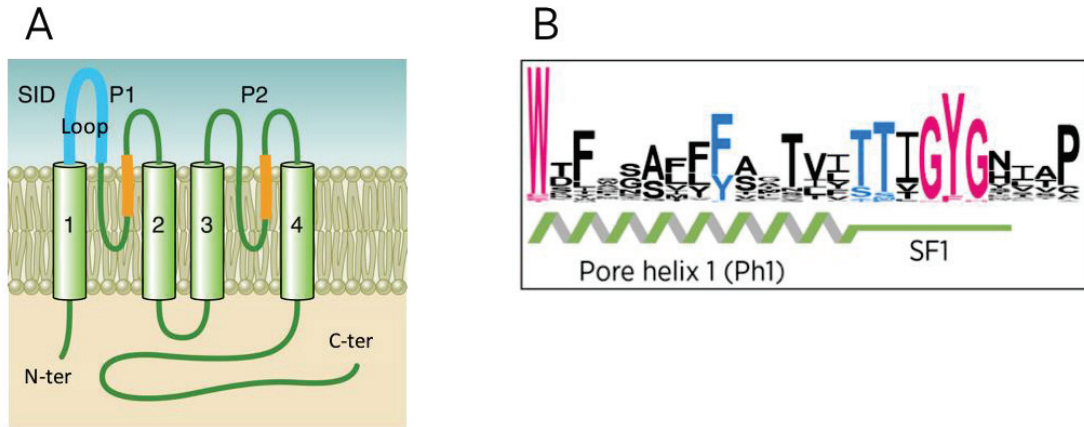


Figure 1 K2P potassium channels structure.

A: Schematic representation of one K2P channel subunit, composed of 4 transmembrane domains (1-4). Extracellular part on top. P1 and P2 are the pore-domains. The extracellular loop is represented in blue (SID: self-interacting domain). Adapted from [Spúlveda \*et al.\*, 2015](#) B: In K2P, channels the sequence GYG is conserved in the first pore-domain helix, forming a signature sequence specific for the potassium selectivity filter. Our published data in [Ben Soussia \*et al.\*, 2019](#).

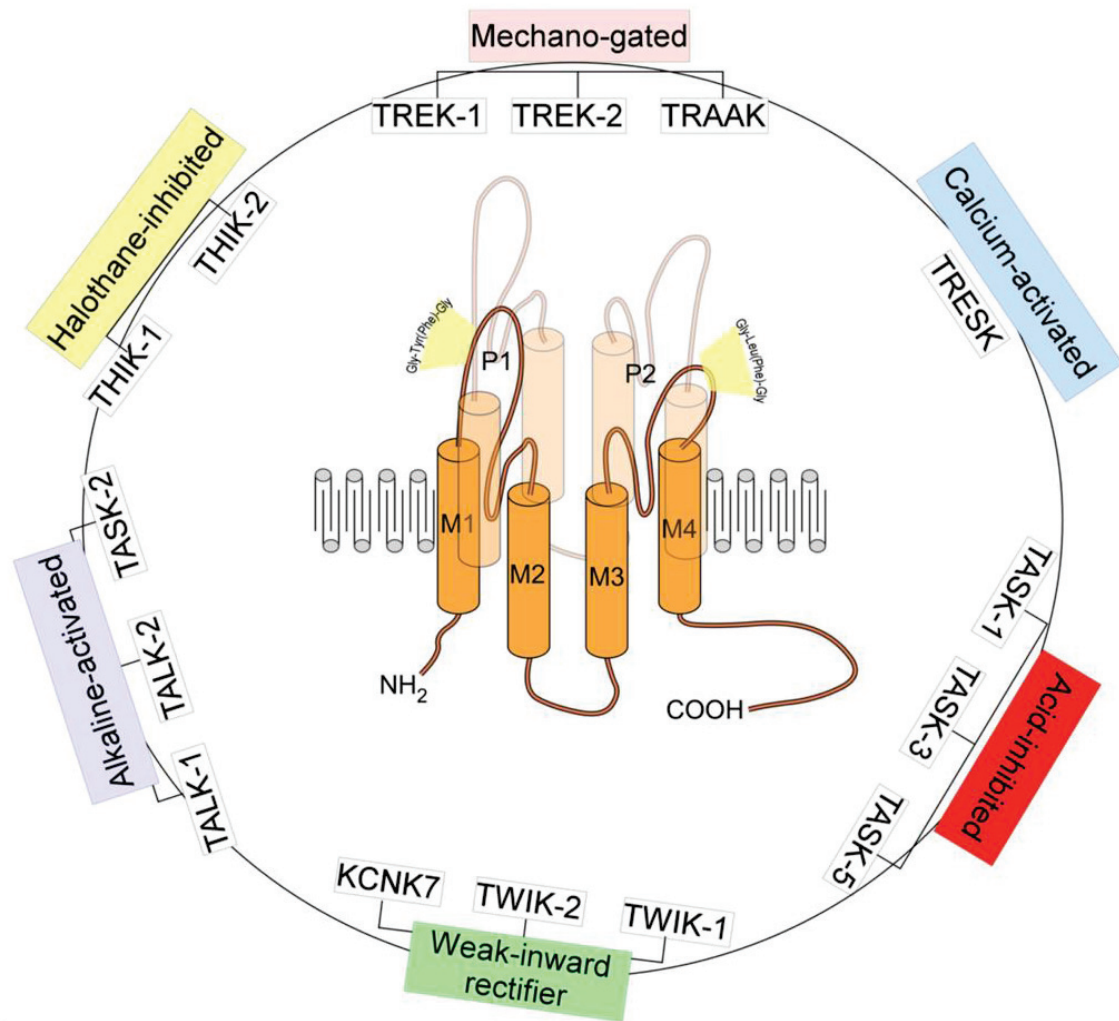
- Regulation and function of K2P potassium channels

There are 15 K2P channels in humans, representing a heterogeneous group in terms of sensitivity. We find channels that are sensitive to calcium, mechanical stimulation, or even pH-sensitive channels ([Figure 2 A](#)). One of the most studied K2P channels is TREK-1 (KCNK2). TREK-1 is strongly expressed in brain, being highly abundant in GABAergic interneurons, which involves this channel in the control of presynaptic transmission ([Hervieu \*et al.\*, 2001](#)). Moreover, TREK-1 has been related to different neurological diseases such as depression ([Heurteaux \*et al.\*, 2006](#)) and epilepsy ([Dey \*et al.\*, 2014](#); [Heurteaux \*et al.\*, 2004](#)). Its association with other processes such as pain perception ([Maingret \*et al.\*, 2000](#)) or general anesthesia ([Patel \*et al.\*, 1999](#)) has also been widely studied.

K2P channels are also involved in cell excitability, where their semi-permanent opening at rest ensures a constant negative membrane potential. This aspect of the functions of K2P channels is the main emphasis of my thesis, reason why I am going to focus more on items related to the involvement of these channels in cell excitability.



A



B

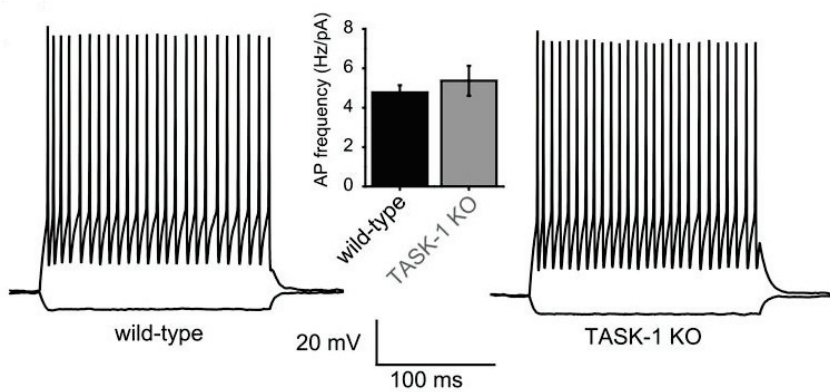


Figure 2 K2P potassium channels regulation.

A: 15 K2P channels in humans are classified in different groups, depending on their regulation. The dimerization of two subunits compose a functional channel. Adapted from [Djillani et al., 2019](#) B: Current-clamp recording showing no difference in action potential frequency in TASK-1 KO mice, compared with wild-type mice. Adapted from [Aller et al., 2005](#).

The cell excitability associated with K2P channels has been most studied in the nervous system, although they are also present in muscle tissue. For example, in brain the currents carried by TASK1/TASK3 are directly involved in maintaining the resting electrical tone of granular neurons, thus determining their excitability. In studies where these channels have been inhibited (muscarine), a significant reduction in potassium current has been observed, inducing a strong depolarization of the cell and, thus, making it more excitable. When current-clamp is performed, ([Figure 2 B](#)), however, no difference in the frequency of action potential discharges was observed between TASK-1 KO and wild-type mice. ([Millar et al., 2000](#); [Aller et al., 2005](#)).

Finally, another K2P channel that plays an essential role in cell excitability, this time of cardiac cells, is TWIK-1 (which is also present in other tissues, such as renal or pancreatic). TWIK-1 has widely been associated with cardiac arrhythmias. However, this channel has a peculiarity that cannot go unnoticed: despite being a mainly potassium-permeant channel, in extreme conditions its selectivity changes becoming highly permeable to sodium ions. Thus, thanks to this peculiar characteristic, in conditions where the pH is below 6 or potassium concentrations are low, the activity of TWIK-1 leads to a depolarization of the cardiomyocytes ([Chatelain et al., 2012](#)).

Although these channels are involved in several functions and their deregulation leads to different diseases, it remains unclear what basic mechanisms regulate both their activity and level of expression.

In summary, how K2P channels are regulated from a cellular and molecular point of view remains an issue to be investigated. Perhaps, one of the limitations has been the almost non-existence of drugs targeting specifically K2P channels. Therefore, one of the major topics in our laboratory is the genetic study of the mechanisms and regulatory factors of K2P channels in the invertebrate model *Caenorhabditis elegans*. In the following, we will consider some examples of studies that have been carried out with the aim of elucidating different K2P channels regulation mechanisms in different models.

## II. Mechanisms that regulate K2P channel density at the cell surface

### A. $\beta$ -spectrin localizes TREK-1 at intercalated discs in the heart

TREK-1 is a K2P potassium channel that has been widely studied in brain, being associated with depression, pain perception and other processes. However, this channel is also present in the heart muscle, where it has been less extensively explored. The interaction between spectrin and the TREK-1 channel has been highlighted in a study conducted by Hund *et al.* in 2014.  $\beta_{IV}$ -spectrin is a structural protein that binds to ankyrin-G, both proteins being strongly involved in the organization of different ion channels in the membrane.

When using a mutant mouse where  $\beta_{IV}$ -spectrin contains a stop codon before the binding site to ankyrin-G ( $qv^{4J}$ ), the two proteins are no longer able to interact with each other in cardiac muscle ([Figure 3](#) A and B). Interestingly, a longer duration of heart muscle action potentials (AP) is observed in these mutants, although the amplitude of the AP is not affected. This could be caused by an alteration in the ion channels present in the membrane of these cells, so a detailed study of different ion channels is carried out. First, the authors looked at both the expression and protein amount as well as the current of different ion channels ( $K_{ir}2.1$ ,  $K_v4.2$ ,  $K_v4.3$ ,  $K_v2.1$ ,  $K_v1.5$  or  $K_v\beta1.2$ ) and they did not observe any alteration. Interestingly, however, this was not the case for the TREK-1 channel. TREK-1 is expressed in the heart specifically in the intercalated discs (ID), together with other K2P potassium channels such as TREK-2 or TASK-1. Although all three channels are expressed in the same region of cardiomyocytes, only TREK-1 is affected in the  $\beta_{IV}$ -spectrin  $qv^{4J}$  mutant, whose location is altered by accumulating partially in the cell's cytoplasm ([Figure 3](#) C). The next question was whether the activity of TREK-1 would also be affected. Then, taking advantage of the fact TREK-1 is sensitive to arachidonic acid (AA), electrophysiological studies were performed to analyze the AA-dependent current of TREK-1 in the ventricle of  $qv^{4J}$  and wild-type (WT) mice. A 66% reduction in current is observed when using mutants for  $\beta_{IV}$ -spectrin compared to WT ([Figure 3](#) D and E). It is clear that  $\beta_{IV}$ -spectrin and TREK-1 interact somehow, but is it a physical interaction? To answer this question Hund *et al.* performed coimmunoprecipitation assays and observed an association between both proteins in the heart lysate of wild-type mice, which interestingly was not seen in  $qv^{4J}$  mutants ([Figure 3](#) F). To go further and know exactly what portion of the  $\beta_{IV}$ -spectrin is necessary for its

union to TREK-1, two constructions were performed: a first one with the entire  $\beta_{IV}$ -spectrin, with fragments that are missing in the mutant  $qv^{4J}$  (repeats 10-17), and a second construction where the ankyrin-G binding-site is removed (repeats 10-14). GST pull-down experiments with these fragments reveal that TREK-1 is able to bind to both constructions of  $\beta_{IV}$ -spectrin ([Figure 3 G](#)).

To conclude, it has been shown that  $\beta_{IV}$ -spectrin is required for the correct localization of the TREK-1 channel in the intercalated discs of cardiomyocytes as well as for its arachidonic acid- dependent activity in mice. Also, TREK-1 and  $\beta_{IV}$ -spectrin are physically associated with each other regardless of the binding of  $\beta_{IV}$ -spectrin to ankyrin-G ([Hund \*et al.\*, 2014](#)).

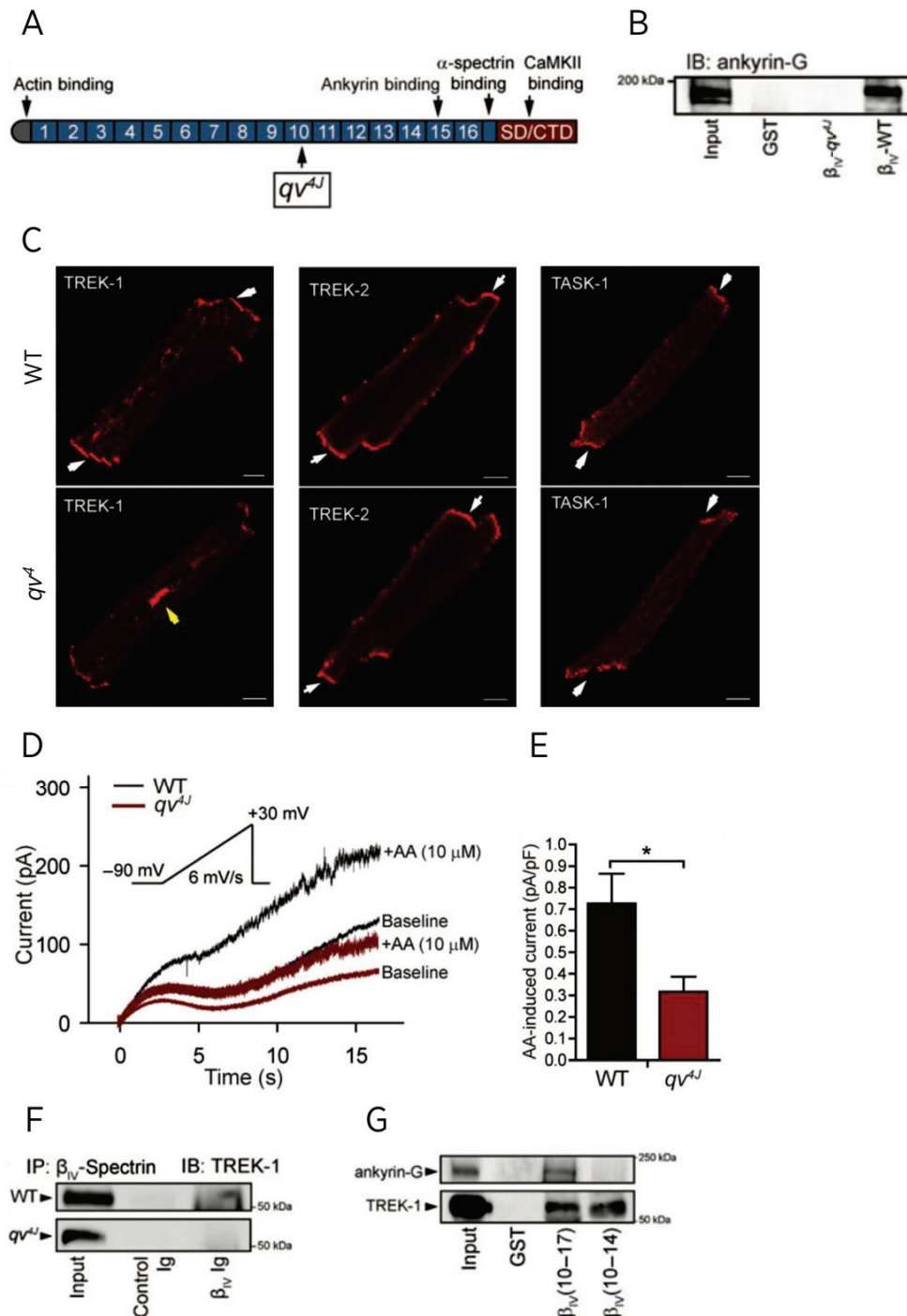


Figure 3  $\beta_{IV}$ -spectrin is involved in the regulation of TREK-1 localization and function in mice heart.

A: Schematic representation of  $\beta_{IV}$ -spectrin structure.  $qv^{4J}$  mutation is an early stop that removes the ankyrin-binding domain on  $\beta_{IV}$ -spectrin. B:  $qv^{4J}$  is no more able to bind ankyrin in pull-down experiments. C: TREK-1, TREK-2 and TASK-1 are expressed in cardiomyocytes at the intercalated discs. Only TREK-1 localization is disturbed in  $qv^{4J}$   $\beta_{IV}$ -spectrin mutants. D: The TREK-1 arachidonic acid-induced current is significantly lower in  $qv^{4J}$  mutants. F and G: immunoprecipitation (F) and immunoblot (G) experiments showing an interaction between TREK-1 and  $\beta_{IV}$ -spectrin. Adapted from [Hund et al., 2014](#).

## B. P11 is required for TASK-1 cellular trafficking

TASK-1 is a K2P potassium channel expressed in many cell types, with abundant levels in brain and heart muscle. A major characteristic of TASK-1 is its sensitivity to variations of external pH, losing its activity at pHs below 6.9 (Duprat *et al.*, 1997). Its inactivity in acid conditions causes changes in the resting potential of the cell membrane, thus modifying its excitability (Millar *et al.*, 2000). Accordingly, a pivotal function of this channel directly related to its sensitivity to pH is the control of respiration, since it is present in carotid bodies. Since little is known about the auxiliary subunits of K2P channels, Girard *et al.* carried out a study with the purpose of identifying TASK-1 regulatory proteins. They began by a screen in the yeast two-hybrid system (Y2H), using the C-terminus region of TASK-1 (amino acids 242-394) and looking for associated proteins. One of the interesting proteins they found was p11 protein, also known as calpactin I or annexin II light chain (Figure 4 A). p11 belongs to the S100 proteins family, and it is known to interact with diverse proteins including ion channels. The authors made an interesting experiment with a construction of the C-terminus of TASK-1 where the last 3 amino acids, SSV, are missing. The results show that in the absence of the SSV sequence, TASK-1 does not bind to p11. Moreover, this binding is specific to TASK-1, since it does not reproduce with TRAAK or TASK-3 (Figure 4 A), which are other K2P channels that do not possess the SSV sequence in their C-terminus region; although TASK-3 presents high homology to TASK-1. On the other hand, in a complementary approach, this interaction of TASK-1 and p11 was confirmed with GST pull-down and coimmunoprecipitation (COS cells) experiments (Figure 4 B).

The electrophysiological experiments in this study had to be carried out in a peculiar way. Considering that p11 is constitutively expressed in different cell types, including the COS cells utilized, the authors decided to decrease the amount of p11 free in the cells by overexpressing two different constructs (PEP21 and PEP35), containing only the C-terminus of TASK-1 that interacts with p11. When both constructions are coexpressed with the whole channel, a lower current is recorded compared to when expressing TASK1 alone (Figure 4 C). This reduction indicates that free p11 might be necessary for TASK-1 channel activity.

The model of interaction proposed by the authors is the following (Figure 4 E): first, they demonstrated that TASK-1 $\Delta$ SSV, which has poor electrophysiological activity (Figure 4 C), is not transported correctly to the membrane compared to wild-type, but is instead

retained inside the cell (observed by fusion of a GFP protein to both TASK-1 WT and TASK-1 $\Delta_{SSV}$ ) ([FIGURE 4 D](#)). Second, there is an MKRR sequence in TASK that seems to be crucial since it makes the difference between an active channel and a non-active channel (TASK-1 $\Delta_{SSV}$ ). This MKRR sequence resembles a retention sequence (RKR) to the endoplasmic reticulum (ER), that was previously described in a  $K_{ir}$  potassium channel ([Zerangue \*et al.\*, 1999](#)). The authors hypothesize that this sequence would be masked by the p11 protein when it binds to TASK-1, thus allowing the correct transport of the channel to the cell membrane rather than being retained in the ER.

To conclude, p11 is an auxiliary subunit that interacts with the TASK-1 channel and is necessary for its electrophysiological activity. Also, the last three amino acids in TASK-1 (SSV) are crucial for this interaction. Finally, p11 would play an essential role in the trafficking of TASK-1 to the cell membrane since by binding to SSV it masks a retention site to the ER, thus allowing the transport and subsequent correct localization of the channel in the membrane ([Girard \*et al.\*, 2002](#)).



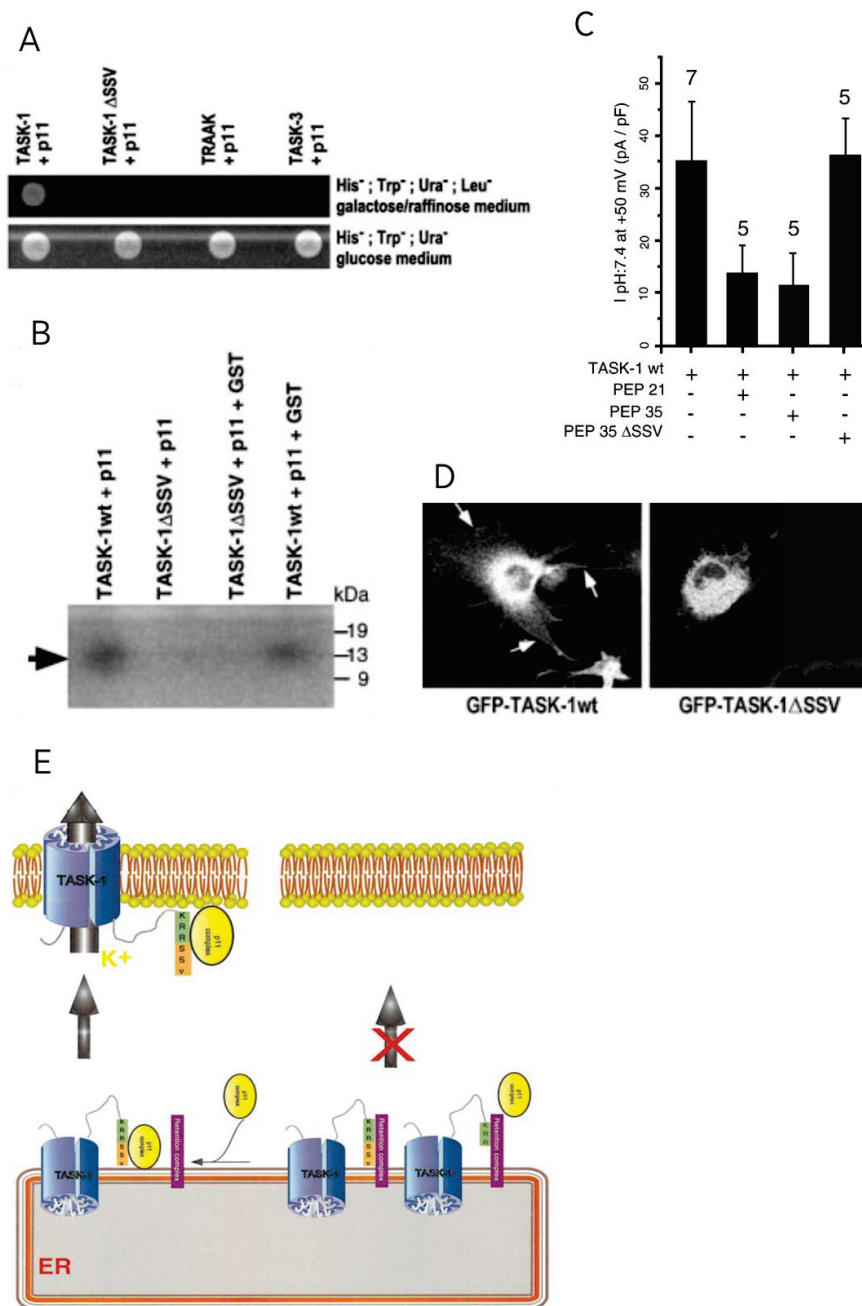


Figure 4 TASK-1 requires p11 to reach the cell membrane.

A: p11 protein interacts specifically with TASK-1 wild-type channel in two-hybrid yeast assays. The TASK-1 C-terminus SSV sequence is required for its interaction with p11. p11 does not interact with TRAAK-1 nor TASK-3, another K<sub>2</sub>P channels. B: GST pull-down experiments confirm the SSV-dependent and specific interaction of TASK-1 and p11. C: PEP21 and PEP35 are constructions where p11 free amount has been strongly reduced by proportioning high levels of the C-terminus fragments of TASK-1, known to bind to p11. The current density recordings on COS cells show no difference in TASK-1 activity when PEP35 missing the SSV C-terminus sequence is used, thus, p11 is free to bind to TASK-1. The current is, however, strongly decreased when p11 is no more able to bind to TASK-1 in PE21 and PEP35. D: TASK-1 requires p11 presence to reach the cell membrane. E: Model proposed of the interaction



of TASK-1 and p11. p11 requires the SSV sequence in TASK-1 C-terminus to bind to it and, thus, allow its trafficking to the cell membrane. Adapted from [Girard et al., 2002](#).

### C. UNC-44/Ankyrin is involved in the trafficking of the K2P channel UNC-58 in *C. elegans*

A last example of a K2P channel regulatory protein, this time in *C. elegans*, is UNC-44. Our laboratory has demonstrated that UNC-44, which is the homologous of ankyrin in worms, mediates the regulation of the K2P channel UNC-58. Philippe Tardy, through a genetic screen, revealed that ankyrin in the nematode is imperative for the correct localization of UNC-58 at the cell membrane, which is expressed mainly in body wall muscle (BWM) and mechanosensory neurons ([Figure 5 A](#)) (unpublished data). Ankyrin is known for its interactions with the protein  $\beta$ -spectrin, whereby both proteins play different roles in locating several ion channels. In this study, Philippe Tardy has shown that this interaction between ankyrin and  $\beta$ -spectrin is dispensable for the localization of UNC-58. Interestingly, ankyrin acts to localize UNC-58 thanks to a structure called lipid-binding pocket which is found in the ZZU super-module of UNC-44 ([Figure 5 B](#)).

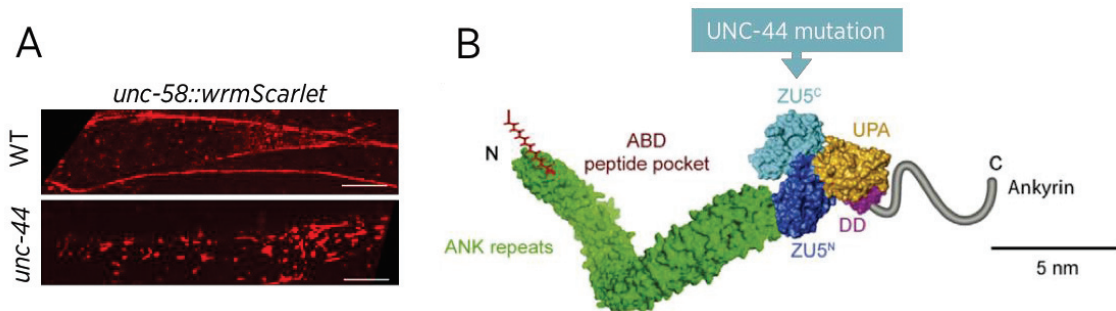


Figure 5 UNC44/Ankyrin regulates the K2P channel UNC-58.

**A:** Ankyrin/UNC-44 is required for the UNC-58 K2P channel localization at muscle cell surface. **B:** UNC-44 structure showing the ZU5 domain, which is necessary for the correct localization of UNC-58. (Unpublished data, from Philippe Tady).

The role of UNC-44 would then be to counteract endocytosis, thus, allowing the channel to be maintained longer in the membrane. For this reason, in the mutants that invalidate the lipid-binding pocket of UNC-44/Ankyrin, UNC-58 is totally delocalized at the membrane, being part of it retained inside the cell, generating phenotypes similar to those obtained in animals that lack *unc-58* (unpublished data).

### III. *In vivo* expression and localization of K2P channels in *C. elegans*

#### A. Distribution of K2P channels in body wall muscle

In *C. elegans* striated muscle (see more [here](#)) there are different types of ion channels co-expressed in the same cell ([Figure 6 A](#)). Most of them are potassium channels, and many belong to the K2P potassium channels class. In our laboratory, we have studied the expression and subcellular localization of most K2P channels present in the worm's striated body wall muscle, by inserting via CRISPR/Cas9, different fluorescent proteins, both using transcriptional and/or translational reporters. As we expected, we saw that in the same cell of the body wall muscle, numerous K2P channels coexist, and although they are all on the same surface, these channels follow different distribution patterns ([Figure 6 B](#)). Figure 6 shows the location of some muscle channels. If we take the example of channel TWK-18, we see that it fills the entire surface of the muscle cell except the anchor points of the integrins, which are shown with yellow arrows in [figure 6](#). (for more detail on the location of the integrins see [results part I](#)). Other channels, such as TWK-42 and TWK-24, show a rather cluster distribution, leaving areas on the membrane that are not occupied by the channel, unlike TWK-18. The third type is the one where the channels are positioned at the lateral membranes, as is the case with TWK-12 and UNC-58 channels, delimiting the shape of the muscle cell. Finally, the most striking case is the one of TWK-28, which has a very peculiar "polarized" localization, since it is restricted to the anterior tip of the cell. TWK-28 makes a "comet" that does not occupy more than one third of the muscle cell surface. These differences in distribution that we observe in the channels clearly indicate the existence of different specific regulatory mechanisms.

A

Calcium channels (4)	Potassium channels (21)	
<i>egl-19</i>	<i>kcnl-1</i>	<i>sup-9</i>
<i>unc-36</i>	<i>kcnl-2</i>	<i>twk-12</i>
<i>cca-1</i>	<i>kvs-5</i>	<i>twk-13</i>
<i>ccb-1</i>	<i>shk-1</i>	<i>twk-17</i>
	<i>shl-1</i>	<i>twk-18</i>
	<i>shw-1</i>	<i>twk-24</i>
	<i>slo-1</i>	<i>twk-28</i>
	<i>slo-2</i>	<i>twk-31</i>
	<i>unc-103</i>	<i>twk-42</i>
		<i>twk-43</i>
		<i>twk-8</i>
		<i>unc-58</i>

B

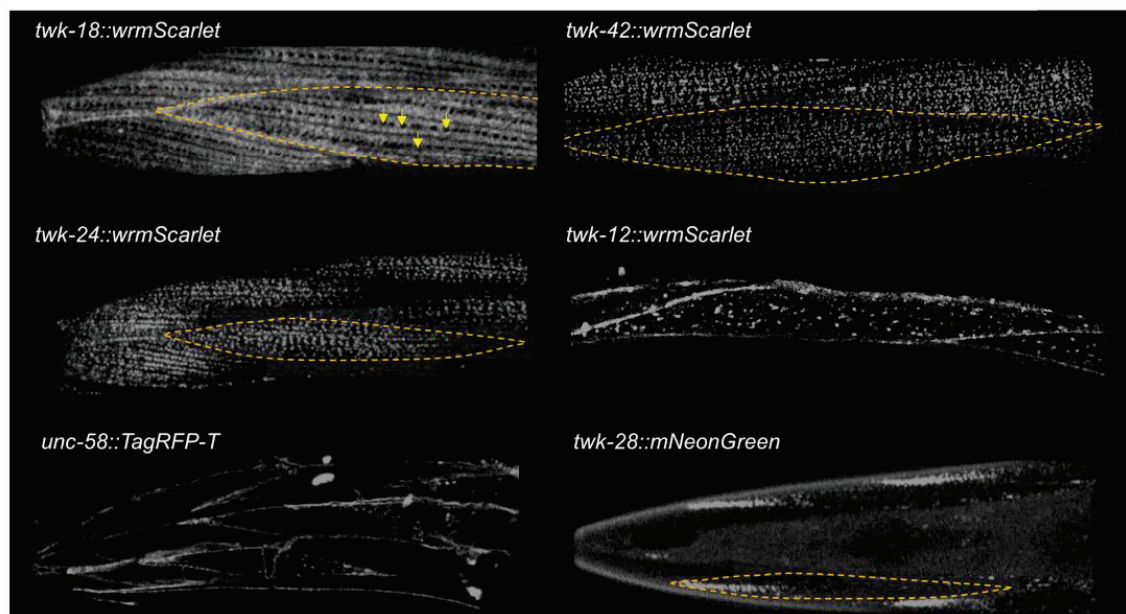


Figure 6 Numerous potassium channels coexist in muscle cells, exhibiting different distributions.

A: List of calcium, chloride and potassium channels present in body wall muscle of worms. K2P channels are the most represented potassium channels (right). B: Representing images of six examples of K2P channels in body wall muscle. The distributions are different from one channel to another. All the strains are CRISPR/Cas9 knock-in lines. (Unpublished data).

The compartmentalized distribution of TWK-28 gave rise to my thesis project, where one of the main objectives was to identify and analyze the factors and molecular mechanisms responsible for this uncommon distribution. It should be noted that, as far as we know, the region where this channel is located does not correspond to any delimited anatomical domain in the muscle cell. The results of the TWK-28 study brought us to the dystrophin complex, establishing for the first time a link between this complex and a channel of the K2P potassium channels family (for more details, see [Results, part I](#)).

#### IV. Identification of regulatory mechanisms – principle of *gain-of-function* genetic screens

Multiple regulatory proteins have been identified thanks to genetic screens. In *C. elegans*, several such studies have been undertaken, most of them involving mutants exhibiting easily identifiable phenotypes, such as problems in locomotion or egg-laying defects. In the following paragraphs, we will see two examples of K2P channels characterization published in the literature, which are SUP-9 and TWK-18. We will also see a new K2P *gain-of-function* (*gof*) mutant, studied during my thesis, which is TWK-28, as well as how the dystrophin complex was identified as a potential regulator.

##### A. SUP-9 likely forms a complex with the regulator subunits SUP-10 and UNC-93

SUP-9 encodes for a K2P family potassium channel which is closely analogous to the human TASK-1 and TASK-3 K2P channels. In this study, De la Cruz *et al.* showed that SUP-10 and UNC-93, two transmembrane proteins, interact with SUP-9 in a single complex in muscle tissue. They initially observed that *gain-of-function* mutants of the three genes give indistinguishable phenotypes in worms: a flaccid paralysis called Rubberband Unc phenotype, as the animals contract when mechanically stimulated in the head and relax back in an "elastic" way, without moving. In addition, they also found that regardless of which gene is mutated (*gof*), a *loss-of-function* (*lof*) mutation in any of the three genes can suppress the Rubberband Unc phenotype associated with the *gain-of-function* mutation. This suggests that all three proteins probably act in a single complex. In parallel, they studied the expression pattern and subcellular location of the three proteins and revealed that all of them are predominantly expressed in the body wall muscle and are also co-localized at the same subcellular level ([Figure 7](#)).

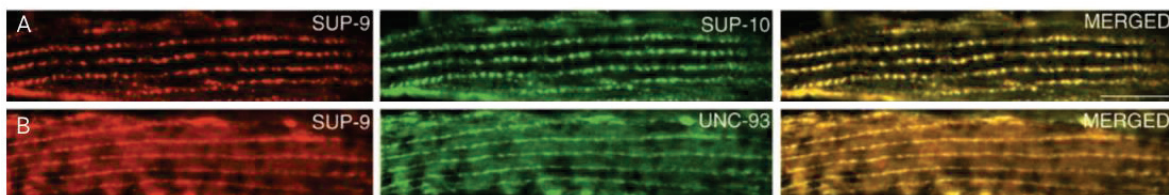


Figure 7 SUP-9 interacts and co-localizes with the regulatory proteins SUP-10 and UNC-93 in body wall muscle. Adapted from [de la Cruz \*et al.\*, 2003](#).

They conclude that the proteins SUP-9, SUP-10 and UNC-93 form a sub-complex in the muscle cells of *C. elegans*, which is involved in the control of body wall muscle contraction ([de la Cruz et al., 2003](#)).

## B. TWK-18 first characterization

TWK-18, formerly called UNC-110, was first characterized by Kunkel *et al.*, where they showed that it is expressed in body wall muscle and allows potassium current to pass through. They carried out both genetic and electrophysiological studies in order to shed some light on the structure and function of this channel. By constructing transgenic animals that express a GFP protein under the control of the *twk-18* (2.75 kb) promoter, it was demonstrated that TWK-18 is present in body wall muscle cells ([Figure 8 A](#)). This expression pattern was confirmed by further studies performed in our laboratory, using different fluorescent proteins fused to the channel by CRISPR/Cas9 ([Figure 8 B](#)).

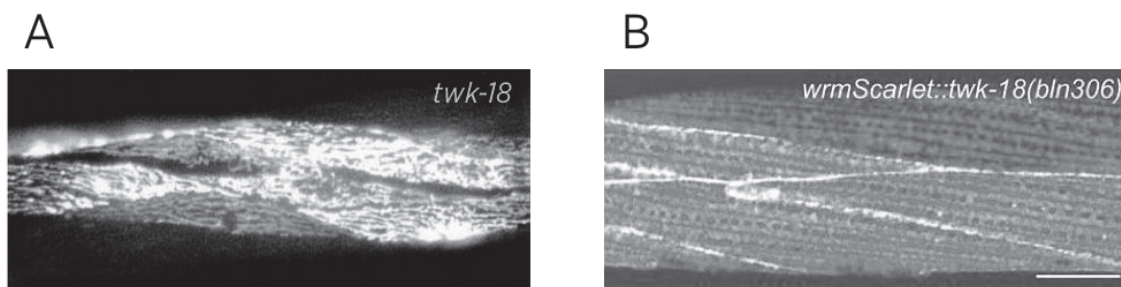


Figure 8 TWK-18 is expressed in body wall muscle.

A: *twk-18::gfp* gene reporter showing the expression of *twk-18* in body wall muscle. Adapted from [Kunkel et al., 2000](#). B: CRISPR/Cas9 protein fusion showing the subcellular localization of TWK-18 in body wall muscle in *C. elegans*. Our published data in [El Mouridi et al., 2017](#).

Mutant alleles of *twk-18* are available (*e11913* or *cn110*), which are temperature sensitive *gain-of-function* mutants. However, no study has gone further into the characterization of this channel, so that the regulation mechanisms of TWK-18 are not known so far.





3) Using the CRISPR/Cas9 strategy, we have been able to reproduce these mutations *in vivo* in *C. elegans*. Before our publication, only 4 K2P *gof* mutants (*egl-23*, *unc-58*, *sup-9* and *twk-18*) were known. When TM2.6 mutations are inserted endogenously into these four genes, the resulting mutants exhibit phenotypes indistinguishable from the canonical alleles. That is, we can generate new gain of function mutants by modifying the TM2.6 residue.

4) This increase in activity observed is not due to a larger expression of the channels on the surface, but is an amplification in the channel's activity.

5) This current increase is also adjustable. Depending on the amino acid inserted in position TM2.6, it is possible to obtain more (if N or D used) or less (if S or T inserted) channel activity, both of which are stronger than the wild-type activity. For more details, see our publication on [results part 3](#).

To conclude, this study describes a new strategy that allows the systematic modulation of the activity of the whole K2P potassium channels family in different models. Also, an innovative facility to generate new *gain-of-function* mutants *in vivo* in *C. elegans*, which previously had to be simulated through a gene over-expression that did not preserve the native physiology of the cell or by performing genetic screens to look for this kind of mutants. Finally, these newly generated *gof* mutants open new doors for genetic studies to further characterize the K2P channels.

#### A. EMS forward genetic screen on TWK-28

Throughout my thesis, one of the genetic screens I performed was on the *gain of function* TWK-28 L210T mutant. The *twk-28* gene is mainly expressed in body wall muscle ([Figure 10 A](#)) of *C. elegans* ([Cao et al., 2017](#)). Thanks to a transcriptional reporter (CRISPR/Cas9), we have been able to see the location of TWK-28 at the subcellular level. Interestingly, this channel shows a very peculiar localization, which is unique in the muscular K2P potassium channels of *C. elegans*. The protein is located only in the anterior tip of each muscle cell ([Figure 10 B](#)), generating a "comet" pattern that is repeated in each body wall muscle cell. The first question that came to our minds was what cellular and molecular mechanisms are involved in the distribution of this channel. Therefore, based on the results of our last study, we were able to create a new *gain-of-function* mutant for the TWK-28 (L210T) channel. TWK-28 L210T showed a strongly higher activity compared to wild-type in *Xenopus* oocytes ([Figure 10 D](#)). Therefore, when we introduce



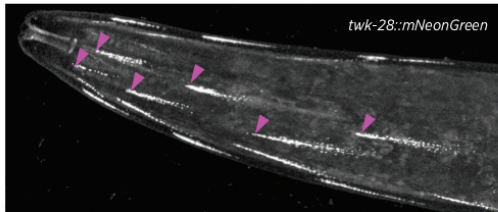
the TWK-28 L210T mutation *in vivo*, mutant worms exhibit a strong paralysis phenotype, which is consistent with a *gain-of-function* muscular potassium channel mutation. The paralyzed TWK-28 L210T strain served as a starting point for a phenotypic suppressor genetic screen, whose objective was to look for regulatory factors of TWK-28 in a native context. Unlike other approaches, a genetic screen develops without preconceptions, since we target the entire genome with random mutations. Thus, we can find genes that participate in different regulatory pathways of TWK-28, from gene expression, post-translational modifications, trafficking and maintenance at the cell membrane as well as modulation of the channel activity. One of the advantages of *C. elegans* in this way, is its clonal hermaphrodite reproduction (300 embryos per animal) and its relatively short reproduction cycle (3 days at 20°C).

A

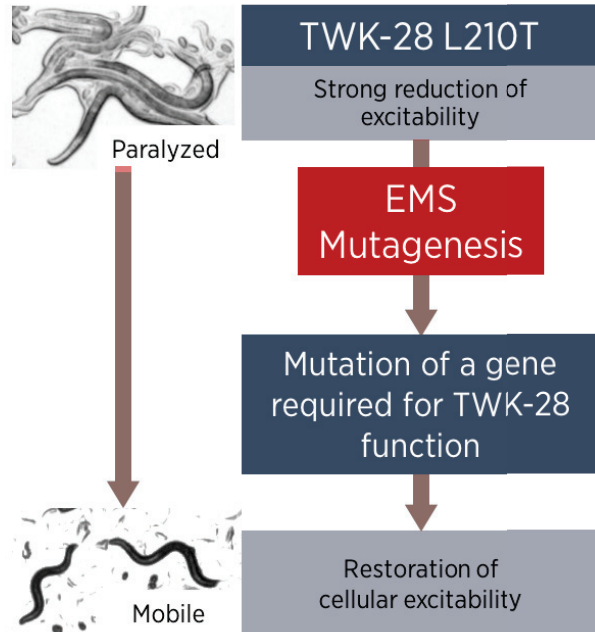
Tissue-level consensus expression profiles. (Values listed are transcripts per million)

Gene	Neurons	Gonad	Hypodermis	Pharynx	BWM	Glia	Intestine
twk-28	0,695	0,295	0,000	0,000	<b>44,423</b>	0,000	18,727

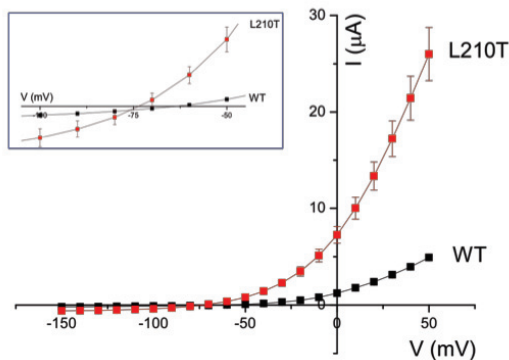
B



C



D



E

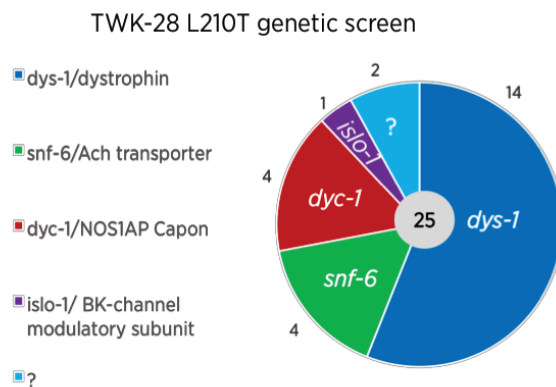


Figure 10 TWK-28 has a particular localization in body wall muscle.

A: RNA-seq data showing that *twk-28* is mostly expressed in body wall muscle. From [Cao et al., 2017](#). B: CRISPR *knock-in* of TWK-28::mNeonGreen showing a comet-like localization of the channel at the anterior tip of each body wall muscle cell. Unpublished data. C: Strategy followed in the genetic screen performed on TWK-28 L210T *gain-of-function* paralyzed worms. After random mutagenesis with EMS, we looked for worms that were able to move again. D: *In vitro* *Xenopus* oocytes electrophysiological recordings show a higher current in TWK-28 L210T compared to wild-type TWK-28. E: Different alleles for four genes were isolated from the *twk-28* genetic screen: *dys-1*/dystrophin, *snf-6*/acetylcholine

transporter, *dyc-1*/NOS1AP Capon and *islo-1*/Big channel (SLO-1) modulatory subunit. Two more genes were not identified (?).

The idea of the genetic screen on TWK-28 is to start from paralyzed animals (L210T) and, after a random mutagenesis with EMS (ethyl methane-sulfonate), look for mobile animals in the offspring ([Figure 10 C](#)). These mobile animals will have one of the two following situations:

- 1) A mutation in the *twk-28* gene itself, so that the *gain-of-function* phenotype initially present in the animals is invalidated as there is no more TWK-28 after mutagenesis.

- 2) A mutation external to *twk-28*, but affecting a gene required for the functioning of the channel, so that its absence would also suppress the *gain-of-function* phenotype of TWK-28 L210T. This last situation is what interested me during my thesis, since it would allow me to identify factors involved in the regulation of TWK-28.

In conclusion, in the forward genetic screen on TWK-28 L210T 182 mutants ([Figure 10 E](#)) were obtained, of which most are genes related to dystrophin: *dys-1*/dystrophin, *snf-6*/acetylcholine transporter, *dyc-1*/NOS1AP Capon, *islo-1*/BK-channel (SLO-1) modulatory subunit. During my thesis, I focused on the characterization of dystrophin and its associated protein complex (DAPC) as well as its involvement in the regulation of the TWK-28 channel. The results obtained from this study are described in the section of [results part I](#).

## Chapter 2 Body wall muscle of *C. elegans*

*Caenorhabditis elegans* was introduced in laboratories in the 1960s by Sydney Brenner as an ideal genetic model to study topics such as developmental biology, genomics and neurobiology ([Brenner, 1974](#)). In recent years, the nematode has been widely used in the study of the development, organization and function of muscle tissue. *C. elegans* has two muscle cell types:

1) Non-striated or smooth muscle: these cells are found in structures like pharynx, which allows the worm to pump bacteria for food. Non-striated muscle is also found in gonad, vulva, uterus, stomatointestinal and anal depressor and sphincter muscles.

2) Striated muscle, most of this tissue is found in the body wall muscle, which is necessary for the movement of the animal.

In this chapter, we will cover general notions about the organization and morphology of the striated muscle (body wall muscle) of *C. elegans*, providing insights about the ionic channels present and implicated in the muscle cell excitability; as well as the attachment structures that finally allow the transduction of the force executed and the consequent movement of the worm.

## I. Organization and structure of striated muscle tissue in *C. elegans*

### A. Body wall muscle organization and development

The body wall muscle (BWM) is the analogue of the skeletal striated muscle in *C. elegans* and consists of a total of 95 rhomboidal cells. These cells are arranged in four quadrants, each one consisting of a monolayer muscle cells partially overlapping with each other creating a row, going from the worm's head to its tail ([Figure 11 A and B](#)). There are two ventral and two dorsal quadrants (right and left in each case). All quadrants, except the left ventral one, which houses 23 cells, contain 24 cells per band ([Sulston and Horvitz, 1977](#)).

In *C. elegans*, BWM comes from D, C, AB and MS lineages ([Sulston et al., 1983](#)). Briefly, the life cycle of the worm consists of an embryonic, a larval and an adult phase. Thus, most BWM cells are formed during embryonic development, but 14 of them are generated later. Accordingly, after hatching we find a premature BWM formed by only 81 cells, the rest being added during larval development. New sarcomeres are also added to each cell. The unique factor that controls muscle genesis (myogenic regulatory factor) in the worm is encoded by *hll-1*, homologous to MyoD. Mutants lacking HLH-1 do not develop and present numerous defects at the level of musculature, supporting the evident relevance of this factor ([Gieseler et al., 2017](#)).

The body wall muscle cells lie on a basal lamina, which separates them from the hypodermis and the nervous tissue. A very interesting fact is that the development of this muscle tissue occurs invariably from one animal to another, so that in each worm each cell is identified and occupies the same position. In addition to the fact that all animals have exactly 95 cells, a particular cell can be followed over time, making it possible to carry out studies, for example, of muscle degeneration.

The BWM cells are fusiform and their structure clearly differentiates an area that holds in the cytoplasm all the contractile apparatus (myofilaments). In a separate region of the cytoplasm, we find the typical organelles of these cells, including nucleus, endoplasmic reticulum, etc. Unlike in mammals, *C. elegans'* BWM cells do not form fibers as they do not fuse together, so they preserve only one nucleus per cell. In addition, these cells are completely post-mitotic and have no regenerative capacity; there are no satellite cells (muscle stem cells) in *C. elegans*. Another difference with mammals, is the innervation

at neuromuscular junctions. Peculiarly, it is the muscle that projects prolongations, called muscle arms, towards the axons of the nerve cells to build the synapse.

Comparable to vertebrates, the functional unit of the worm muscle is the sarcomere, which is responsible for giving the striated appearance to the BWM. The almost total transparency of *C. elegans* allows us to visualize such structures ([Gieseler et al., 2017](#)) ([Figure 11 C](#)). These striations, instead of being straight as in vertebrates, they are slightly inclined forming an angle of approximately 5.9 degrees with respect to the longitudinal axis of the cell ([Figure 11 E](#)). This is why the roundworms of the phylum Nematoda are said to have an obliquely striated muscle ([Moerman and Williams, 2006](#)). Interestingly, the proteins that form the sarcomere have been widely conserved in evolution. So, we find thin actin and thick myosin filaments, both responsible for generating the contraction as it is known in vertebrates. Actin thin filaments are encoded by four genes (*act-1* to *act-4*), and in the sarcomere this actin is coupled to other proteins such as tropomyosin (LEV-11) or troponins (PAT-10, MUP-2, TNI). Concerning the thick myosin filaments, in BWM there are two heavy chains encoded by two genes: *myo-3* for the myosin heavy chain A (MHC A) and *unc-54* for the MHC B chain; although there are two other genes that code for heavy chains of myosin in another muscle organ, the pharynx, which are *myo-1* and *myo-2*. The myosin light chains are coded by *mlc-1* and *mlc-2* ([Gieseler et al., 2017](#)).

The arrangement of the *C. elegans* sarcomeric myofilaments follows the path of its vertebrate counterparts, with an A-band consisting of myosin filaments and an I-band containing actin. We also find that the myosin filaments are anchored to the M line ([Figure 11 E](#)). However, the first difference is that the anchoring zone of the actin filaments is called dense body, being the analog of the Z discs. Accordingly, a sarcomere corresponds to the region delimited by two dense bodies, as in the mammalian costamers ([Francis and Waterston, 1985](#)). Thus, in *C. elegans* we find three anchor points of the sarcomere to the sarcolemma: the dense bodies, the M lines and the attachment plaques. These structures will be described in more detail in the next section.

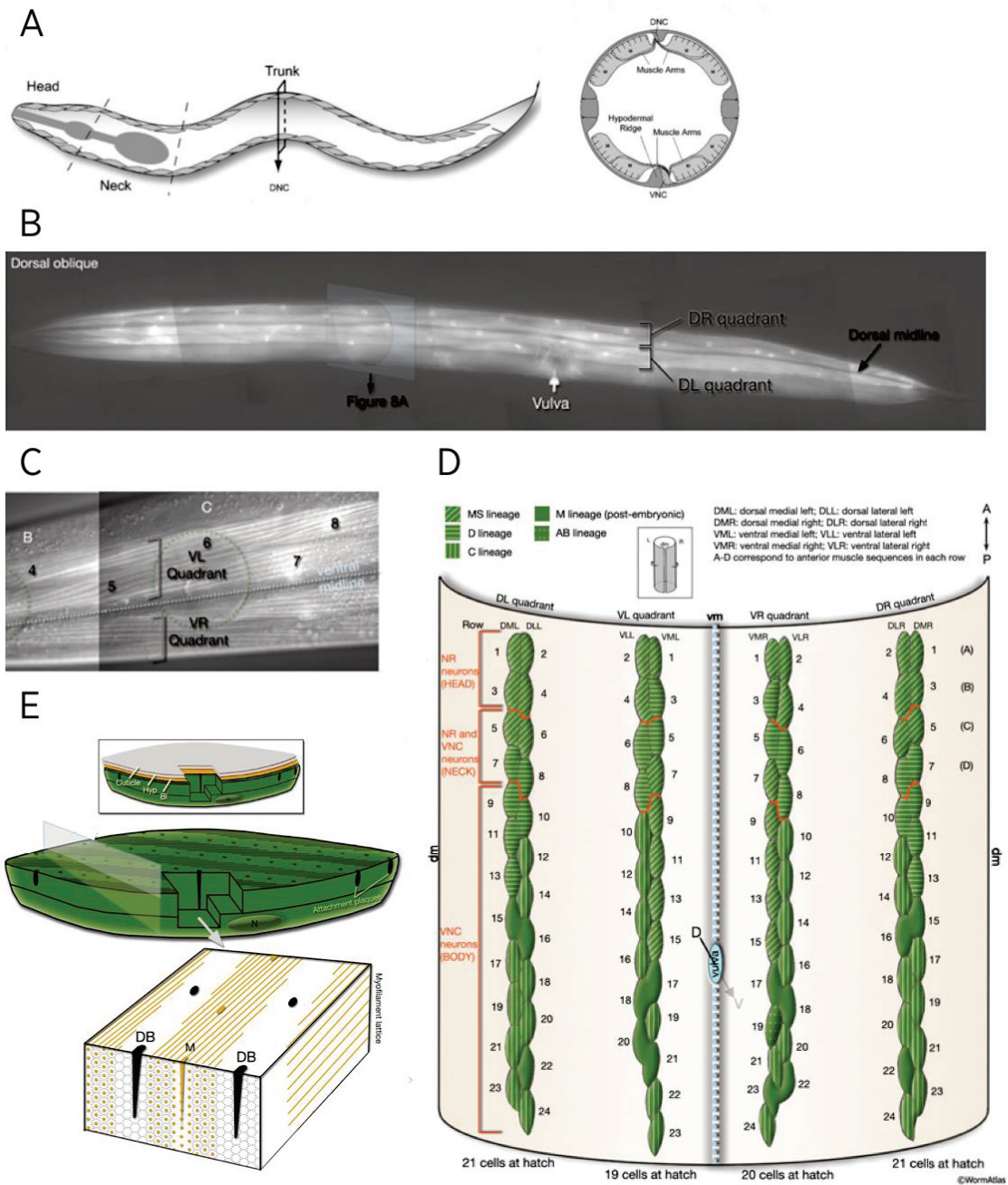


Figure 11 *C. elegans* striated muscle corresponds to body wall muscle and is arranged in four quadrants.

A: Schematic representation of body wall muscle organization in four longitudinal quadrants. B and C: *C. elegans* transparency allows the visualization of muscle quadrants from the worm's head to the tail (B) and the striations in each body wall muscle cell (C). D: Representation of the four muscle quadrants in L1 larval stage. E: In body wall muscle, myosin filaments are anchored the M line and the actin filaments to the dense bodies. Myofilaments form an oblique striation. Adapted from WormAtlas®.



## B. Muscle cells attachments allow the force transduction

The Z-disk analogue, called dense body in *C. elegans*, together with the M lines, form the anchor points of the sarcomere to the muscle cell membrane and the underlying basement membrane ([Figure 11 E](#)). Integrins are crucial as they represent the main proteins allowing the establishment and maintenance of the sarcomere point-attachments to the sarcolemma. Integrins in *C. elegans* show a great conservation in evolution. We find PAT-2, which is analogous to  $\alpha$ -integrin, and PAT-3 for  $\beta$ -integrin; both interacting with components of the extracellular matrix ([Figure 12 A](#)) ([Gieseley et al., 2017](#)). In the dense body, the role of the vinculin (DEB-1) is also to form a complex associated with PAT-2 and PAT-3, as well as the perlecan (UNC-52), establishing the base of the anchor of the dense body in the muscle cell membrane. Finally, in the extracellular matrix (ECM) associated to dense bodies and M line, we find collagen IV. There are also fibrous organelles, which serve to connect the muscle tissue and the surrounding hypodermis to the cuticle. The fibrous organelles are the homologues of vertebrate hemi-desmosomes. The muscle contraction in *C. elegans* takes place in a similar way to the mammalian one, where the myosin filaments attract the actin filaments towards the M line ([Figure 12 B](#)). This contractile force will be propagated to the outside with the help of the dense bodies, which are directly linked to the ECM. This bridge is crucial for the transmission of the force generated by the muscle cell to the underlying basal lamina, which then, thanks to the fibrous organelles, will pass through the hypodermis and reach the cuticle (the exoskeleton of the worm) ([Cox and Hardin, 2004](#)). Finally, it should be noted that at the moment of the contraction of the BWM cells, the signal is propagated to the neighboring cells along the quadrant thanks to the electrical coupling between these cells, since they are linked together by gap junctions ([White et al., 1986](#)).



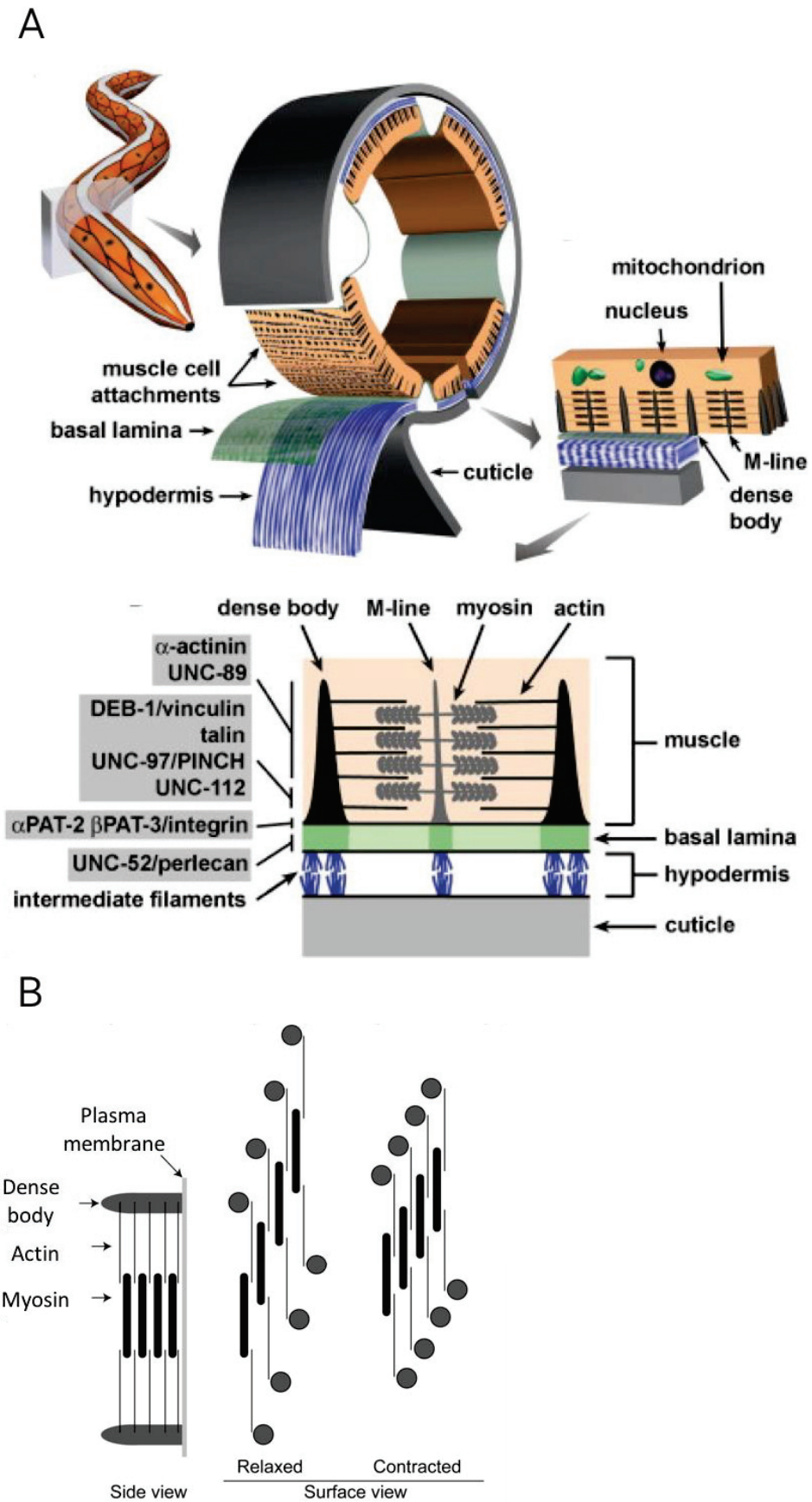


Figure 12 The body wall muscle functional unit, the sarcomere, is conserved.

A: Schematic representation of different levels of body wall muscle organization. BWM is separated from the external cuticle by first a basal lamina and a hypodermis tissue. The functional subunit of BWM is the sarcomere, delimited by two dense bodies (thin actin filaments anchor) containing an M line (thick myosin filaments anchor). Adapted from [Mackinnon et al., 2002](#). B: Myofilaments in BWM form a 5,9 degrees angle with the muscle cell longitudinal axis, giving rise to an obliquely striated body wall muscle. Adapted from [Ono et al., 2014](#).

### C. Innervation through muscle arms projections

The striated muscle cells of the body wall muscle, depending on how they are innervated, define three areas: 1) the anterior area closest to the head, consisting of 4 cells in each quadrant (16 in total). These cells obtain their innervation from the nerve ring. 2) area of the pharynx, where 16 cells called neck cells (4 from each quadrant) are innervated from both the nerve ring and the nerve cord. 3) finally, the rest of the body's muscle cells (63 cells), whose innervation proceeds exclusively from the nerve cord (reviewed in [White, 2018](#)).

The neuromuscular junction synapses in *C. elegans*, unlike in mammals, can be both excitatory (acetylcholine, Ach) and inhibitory ( $\gamma$ -aminobutyric acid, GABA) ([Figure 13 A](#)). Thus, the release of acetylcholine will cause an excitation in the muscle, which results in consequent contraction; while the release of GABA will cause the opposite effect, hence, the relaxation of the muscle cells. The balance between both processes is crucial for the locomotion of these animals. During its movement, the worm will contract the muscle cells on one side while relaxing those on the opposite side, creating a sinusoidal movement characteristic of these animals ([Figure 13 B](#)).

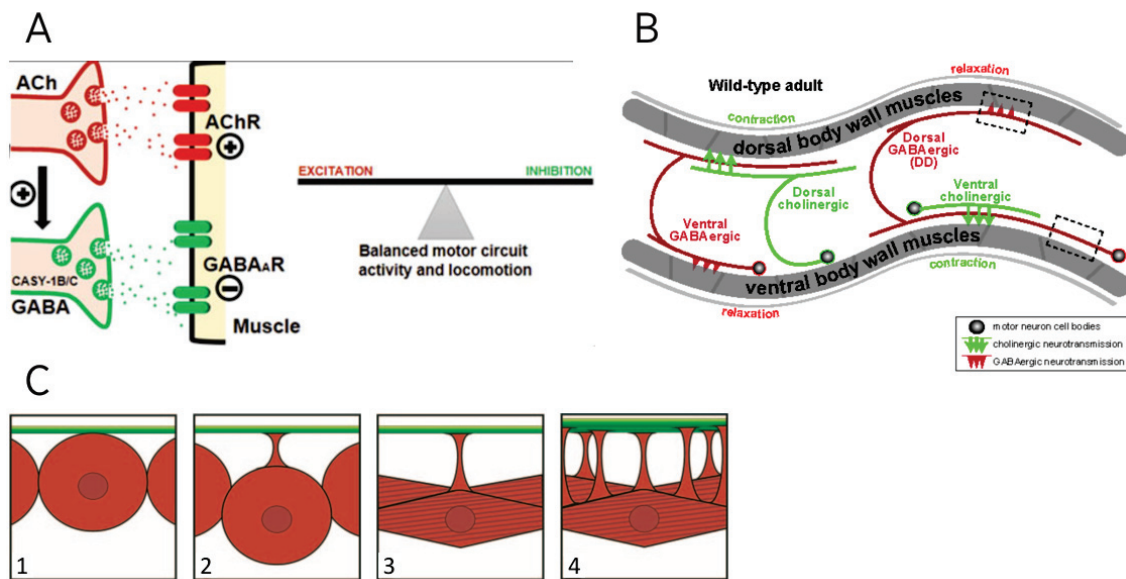


Figure 13 In *C. elegans*, the muscle project muscle arms toward axons, where muscle can be excited (ACh) or inhibited (GABA).

A: In *C. elegans* body wall muscle GABAergic and Cholinergic innervation coexist, and the balance between them lead to worm locomotion. Adapted from [Thapliyal and Babu, 2018](#). B: For locomotion, muscle cells on one side contract (ACh) while the opposite cells are inhibited (GABA), originating a typical sinusoidal movement. Adapted from [Han et al., 2015](#). C: Schematic representation of muscle arms development. Muscle arms are projections that muscle cells (red) send towards the axon or nerve chord (green) to establish the neuromuscular junction. Adapted from [Dixon et al., 2005](#).

Interestingly, instead of nerve cells projecting extensions into the muscle in order to innervate it, in *C. elegans* it is the muscle cells that project into the nerves. These muscular projections are called muscle arms, and are extensions that are maintained throughout the life of the animal ([Sulston et al., 1983](#); [White et al., 1986](#); [Dixon et al., 2005](#)). Muscle arms develop during embryogenesis and, after hatching, their number increases threefold: 1-2 muscle arms per cell in L1 larval stages versus 3-5 in adults ([Figure 13 C](#)) ([Hedgecock et al., 1990](#); [Hall and Hedgecock, 1991](#)). Finally, muscle arms differ in shape and length, which varies depending on how close or far away the nerve that innervates them is.

## II. Ion channels and regulation of *C. elegans* muscle excitability

### A. TWK-18, the first TWK channel characterized

TWK-18, a K<sup>2</sup>P channels in *C. elegans*, was the first TWK channel to be fully characterized (Kunkel *et al.*, 2000). To analyze its electrophysiological role, the authors utilized the *Xenopus* model, where oocytes are used to express RNA from the channel's subunits, both under wild-type and mutant conditions. In oocytes, two electrode voltage-clamp and patch-clamp experiments were performed. The results show that: 1) outwardly rectifying currents are generated by these channels and 2) *cn110* and *e1913* *gof* mutants permit significantly higher current to pass than wild-type channels (Figure 14 A). Furthermore, this study showed that both WT and mutants channels have a temperature-dependent function, that is, at higher temperatures the activity is stronger (Figure 14 B). To conclude, TWK-18 is a channel present in muscle that allows the passage of potassium ions in a temperature-dependent manner. *Gain-of-function* mutations in this channel result in animals with uncoordinated locomotion phenotypes and paralysis, which is consistent with a higher potassium output that hyperpolarizes the muscle cell making it less excitable. Thus, the most sustained hypothesis defends that this channel could be involved in the control of *C. elegans* muscle excitability (Kunkel *et al.*, 2000).

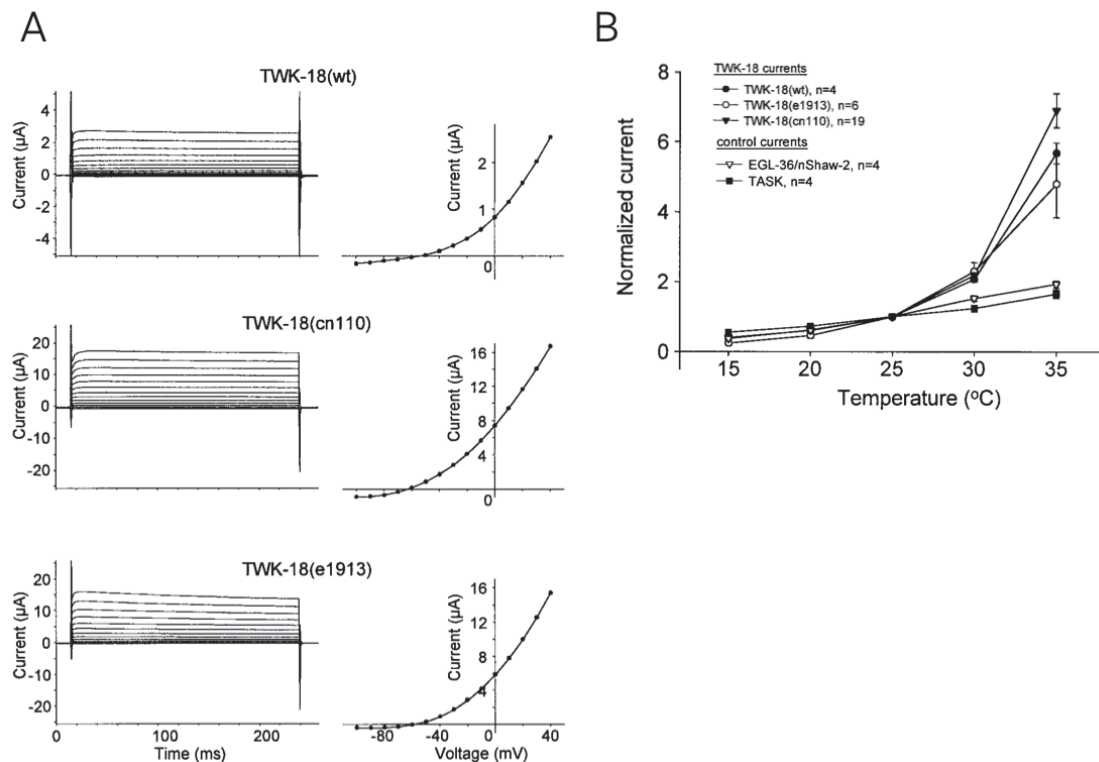


Figure 14 TWK-18 is a K<sup>2</sup>P potassium channel that controls body wall muscle excitability.

A: Electrophysiological recording from *Xenopus* oocytes show a greater current in the two *gain-of-function* mutants *twk-18(cn110)* and *twk-18(e1913)* channels compared to wild-type (wt). B: TWK-18 associated current is temperature-sensitive, being increased at higher temperatures. EGL-36 and TASK are temperature-insensitive channels used as control. Adapted from [Kunkel et al., 2000](#).

## B. SUP-9 is also involved in muscle excitability

Among the 47 K2P channels present in *C. elegans*, only 4 of them have a direct human counterpart, they are: SUP-9, TWK-14, TWK-46 and TWK-20. SUP-9 presents high similarities with the TASK-1 and TASK-3 K2P human channels. In *C. elegans*, it is expressed mainly in the body wall muscle cells. One of the first research groups to study this K2P channel was the Horvitz team, who built a GFP reporter expressed under the control of the *sup-9* promoter and demonstrated a muscle expression pattern ([Figure 15 A](#)) ([de la Cruz et al., 2003](#)). Continuously, our laboratory used CRISPR/Cas9 to confirm the location of SUP-9 in the striated muscle of the worm ([Figure 15 B](#)).

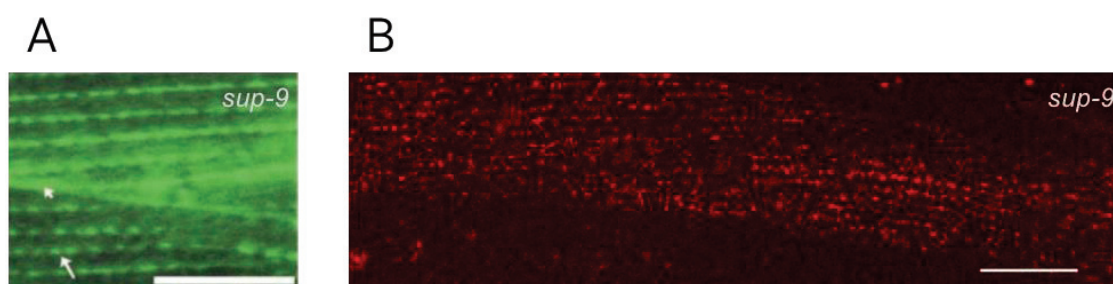


Figure 15 SUP-9 is a K2P channel which is expressed in *C. elegans* body wall muscle.

A: Gene reporter showing the *sup-9* localization in muscle. Adapted from [de La Cruz et al., 2003](#). B: CRISPR/Cas9 knock-in showing more clustered subcellular localization of SUP-9. Scale: 10 $\mu$ m. (Unpublished data).

The mutants for *sup-9*, such as *sup-9(n1550)*, show a visually recognizable phenotype of flaccid paralysis that is called Rubberband Unc. When animals receive a mechanical stimulus, they contract and then relax in an "elastic" way. The hypothesis here is similar to the one made in TWK-18 study: the *gof* mutation leads to increased transport of K<sup>+</sup> ions through SUP-9, resulting in cell hyperpolarization and thus loss of excitability, originating paralysis. However, electrophysiological experiments on SUP-9 were not performed, although an indirect approach using muscimol was used ([de la Cruz et al., 2003](#)). Muscimol is a GABA Cl<sup>-</sup> channel agonist and is known to induce hyperpolarization of BWM ([Richmond and Jorgensen, 1999](#)). Muscimol was used on

wild-type worms and, as expected, triggered the same Rubberband Unc phenotype as *sup-9(n1550)* *gof* allele. Finally, when they added muscimol to the *gof* mutants of *sup-9*, they saw an additive effect. Thus, muscimol and *sup-9* mutants, although they originate the same phenotype, function independent and additively. They conclude that the phenotype observed in *sup-9(n1550)* could be due to a hyperpolarization similar to the one carried by muscimol ([de la Cruz et al., 2003](#)).

### C. SLO-1, a BK potassium channels in *C. elegans*

SLO-1 belongs to the BK (big potassium) channels family, presenting high homology with the mammals Slo1 channel ([Wei et al., 1996](#)), and sensitivity to both intracellular calcium concentration and voltage. Already in 2001, this characteristic was confirmed by *in vitro* measurement of the current of this channel expressed in *Xenopus* oocytes. Wang *et al.* showed that there is a variation in the current transported by SLO-1 when a modification in the membrane potential is induced, keeping the calcium concentration fixed, and vice versa ([Figure 16 A](#)) ([Wang et al., 2001](#)). This channel in *C. elegans* is expressed in both neurons and muscle, including the body wall muscle ([Carre-Pierrat et al., 2006](#)). To further investigate the function of this channel, the E350Q mutation was created ([Chen et al., 2010](#)), based on previous studies that demonstrated the importance of this residue for the channel activity ([Davies et al., 2003](#)). SLO-1 is known to play an important role in the neuromuscular junction, where it is involved in the regulation of neurotransmitter release. Based on this, Chen *et al.* conducted electrophysiological studies where they measured ePSC (excitatory postsynaptic current) in the muscle near the NMJ. They saw that in the SLO-1 E350Q *gain-of-function* mutant, the ePSCs were significantly reduced ([Figure 16 B](#)), which was expected since increased SLO-1 activity would lead to increased potassium transport out of the cell, making it hyper-polarized and therefore less excitable. They repeated the same experience with SLO-1 *loss-of-function* mutant ([Figure 16 B](#)), and saw the opposite effect ([Chen et al., 2010](#)). However, in another study ([Sancar et al., 2011](#)), the authors induced an optogenetic stimulation of the ventral cord (specifically the cholinergic motor neurons), and measured the synaptic current evoked in the muscle. No difference between wild-type animals and *slo-1(js379)* *loss-of-function* mutants was observed ([Figure 16 C](#)). Current-clamp was also performed on the BWM, where responses in the form of action potentials near the NMJ, caused by induced stimulation, were analyzed. It was shown that loss of SLO-1 increases stimulated AP



bursts (Figure 16 D). However, the absence of the channel does not generate a change in the resting potential (Figure 16 D). Thus, although these channels are involved in muscle excitability, they do not intervene in establishing or maintaining the resting electrical tone of the membrane. The hypothesis of the involvement of SLO-1 in excitability argues that these channels are necessary to correctly repolarize the cell membrane after an action potential. So, if lost, repolarization is deficient and the cell becomes excitable and can more easily generate a second action potential (Sancar *et al.*, 2011).

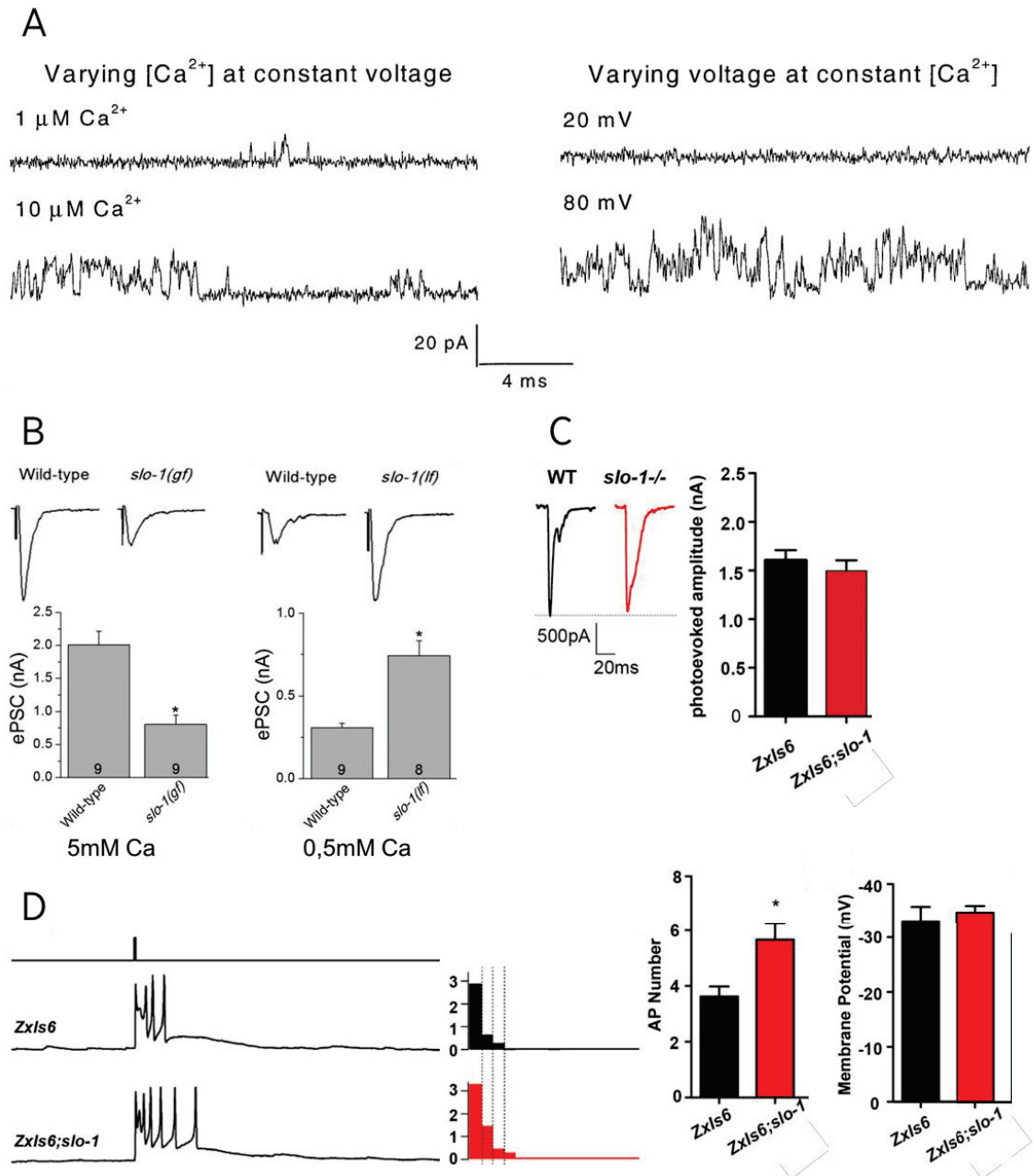


Figure 16 SLO-1 is a BK channels in *C. elegans*, involved in muscle excitability, through repolarization regulation.

A: Electrophysiological recording of single channel currents of SLO-1 shows the sensitivity of the channel to both voltage and calcium concentration. Adapted from Wang *et al.*, 2001. B: ePSC amplitude recorded

at neuromuscular junction is decreased in SLO-1 *gain-of-function* and higher in *loss-of-function* mutants when compared to wild-type. Adapted from [Chen et al., 2010](#). **C:** Synaptic current recorded from body wall muscle shows no difference between *slo-1 loss-of-function* mutant and wild-type. ZxIs6 is the transgenic channel-rhodopsin strain, used as control. **D:** *slo-1 loss-of-function*, however, induce an increase in action potential frequency, without changing the membrane potential. Adapted from [Sancar et al., 2011](#).



## Chapter 3 Dystrophin-Associated Protein Complex (DAPC)

Muscular dystrophies belong to the group of myopathic diseases, which are characterized by the deterioration of muscle tissue function, resulting in progressive muscle weakness and atrophy. A well-studied class of muscular dystrophies in the last decades are the dystrophinopathies, which are hereditary myopathies in which the causal mechanism is the total or partial absence of dystrophin. The underlying mechanisms are diverse, in this manuscript we will focus on the genetic mutations that interfere in the production of some proteins, including dystrophin, necessary for the proper functioning of the muscle tissue, focusing mainly on the model nematode *Caenorhabditis elegans*.

## I. The dystrophin-associated proteins complex and its conservation in *C. elegans*

### A. General overview

In 1987 Kunkel and his co-workers opened the door to the new era of research into muscular dystrophies, by cloning the cDNA of the dystrophin gene. This finding confirmed the results of previous studies in proposing the dystrophin gene as a candidate of Duchenne Muscular Dystrophy in 1986 ([Monaco et al., 1986](#); [Koenig et al., 1987](#)).

The dystrophin is the largest known gene present in our genome. Thanks to the work of Kunkel's group and other researchers, this gene has been mapped on the X-chromosome (Xp21), which explains the prevalence of Duchenne recessive disease in boys, since they only possess one X-chromosome ([Monaco et al., 1986](#); [Hoffman et al., 1987](#)). Also, it has been determined that this gene comprises about 2.4 Mb of genomic sequence, being composed of 79 exons as well as very long introns, representing themselves about 1-1.5% of the X-chromosome content.

Few years after the discovery of dystrophin, numerous studies showed that this protein is in fact part of a complex called the dystrophin-associated protein complex or DAPC ([Ervasti et al., 1990](#)). DAPC was first isolated from skeletal muscle, ([Ervasti and Campbell, 1991](#); [Anderson and Kunkel, 1992](#)) and it is constituted by a group of proteins that can be transmembrane, extracellular or intracellular ([Ervasti and Campbell, 1992](#); [1993](#)). Interestingly, when mutations occur in other proteins than dystrophin, they also can lead to muscular dystrophies, as is the case for example with limb-girdle muscular dystrophies or congenital muscular dystrophies ([Roberds et al., 1994](#); [Noguchi et al., 1995](#); [Bonnemann et al., 1995](#)).

In the following point, I will describe the composition of this complex and its evolutionary conservation in the model I used during my thesis, the nematode *Caenorhabditis elegans*.

### B. Molecular composition of the DAPC in vertebrates' muscle: differences and commonalities with *C. elegans*

The dystrophin-associated protein complex (DAPC) is a group of different classes of proteins located at the sarcolemma level in the muscle cells. The DAPC provides a

structural bond that links the cytoskeleton to the extracellular matrix, making the myocyte more stable and resistant to contraction and relaxation cycles ([Ervasti, 2006](#)). Depending on their biochemical characteristics, the proteins that form the DAPC can be classified into 3 sub-complexes ([Figure 17](#)):

- **A cytoplasmic component:** consisting essentially of dystrophin, syntrophin and dystrobrevin. With a molecular weight of 427KDa, dystrophin is one of the largest proteins present in the costamere, and it acts as a bridge between the actin cytoskeleton and the dystroglycan sub-complex directly linked to the extracellular matrix (ECM). The other cytoplasmic proteins in DAPC are  $\alpha$ -dystrobrevin and syntrophins ( $\alpha 1$ ,  $\beta 1$  and  $\beta 2$ ) ([Roberts, 2001](#)).
- **Dystroglycan sub-complex:** this group consists of two proteins,  $\alpha$  and  $\beta$ -dystroglycan, both encoded by a single gene ([Ibraghimov-Beskrovnaya et al., 1992](#)). The  $\alpha$ -dystroglycan subunit is located outside the cell, interacting with ECM compounds, such as laminin. The  $\beta$ -dystroglycan subunit is responsible for keeping the subcomplex anchored to the membrane, as it contains a transmembrane fragment. In addition,  $\beta$ -dystroglycan connects to dystrophin through its cytoplasmic part, thus providing an additional anchorage point of the DAPC to the sarcolemma ([Ervasti and Campbell, 1993](#); [Huang et al., 2000](#)).
- **Sarcoglycan sub-complex:** there are several classes of sarcoglycans, we find principally  $\alpha$ ,  $\beta$ ,  $\gamma$  and  $\delta$ -sarcoglycan in the muscle, all being transmembrane proteins ([Holt and Campbell, 1998](#)). These proteins interact both with dystroglycans and with another DAPC component called sarcospan ([Crosbie et al., 1999](#); [Noguchi et al., 2000](#)).

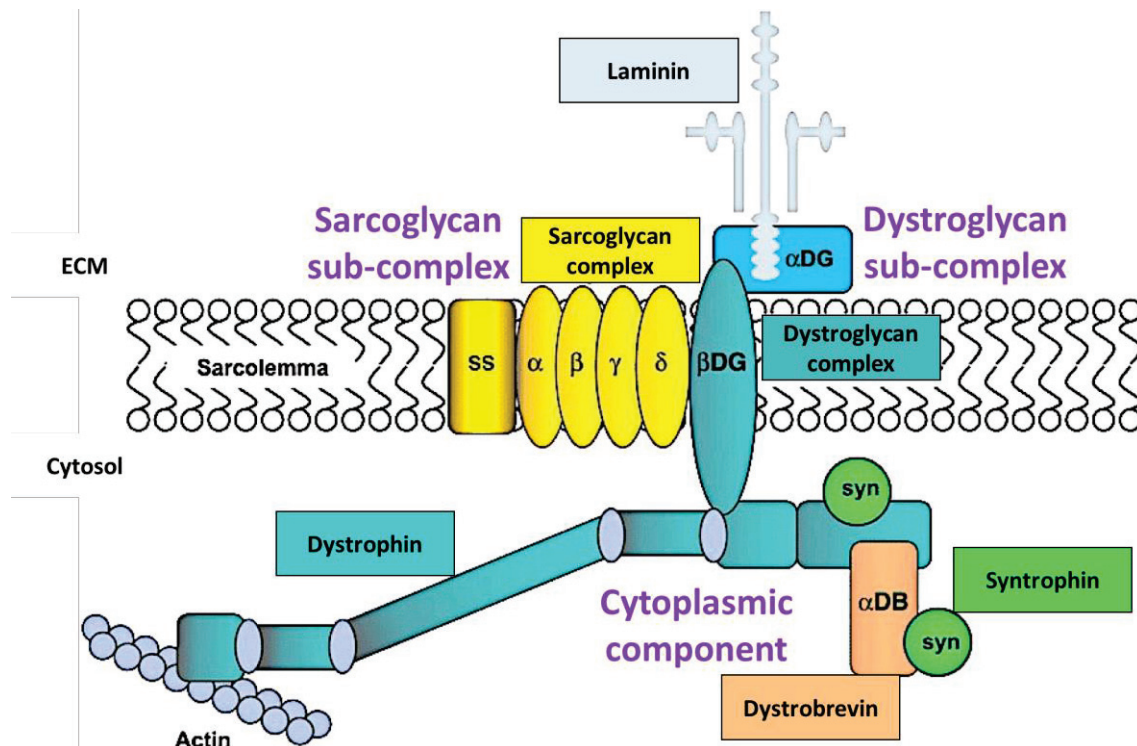


Figure 17 Dystrophin-Associated Protein Complex (DAPC) in skeletal muscle.

Adapted from [Blake et al., 2002](#).

During my thesis, I became interested in the study of this proteins complex in the invertebrate model *Caenorhabditis elegans*. Interestingly, the DAPC has shown great conservation along the evolution, so that we find most of its components identified in vertebrates already existing in the nematode.

In *C. elegans*, the homologous gene of dystrophin is *dys-1*, which was first identified and described in 1998 in the laboratory of Laurent Ségalat. Although the *dys-1* gene contains 47 exons, unlike the 79 found in humans, the encoded protein is about the same length, 3674 amino acids in the worm, compared to 3685 aa in human dystrophin ([Bessou et al., 1998](#)); suggesting that both proteins may have the same structural function. Moreover, in addition to the similarity in length, most of the functional domains identified in human dystrophin are again present in *DYS-1*. The structure, function and conservation of *DYS-1* domains are detailed in [section II](#) of this chapter.

Likewise, in worms, the two cytoplasmic proteins associated to dystrophin, dystrobrevin and syntrophin are present in the genome showing a strong evolutionary conservation. *C. elegans* also contains a subfamily of dystroglycans and sarcoglycans ([Johnson et al., 2006](#)). Finally, mutations in the different proteins that compose the DAPC of the nematode, give rise to consistent and similar phenotypes between the different genes (for

more details, see [chapter 3, point II](#)), suggesting a common function as a complex, just as occurs in vertebrates. Nevertheless, because worms have striated muscle whose characteristics differ substantially from skeletal muscle in vertebrates, *dys-1* mutants do not show phenotypes directly comparable to those observed in DMD patients. The advantage of this model, however, resides in the ability to study a highly conserved protein complex at the molecular and cellular level, being able to analyze both biochemical interactions and genetic interdependences on a large scale comparing multiple strains.

## II. Dystrophin as a structural linker in muscle

### A. Evidence in vertebrates

Since the discovery of the dystrophin gene, multiple genetic and biochemical studies have been performed in order to elucidate the biological functions of this protein. Although the most sustained hypotheses are the structural role of dystrophin in the sarcolemma, the exact pathophysiological mechanism of dystrophin in degenerative Duchenne disease remains unclear.

#### *Expression of DMD gene*

The expression of the full length of dystrophin is controlled by three initial promoters ([Figure 18 A](#)): (1) a "B" promoter that leads the expression to the brain ([Boyce et al., 1991](#)), a second "M" promoter, whose expression is muscular ([Klamut et al., 1990](#)) and a third "P" promoter, for the Purkinje cells ([Górecki et al., 1992](#)). In muscle tissue, the highest level of dystrophin is found in the striated muscle, both cardiac and skeletal.

Additionally, there are other internal promoters that control the expression of the dystrophin gene (R: retina, B3: brain, S: Schwann cells and G: general), in this case, giving rise to shorter proteins on the N-terminus side but still retaining their C-terminus end, even if they lose part of the WW domain ([Figure 18 B](#)). The precise role of these isoforms is not yet well known.

#### *Protein structure, subcellular localization and functions of DMD*

Dystrophin is a large protein in which five main domains can be distinguished ([Figure 18 B](#)):

- **N-terminus domain:** containing a sequence with a strong homology to the structural proteins spectrin and actinin; it is assumed that dystrophin belongs to the family of the  $\beta$ -spectrin/ $\alpha$ -actinin proteins. The most important aspect of this region is the presence of two calponin homology domains (CH), which are responsible for the interaction of dystrophin with actin ([Hemmings et al., 1992](#); [Rybakova et al., 1996](#)). It is important to note that the  $\gamma$ -actin to which dystrophin binds is different from the  $\alpha$ -actin involved in the formation of the sarcomere ([Rybakova et al., 2000](#)).
- **Central rod domain:** composed of 24 spectrin repeats, this domain is assumed to be responsible for conferring the characteristic flexibility to dystrophin ([Koenig and Kunkel, 1990](#)). Each unit of these spectrine repeats is

analogous to the triple helical repeats found in the spectrine. In addition to the helical structures, four hinge regions (H1-4) are present in a "dispersed" way as shown in [figure 18 B](#).

- **WW domain:** this protein binding module was recently described as recognizing proline rich regions; hence it is the part of dystrophin responsible for its binding to the dystroglycan complex. WW domain specifically recognizes the PPxY sequence at the cytoplasmic C-terminus end of  $\beta$ -dystroglycan ([Zarrinpar et al., 2003](#)).
- **Cystein-rich domain:** contains 2 EF-hand motifs that have been shown to bind intracellular calcium ([Koenig et al., 1988](#)). Also, it contains a ZZ-domain which, thanks to cysteine repeats, is predicted to bind zinc anions ( $Zn^{2+}$ ), creating a region that resembles the zinc fingers existing in other proteins. The ZZ-domain also interacts with calmodulin in a  $Ca^{2+}$  dependent manner ([Rentschler et al., 1999](#)).
- **C-terminus domain:** it contains a sequence unique to dystrophin and its associated proteins. It is characterized by comprising two  $\alpha$ -helical regions called coiled-coil (CC) domains, which are similar to the helical regions found in the spectrin repeats region. The CCs are typical protein-protein interaction domains, by which dystrophin is able to bind to dystrobrevin or syntrophin.

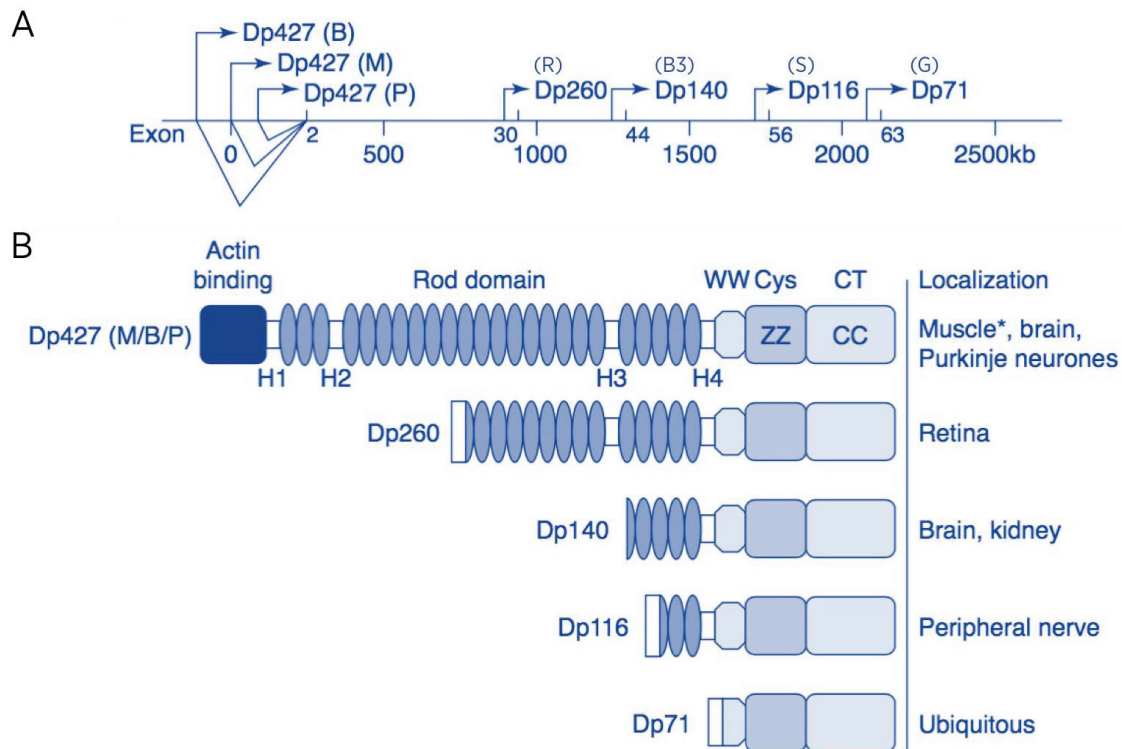


Figure 18 Dystrophin gene and protein structure.

A: Representation of the dystrophin gene localizing the promoters that give seven different protein isoforms. B: Structure of dystrophin representing the main functional domains in tissue-specific isoforms. A and B are adapted from [Blake \*et al.\*, 2002](#).

Dystrophin is localized in the sarcolemma of the muscle fibers in a non-homogenous way, it is enriched in various regions such as the costamere, the myotendinous junctions or contact area between two muscle cells, as well as in the neuromuscular junctions (reviewed in [Davies and Nowak., 2006](#)). The function of dystrophin in the intracellular periphery of the sarcolemma is thought to be providing protection against the stress of the muscle contraction/relaxation cycles by giving “*cushioning*” to the membrane. This would be partly thanks to the flexibility of the protein given by its central region with the spectrin repeats ([Petrof \*et al.\*, 1993](#); [Grum \*et al.\*, 1999](#)). In summary, dystrophin is part of a protein complex where it plays an essential role in the maintenance and stability of multiple associated proteins, whose absence destabilizes the entire DAPC and alters the location of associated proteins ([Ervasti \*et al.\*, 1990](#)) ([Yoshida \*et al.\*, 2000](#)).



## B. DMD diseases

Dystrophinopathies are muscular diseases caused by mutations in the dystrophin gene and can occur in two forms: a severe form called Duchenne Muscular Dystrophy (DMD), and a less severe form called Becker Muscular Dystrophy (BMD) ([Hoffman et al., 1987](#)). Duchenne muscular dystrophy owes its name to the researcher and physician Guillaume Duchenne who, in 1861, completed the characterization of this myopathy. DMD is primarily seen in boys and is estimated to affect an average of 1 in 3500 birth males ([Emery, 1991](#)). This higher proportion in boys is due to the location of the dystrophin gene on the X chromosome and the transmission is carried out in a recessive manner. Then, DMD, unlike BMD, is due to mutations that change the reading frame in the dystrophin gene, resulting in early stops that lead to a total or partial absence of the protein in muscle and other tissues, such as the brain.

Dystrophin's pattern of expression, found mainly in muscle and nerve tissue, explains the symptoms of Duchenne disease. The first indications are muscular, mostly affecting the lower limbs at first, resulting in problems in locomotion. Usually, a delay in learning to walk is observed, and often when the boys start to walk they have difficulties in getting up and cannot even run due to muscle weakness. Other manifestations, not less important, are cognitive complications. Above all, these are difficulties in abstraction and reasoning, and there may even be cases of pseudo-autism.

The complexity of DMD comes at the end, when the respiratory and cardiac muscles begin to weaken. Thus, by the age of 20-30, deaths occur from respiratory or cardiac failure ([Khirani et al., 2014](#)).

In the other hand, the most attenuated form of dystrophinopathy, so-called Becker Muscular Dystrophy, arises when mutations that preserve the reading frame in the dystrophin gene occur. The appearance of clinical manifestations in this case is later and less acute, so that usually motor symptoms start to be observed around the age of 12-14 years and become more aggravated after 40 years. As for the nature of the symptoms, they are similar to those seen previously in DMD, but in this case, they are less severe since there is a truncated and partially functional protein ([Hoffman et al., 1988](#)).

## C. Dystrophin/*dys-1* in *C. elegans*: consequences of different mutations

### *Dystrophin gene in C. elegans (dys-1)*

The gene coding for dystrophin in *C. elegans* is *dys-1*, which was identified more than twenty years ago, in the laboratory of Laurent Ségalat and Kathrin Gieseler ([Bessou et al., 1998](#)). *dys-1* is located on chromosome I, covers 31 kb of genomic sequence and consists of 47 exons ([Wormbase](#)), although only 46 were initially described when first characterizing the gene. Using a GFP-reporter expressed under the control of the *dys-1* gene promoter, it was shown that the dystrophin in the worm is expressed in muscle tissue, either in the body wall muscle (1) or in other muscles such as the vulva (2) or the pharynx muscles (3), as shown in [figure 19 B](#). Thanks to advances in genetic engineering, it is now relatively easy to obtain a *knock-in* line. Thus, we took advantage of the simplicity of the model and the rapidity of the genomic modifications by CRISPR/Cas9 to perform a transcriptional *knock-in* (*dys-1::sl2::wrmScarlet*) to visualize the expression of dystrophin under physiological conditions (data not published). Our results confirm the expression of dystrophin in the muscle tissue as described in 1998 by Bessou *et al.*, in addition to the exclusion of neurons in the nematode ([Figure 19 C](#)). No other dystrophin-like genes have been described in the worm, as counterparts to the vertebrate utrophin or DRP2 ([Grisoni et al., 2002a](#)).

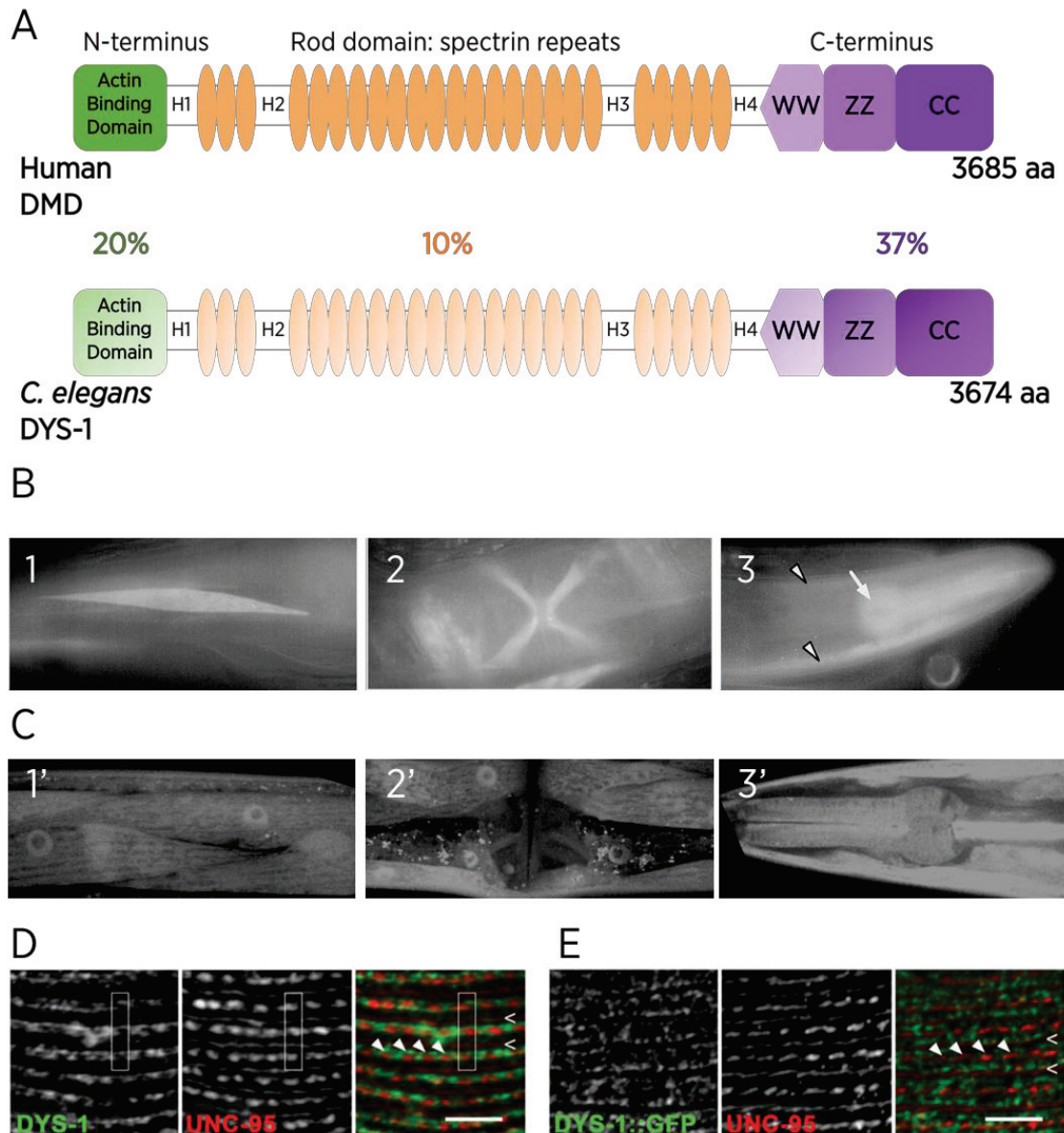


Figure 19 Dystrophin/dys-1 in *C. elegans* is highly conserved and is expressed in muscle tissues.

A: DYS-1 shows a high conservation in the functional domains compared to human dystrophin. B: Transgenic animals carrying *dys-1* GFP gene reporter show expression in body wall muscle (1), vulva (2) and pharynx (3) muscles. Adapted from [Bessou et al., 1998](#). C: CRISPR/Cas9 transcriptional fusion of wrmScarlet to *dys-1* shows the expression pattern of dystrophin in body wall muscle (1'), weak signal in vulva muscles (2') and pharynx muscles (3'). Our unpublished data. D and E: Immunostaining revealing the subcellular localization of DYS-1 using antibodies against DYS-1 (D) or against GFP (E) fused to *dys-1*. Adapted from [Brouilly et al., 2015](#).

### *Dystrophin protein in C. elegans (DYS-1)*

The DYS-1 protein presents a high homology in its different functional domains, especially in the C-terminus part, compared to human DMD ([Figure 19 A](#)). A structural

analysis of the longer DYS-1 isoform showed the presence of the following domains ([Bessou et al., 1998](#); [Gieseler et al., 1999a](#)):

- **N-terminus region** (1-234): is also an  $\alpha$ -actinin type sequence, as occurs in vertebrates. It is estimated that the percentage of homology of this region is about 20%.
- **Central domain** (235-3032): as in human DMD, DYS-1 also presents a flexible central domain composed of spectrin repeats. The homology in this region is lower, about 10%.
- **WW-domain** (3047-3081) and **cysteine rich domain** (3082-3353).
- **C-terminus end** (3354-3674): this region, responsible for the binding of dystrophin to other DAPC proteins, has the highest homology respect to the human one, about 37%. The interactions between DYS-1 and other DAPC proteins will be discussed in further sections of this chapter.

DYS-1 has a length of 3674 amino acids, compared to the 3685 amino acids of human DMD, which suggests a conservation in the structural function of both proteins. It was shown that the dystrophin in *C. elegans* is located in the I-bands of the body wall muscle, co-localizing with the actin filaments and the dense bodies, being excluded from the A-bands ([Figure 19 D and E](#)) ([Brouilly et al., 2015](#)). As shown in [figure 19 D and E](#), depending on whether an antibody against DYS-1 or GFP is used, the localization patterns are slightly different and may result in inaccurate conclusions. The experiments performed at that period, under the technological limitations of both genetic engineering and confocal microscopy, could be rebuilt today with improved resolution. For this reason, we decided to build a *knock-in C. elegans* strain by fusing a fluorescent protein in the *dys-1* genomic sequence by CRISPR/Cas9. The results of this experiment are detailed in the results chapter, [part I](#) (article in preparation).

#### Mutations in *dys-1* and associated phenotypes

Various alleles with different mutations in the *dys-1* gene exist, but only *dys-1(cx18)* has been widely used for the characterization of dystrophin in *C. elegans*. As a result of an EMS (ethyl methane sulfonate) induced chemical mutagenesis, *dys-1(cx18)* and *dys-1(cx26)* were isolated. *cx18* shows a substitution mutation (g in a) that generates a premature stop codon in exon 33 (amino acid 2721), and in *cx26* a stop codon also occurs but this time in exon 39. By a different approach (UV) *cx35* and *cx40* were also isolated ([Figure 20 A](#)). Most of the phenotypes described in these alleles belong to a study conducted by Bessou et al. in 1998. Mutant strains of *dys-1* are characterized as

hyperactive and hyper-contracted, as well as hypersensitive to aldicarb, which is an inhibitor of the enzyme acetylcholinesterase.

Hyperactivity was defined by a locomotion test in which the number of body bends performed by the animal when moving on a solid medium was counted. The results show a significant increase in body bends/minute in *dys-1* mutant animals compared to the wild-type (N2 strain). Beyond that, worms tend to contract their bodies when moving backwards. Intriguingly, these mutants exhibit a typical and unusual characteristic which is to twist their heads very tightly to one side or the other when they move forward. This phenomenon of exaggerated head movement was called "overbent" or "head-bending" phenotype ([Figure 20 B](#)).

A typical hallmark of Duchenne disease is the muscle degeneration that is observed in patients. Concerning this feature in worms with dystrophin mutations, no degeneration of the body wall muscle is observed (very occasionally one or two affected cells are detected). This was determined using a specific muscle marker (*unc-54::gfp*), with which no difference in the arrangement of sarcomere myofilaments was observed between *dys-1* mutants and wild-type animals ([Figure 20 C](#)).

The non-presence of degeneration in muscle tissue when dystrophin is mutated is not limited to *C. elegans*, but it is also the case in the murine model of DMD (*mdx* mice). In a study conducted by Megeney *et al.* in 1996, a mutation in MyoD, a factor required for muscle development and differentiation, was inserted in the context of *mdx* mice, resulting in more deteriorated and impaired muscle increasing the severity of the myopathy, coming closer to what is observed in Duchenne disease ([Megeney \*et al.\*, 1996](#)). Based on these findings, Kathrin Gieseler's team generated a new model of DMD by combining *dys-1* mutants with *hll-1* mutants. For *hll-1*, which is the homologous gene of MyoD, a thermosensitive allele (*cc561*) was used as it is more permissive, since the null *hll-1* mutant is lethal. The double mutant *dys-1(cx18);hll-1(cc561)* shows an aggravation in the phenotypes previously observed in the single mutant *dys-1(cx18)*, showing an increased and progressive muscle degeneration, deteriorating over time ([Figure 20 D](#)) ([Gieseler \*et al.\*, 2000](#)).



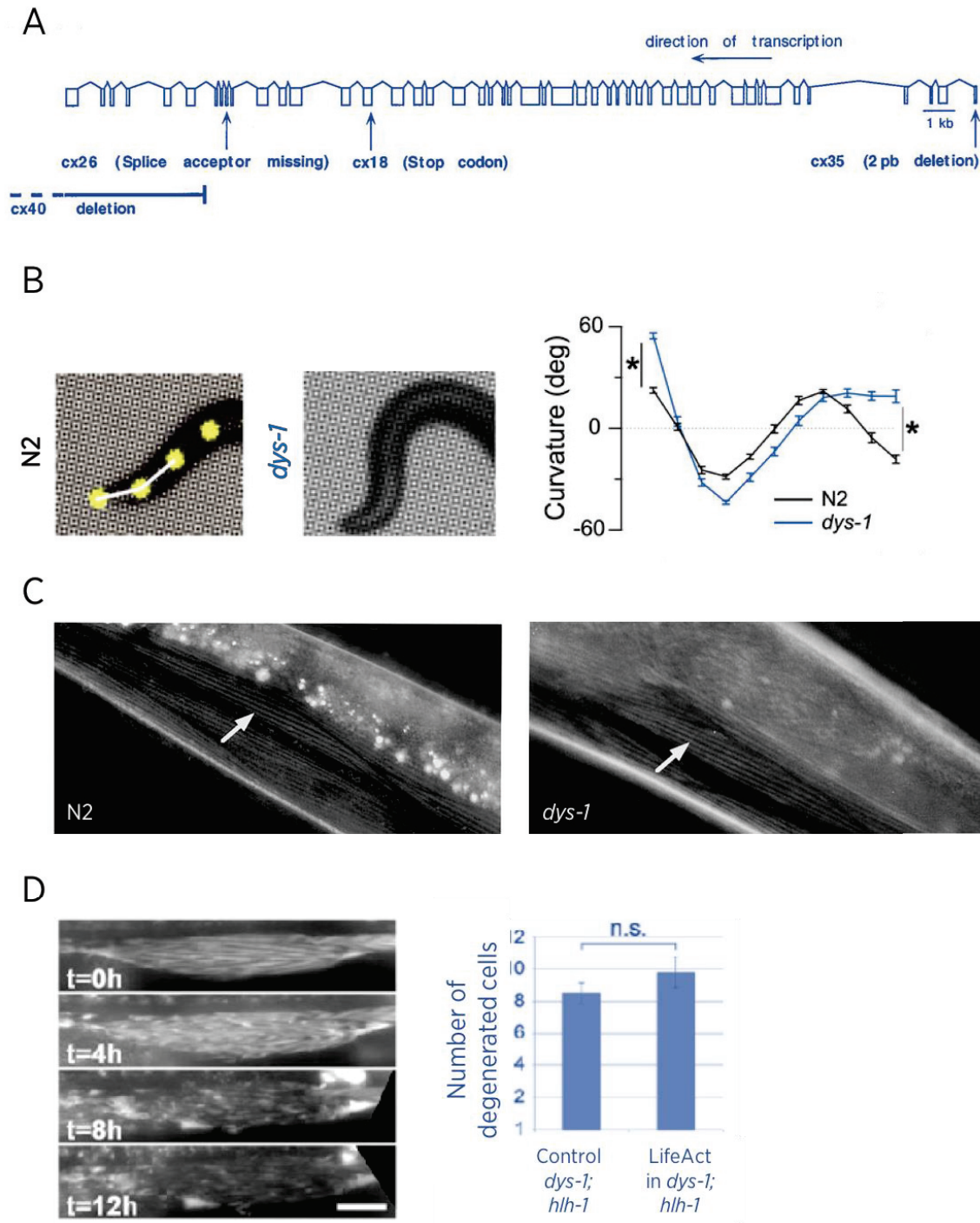


Figure 20 *dys-1* mutants in *C. elegans* present a "head-bending" phenotype but not muscular degeneration, unless combined with *hlh-1* mutants.

A: Dystrophin gene structure showing the location of the existent alleles. Adapted from [Bessou et al., 1998](#).  
 B: *dys-1* mutants exhibit an exaggerated head-bending curvature when moving forward. Adapted from [Kim et al., 2009](#).  
 C: Polarized light do not show any difference in muscle striations in *dys-1(cx18)* mutants compared to wild-type. Adapted from [Bessou et al., 1998](#).  
 D: Actin staining (mCherry) show progressive degeneration over time in double *dys-1(cx18);hlh-1(cc561)* mutants. Adapted from [Brouilly et al., 2015](#).

### III. Dystroglycan in vertebrates

#### A. Biosynthesis and functions

The dystroglycan (DG) sub-complex is a central component of the muscular DAPC with a predominant structural role: connecting the components of the cytoskeleton to the extracellular matrix. Dystroglycan is encoded by a single gene of 2 exons, which gives rise to a precursor protein ([Figure 21 A](#)). The expression of this gene is ubiquitous ([Montanaro \*et al.\*, 1995](#)) ([Durbiej \*et al.\*, 1998](#)). Following its synthesis, the precursor protein derived from a single mRNA, undergoes several post-translational modifications, including the cleavage process (Ser654), targeting to separate the precursor protein into two subunits:  $\alpha$ - and  $\beta$ -dystroglycan ([Ibraghimov-Beskrovnaya \*et al.\*, 1992](#)).

The  $\alpha$ -dystroglycan subunit is a 156KDa highly glycosylated peripheral extracellular protein. Along with  $\beta$ -dystroglycan, it was isolated from muscle as part of DAPC ([Ervasti \*et al.\*, 1990](#)).  $\alpha$ -dystroglycan consists of an N-terminus domain (1-312 aa), a mucin-like domain with numerous O-glycosylation sites (313-385 aa), and a C-terminus domain (386-653 aa) ([Figure 21 A](#)). Both the N-terminus and C-terminus ends have N-glycosylation sites ([Brancaccio \*et al.\*, 1997](#); [Nilsson \*et al.\*, 2010](#); reviewed in [Yoshida-Moriguchi and Campbell, 2015](#)). Finally, we find  $\alpha$ -dystroglycan associated, on the one hand, with components of the extracellular matrix, such as laminin and agrin (by binding to globular G-domains on the C-ter of these), and on the other hand, with the  $\beta$ -dystroglycan subunit ([Gee \*et al.\*, 1993](#); [Montanaro \*et al.\*, 1999](#)).

The other subunit, much smaller (43KDa), is  $\beta$ -dystroglycan. It contains a single transmembrane segment (aa 751-774, in the precursor), representing an anchorage site of the DG and DAPC to the plasma membrane. In addition to its interaction with the  $\alpha$  subunit, the cytoplasmic -COOH part of the  $\beta$ -DG is associated with the cystein-rich region of the dystrophin.

#### B. Interaction with DAPC

Dystroglycan  $\beta$  subunit binds to dystrophin. The part of the dystroglycan that participates in this interaction is highly conserved that is situated at the C-terminus end (last 15 aa). This region is also rich in proline, being the PPPY motif the specific sequence that links to the WW domain of the DMD ([Figure 21 B](#)) ([Rentschler \*et al.\*, 1999](#); [Hnia \*et al.\*, 2007](#)).



Furthermore, it was shown that an additional interaction with the EF-hands domains of DMD is also needed ([Ishikawa-Sakurai et al., 2004](#)). Thus, both the WW and the EF-hands are required to form a recognition surface in the dystroglycan PPPY sequence to its interaction with dystrophin.

Interestingly, it was shown for the first time in 1999 that dystrobrevin, a cytoplasmic protein of DAPC associated directly to dystrophin, also interacts with  $\beta$ -dystroglycan, even if it lacks the WW-like domain but contains the EF-hand domain ([Chung and Campanelli, 1999](#)). Also, in several biochemical co-immunoprecipitation studies, dystroglycan and sarcoglycan sub-complexes were also reported to interact with each other ([Yoshida et al., 2000](#)).

Finally,  $\beta$ -dystroglycan binds to caveolin-3 (Cav-3). Cav-3 also contains a WW-domain through which it binds to the PPPY sequence of the  $\beta$ -dystroglycan, thus competing with dystrophin, since both proteins bind to the same dystroglycan site ([Sotgia et al., 2000](#)).

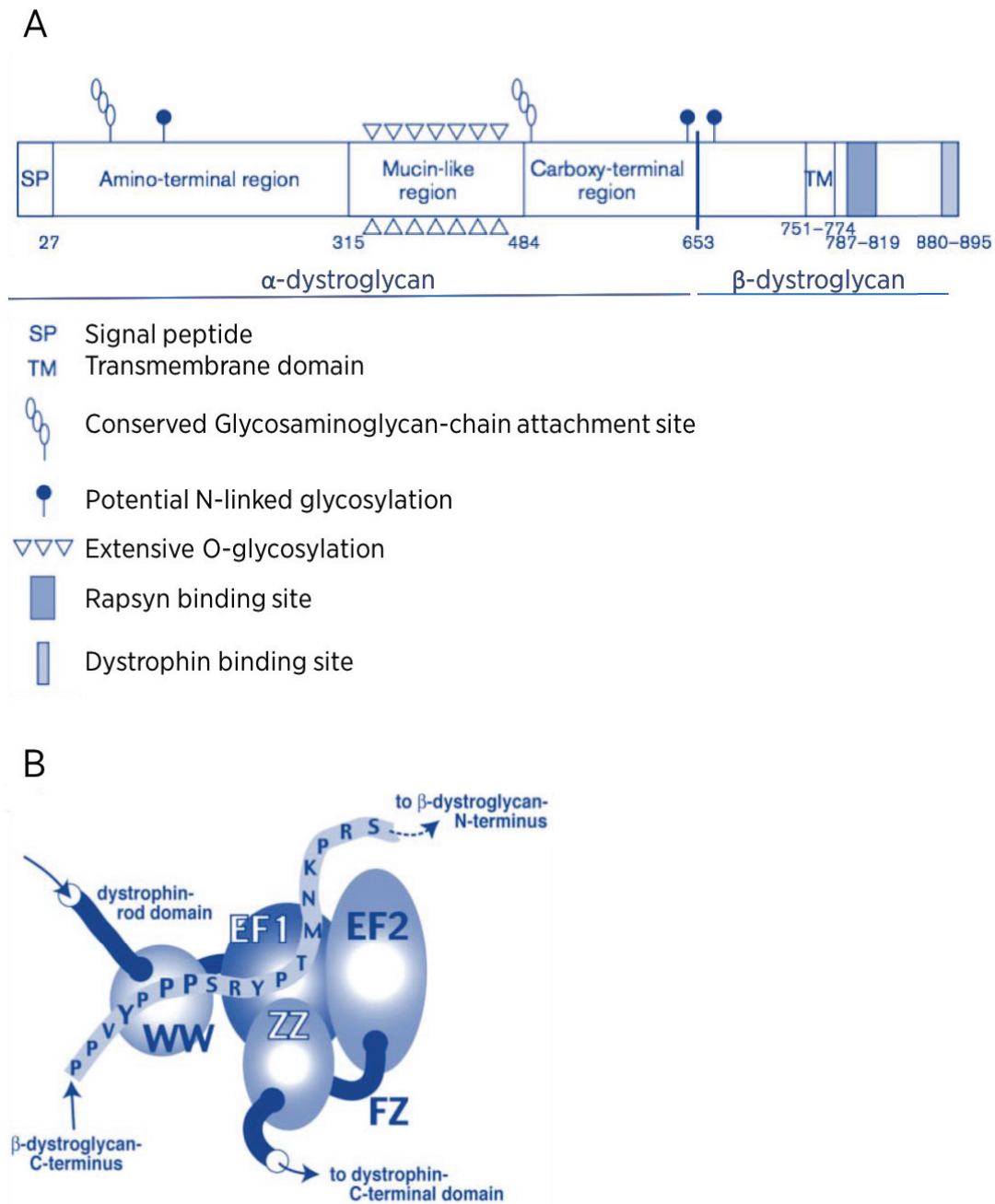


Figure 21 A single precursor give rise to  $\alpha$  and  $\beta$ -dystroglycan.

A: Precursor of  $\alpha$  and  $\beta$ -dystroglycan proteins structure. B: Schema of the  $\beta$ -dystroglycan C-terminus sequence interaction with C-terminus domains (WW and EF) of dystrophin. A and B are adapted from [Ishikawa-Sakurai \*et al.\* 2004.](#)

### C. Interaction with ECM

The  $\alpha$  subunit of the dystroglycan subcomplex is characterized by binding to different non-collagenous proteins of the extracellular matrix, including laminin, agrin and perlecan, among others.

In the literature, one of the most studied interactions of dystroglycan with ECM is the one between  $\alpha$ -DG and laminin. Laminin is probably the most abundant protein present in the extracellular matrix at the basal lamina level. It has been shown in 1993 that the  $\alpha$ -DG subunit interacts with globular G-domains located at the C-terminus end of laminin. This same interaction was also shown to exist between  $\alpha$ -DG and the ECM agrin protein ([Gee et al., 1993](#); [Bowe et al., 1994](#); [Rentschler et al., 1999](#)). Finally, a strong interaction between the  $\alpha$ -DG subunit and fragment V of perlecan was also reported, with a higher affinity than that observed for laminin ([Talts et al., 1999](#)).

A crucial aspect to keep in mind is that, for this interaction to occur properly, the  $\alpha$ -DG subunit needs to be properly glycosylated, where the O-mannose-glycosylation that takes place during the post-translational modifications of dystroglycan is especially important. Then, when a mutation occurs in the enzymes required for O-linked glycosylation of DG, a pathology called  $\alpha$ -dystroglycanopathy occurs, which represents a new category of myopathies with a generic feature and synthetic manifestations ([Xu et al., 2015](#)).

## IV. Everything we know about DG in worms

### A. Dystroglycan structure and conservation in *C. elegans*

DGN-1 is the homologous of the dystroglycan in the nematode *C. elegans*. It was first identified by Grisoni *et al.* in 2002, through a sequence alignment analysis ([Figure 22 A](#)), where in addition to DGN-1, other conserved components of DAPC were revealed. In this study, it was assumed that only one homologue exists, however, few years later, DGN-2 and DGN-3 were identified, whose sequences are much less conserved ([Grisoni \*et al.\*, 2002a](#)).

It was only in 2006 that a first complete characterization of *C. elegans* dystroglycan was performed by Johnson *et al.* The DGN-1 protein has a well-preserved N-terminus region, which also contains an immunoglobulin domain, as in vertebrates. Continuously, it contains a short mucin-like region and several glycosylation sites ([Figure 22 B](#)). The most conserved region in evolution, however, is the C-terminus part, as described in the paper of Grisoni *et al.* in 2002a.

Nevertheless, despite the fact that the C-ter region presents more than 30% of homology with vertebrate sequences, the PPPY motif necessary for the binding of dystroglycan to dystrophin, is not found in *C. elegans* ([Figure 22 C](#)) ([Johnson \*et al.\*, 2006](#)).

Interestingly, unlike humans, where the dystroglycan is derived from a single precursor that gives rise to two subunits, in the worm the dystroglycan does not cleave, but it does glycosylate.



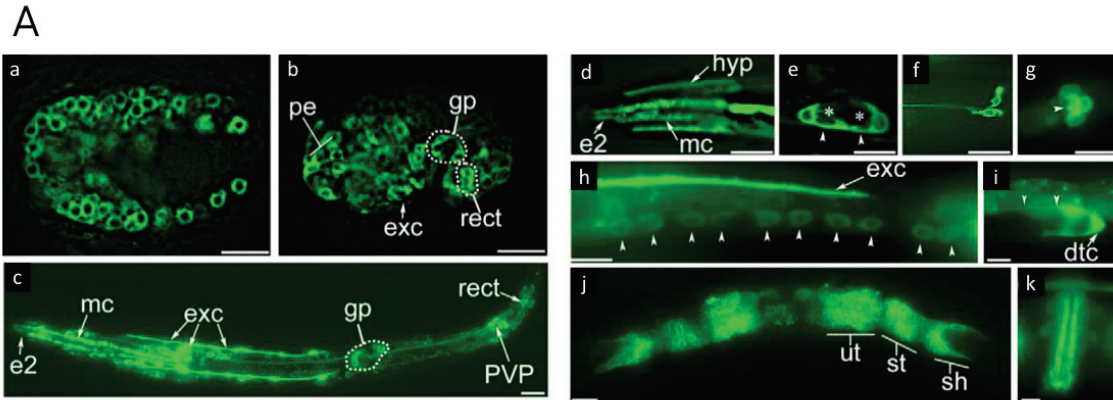
## B. Dystroglycan expression in worm muscle

To determine which tissue express *dgn-1* in *C. elegans*, a transgene was constructed containing, on the one hand, 2680bp of genomic DNA upstream the first exon, reaching the second exon on the 3' side. On the other hand, an artificial transmembrane domain and, finally, a GFP-coding sequence. Thanks to this GFP-reporter, the expression of *dgn-1* was observed mainly in epithelial and neural tissue, but not in muscle ([Figure 23 A](#)). This experience was repeated, with different promoters, and it was shown that the expression was identical, confirming that *dgn-1* is not expressed in the muscle ([Johnson et al., 2006](#)).

This result was surprising, since, on one hand, it is inconsistent with the expression and function of the dystroglycan in the vertebrate muscle, and on the other hand, because of a transcriptome analytical study conducted many years later by Cao *et al.*, in which it was reported a high expression of *dgn-1* in the body wall muscle of *C. elegans* ([Figure 23 B](#)) ([Cao et al., 2017](#)).

Consequently, taking advantage of the genomic modification rapidity with the CRISPR/Cas9 system, we were able to construct a *knock-in* line of *dgn-1* fused to a fluorescent protein. Our results clearly show a great expression of *dgn-1* in the body wall muscle of *C. elegans*, whose subcellular location, interestingly, is similar to that observed for DYS-1 ([Figure 23 C](#)).





B

Tissue-level consensus expression profiles. (Values listed are transcripts per million)

Gene	Neurons	Gonad	Hypodermis	Pharynx	BWM	Glia	Intestine
<i>dgn-1</i>	160,148	128,459	27,370	52,657	180,676	170,179	46,607
<i>dgn-2</i>	0,000	0,000	0,000	0,000	0,092	0,000	0,000
<i>dgn-3</i>	0,000	0,000	0,172	0,000	0,000	0,000	0,000

C

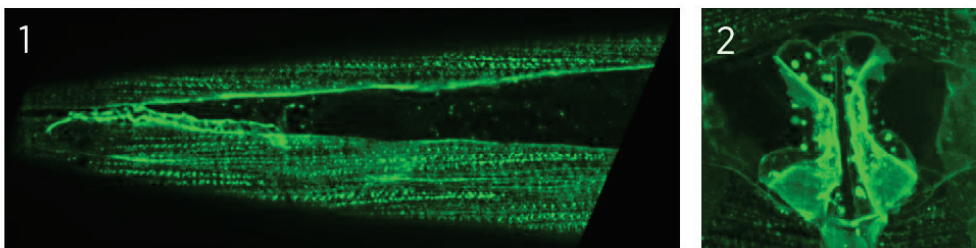


Figure 23 DGN-1 is expressed in body wall muscle of *C. elegans*, unlike previously reported.

A: GFP gene reporter showing the expression of *dgn-1* in embryos (a and b) and in L1 larvae stage (c). *dgn-1* is present in pharyngeal epithelium (d), gonad precursor cells (e), PVP neurons (f), rectal epithelium (g), ventral cord neurons (arrowheads in h). In L3 larvae stage *dgn-1* is present in gonad epithelium (i). In L4 animals *dgn-1* is found in gonad and uterus (j) as well as vulval epithelium (k). Scale: 10µm. Adapted from [Johnson et al., 2006](#). B: Table showing the expression level of the three dystroglycan genes (*dgn-1*, *dgn-2* and *dgn-3*) in different tissues in *C. elegans*. *dgn-1* is the most abundant and, so, considered the dystroglycan homolog in worms. Adapted from [Cao et al., 2017](#). C: CRISPR/Cas9 *dgn-1::mNeonGreen* knock-in showing the subcellular localization of DGN-1 in body wall muscle cells (1) and vulva muscles (2). Unpublished data.



### C. DGN-1 functions and mutations consequences

When the first dystroglycan-deficient worm (dsRNA) was generated, the animals appeared to be sterile, suggesting that DGN-1 may be involved in gametogenesis ([Grisoni et al., 2002a](#)). This was confirmed in further studies. However, Johnson *et al.* showed that this sterility was due to a malformation of the gonad. It is important to remember that dystroglycan is a membrane receptor that interacts with several components of the ECM. Therefore, a deficiency of DGN-1 leads to alterations in the basal lamina formation of the gonad during development, giving rise to a non-functional gonad with an aberrant morphology and, consequently, to sterile animals ([Johnson et al., 2006](#); [McClatchey et al., 2016](#)). Similarly, in a later study it was reported that DGN-1 and TEN-1, the homologous of teneurin, are involved in the formation and integrity of both the gonadal and pharyngeal basal lamina ([Trzebiatowska et al., 2008](#)).

Finally, when *dgn-1* mutants were first studied, they were suspected of having the head bending phenotype typically present in *dys-1* mutants (and other DAPC components). However, it was later found that these mutants don't show any head bending appearance. Also, *dgn-2* and *dgn-3* mutants do not have any visible phenotype.

## V. Sarcoglycans as organizers of the DAPC?

### A. Expression and localization

Sarcoglycan (SG) and sarcospan form a transmembrane sub-complex of DAPC in the skeletal muscle of vertebrates. Four subunits are needed to form a SG complex:  $\alpha$ ,  $\beta$ ,  $\gamma$  and  $\delta$ -sarcoglycan, that are highly expressed in skeletal muscle, but not exclusively. A fifth SG subunit exist, the  $\epsilon$ -sarcoglycan, which is present in different tissues. Sarcoglycans are glycosylated proteins, unlike sarcospan. Besides, each subunit within its sequence has a transmembrane domain that allows it to anchor to the sarcolemma, and a cystein-rich zone that is located in the extracellular part ([Figure 24 A](#)) ([Ozawa \*et al.\*, 2005](#)).

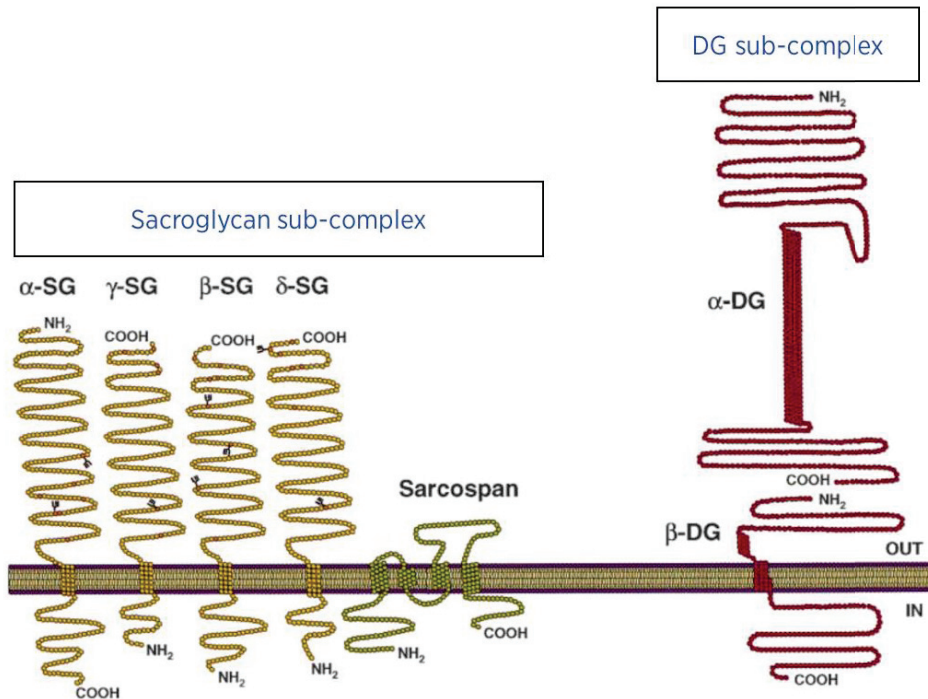
Additionally, a study based on the structural analysis of this sub-complex, showed that the  $\beta$ ,  $\gamma$  and  $\delta$  subunits have the N-terminus ends inside the cell, while the  $\alpha$  and  $\epsilon$  subunits have an extracellular N-terminus. It is now currently known that sarcoglycans are proteins that have a relatively long extracellular domain, with several N-glycosylation sites ([McNally \*et al.\*, 1996](#); [Chan \*et al.\*, 1998](#)). A very interesting fact that was put in evidence by [Ettinger \*et al.\*](#), is that, among all SG, the  $\alpha$  and  $\epsilon$  subunits have a high homology with each other, reaching 60% at the amino-acid level. Also, in another study conducted by K. Campbell's laboratory three years later, it was found that in smooth muscle, the  $\epsilon$ -sarcoglycan subunit replaces the  $\alpha$  subunit, which seems to be reasonable since they are two highly similar proteins ([Ettinger and Sanes, 1997](#); [Barresi \*et al.\*, 2000](#)). Similarly, the  $\delta$  and  $\gamma$  subunits are also close regarding the protein composition, sharing almost 70% of their amino acids ([Hack \*et al.\*, 2000](#)). Finally,  $\beta$ -SG has been shown to be the furthest in sequence of all sarcoglycans ([Lapidos \*et al.\*, 2004](#)).

### B. Regulation of surface expression

Both for the correct formation of the sarcoglycan sub-complex and for its trafficking to the plasma membrane of the muscle cell, several studies have shown that all its subunits need to be translated before assembly ([Holt \*et al.\*, 1998](#); [Noguchi \*et al.\*, 2000](#)). Once all four subunits are translated, the beginning of assembly ([Figure 24 B](#)) occurs in the endoplasmic reticulum (ER) where the  $\beta$  and  $\delta$  subunits are first associated. Both subunits are reported to be strongly linked together and form a core of the complex, with the  $\beta$

subunit being responsible for initiating the assembly. The core will then recruit the remaining sarcoglycans,  $\gamma$  and  $\alpha$ , respectively (Shi *et al.*, 2004).

A



B

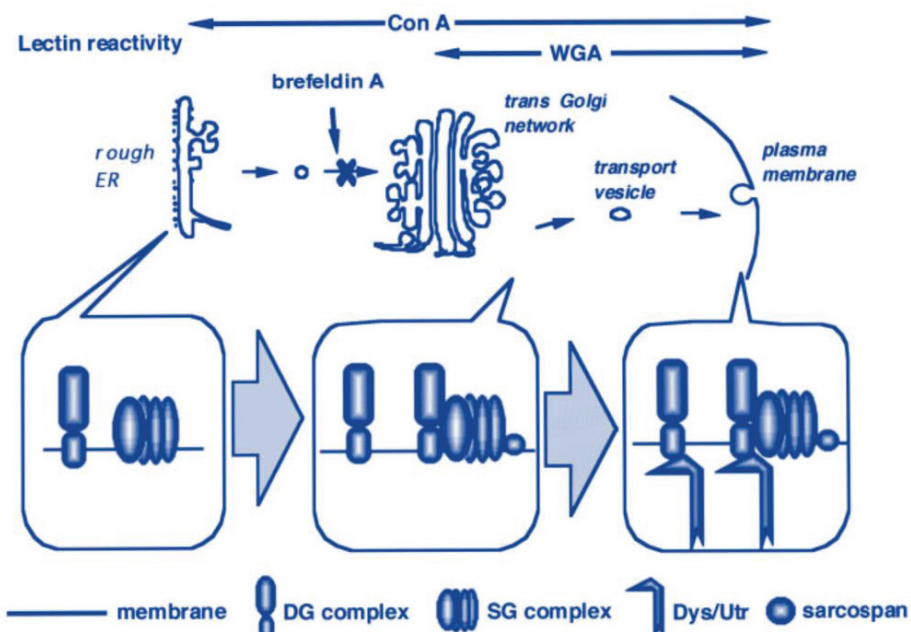


Figure 24 Four subunits compose the sarcoglycan sub-complex.

A: Schematic representation showing the disposition of the four sarcoglycan (SG) subunits ( $\alpha$ ,  $\beta$ ,  $\gamma$  and  $\delta$ ) in interaction with sarcospan forming the sarcoglycan-sarcospan subcomplex (left). Right: dystroglycan (DG) subcomplex disposition with the extracellular  $\alpha$  subunit binding to the transmembrane  $\beta$  subunit. Adapted from Crosbie *et al.*, 1999. B: During the formation of the sarcoglycan subcomplex, the

simultaneous co-synthesis of the four subunits is required. SGs interact with dystroglycans during their trafficking from Golgi to reach the cell membrane. Adapted from Noguchi *et al.*, 2000.

### C. Absence of SG

Mutations in Sarcoglycans are also known to lead to genetic muscle diseases. In this case, the myopathies that are generated are called limb girdle muscular dystrophies (LGMD), and are characterized by affecting more acutely the pelvic area and back muscles ([Hack \*et al.\*, 2000a](#)).

Interestingly, the  $\beta$  subunit seems to be the responsible for recruiting the rest of the subunits to form the sarcoglycan sub-complex. Therefore, one may contemplate that the loss of this subunit would lead to the destabilization of the whole complex. And indeed, Shi *et al.* demonstrated that when a defect occurs in the glycosylation process of the  $\beta$  subunit, the entire sarcoglycan subcomplex is disrupted. And not only so, but even when missense mutations in  $\beta$ -SG occur, the structure of the complex is lost, which highlights the indispensability of this subunit ([Shi \*et al.\*, 2004](#)).

Similarly, and since the  $\delta$  subunit also intervenes early in the formation of the sarcoglycan complex, as it, together with the  $\beta$  subunit, forms the core that initiates the assembly, it has been shown that the loss of  $\delta$ -SG also results in the complete absence of the complex. Mutations in the  $\gamma$  subunit only involves a simple reduction of the remaining subunits and not the total loss of the SG complex ([Hack \*et al.\*, 2000b](#)). Thus, in null mice for sarcoglycans, it was confirmed by immunohistochemical analysis that the SG complex has completely lost its components. These mice also show symptoms of muscular dystrophy ([Bonnemann \*et al.\*, 1996](#)). In parallel, it seems that the fact of simply removing the  $\alpha$  subunit also produces progressive muscular dystrophy in mice, characterized by weakness, necrosis and an increase in the permeability of the plasma membrane of the muscle fibers; as occurs in the type 2D of limb girdle muscular dystrophy (LGMD2D), which is the type of LGMD produced in humans by the absence of the  $\alpha$ -SG subunit ([Dulcos \*et al.\*, 1998](#)).

All these results indicate that the subunits of the sarcoglycan subcomplex are strongly interdependent, and that the absence of one of them leads to alterations at a greater level, resulting eventually in the total loss of the SG complex structure.

#### D. Interaction with extracellular and intracellular factors

The first characterized subunit of the sarcoglycan complex is  $\alpha$ -SG or *adhalin*, as it was originally called, which was cloned by Roberts *et al.* in 1993 from rabbit skeletal muscle tissue. This unit has a molecular weight of 50KDa and has been shown to possess a domain that has  $\text{Ca}^{2+}$  and  $\text{Mg}^{2+}$  dependent ATPase activity ([Roberds \*et al.\*, 1993](#); [Sandonà \*et al.\*, 2004](#)).

The sarcoglycan sub-complex is part of the DAPC. In this context, several studies have sought to study the possible interaction that could exist between sarcoglycans and different components of DAPC.

In 1998, Chan *et al.* suggested an interaction between the  $\delta$ -sarcoglycan subunit and the dystroglycan complex, which was tested in cultured mouse myotubes and was indeed found that the extracellular domain of  $\delta$ -SG binds to both  $\alpha$  and  $\beta$ -DG ([Chan \*et al.\*, 1998](#)). This interaction between the two complexes was corroborated by a later study, which additionally showed that the interaction occurs during the transport of the sarcoglycan sub-complex before it reaches the muscle cell membrane ([Noguchi \*et al.\*, 2000](#)). Also, since the dystroglycan complex show a significant reduction in western blot analysis when  $\alpha$ -sarcoglycan is absent, it was reported that sarcoglycan may have an additional role in stabilizing the interaction that takes place between both components ([Sakamoto \*et al.\*, 1997](#)).

Analogously, it has traditionally been assumed that the sarcoglycan complex does not interact directly with dystrophin, however, Vainzof *et al.* proposed that the  $\gamma$ -SG subunit could be associated with dystrophin, which was suggested following an observation of the immunofluorescent pattern of DMD in muscles of patients with sarcoglycanopathies, but it was not conclusive since it was observed in only two patients, and in one the decrease of fluorescence was not total ([Vainzof \*et al.\*, 1999](#)). Likewise, a more recent study based on co-immunoprecipitation analysis showed that the intracellular parts of both  $\beta$  and  $\delta$ -sarcoglycan are associated with dystrophin at its C-terminus end. In this assay, the short DMD isoform (*dp71*) was used, in which the entire N-terminus and central region are missing, preserving only the C-terminus interaction domains ([Chen \*et al.\*, 2006](#)).

Finally, there are indications to contemplate that sarcoglycans could also associate to dystrobrevin, another DAPC protein. This was demonstrated by a biochemical analysis

of a purified DAPC complex, where the N-terminus end of the  $\alpha$ -dystrobrevin has been found to be associated with the sarcoglycan sub-complex ([Yoshida \*et al.\*, 2000](#)).

## VI. All we know about SG in *C. elegans*

### A. Conservation, expression and localization in muscle

Protein and genomic sequence alignment analysis showed the existence of homologues for the sarcoglycan sub-complex subunits in *C. elegans* ([Figure 25 A](#)): SGCA-1 (H22K11.4) for  $\alpha$ -sarcoglycan, SGCB-1 (K01A2.1) for  $\beta$ -sarcoglycan and finally SGN-1 (F07H5.2), as a  $\delta/\gamma$ -sarcoglycan homologue ([Grisoni et al., 2002a](#)).

In the literature, few studies have tried to bring clarity to the SG complex in *C. elegans*. So, the only sarcoglycan whose expression pattern is known in worms is SGCA-1.

The first studies carried out to identify the tissues that express *sgca-1* and to explore its localization, on the one hand, were based on the construction of a transgene containing a fluorescent protein (GFP) fused in frame to the sequence of *sgca-1*, which was injected and integrated into the worm genome. On the other hand, anti-SGCA-1 antibodies were used as well. In both cases an extended expression was observed in the muscle tissue, specifically in the body wall muscle. SGCA-1, in addition, had a puncta pattern distribution that is excluded from the A lines but positioned along with the dense bodies ([Figure 25 B](#)). In addition, a recent study conducted by Oh *et al.* showed that the fluorescence associated to SGCA-1 is reduced in *dys-1(eg33)* mutants ([Figure 25 C](#)) ([Grisoni et al., 2002a](#); [Kim et al., 2009](#); [Oh et al., 2012](#)).



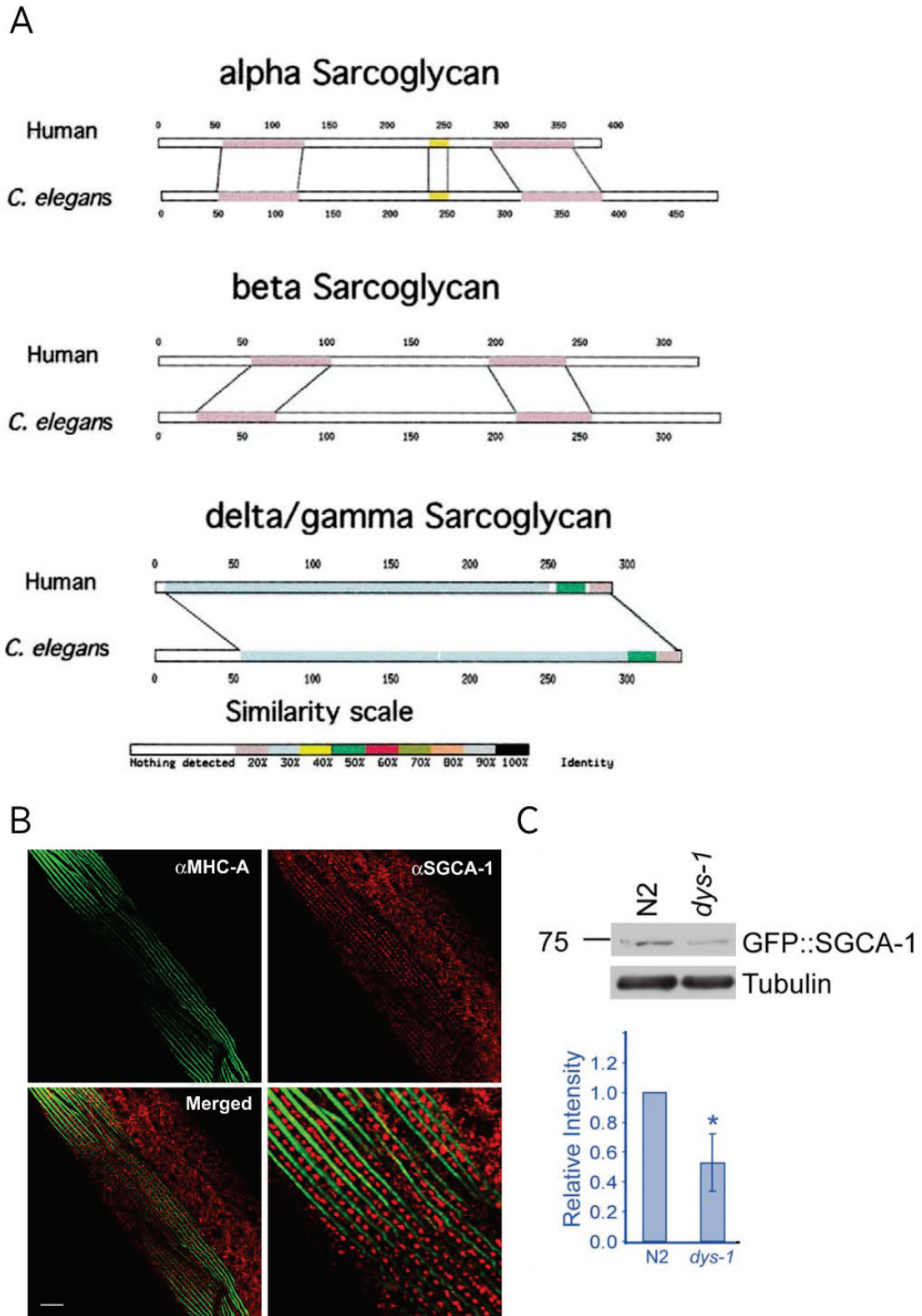


Figure 25 Sarcoglycans are conserved in *C. elegans* and found in muscle.

A: Protein structure of the three *C. elegans* sarcoglycans: SGCA-1/ $\alpha$ -sarcoglycan, SGCB-1/ $\beta$ -sarcoglycan and SGN-1/ $\gamma$ - $\delta$ -sarcoglycan showing a small conservation with human sarcoglycans when looking at the functional domains. Adapted from [Grisoni et al., 2002a](#). B: SGCA-1/ $\alpha$ -sarcoglycan immunostaining reveals the subcellular localization of *C. elegans* SG (red) in contrast with the Myosin Heavy Chain-A

(green). Adapted from [Kim et al., 2009](#) (sup. data). C: Western Blot analysis showing a decrease in SGCA-1 amount in *dys-1(eg33) lof* mutants compared to wild-type. *eg33* is a nonsense mutation at AA3287. Adapted from [Oh et al., 2012](#).

To date, no studies have published the expression pattern of SGCB-1 or SGN-1. Therefore, we construct CRISPR/Cas9 *knock-in* lines of fluorescent proteins fused to the three sarcoglycan genes of *C. elegans*: *sgca-1::wrmScarlet*, *sgcb-1::wrmScarlet* and *sgn-1::wrmScarlet*. The results of the first two show an asymmetric muscle expression in puncta pattern and are detailed in [part I](#) of the results chapter. For SGN-1, incomplete results are not included in this manuscript.

## B. Sarcoglycans mutants

When sarcoglycans were identified in *C. elegans*, a behavioral study was done in the absence of the SG subunits using dsRNA for each of the *sgca-1*, *sgcb-1* or *sgn-1* genes. Grisoni *et al.* reported that in all three cases the head-bending and hyperactivation typically observed in *dys-1* mutants were phenocopied ([Grisoni et al., 2002a](#)). Also, in the first study describing the expression pattern of SGCA-1, carried out by Kim *et al.*, it is also mentioned that the SGCA-1::GFP construction performed can rescue the phenotypes of the *sgca-1(tm1232)* mutant ([Kim et al., 2009](#)). Moreover, in a more recent study it is reported that another allele, also considered null, of *sgca-1(ok1529)* does not have any visible phenotype. Neither is the case for an allele of the subunit *sgn-1(ok2432)* ([Johnson and Kramer, 2012](#)). Plus, the *tm1232* allele has been analyzed in the laboratory and we have not been able to observe any locomotor defect or the head-bending phenotype. In order to continue exploring the phenotypes triggered by the absence of sarcoglycans, we have analyzed recently performed CRISPR/Cas9 *knock-out* lines, which are null molecular for *sgcb-1* (of which no mutant allele was available), and for *sgn-1*. The phenotype of head-bending is still weakly perceptible and unclear.

With regard to phenotypes related to muscle degeneration, unpublished data from K. Gieseler's team show that the combination of the mutants *sgca-1* and the thermosensitive *hll-1(cc561)* allele, which is a MyoD homologue, shows a marked degeneration of the body wall muscle of *C. elegans* (reviewed in [Gieseler et al., 2017](#)).

Finally, even if mutant alleles exist for sarcoglycans in *C. elegans*, the phenotypes associated with these mutations remain unclear in the literature.

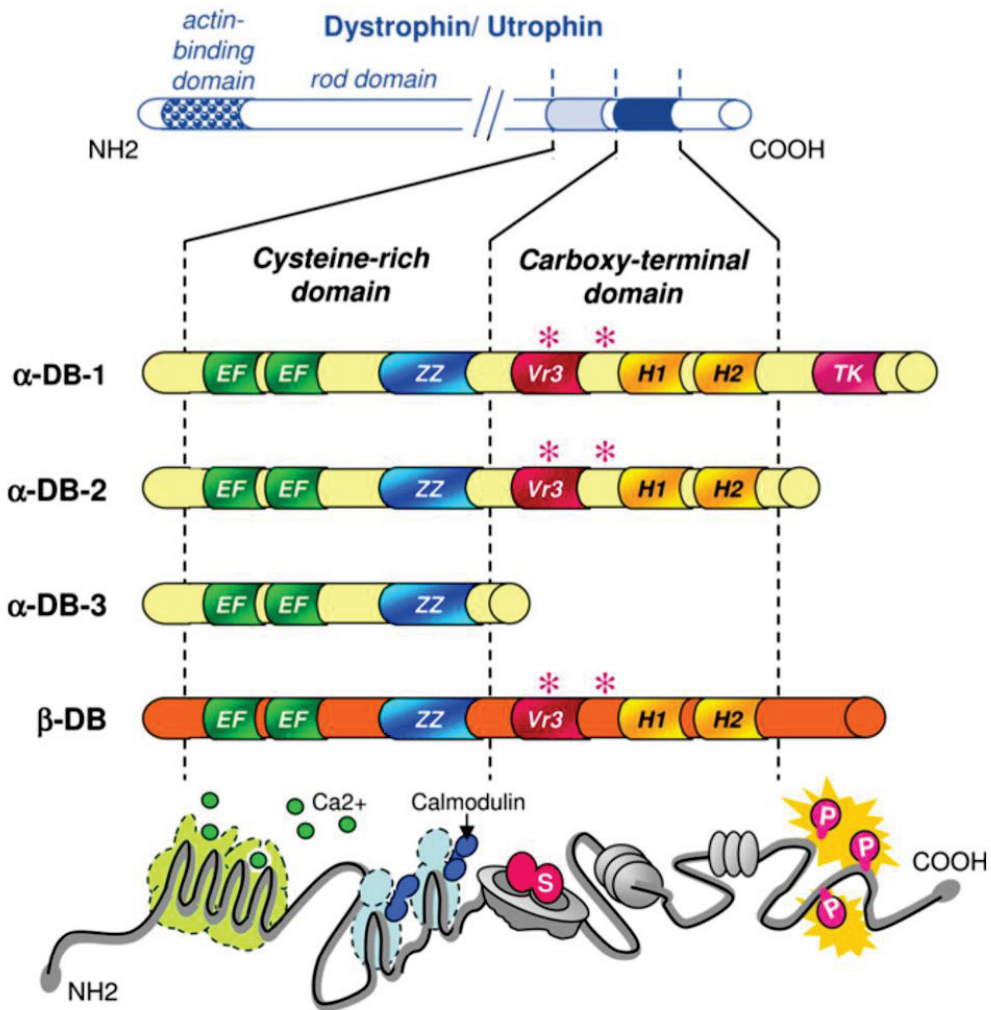
## VII. Syntrophin and dystrobrevin are associated to dystrophin in the DAPC

### A. Dystrobrevin structure and expression in muscle

Dystrobrevin (DB) is one of the cytoplasmic components of the dystrophin-associated protein complex. It has a molecular weight of 87KDa and was initially isolated from muscle tissue of *Torpedo californica* ([Carr et al., 1989](#)). Previous to knowing its affiliation to DAPC, this protein was mainly known by its association with acetylcholine receptors (AChR), since it was identified thanks to its coimmunoprecipitation with AChR ([Wagner et al., 1993](#)).

In vertebrates, dystrobrevin is the product of two independent genes, which give rise to two proteins:  $\alpha$  and  $\beta$ -dystrobrevin. Each dystrobrevin comprises multiple isoforms ([Figure 26 A](#)), and, despite their high homology, they show different expression patterns. In general,  $\alpha$ -dystrobrevin is expressed mostly in muscle tissue, both skeletal and cardiac, and in brain. While  $\beta$ -dystrobrevin shows a rather extensive, although not muscular, expression (brain, kidneys, etc.) ([Blake et al., 1996](#)). It has been shown that not all dystrobrevins are associated with dystrophin in DAPC, but only  $\alpha$ -1,  $\alpha$ -2 and  $\alpha$ -3 (and not  $\alpha$ -4 and  $\alpha$ -5).  $\alpha$ -dystrobrevin-1 is mostly located at the neuromuscular junction, whereas  $\alpha$ -DB-2 is located both at the neuromuscular junction and in other areas of the sarcolemma, in interaction with DAPC. Finally, of the  $\alpha$ -DB-3, which lacks the domain of interaction with both dystrophin and syntrophin, little is known about its exact subcellular localization in muscle ([Peters et al., 1998](#)).

A



B

Helix 1

		defg	abcdefg	abcdefg	abcdefg	abcdefg	abcdefg	abcd
Dys	<u>HYCQSLNQDSPLSQP</u> ...RSP	<u>AQIL</u>	<u>ISLESEE</u>	<u>RGELERI</u>	<u>LADLEEE</u>	<u>NRNLOAE</u>	<u>YDRLKQO</u>	<u>HEHK</u> <u>GLSPLPSP</u>
Dtn	<u>RYAARLAAESSSSQPQORSA</u>	<u>PD</u> ...	<u>ISFTIDA</u>	<u>NKQORQL</u>	<u>IAELENK</u>	<u>NREILQE</u>	<u>IQLRLLE</u>	<u>HEQA</u> S.....

Helix 2

		abcdefg	abcdefg	abcdefg	abcdefg	abcdefg
Dys	<u>PEMPTSPQS</u> PR	<u>DAELIAE</u>	<u>AKLLRQH</u>	<u>KGRLEAR</u>	<u>MQILEDH</u>	<u>NKQLESQ</u> <u>LHRLRQL</u> <u>LEQPQAE</u>
Dtn	... <u>QPTPEKA</u> QQ	<u>NPTLLAE</u>	<u>LRLLRQR</u>	<u>KDELEQR</u>	<u>MSALQES</u>	<u>RRELMVQ</u> <u>LEGLMKL</u> L.....K

Dys pI= 5.44

Figure 26 Four dystrobrevin isoforms are products of two genes:  $\alpha$  and  $\beta$  dystrobrevin.

A: Schematic representation of the dystrobrevin (DB) protein structure showing the different functional domains and its conservation in all dystrobrevin isoforms ( $\alpha$ -1,  $\alpha$ -2,  $\alpha$ -3 and  $\beta$ -DB), that are similar to C-terminus domains of dystrophin/utrophin (top). Adapted from [Rees et al., 2007](#). B: Dystrophin (Dys) and dystrobrevin (Dtn) sequence alignment. 3474-3603 aa and 436-551 aa fragments are shown, respectively. a-g: residues of coiled-coil domain. Underlines: dystrophin-binding site in dystrobrevin and vice versa. Adapted from [Sadoulet-Puccio et al., 1997](#).

Possibly the clearest characteristic of  $\alpha$ -dystrobrevin is its high similarity to dystrophin in the C-terminus part ([Figure 26 A and B](#)). Dystrobrevin is well known for sharing the functional domains found in the C-terminus region of DMD, which are responsible for the interaction of dystrophin with other DAPC proteins such as syntrophin. Therefore, one can already imagine that dystrobrevin will, likewise, associate through these domains with the same proteins. Among the regions that can be identified at the C-terminus end of dystrobrevin, we find: cysteine-rich regions, the EF-hand motifs, ZZ finger and, as expected, a syntrophin binding site ([Sadoulet-Puccio \*et al.\*, 1997](#)). In addition, the protein contains regions rich in tyrosine, which represent target areas for regulation by phosphorylation ([Balasubramanian \*et al.\*, 1998](#)). Finally, given that dystrobrevin is part of the DAPC, it has become common to assign it a structural function, however, several studies have shown a possible role of  $\alpha$ -DB in the development (changing expression profile) and in the transmission of intracellular signals (in association with nNOS, via syntrophin) (reviewed in [Rees \*et al.\*, 2007](#)).

## B. Syntrophin structure and expression in muscle

The last component of DAPC that we will cover in this manuscript are syntrophins, which represent a family of cytoplasmic proteins associated to dystrophin and dystrobrevin ([Yang \*et al.\*, 1995](#)). Syntrophins are considered scaffolding proteins or adaptors, which is due to the multiple domains of interaction with other proteins present in their structure. There are five classes of syntrophins, derived from five different genes:  $\alpha$ -syntrophin (also called  $\alpha$ 1-syntrophin),  $\beta$ 1-syntrophin and  $\beta$ 2-syntrophin, which are muscular; and the non-muscular  $\gamma$ 1-syntrophin and  $\gamma$ 2-syntrophins. In general, the pattern of expression of syntrophins is heterogeneous, although with a greater presence in muscle and brain.  $\alpha$ 1-syntrophin, in addition to being the most predominant in muscle tissue, is located throughout the sarcolemma, whereas  $\beta$ -syntrophin is more strongly enriched at NMJ ([Peters \*et al.\*, 1994](#); for review, see [Bhat \*et al.\*, 2019](#)).

All syntrophins share a common structure, consisting of three main types of functional domains ([Figure 27](#)): 1) two PH (Pleckstrin Homology) domains, a first one close to the N-terminal part, which is in fact split in two parts, hosting the PDZ domain in the middle; and second entire PH domain, closer to the C-terminus end. These domains are known to provide the protein with a role in intracellular signaling transduction; 2) a type-I PDZ domain, which enables its association with multiple proteins; 3) and finally, the



syntrophins have a unique domain called syntrophin unique domain or SU, consisting of highly conserved 57 amino acids (reviewed in [Bhat et al., 2019](#)).

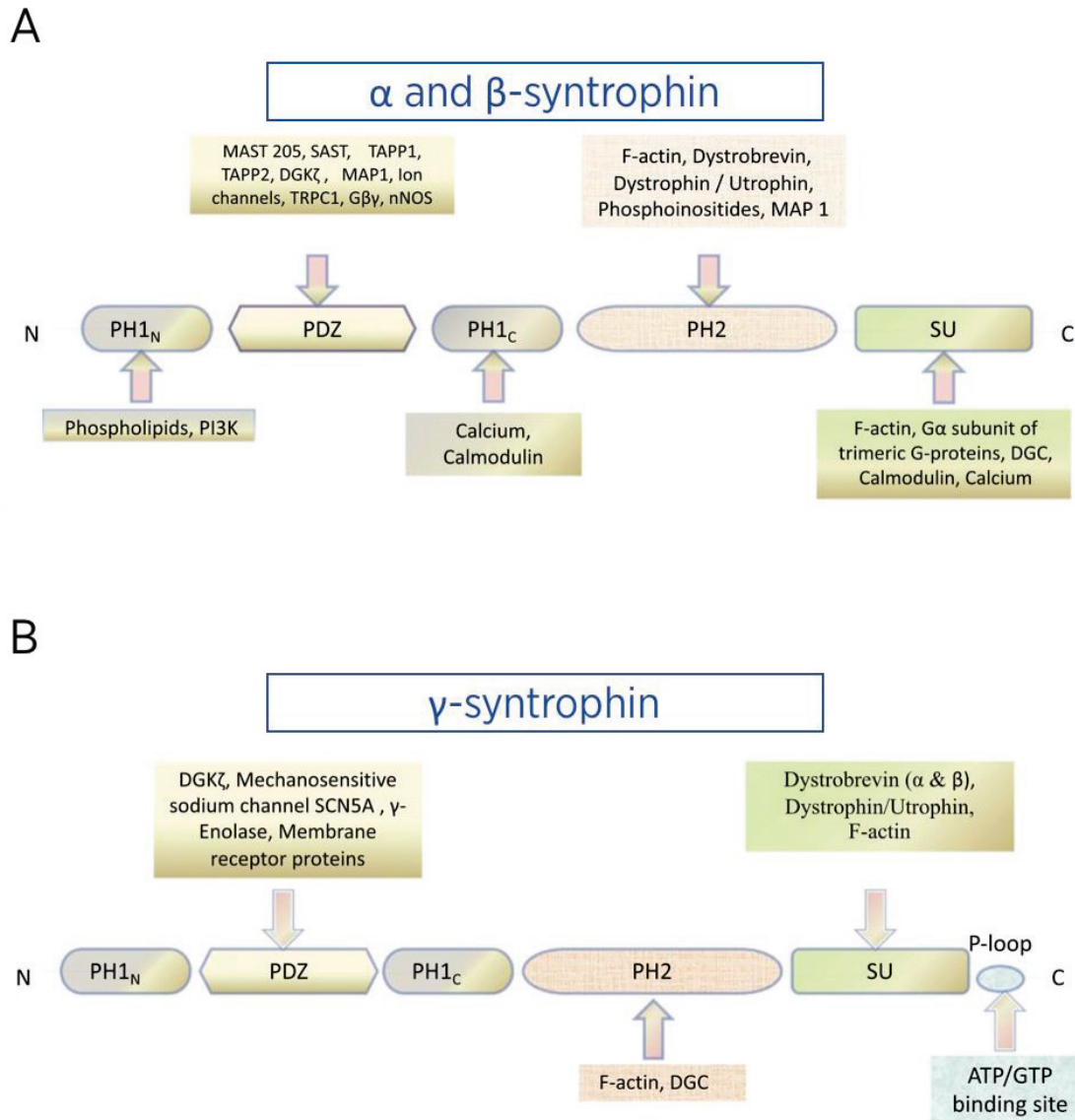


Figure 27 Syntrophins present functional domains that are conserved.

Muscular  $\alpha$  and  $\beta$ -syntrophins (A) share the same functional domains with the non-muscular  $\gamma$ -syntrophin (B). Adapted from [Bhat et al., 2019](#).

The syntrophins are mainly coupled to two DAPC proteins: dystrophin and dystrobrevin. Interestingly, several studies have shown that in both the dystrophin and dystrobrevin C-terminus sequences, there are not only one, as anticipated, but two sites of interaction with syntrophin; meaning that each complex would bind four molecules of syntrophin ([Ahn et al., 1995](#); [Sadoulet-Puccio et al., 1997](#)). Additionally, thanks to the PDZ domain, syntrophin can associate with multiple proteins, some of which are essential for intracellular signaling. Thus,  $\alpha$ 1-syntrophin binds to nNOS (neuronal Nitric Oxide



Synthase) ([Brenman et al., 1996](#)), to diverse classes of kinase proteins ([Chamberlain et al., 2000](#)), as well as to ion channels.

The association of syntrophin with ion channels is the aspect that has interested me the most over the last four years, so it will be elaborated with more details in the introduction [chapter 4](#) of this manuscript.

### C. Characterizing syntrophin and dystrobrevin in *C. elegans*

When *C. elegans* dystrophin was identified in Laurent Ségalat's laboratory, a genetic screen based on the use of RNAi was subsequently performed to identify other dystrophin-associated proteins. The authors looked for animals that had the same phenotype of head bending and hyperactivity, among others, as the *dys-1* mutants. Hence, they were able to identify the genes homologous to syntrophin/*stn-1* and to dystrobrevin/*dyb-1*, among others ([Grisoni et al., 2002b](#)).

#### - *Syntrophin in C. elegans*

In *C. elegans* there are two genes that code for syntrophin: *stn-1*, which produces a protein with high homology to the muscular  $\alpha$  and  $\beta$ -syntrophins of vertebrates; and *stn-2*, whose sequence is most closely related to the non-muscular  $\gamma$ -syntrophin.

#### **Syntrophin/STN-1** ([Grisoni et al., 2003](#)):

The first syntrophin in the worm (F30A10.8) was identified using sequence alignment by Grisoni *et al.* in 2002 ([Figure 28](#) A). Later, in 2003 it was named *stn-1*, for syntrophin 1. The structure of STN-1 is highly conserved. STN-1 has a PDZ domain (amino acids 42-125), which is 80% similar to its human counterpart; and a PH domain (amino acids 227-340), which has a 58% homology ([Grisoni et al., 2002b](#); [Grisoni et al., 2003](#)).

To determine which tissue express *stn-1* in the worm, a transgene was constructed containing 2kb of the genomic sequence upstream to *stn-1*, which was fused to a GFP coding sequence. The injection of this *stn-1::gfp* reporter highlighted muscle tissue (head, vulva and body wall muscle) and worm neurons as the primary and unique tissues expressing syntrophin ([Figure 28](#) B). To confirm this pattern, a second construction was made, this time including more upstream sequence to *stn-1*; the results were identical. Interestingly, fluorescence was observed at very early stages of development, as shown in [Figure 28](#) B, image 1.

The syntrophin mutant allele characterized by Grisoni *et al.*, *stn-1(ok292)*, which carries a deletion that removes the amino acids 230-417, presents the same phenotypes that the

previously observed and described in *dys-1(cx18)*. These include hyperactivity, exaggerated head-bending phenotype, as well as hypercontraction observed when animals move backwards. In addition, *stn-1* mutants were also found to exhibit hypersensitivity to the acetylcholinesterase inhibitor aldicarb, just as seen in *dys-1* mutants. Also, a double mutant strain was constructed for *stn-1* and *dys-1*, showing that the phenotypes are not additive, probably because both proteins function in the same complex. Interestingly, it was demonstrated that these phenotypes are the result of the absence of syntrophin from the muscle and not from the neurons.

With respect to muscle degeneration, similar to *dys-1*, the single mutant *stn-1* shows no signs of degeneration in the body wall muscle cells. However, contrary to *dys-1*, *stn-1* in combination with the MyoD homologous mutant *hlh-1(cc561)* does not show significant degeneration.



### **Syntrophin/STN-2:**

Similarly, by sequence alignment, *stn-2* (F27D9.8) was identified as a  $\gamma$ -syntrophin homologue. The expression pattern of this gene was elucidated by a GFP reporter coupled to a 3.82 Kb DNA genomic sequence upstream to *stn-2*. The results showed expression in neurons, neural commissures and muscle tissue ([Figure 28 C](#)) ([Zhou et al., 2008](#)). Although *stn-2* has not been as studied as *stn-1*, there are two mutant alleles that have been partially characterized. *stn-2(tm1869)* has an 811-bp deletion, removing the PDZ domain; and *stn-2(ok2417)*, that presents an *indel* also affecting the PDZ domain and other sequences near to the C-terminus end. These mutants show the same hyperactivity and head-bending phenotypes, as *dys-1* and *stn-1* mutants.

#### **- *Dystrobrevin in C. elegans***

*dyb-1*, which is the only gene encoding for dystrobrevin in the worm, was mapped on chromosome I. After its identification, the DYB-1 protein was sequenced, revealing that it possessed a 38% match to human  $\alpha 1$ -dystrobrevin. In addition, as it happens with the dystrophin and dystrobrevin proteins of vertebrates, DYB-1, like DYS-1, also contain at their C-terminus coiled coil domains. Also, there are two helices H1 and H2, in which the percentage of identity with respect to the sequence of vertebrates is greater in H2 ([Figure 29 A](#)) ([Gieseler et al., 1999b](#)) The interaction between both proteins will be discussed more extensively in the next point of this chapter.

With regard to the expression pattern of *dyb-1*, a GFP reporter was used to determine it by including 60bp of the 3' sequence of the *dyb-1* gene. It showed an abundant expression of dystrobrevin in the muscle tissue of *C. elegans*, including body wall muscle, head, pharynx and vulva muscle. In addition, numerous neurons were also observed expressing *dyb-1* ([Figure 29 B](#)). Both neurons and muscle showed an expression of dystrobrevin in early stages of embryonic development. Interestingly, no difference in the expression of *dyb-1* was noticed between the N2 and *dys-1(cx18)* worms, suggesting that dystrophin is probably not required for the expression of dystrobrevin in the worm.



A

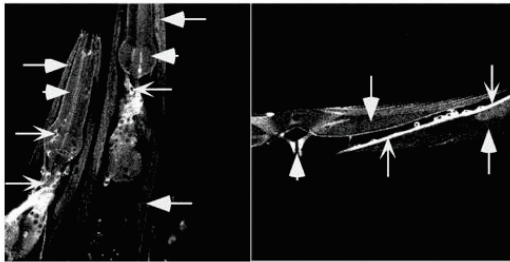
### Dystrophins

	defg abcdefg abcdefg abcdefg abcdefg abcdefg	
hsDYS	AQIL ISLESEE RQELERI LADLEEE NRNLQAE YDRLKQQ	<b>Helix 1 :</b>
ceDYS	LQII NQVEQLQ RDEMDQM LHRLQFE NKQLRKE LEWKRGA	Identity : 28%
	abcdefg abcdefg abcdefg abcdefg abcdefg abcdefg	
hsDYS	DAELIAE AKLLROH KGRLEAR MQILEDH NKQLESQ LHRLRQL	<b>Helix 2</b>
ceDYS	QNDVMDE AKALRLH KORLEHR SRILEQQ NEQLEMQ LQRLKKV	Identity : 52%

### Dystrobrevins

	abcdefg abcdefg abcdefg abcdefg abcdefg abcd	
hsDYB	ISFTIDA NKQQRQL LAELENK NREILQE IQRLRLE HEQA	<b>Helix 1</b>
ceDYB	RSMNSSM VGDERIL IAQLEEE NSMMVRE MARLESQ TTSD	Identity : 25%
	abcdefg abcdefg abcdefg abcdefg abcdefg abcd	
hsDYB	LRLLRQR KDELEQR MSALQES RRELMVQ LEGLMKL LKEE	<b>Helix 2</b>
ceDYB	LACLRDR KMELEEK MFEMQQR RRELMVQ LEHLMAQ LNTG	Identity : 53%

B



C

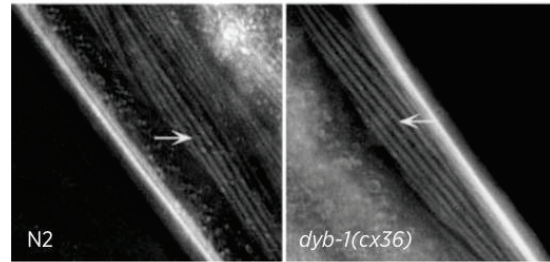


Figure 29 A highly conserved dystrobrevin is expressed in worms' muscle and neurons.

A: *C. elegans* (ce) and human (hs) dystrophin (DYS) and dystrobrevin (DYB) protein sequences alignment showing their conservation in helix 1 and 2, being greater in helix 2 for both proteins. Adapted from [Gieseler et al., 1999b](#). B: GFP gene reporter showing the expression of *C. elegans* dystrobrevin/*dyb-1* in pharyngeal and body wall muscle as well as in neurons. C: Polarized light showing no defect in muscle morphology in *dys-1(cx36)* mutants compared with wild-type (N2). B and C are adapted from [Gieseler et al., 2001](#).

The most commonly used mutant allele is *dyb-1(cx36)*, in which only 38 amino acids remain preserved. As expected, the dystrobrevin mutants reveal identical phenotypes to those observed in *dys-1*'s, including hyperactivity, hypercontraction when animals move backwards and head-bending phenotype. In addition, as occurring in *dys-1(18)*, *dyb-1(cx36)* also shows a higher pharmacological sensitivity to aldicarb (acetylcholinesterase inhibitor). Electrophysiology experiments were also performed on the worm's terminal bulb muscle, showing that depolarization of these muscle cells takes place at considerably lower acetylcholine concentrations when compared to the wild-type strain. This clearly

indicates that *dyb-1* mutants are more sensitive to Ach than wild-type worms, just like *dys-1* mutants. Important to be noted, the double *dys-1(cx18),dyb-1(cx36)* show the same phenotype as the single mutants. ([Gieseler et al., 1999a](#); [Gieseler et al., 2001](#)).

## VIII. Most of the DAPC proteins are interdependent

### A. Dystrophin, dystrobrevin and syntrophin interactions in vertebrates

In the dystrophin protein, the C-terminus region hosts numerous domains of interaction with various proteins, including dystrobrevin and syntrophin.

One of the domains found at the C-terminus end of DMD is the coiled-coil domain, which consists of two  $\alpha$ -helicoidal motifs ([Blake \*et al.\*, 1996](#)), that have been directly involved in the binding of dystrophin to syntrophin in multiple studies. Furthermore, between 1994 and 1997 numerous researchers pointed to the fact there are not only one, but two sites of interaction with syntrophin in the -COOH region of dystrophin. First, Suzuki *et al.* conducted studies based on a blot-overlay approach to determine the exact portion of DMD that is necessary for its binding to syntrophin. To do so, they made different constructions with C-terminus fragments of different sizes and studied their ability to bind both  $\alpha$ 1 and  $\beta$ 1-syntrophin. They showed that both  $\alpha$ -1 and  $\beta$ -1-syntrophins bind to the COOH part of DMD, and that this association is carried out by the amino acids 3444-3535 in DMD (exons 73-74), an area that is just in the proximity of the cystein-rich region, which is responsible for the binding of DMD to  $\beta$ -dystroglycan (3080-3408 amino acids). Additionally, in this study they suggest a possible second syntrophin binding site in this region of the dystrophin; which was confirmed in further studies. Complementarily, they also showed that DMD isoforms lacking this Ex-74-coded region are rarely present in skeletal muscle, but are more abundant in smooth and cardiac muscles and in the brain. Thus, suggesting that the interaction with syntrophin is important for the role of dystrophin in skeletal muscle ([Suzuki \*et al.\*, 1995](#)).

To complement this study, a second one was conducted to analyze the dystrophin-syntrophin interaction, using this time *in vitro* expression system. Here, portions of the human DMD gene, that had previously been shown to be involved in syntrophin binding in co-immunoprecipitation experiments, were utilized. The results show that the 53 amino acids of exon 74 are necessary and sufficient for the binding of dystrophin to  $\beta$ 1-syntrophin *in vitro* ([Figure 30 A](#)). Another isoform of DMD, which is missing 110 amino acids, including the 53 mentioned above, was shown to not able to bind syntrophin ([Ahn and Kunkel, 1995](#)). Curiously, it has been shown that even non-muscular dystrophins that preserve the C-terminus region are also able to bind syntrophin *in vitro* ([Yang \*et al.\*, 1995](#)).



Finally, it should be noted that in the *mdx* model mice, the syntrophin is strongly reduced and almost disappeared, except in regions corresponding to the neuromuscular junction, as shown in [Figure 30 B](#). Interestingly, similar results were obtained regarding the localization of dystrobrevin in the *mdx* mice, where both  $\alpha$ -1 and  $\alpha$ -2-dystrobrevins are lost from the sarcolemma, although they remain present at the NMJ ([Figure 30 B](#)) ([Deconinck et al., 1997](#)). Their maintenance in NMJ was hypothetically related to utrophin. However, another study showed that dystrobrevin was correctly located in utrophin *knockout* mice ([Figure 30 C](#)). Thus, it remains unclear with which complex both syntrophin and dystrobrevin could interact at the neuromuscular junctions.

Finally, a recent study shows that syntrophin not only binds to dystrophin in its coiled-coil domain in the C-terminus region, but curiously there are also syntrophin-binding sites in the spectrin repeats, contained in the central rod domain of DMD. Also, only  $\alpha$ -syntrophin bound to spectrin repeats is capable of associating with nNOS ([Adams et al., 2018](#)).

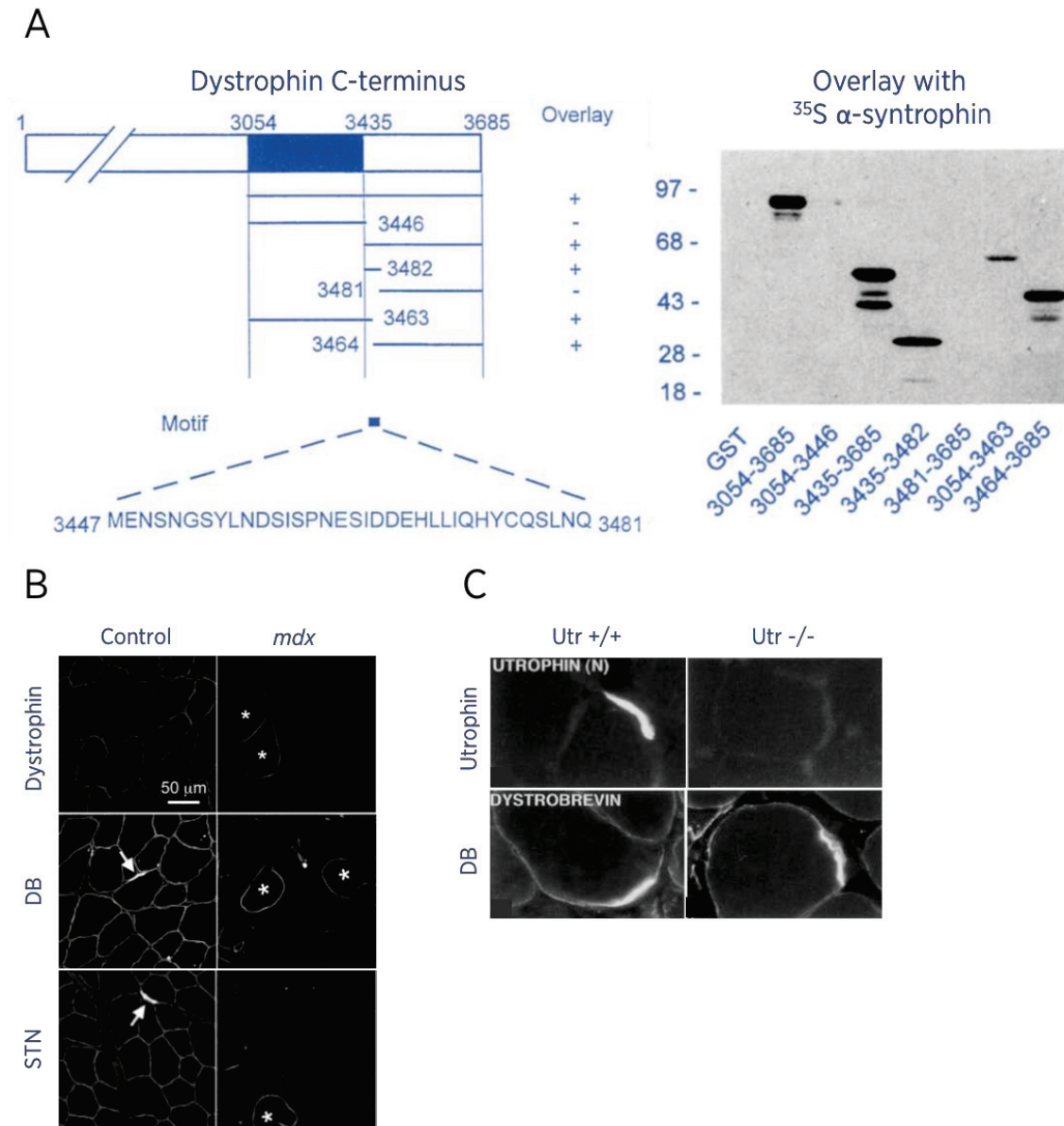


Figure 30 Dystrophin, dystrobrevin and syntrophin interact with each other in muscle.

A: Revelation of syntrophin binding-sequence in dystrophin (left) by GST pull-down analysis (right) performed in seven different fragments of the dystrophin C-terminus sequence. Adapted from [Yang et al., 1995](#). B: Immunostaining shows a strong decrease of dystrobrevin (DB) and syntrophin (STN) signal in dystrophin deficient *mdx* mice muscle. Adapted from [Li et al., 2009](#). C: Dystrobrevin (DB) expression does not differ in utrophin null mice (Utr<sup>-/-</sup>) compared with wild-type (Utr<sup>+/+</sup>) in immunohistochemical analysis from mice skeletal muscle sections. Adapted from [Grady et al., 1997](#).

Regarding dystrobrevin, a coiled-coil zone its C-terminus is found. In this region, as in dystrophin, we find two  $\alpha$ -helicoidal motifs showing a great homology ([Figure 26 B](#)). Based on this, numerous studies pointed out that in dystrobrevin, the region responsible for the interaction with syntrophin is contained in exons 13-14 (amino acids 427-480)

([Sadoulet-Puccio et al., 1997](#)). It is also argued that there are two syntrophin-binding sites in both dystrophin and dystrobrevin, so that in a single DAPC complex four syntrophins would be associated, two to each protein ([Newey et al., 2000](#)).

## B. Dystrophin, dystrobrevin and syntrophin interactions in *C. elegans*

Analogously to the studies on vertebrates, in the worm the possible interaction between DYS-1, DYB-1 and STN-1, the homologues to dystrophin, dystrobrevin and syntrophin, respectively, has also been investigated.

In 1999, an *in vitro* association test was performed using 273 amino acids of DYS-1 and 154 amino acids of DYB-1, both containing the C-terminus region that encompasses the coiled-coil domains of both proteins. The authors found that GST-DYS-1 was able to retain labeled DYS-1 and vice versa. Thus, an *in vitro* association of both protein takes place. Interestingly, when they removed the region comprising the  $\alpha$ -helicoidal motif H2 of DYB-1, they saw that the binding was drastically reduced, suggesting that the dystrophin H2 helix is indeed critical for its binding to dystrophin ([Gieseler et al., 1999b](#)). Years later, this binding site between dystrophin and dystrobrevin was further refined, showed that the first part of H2 seems to be the most relevant of this helical motif, but, they were curiously not able to reproduce the same *in vitro* association experiments when replicating them in yeast two hybrid (Y2H) assays ([Grisoni et al., 2002a](#)). It should be noted that this is not the case in mammals, where H1 was shown to be more critical for the interaction of dystrophin with dystrobrevin ([Sadoulet-Puccio et al., 1997](#)).

Additionally, syntrophin can bind both dystrophin and dystrobrevin in the worm. Y2H assays showed that the full length of STN-1 does not bind to fragments of the C-terminus region of DYS-1. Two fragments of DYS-1 were used, amino acids 2857-3674 and amino acids 3402-3674, which had previously been identified as necessary sites for *in vitro* interaction with STN-1 ([Gieseler et al., 1999b](#)). These results indicate that, contrary to what was obtained *in vitro*, STN-1 and the used fragments of DYS-1 do not interact *in levuro* ([Grisoni et al., 2003](#)). Regarding DYB-1 and STN-1 interaction, the results show that the fragment containing amino acids 390-543 is sufficient for the binding *in levuro*. To conclude, *in vitro* pulldown experiments detect an interaction of syntrophin with both dystrophin and dystrobrevin, however, Y2H assays were unable to replicate the results of the association of STN-1 with DYS-1, although they were successful with DYB-1. One of the hypotheses is that the syntrophin in the worm does not bind directly to dystrophin,

but it does so through dystrobrevin. This seems to be consistent with a result obtained by Newey *et al.* in 2000, where a sequence alignment analysis was performed and it was found that *dys-1* does not possess any syntrophin conserved binding motif ([Newey \*et al.\*, 2000](#)).

### C. Dystroglycans are strongly reduced in *mdx* mice

Multiple studies have characterized the  $\beta$ -DG subunit which, through its C-terminal ends found in the cytoplasm, has been shown to bind to cystein-rich regions on dystrophin. The WW domains of dystrophin have been shown to be particularly relevant for its association to the  $\beta$ -dystroglycan subunit. These WW-domains are of type I and can be associated with PPxY-proline rich motifs.

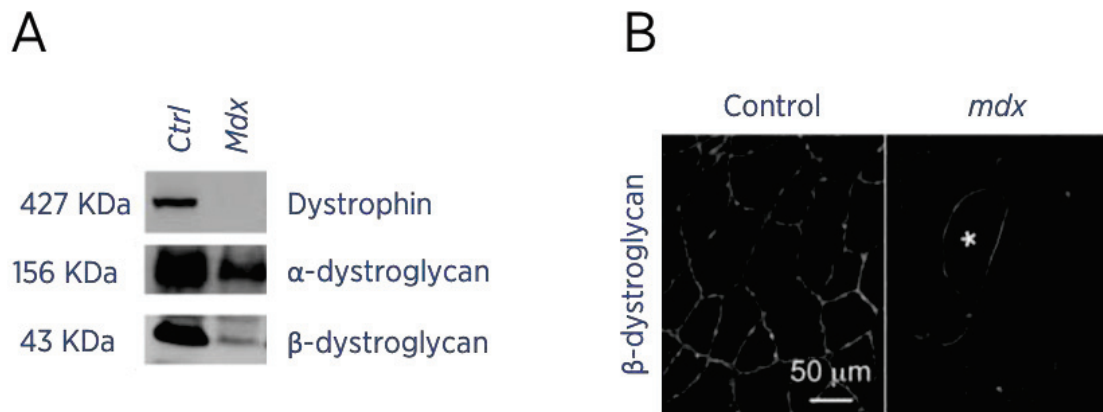


Figure 31 Dystroglycan is reduced in *mdx* mice.

A:  $\alpha$ - and  $\beta$ -dystroglycans amounts are reduced in dystrophin deficient *mdx*, mice compared with wild-type (BL10) control mice in western blot analysis. B: Immunostaining showing a strong decrease of  $\beta$ -dystroglycan in *mdx* skeletal muscle compared with wild-type mice. A and B are adapted from [Li \*et al.\*, 2009](#).

Comparable to most of the components of the dystrophin-associated proteins complex, the location of the dystroglycans is strongly disturbed in dystrophin mutant models, as is the case with the *mdx* mice. On one hand, western-blot analyses have shown that about 80% of  $\beta$ -dystroglycan is lost from whole muscle lysate in *mdx* compared to wild-type mice ([Figure 31 A](#)). On the other hand, and complementarily, when immunofluorescence staining is performed, the muscle of *mdx* mice shows a strong reduction of  $\beta$ -DG, which is almost inexistent in selected areas ([Figure 31 B](#)) ([Li \*et al.\*, 2009](#)).

#### D. Loss of one of the sarcoglycan complex subunits destabilizes the whole sub-complex

Sarcoglycans constitute a transmembrane sub-complex that interacts with several DAPC proteins. In addition, numerous studies have led researchers to agree that the absence of a single subunit of the sarcoglycan subcomplex entails the loss of the entire complex.

In 1998, Duclos *et al.* examined the presence and localization of various DAPC proteins in the skeletal and cardiac muscle of  $\alpha$ -sarcoglycan (*Sgca*) null mice. Interestingly, as a result of immunofluorescence analysis, they found that although only the  $\alpha$ -sarcoglycan was missing, the other subunits of the subcomplex had also disappeared from the muscle, resulting in a loss of the entire SG complex. Not only, but they also observed that the localization of other DAPC proteins, such as dystrophin or dystroglycan, were also severely affected, reducing the amount of these proteins at skeletal muscle ([Figure 32 A](#)) ([Duclos \*et al.\*, 1998](#)). In parallel, Yoshida *et al.* showed that dystrobrevin is also affected when the sarcoglycan complex is destabilized, since a clear loss of  $\alpha$ -dystrobrevin is observed in the sarcoglycan *knockout* mice muscle. This study also demonstrates that both proteins can be associated, with sarcoglycan binding to the N-terminus end of  $\alpha$ -dystrobrevin ([Yoshida \*et al.\*, 2000](#)).

The impact of the loss, this time of the  $\beta$ -sarcoglycan subunit, has also been deeply analyzed. Animal models with mutations in  $\beta$ -SG also show signs of muscular dystrophies, in addition to the fact that northern blot analysis shows that the remaining subunits,  $\alpha$ ,  $\gamma$  and  $\delta$ -SG, are extremely reduced and almost disappeared from the muscle of these animals ([Figure 32 B](#)) ([Araishi \*et al.\*, 1999](#)).

In conclusion, the loss of a single subunit of the sarcoglycan complex leads to the destabilization and alteration of the localization of the other subunits, giving rise to a totally unstable complex that is eventually lost. It also affects the distribution of other DAPC proteins, such as dystrophin, dystrobrevin or dystroglycan. These results have been seen both in animal models and in patients' biopsies.

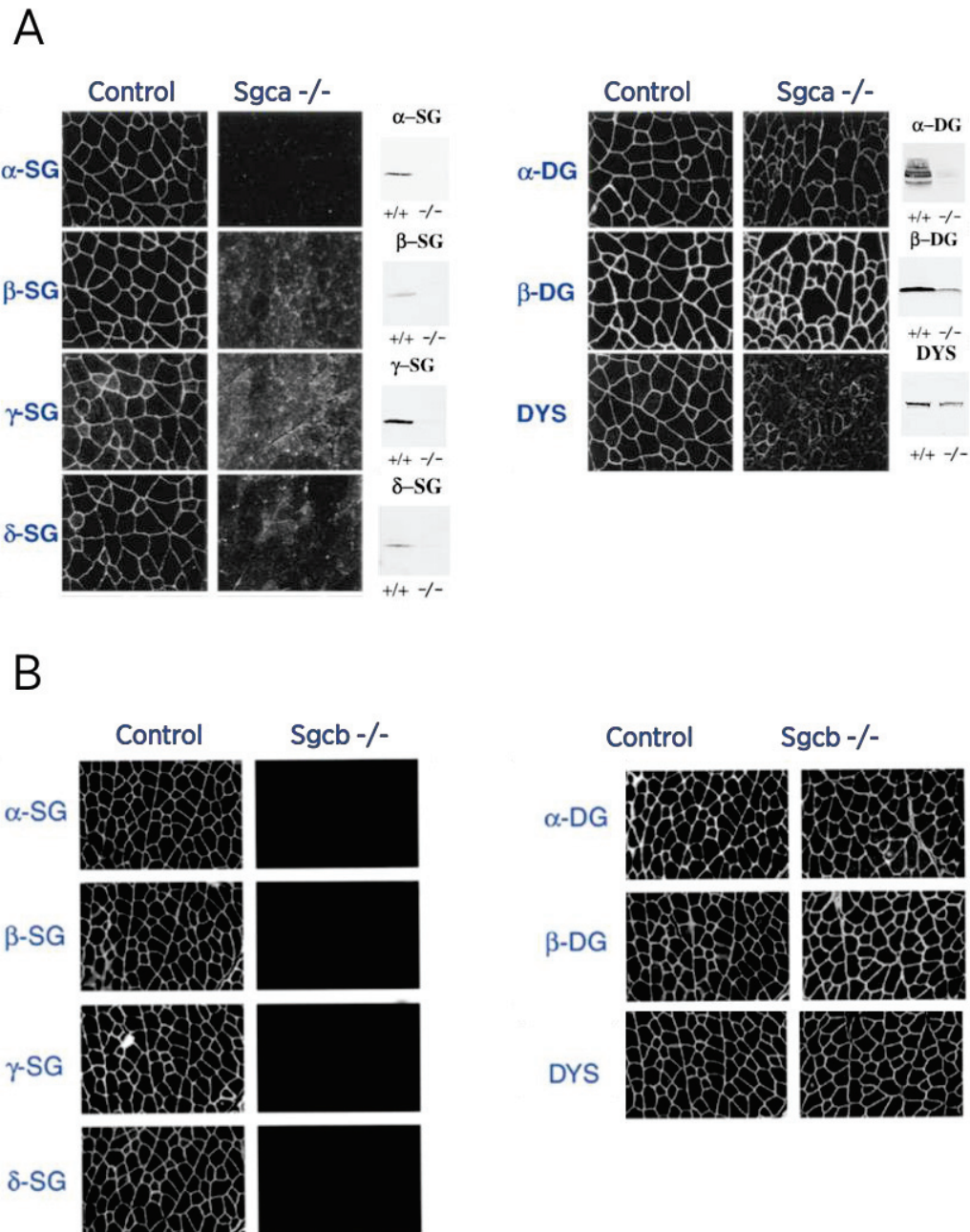


Figure 32 Mutations in one sarcoglycan subunit lead to the total loss of the SG complex and other DAPC proteins.

Most of sarcoglycan (SG) subcomplex subunits are reduced or even disappeared in skeletal muscle immunostaining analysis of KO mutants of  $\alpha$ -sarcoglycan Sgca<sup>-/-</sup> (A) and  $\beta$ -sarcoglycan Sgcb<sup>-/-</sup> (B). Dystrophin (Dys) and  $\alpha$ -dystroglycan (DG) localizations are altered in Sgca<sup>-/-</sup> but not in Sgcb<sup>-/-</sup> KO adapted from [Dulcos et al., 1998](#).



## Chapter 4 Dystrophin-associated proteins complex and ion channels

The dystrophin-associated protein complex is composed of intra- and extracellular proteins and is mainly involved in the binding between the cytoskeleton and the extracellular matrix. The absence of dystrophin or any other protein component of DAPC leads to several alterations in the functioning of these cells, including muscle degeneration. The exact molecular mechanism underlying this degeneration remains poorly understood. One of the hypotheses under debate is the deregulation of calcium flux in the muscle cell, where this increase in the intracellular concentration of  $\text{Ca}^{2+}$  could trigger protein degradation and thus muscle degeneration. This calcium influx depends extensively on the resting membrane voltage, which is controlled by the expression and activity of different ion channels. In this chapter, we will discuss and provide some practical examples of the interaction taking place between the dystrophin complex and the ion channels in the membrane of both skeletal and cardiac muscle cells.



I. An additional role of the DAPC: interaction with ion channel in vertebrates

A. Dystrophin complex interacts with voltage-dependent sodium channels ( $\text{Na}_v$ ) in skeletal and cardiac muscle

$\text{Na}_v$  channels represent a family of voltage-dependent sodium-selective ion channels that are responsible for the flux of  $\text{Na}^+$  cations within the action potential of excitable cells. We have  $\text{Na}_v$  channels in the skeletal muscle, heart and brain, among others. In the skeletal muscle these channels were called SkM1, then  $\text{Na}_v1.4$ . In the heart, they were known as SkM2, and later  $\text{Na}_v1.5$ . These channels are constituted by an  $\alpha$  subunit and by auxiliary subunits called  $\beta$  subunits ([Gee et al., 1998](#)).

Unlike the regulation of the anchoring and maintenance of synaptic receptors in the postsynaptic membrane, very little is known about the mechanism underlying the location in sub-domains of most transmembrane proteins, including ionic channels such as  $\text{Na}_v$  channels. Interestingly, several studies show that the localization of these ion channels is strongly disrupted in the skeletal and cardiac muscle of models lacking dystrophin, such as the *mdx* mice; suggesting that the DAPC might be involved in the localization of ion channels. Indeed, proteins belonging to DAPC, such as syntrophin, have been shown to bind through their PDZ domain to different ion channels and other transmembrane proteins (reviewed in [Leyva-Leyva et al., 2018](#)).

In muscle tissue, we find three syntrophines:  $\alpha 1$  (the most abundant) and  $\beta 1$ -syntrophins, both present in NMJ and sarcolemma; and  $\beta 2$ -syntrophine, which is more prevalent in NMJ. (For more details, see [chapter 3, point VIII](#)). One of the functional domains found in syntrophin is the PDZ domain, by which it has been shown to bind to proteins such as nNOS (Nitric Oxide Synthase). Considering that other proteins with the PDZ domain bind to proteins containing at their C-ter end sequences of the (S/T)XV-COOH type, and since muscular  $\text{Na}_v$  channels also present this type of motifs at their  $\alpha$  subunit C-ter, [Gee et al.](#) conducted an initial study to investigate the association between  $\text{Na}_v$  channels and DAPC. Later, in the  $\text{Na}_v1.5$ , this PDZ binding motif was mapped to the last three amino acids: Ser-Ile-Val. It should be noted that the brain  $\text{Na}_v$  channels don't share this sequence ([Gee et al., 1998](#); [Gavillet et al., 2006](#)).

Immunoprecipitation and Western Blot experiments showed that in mouse skeletal muscle, when using anti-syntrophin antibodies,  $\alpha$  subunits of the  $\text{Na}_v$  channels are also

detected. These complexes not only precipitated  $\text{Na}_v$  and syntrophin, but also dystrophin, which is bound to syntrophin in the DAPC. The same results were obtained when working with mouse cardiac muscle extract. Interestingly, and although they do not present this (S/T)XV-COOH sequence, the brain channels were also precipitated with syntrophin and dystrophin in brain extracts, following the same method as before. The authors explained this by hypothesizing that the binding of these channels to the DAPC complex is based on other types of interactions not involving the PDZ domain ([Gee et al., 1998](#)).

Years later, another research team demonstrated that  $\text{Na}_v1.5$  channels are indeed associated with syntrophin and dystrophin by pull-down experiments. They utilized human and rodent cardiac muscle extract, in which they tested different constructs containing the last 66 amino acids of the  $\alpha$  subunit of  $\text{Na}_v1.5$  ([Figure 33 A](#)). They showed that both dystrophin and syntrophin can bind to these fragments, and that for this interaction, in addition, the last three amino acids mentioned above are indispensable ([Gavillet et al., 2006](#)). In order to know the exact fraction of syntrophin required for this binding, *Gee et al.* used different constructions containing fragments corresponding to the functional domains of the syntrophin protein (amplified from its cDNA and contained in a vector). These constructs were incubated with extracts from both mouse muscle and brain. Interestingly and as expected, only the fragments containing the PDZ domain of syntrophin captured  $\text{Na}_v$  channels. This interaction was not observed neither for the other domains (not PDZ) or for the brain extracts, where the PDZ domain failed to recruit  $\text{Na}_v$  (since they lack PDZ-binding motif) ([Gee et al., 1998](#)).

On the other hand, since the absence of dystrophin alters the location and amount of syntrophin, one can expect that in the *mdx* mice models we would see an alteration in the  $\text{Na}_v$  channels. In fact, it has been demonstrated by western blot (ventricular lysates) that the amount of  $\text{Na}_v$  protein was significantly reduced in *mdx* mice when compared to wild-type mice ([Figure 33 B.1](#)). To know the source of this reduction, a qRT-PCR was performed and showed that  $\text{Na}_v$  mRNA was not affected ([Figure 33 B.2](#)), which means that DAPC is required for the correct formation of the  $\text{Na}_v$  but it only intervenes in post-transcriptional phases, probably for the localization or function of the proteins at cell membrane. Besides the protein level, they also found that the current associated to  $\text{Na}_v$  channels was significantly reduced by using patch-clamp experiments ([Figure 33 C](#)); where they also measured the electrical capacitance, which was not different in the *mdx* compared to wild type mice, suggesting that the cell size did not differ either ([Gavillet et al., 2006](#)). Interestingly, the same research team showed recently the effect of a

proteasome inhibitor (MG132) on  $\text{Na}_v$  channels in the context of *mdx* mice. A rescue of both the current associated with these channels and their expression in cardiomyocytes was observed ([Figure 33 D.1 and D.2](#)). It should be noted that with the use of MG132 no rescue in the expression of dystrophin was observed ([Rougier \*et al.\*, 2013](#)).

Last but not least, several studies showed that dystrophin is not homogeneously located in the cardiomyocyte membrane, but instead it is enriched in the lateral membrane (LM) and very weakly present, almost excluded from the intercalated discs (ID) ([Stevenson \*et al.\*, 2005](#)). Considering that the  $\text{Na}_v$  channels are present both in the lateral membrane and in the intercalated discs, one can assume that two pools of these channels exist, the first one associated with the DAPC (LM) and the second one not. Interestingly, a strong colocalization was observed between  $\text{Na}_v$  and the components of the DAPC dystrophin and syntrophin ([Figure 33 E](#)). In addition, they observed a decrease in the amount of  $\text{Na}_v$  channels in the lateral membrane of the cardiomyocytes in the context of the *mdx* mice ([Figure 33 F](#)), which explains the decrease in current observed in the previously cited study ([Petitprez \*et al.\*, 2011](#)).

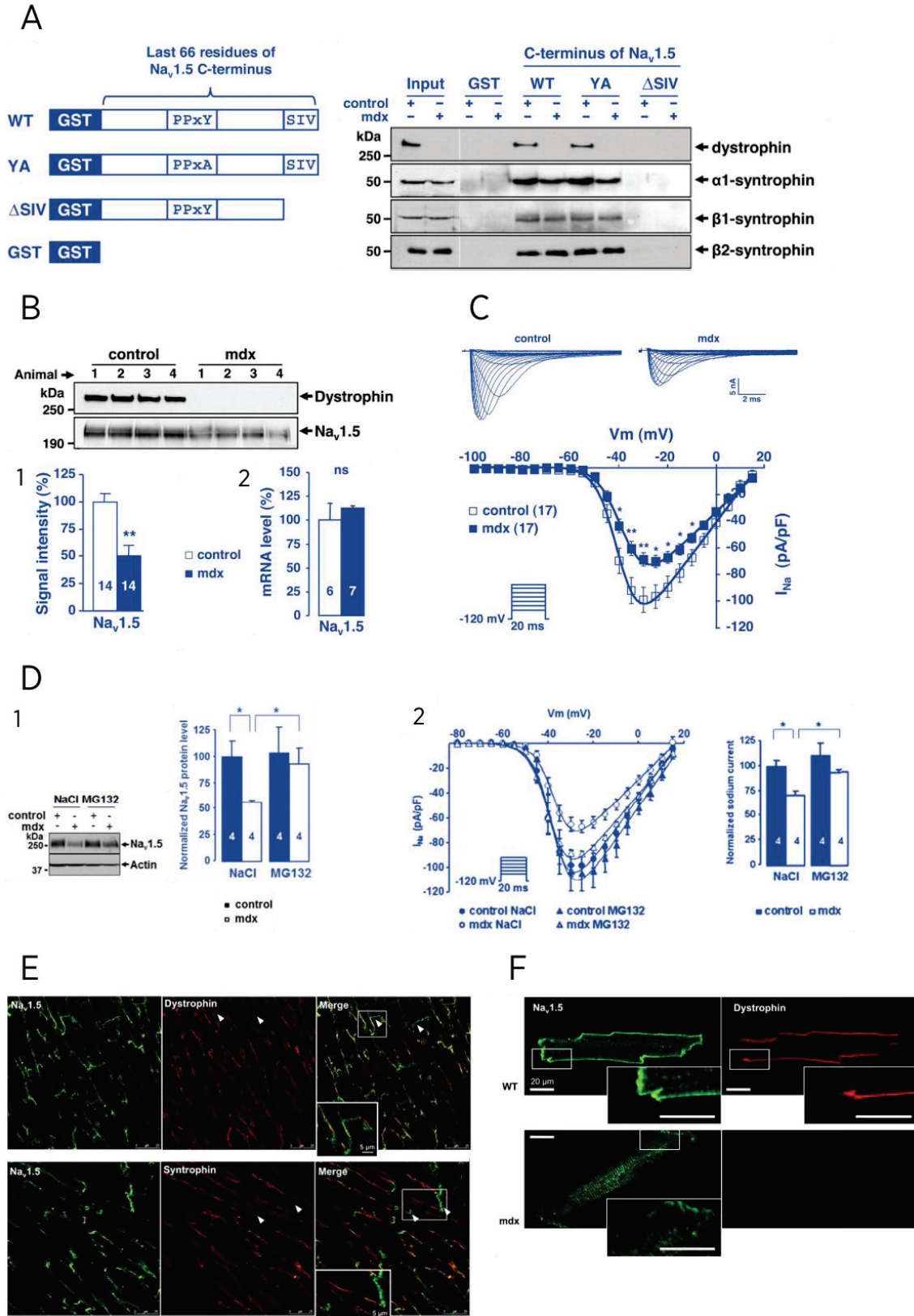


Figure 33 Muscular Na<sub>v</sub> channels localization and function depend on DAPC.

A: GST pull-down experiments with different fragments of the Na<sub>v</sub>1.5 cardiac muscular voltage-sensitive sodium channel. Na<sub>v</sub>1.5 interaction with syntrophins and dystrophin requires the C-terminus SIV sequence of the channel. B: Western blot (top) analysis and RT-qPCR show a strong decrease of Na<sub>v</sub>1.5 protein

amount (1) and mRNA level (2) respectively in *mdx* mice heart. C: Patch-clamp experiments show a reduction in the Na<sub>v</sub>1.5 associated current in *mdx* mice cardiac muscle. A, B and C are adapted from [Gavillet et al., 2006](#). D: Western blot (1) and patch-clamp recording (2) showing the effect of the proteasome inhibitor (MG132) on Na<sub>v</sub>1.5 protein amount and channel activity, respectively, in wild-type and *mdx* mice. Adapted from [Rougier et al., 2013](#). E: Immunostaining analysis showing the localizations of Na<sub>v</sub>1.5 (green), dystrophin (red, top) and syntrophin (red, bottom) in cardiomyocytes. Na<sub>v</sub>1.5 is localized both at lateral membrane and intercalated discs (arrowheads) while dystrophin and dystrophin are only localized at lateral membrane. F: Na<sub>v</sub>1.5 expression is strongly reduced in *mdx* cardiomyocytes. E and F are adapted from [Petitprez et al., 2011](#).

## B. A PDZ domain-dependent interaction of syntrophin and the potassium channel K<sub>ir</sub>4.1 in mice

The K<sub>ir</sub>4.1 channels belong to the class of inward rectifier potassium channels. They are expressed in different tissues, including glial cells in both the central nervous system and in the retina (Müller cells). Its main function in this tissue is to balance the extracellular concentration of potassium cations, acting as a buffer ([Hibino et al., 2004](#)). It was previously suggested that these channels, in the neural tissue, could be in association with the DAPC, being involved in their maintenance. At the beginning of 2002, Connors and Kofuji *et al.* noticed that both the K<sub>ir</sub>4.1 channels and the Dp71 isoform of dystrophin have similar subcellular distribution in the Müller cells of the retina. They immediately demonstrated that Dp71 is involved in the localization of K<sub>ir</sub>4.1. Since in the *mdx* mice models this dystrophin isoform is totally absent, they observed that the distribution of the channel is altered. They concluded that Dp71 is necessary for the correct positioning of K<sub>ir</sub>4.1 in Müller cells ([Connors and Kofuji, 2002](#)). This interaction was shown a few years later by immunoprecipitation experiments, showing that dystrophin and these potassium channels are associated forming a macro-complex in brain.

Another hypothesis argued that the channels could bind to other DAPC proteins known to associate with transmembrane proteins. Interestingly, the K<sub>ir</sub>4.1 channels have at their C-terminus end a PDZ-binding motif (-SNV-COOH), which might allow to interact with proteins containing the PDZ-domain in their structure ([Horio et al., 1997](#)), as is the case with the syntrophins. In 2004, K<sub>ir</sub>4.1 channels were clearly shown to be associated with  $\alpha$ -syntrophin, in addition to Dp71, in both mouse brain extract and cortical astrocyte cell culture, as shown in [figure 34](#). Finally, when mutants lacking syntrophin are used this association is not able to take place. ([Connors et al., 2004](#)).

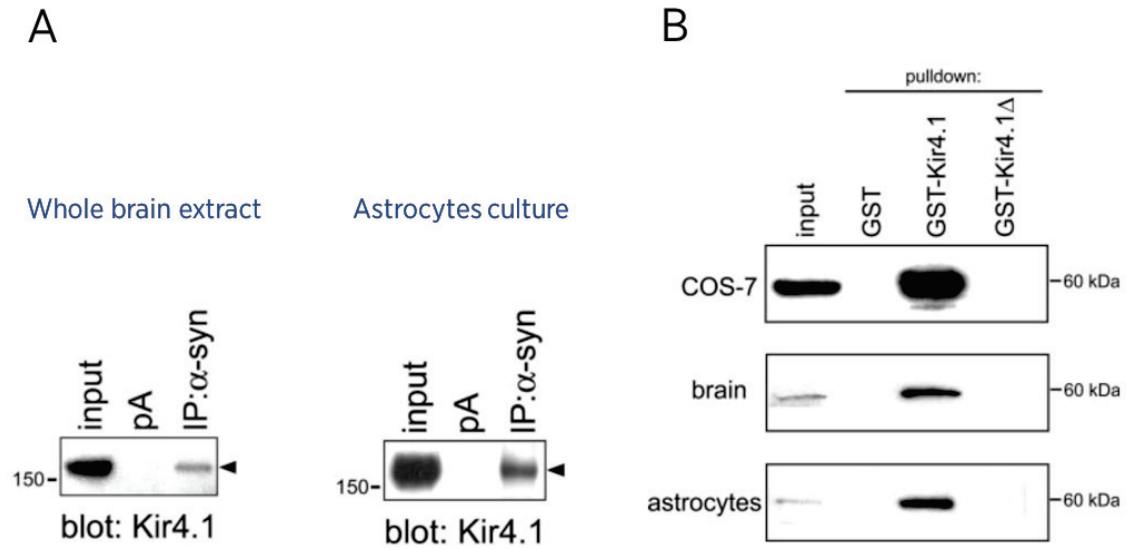


Figure 34  $K_{ir}4.1$  channels are associated to dystrophin and syntrophin in the DAPC.

A: Western blot showing a co-association of the  $K_{ir}4.1$  potassium channel with  $\alpha$ -syntrophin both in whole brain extract and in astrocytes cells culture. B: GST pull-down experiments reveal the requirement of the C-terminus regions of  $K_{ir}4.1$  for its interaction with  $\alpha$ -syntrophin *in vitro*. Adapted from [Connors et al., 2004](#).

Now that an association between syntrophin and these channels is known to exist, the next wonder was whether it was occurring through the PDZ domain. To answer this question, pull-down experiments were carried out using fragments from the C-ter region of  $K_{ir}4.1$ , which contain the PDZ-binding motif, in combination with lysates from COS-7 cells (transfected with  $\alpha$ -syntrophin). Only an association when the C-ter fragment of  $K_{ir}4.1$  was present was observed, which was not the case when using a control lacking this fragment. These results were confirmed by a second *in vitro* experiment, where the same  $K_{ir}4.1$  constructions were used either in combination with brain extract or astrocyte culture (both providing the syntrophin). In [figure 34 B](#) it is observed that interactions between  $K_{ir}4.1$  and  $\alpha$ -syntrophin only occur when the channels preserve their C-terminus, indicating that syntrophin and  $K_{ir}4.1$  potassium channels are associated in a PDZ-dependent way in mouse brain ([Connors et al., 2004](#)).

### C. TRPC1, a non-selective permeant calcium channel, binds to the PDZ domain of syntrophin

TRPC (Transient Potential Canonical Receiver) channels represent a large family of non-selective ion channels consisting of seven members (TRPC1-7). They are mechanosensitive and their main function is to transduce signals of membrane movement



or stretching in ion flux (such as sodium, potassium, calcium or magnesium) across the membrane. These channels were extensively studied in *Drosophila*. The first member of this family to be cloned was TRPC1 ([Wes et al., 1995](#)), which is related to skeletal muscle ([Vanderbrouck et al., 2002](#)). Subsequently, its localization was analyzed and it was found to be embedded in the sarcolemma of mouse muscle fibers. A very interesting finding consists in the observation of a colocalization between TRPC1 and dystrophin in the sarcolemma ([Figure 35 A](#)) by immunostaining analyses ([Vandebrouck et al., 2007](#)). In addition, an interaction between this channel and the dystrophin-associated protein complex was established for the first time, which is described below.

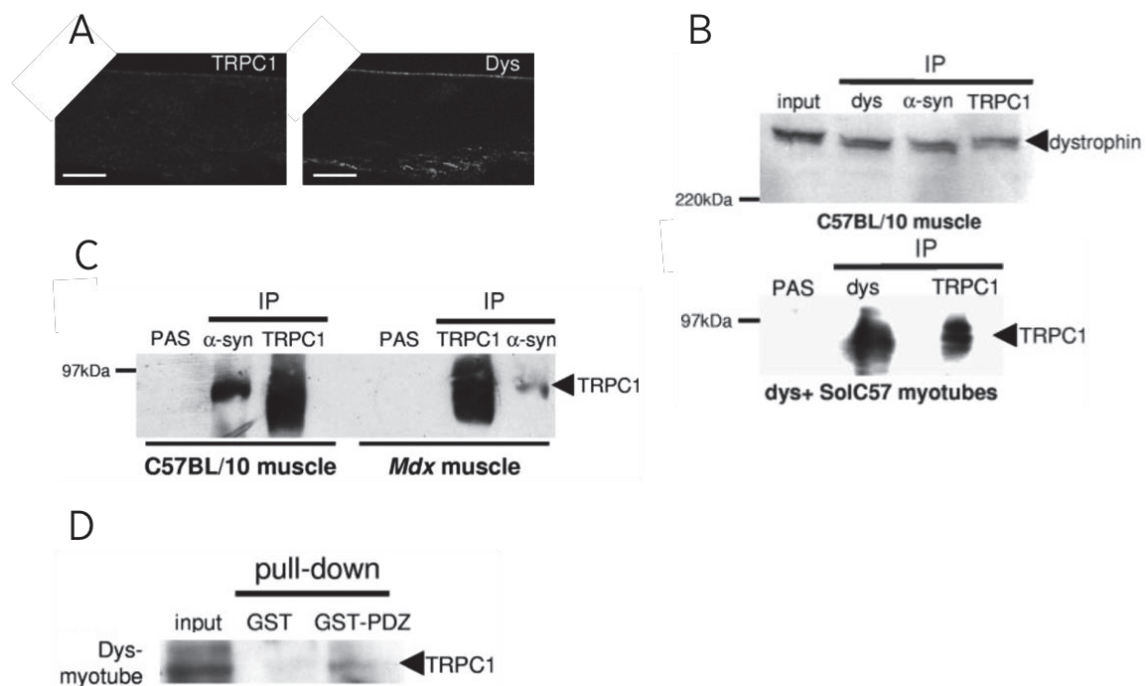


Figure 35 TRPC ion channels are associated with dystrophin and altered in *mdx* mice.

A: Immunostaining co-localization of TRPC1 and dystrophin (Dys) at the sarcolemma of cultured myotubes. Bar: 10 $\mu$ m. B: Co-association of TRPC1 with dystrophin and  $\alpha$ -syntrophin in wild-type mouse (C57BL/10) muscle (top) and with dystrophin in dystrophin-expressing myotubes (SolC57) culture (bottom). C:  $\alpha$ -syntrophin and TRPC1 co-immunoprecipitation from mouse muscle lysates in wild-type and *mdx* conditions. D: GST pull-down experiments showing the implication of the  $\alpha$ -syntrophin PDZ domain in its interaction with TRPC1 in cultured myotubes Adapted from [Vandebrouck et al., 2007](#).

Coimmunoprecipitation studies performed with both mice muscle fiber lysates (C57BL/10) and *in vitro* cultures of myotubes (SolC57) showed an association between dystrophin and the TRPC1 channel ([Figure 35 B](#)). The previously known interaction between dystrophin and  $\alpha$ -syntrophin was also observed ([Figure 35 B](#)). Furthermore, the



most explored hypothesis held that, as is the case with other ion channels in the sarcolemma, TRPC1 could interact with the PDZ domain of syntrophin. Then, Vanderbrouck *et al.* conducted co-immunoprecipitation studies to examine this interaction, employing lysates from both healthy muscle and *mdx* mice. As expected, it was observed that TRPC1 could precipitate with  $\alpha$ -syntrophin under both conditions ([Figure 35 C](#)). They concluded that, even in the absence of dystrophin,  $\alpha$ -syntrophin and TRPC1 were capable of binding together and conforming macro-complexes in the sarcolemma, although the amount of syntrophin is very reduced in *mdx* mice ([Vanderbrouck et al., 2007](#)). Finally, since most of the interactions of syntrophin with other ion channels in sarcolemma occurred through its PDZ domain, they wondered if this was also the case with TRPC1. For this purpose, they performed pull-down assays in which they took only the fragment containing PDZ domain of syntrophin and fused with GST (glutathione S-transferase), then incubated with myotubes lysates and revealed with antibodies against TRPC1. The results show a clear band corresponding to the channel when the fragment containing the PDZ domain is used ([Figure 35 D](#)). Thus, an association between TRPC1 and the PDZ domain of syntrophin was confirmed ([Vanderbrouck et al., 2007](#)).

## II. Implication of the DAPC in the regulation of SLO-1, a muscular BK channel in *C. elegans*

The group of ionic channels called BK (Big K<sup>+</sup>) constitute a class of potassium channels that are characterized by their large conductance and ability to allow high currents to pass through. These channels are reported to be dependent on the intracellular calcium level and also on voltage, being expressed in mammals in muscle and neurons. In *C. elegans*, there are two genes that code for homologues to these channels: *slo-1* and *slo-2*, both present in neurons and muscle in the worm ([Wang et al., 2001](#)). The first connection of these channels with DAPC was evidenced in the worm following the realization that the *slo-1* absence phenocopies the behavior of the dystrophin and other DAPC proteins mutants. Interestingly, *slo-1* mutant alleles were found in a genetic screen performed by L. Ségalat's team, where the purpose was to look for new alleles of genes having the same phenotype as the *dys-1* mutants. Two alleles were collected: *cx29* (436-bp deletion) and *cx42* (Leu to Trp missense mutation), both of which were mapped onto chromosome V ([Carre-Pierrat et al., 2006](#)). The phenotypes observed include hyperactivity, hypercontraction when the animals move backwards, as well as head-bending phenotype, typical of either dystrophin mutants or other components of DAPC. In addition, as occurs with *dys-1(cx18)*, *slo-1(cx29)* combined with *hlh-1(cc561)*, which is the counterpart of MyoD, shows signs of muscle degeneration ([Figure 36 A](#)).

The most plausible hypothesis to explain the fact that both *slo-1* and *dys-1* mutants have the same phenotype is that the absence of dystrophin causes the decrease or disappearance in muscle, since it has been proven that the SLO-1 phenotypes come from its absence in the muscle and not from the neurons ([Carre-Pierrat et al., 2006](#)). One way to check this is to look at the expression of *slo-1* in *dys-1* mutants, by quantifying mRNA through RT-PCR. This showed that there was no alteration in the amount of mRNA, which means that the absence of DYS-1 does not alter the rates of expression of the *slo-1* gene ([Carre-Pierrat et al., 2006](#)). In a further study, the location of SLO-1 in the *dys-1(cx18)* background was observed, which was done using a *slo-1::gfp* reporter gene expressed in the muscle under the promoter of the *slo-1* gene itself. The results show a clear decrease of SLO-1 in both dystrophin mutants and other DAPC proteins, such as syntrophin or dystrobrevin ([Figure 36 B](#)). ([Sancar et al., 2011](#)). Also, another study confirmed DYB-1 to be necessary for the correct localization of SLO-1 both in the body wall muscle and in the neurons of *C. elegans* ([Figure 36 C](#)). Finally, a very interesting fact is that SLO-1

depends on dystrobrevin also for a correct functioning, since *dyb-1* mutants seem to clearly suppress phenotypes observed in *gain of function* mutants of *slo-1*, which show defects especially in locomotion and egg laying ([Chen et al., 2011](#)).

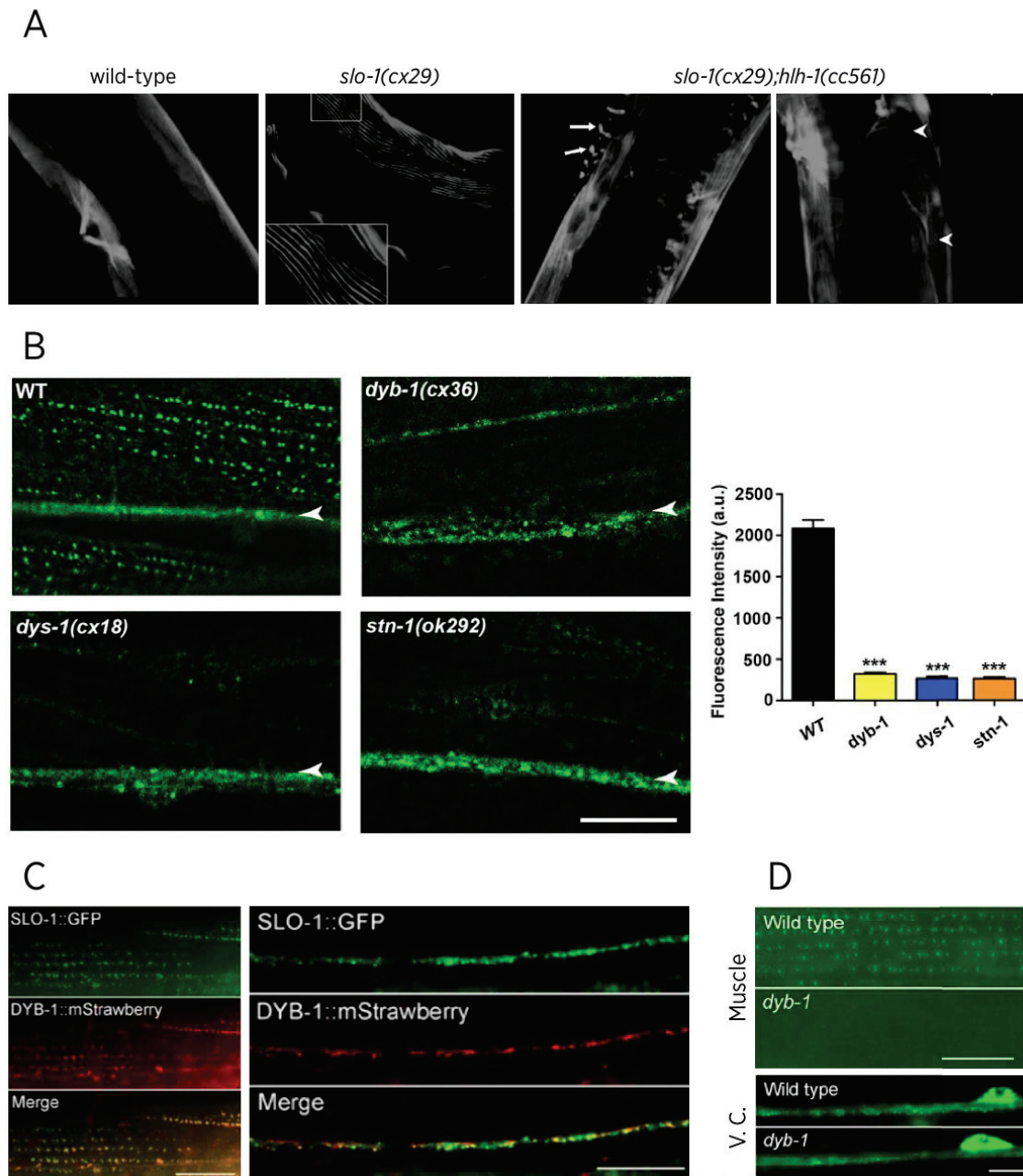


Figure 36 SLO-1, a BK channel in *C. elegans*, interact with DAPC proteins for its localization and function.

**A:** Phalloidin-rhodamine actin staining shows no muscle defect in the *slo-1(cx29)* single mutant but a clear degeneration when combining with the MyoD orthologue in the *slo-1(cx29);hll-1(cc561)* double mutant. Adapted from [Carre-Pierrat et al., 2006](#). **B:** An integrated translational fusion reporter showing the puncta distribution of SLO-1 in body wall muscle. SLO-1 expression is strongly reduced in dystrobrevin/*dyb-1*, dystrophin/*dys-1* and syntrophin/*stn-1* *lof* mutants. Adapted from [Sancar et al., 2011](#). **C:** SLO-1 and dystrobrevin/DYB-1 co-localize at the dorsal nerve chord. **D:** SLO-1 localization is lost in body wall muscle, but not in neurons, in *dyb-1* *lof* mutants. C and D are adapted from [Chen et al., 2011](#).



## RESULTS

**Part I: DAPC and PCP pathways organize asymmetric membrane domains of *C. elegans* muscles**

## **ABSTRACT**

The dystrophin-associated protein complex (DAPC) is a major structural actor in the costamere of vertebrates and invertebrates muscle cells. This complex is able to physically connect the actin cytoskeleton to the extracellular matrix (ECM), which is why generally it is assumed that the DAPC functions to ensure cell cytoskeleton-ECM cohesiveness. DAPC has been associated to different ion channels, such as voltage-sensitive sodium ( $\text{Na}_v$ ) and calcium ( $\text{Ca}_v$ ) channels, inward-rectifying potassium channels ( $\text{K}_{ir}$ ), and big potassium (BK) channels, in different models. Intriguingly, there are no studies in the literature linking DAPC with K2P potassium channels. Two-pore domain potassium (K2P) channels belong to a large and conserved potassium channels family, which is present in almost all animals cell types playing a key role in cell excitability. Here, we report an unexpected functional association between components of DAPC, such as dystrophin/DYS-1, syntrophin/STN-1 and dystrobrevin/DYB-1, and the muscular K2P channel TWK-28 in *C. elegans* muscle. Furthermore, we present a novel characterization of DAPC proteins whose pattern of expression and subcellular location were unknown, as is the case of sarcoglycans/SGCA-1 and SGCB-1. Interestingly, we also show that dystroglycan/DGN-1 is expressed in the body wall muscle of *C. elegans*, contrary to what was previously assumed. Finally, we demonstrate the involvement of WNT pathway proteins, such as Disheveled/DSH-1, as a regulatory mechanism for the polarity observed in TWK-28, providing an innovative example of planar cell polarity in *C. elegans* muscle.



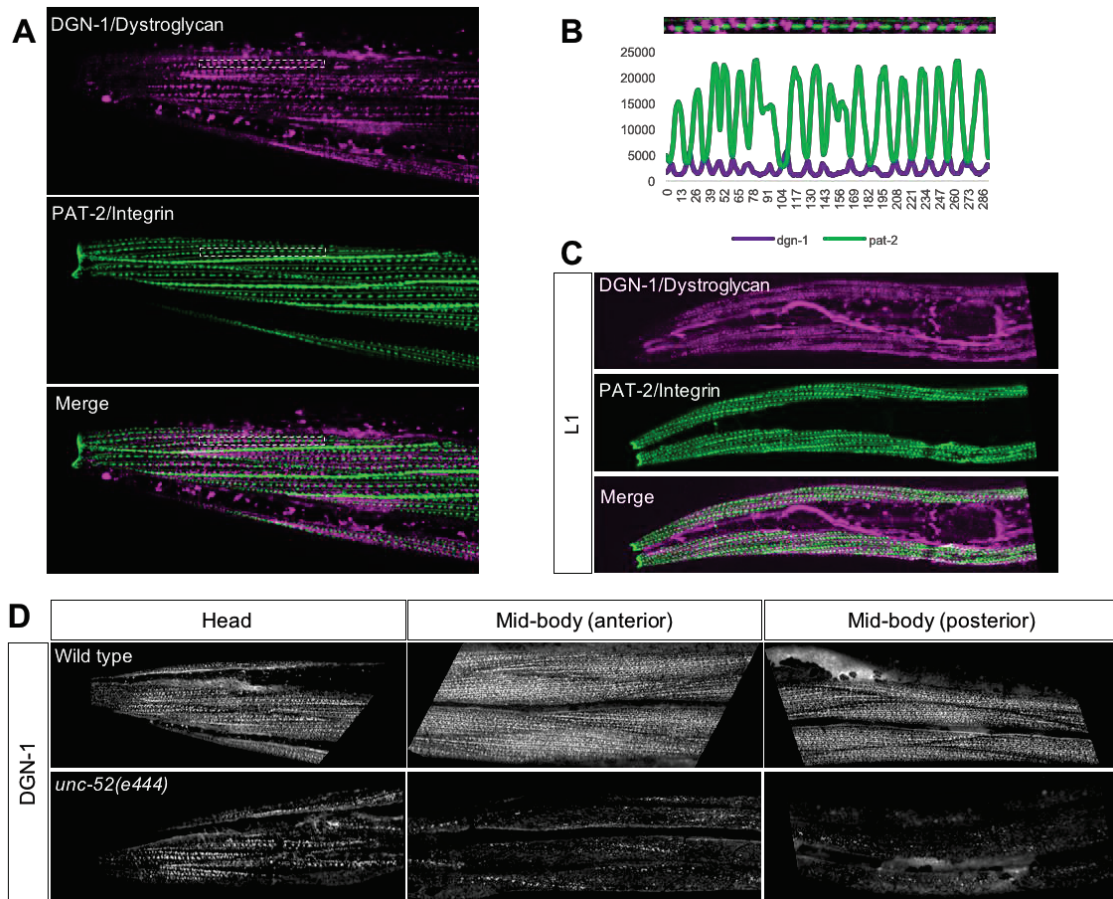
## **Part I: results (article in preparation)**

### **1. DGN-1/DG/Dystroglycan is expressed in *C. elegans* muscle**

In vertebrates, dystroglycan (DG) is a central component of the dystrophin-associated protein complex (DAPC) with a predominant structural role in the muscle. In *C. elegans*, dystroglycan was reported to be expressed in several different tissues, but surprisingly not in muscle cells ([Johnson et al., 2006](#)). However, recent single-cell RNAseq experiments detected significant muscle expression of *dgn-1*, one of the three worm Dystroglycan orthologues ([Cao et al., 2017](#)). To confirm this observation and determine the subcellular localization of DGN-1 in muscle, we used fluorescently-labeled protein fusions generated by CRISPR/*Cas9* gene editing. Contrary to previous findings, DGN-1 was clearly detectable in all body wall muscle cells, and exhibited a non-uniform subcellular localization ([Figure 1 A](#)). We used the dense body marker, PAT-2/integrin, as a cellular landmark to precisely identify DGN-1 localization. Double-labeling revealed that both proteins occupy distinct membrane domains, since DGN-1 was excluded from dense bodies and M lines occupied by PAT-2 ([Figure 1 B](#)). This localization pattern was already established in first stage larvae and maintained throughout development ([Figure 1 C](#)).

Dystroglycans interact with extracellular matrix proteins such as laminins and perlecan through their extracellular domain ([Talts et al., 1999](#)). We tested whether perlecan is also required in *C. elegans* for proper localization of DGN-1 using a viable isoform-specific nonsense allele of *unc-52*/Perlecan (*e444*), that eliminates perlecan isoforms expressed in all but the most anterior muscle cells. In these mutant worms, we observed a profound disruption of DGN-1 surface expression ([Figure 1 D](#)), confirming a conserved genetic link between dystroglycans and perlecan in worms.

The presence of dystroglycan/DGN-1 in *C. elegans* muscle prompted us to revisit the expression, localization and function of dystrophin-associated protein complex using state-of-the-art genetic approaches.



Results Fig. 1 DGN-1/Dystroglycan is expressed in *C. elegans* muscle and requires *unc-52*/perlecan for its surface localization

**A:** DGN-1 localizes to plasma-membrane domains devoid of integrins/PAT-2. Representative images of head muscle cells of DGN-1-wrmScarlet (in magenta) and PAT-2-GFP (in green) translational fusion knockin line. **B:** DGN-1 and PAT-2 occupy juxtaposed optically-separable microdomains. Enlargement of corresponding area in panel A (dashed box). Fluorescence profile of DGN-1 (purple) and PAT-2 (green). **C:** DGN-1 is expressed soon after hatching. Representative images of head muscle of DGN-1::wrmScarlet and PAT-2::GFP at the L1 stage. **D:** The mNeonGreen-tagged of *dgn-1* (from CGC) was used to analyze the localization of DGN-1 in wild-type (WT) and *unc-52(e444)* animals, at the muscle cells of the head, mid-body (anterior) and mid-body (posterior). Mislocalization of DGN-1 in all the muscle cells, except in the head, in the *unc-52* mutant, in compare with the wild type.

## 2. Sarcoglycans are expressed in *C. elegans* muscle and define novel plasma-membrane compartments

In addition to dystroglycans, sarcoglycans (SG) are the other major integral-membrane component of the dystrophin-associated protein complex (DAPC). The SG complex is composed of several sarcoglycan subunits (e.g.  $\alpha$ ,  $\beta$ ,  $\gamma$ ,  $\delta$ -sarcoglycans) in skeletal and cardiac muscles (Holt *et al*, 1998). The *C. elegans* genome encodes three sarcoglycans,

*sgca-1*, *sgcb-1*, and *sgn-1*, which are orthologues of  $\alpha$ -sarcoglycan,  $\beta$ -sarcoglycan, and  $\delta/\gamma$ -sarcoglycan, respectively ([Grisoni et al., 2002](#)). According to previous reports ([Kim et al., 2009](#)) and single-cell RNASeq data ([Cao et al., 2017](#)), all three sarcoglycans are expressed in worm muscles. To examine their subcellular localization, we tagged SGCA-1 and SGCB-1 with fluorescent proteins by CRISPR/*Cas9* gene editing. SGCA-1 and SGCB-1 were indeed expressed in body wall muscles ([Figure 2](#) A and B). Both sarcoglycans localized to the outer face of muscle cells (facing the epidermis) and exhibited a striking asymmetrical distribution pattern. Sarcoglycans occupy distinct membrane domains at the extremities of individual muscle cells. At the anterior tip of muscle cells, they form a dense domain that has a comet-like appearance ([Figure 2](#) A). This narrow portion of the cell contains no integrins ([Figure 2](#) A and B). It is followed by a gap that appears devoid of sarcoglycans, but SG are again visible in the posterior half of each cell. There, SG are organized in a linear pattern of regularly spaced punctate microdomains. Just as in the anterior domain, these puncta are clearly distinct from integrin-containing membrane domains. As for dystroglycan, this striking localization pattern was also visible in freshly-hatched first stage larvae ([Figure 2](#) C and D), albeit somewhat less obvious for the posterior domain. The dense anterior domain was however already visible soon after hatching.

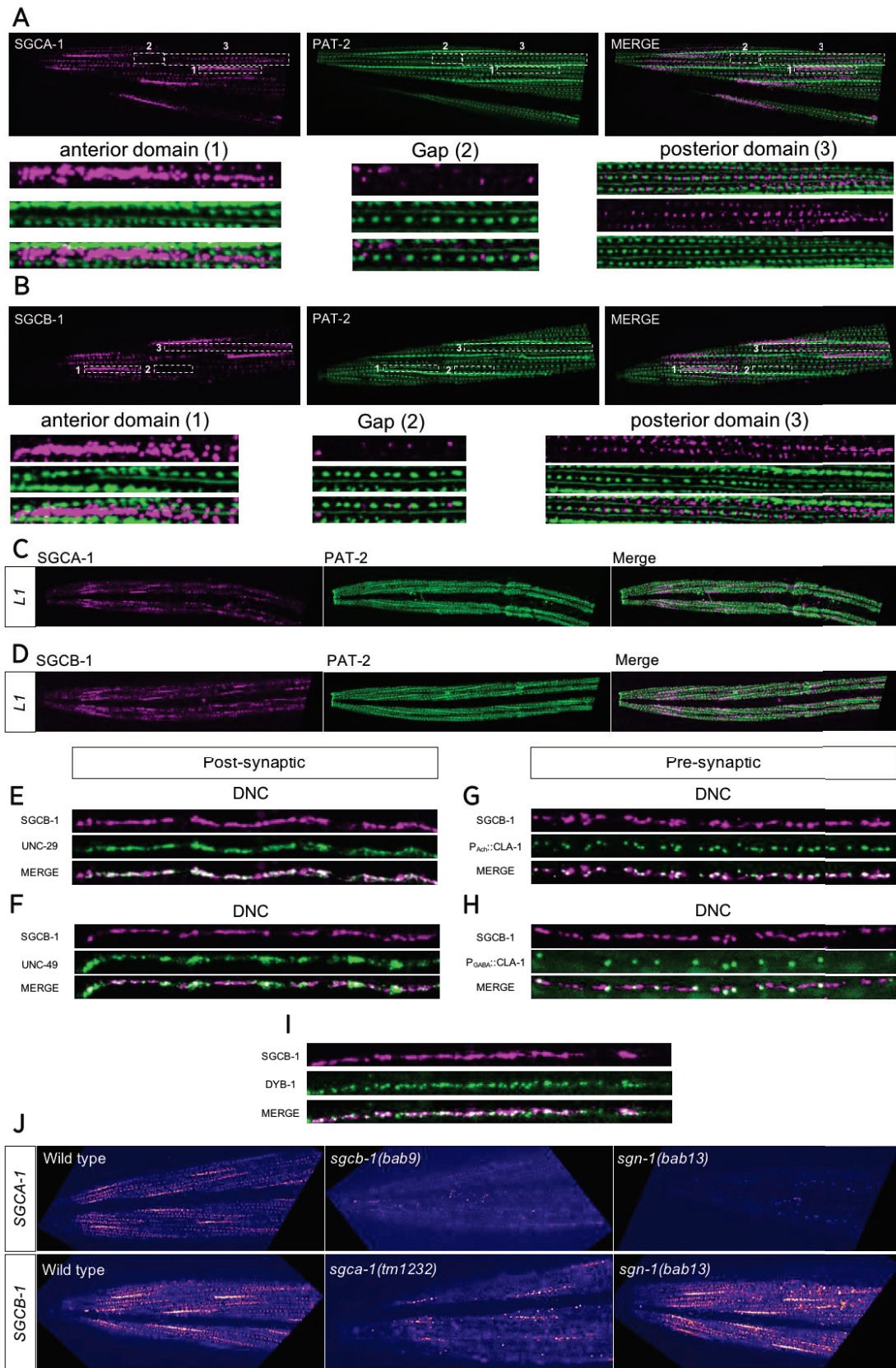
Interestingly, sarcoglycans were also enriched at neuromuscular junctions. We compared SGCB-1 localization with that of pre- and post-synaptic markers for cholinergic and GABAergic neuromuscular synapses. Using diffraction limited confocal microscopy, we found that SGCB-1 was present at cholinergic ([Figure 2](#) E) and GABAergic post-synaptic sites ([Figure 2](#) F). SGCB-1 was also systemically juxtaposed to the respective presynaptic domains ([Figure 2](#) G and H). In contrast, we could not detect SGCB-1 or SGCA-1 along the length of muscles arms suggesting that sarcoglycans are indeed closely associated with synaptic domains. Similarly, dystrobrevin/*dyb-1* was also enriched at the ends of muscle arms, suggesting an association of SG and dystrobrevins in this subcellular compartment ([Figure 2](#) I).

In vertebrates, assembly of individual sarcoglycan subunits into an oligomeric protein complex is necessary for trafficking to the plasma membrane of muscle cells. Loss of individual SG subunits strongly decreases SG complex formation and membrane targeting ([Holt et al., 1998](#)). However, SG subunits play distinct roles in this process. Indeed,  $\beta$ -sarcoglycan appears to initiate complex formation by associating with  $\delta$ -SG

([Shi et al., 2004](#)). We tested the interdependence of worm SG *in vivo* by combining fluorescently-labeled SG reporters with null mutants of individual sarcoglycan subunits. We observed that surface expression of SGCA-1 was strongly affected by the loss of *sgcb-1* or *sgn-1*. In contrast, loss of *sgn-1* did not visibly alter SGCB-1 surface expression, and SGCB-1 was not entirely disrupted in *sgca-1* null mutants. Indeed, while SGCB-1 was no longer detectable in the posterior half the cell, it could still be detected in the anterior tip, albeit at a lower level.

Taken together, these results suggest that the localization of SGCA-1 is dependent on the SGCB-1 and SGN-1 subunits, but that SGCB-1 may be able to properly traffic to the cell surface on its own or in association with SGCA-1. The localization of SGN-1 and its dependence on SGCA-1 and SGCB-1 remains to be investigated.





Results Fig. 2 Sarcoglycans define novel asymmetrical membrane compartments

A, B: SGCA-1 and SGCB-1 partition into distinct membrane domains at the anterior and posterior ends of muscle cells. *Anterior domain*, dense linear sarcoglycan domain at the tip of muscle cells, flanked by PAT-

2-containing membrane domains. *Gap*, absence of sarcoglycan. *Posterior domain*, clustered pattern aligned with but optically-separable from PAT-2-positive dense bodies.

Numbered dashed white boxes indicate corresponding regions of interest. **C, D**: SGCA-1 and SGCB-1 are expressed in muscle at birth, and form clusters at the tip of muscle cells. L1 stage larva. **E-H**: SGCB-1 is a synaptic protein, that co-localizes with cholinergic (*E*) and GABAergic (*F*) post-synaptic domains, facing corresponding pre-synaptic termini (*G, H*). **I**: DYB-1/dystrobrevin is clustered at neuromuscular junctions, with SGCB-1. **J**: Altered surface expression of SGCA-1 and SGCB-1 in sarcoglycan null mutants. DNC, dorsal cord.

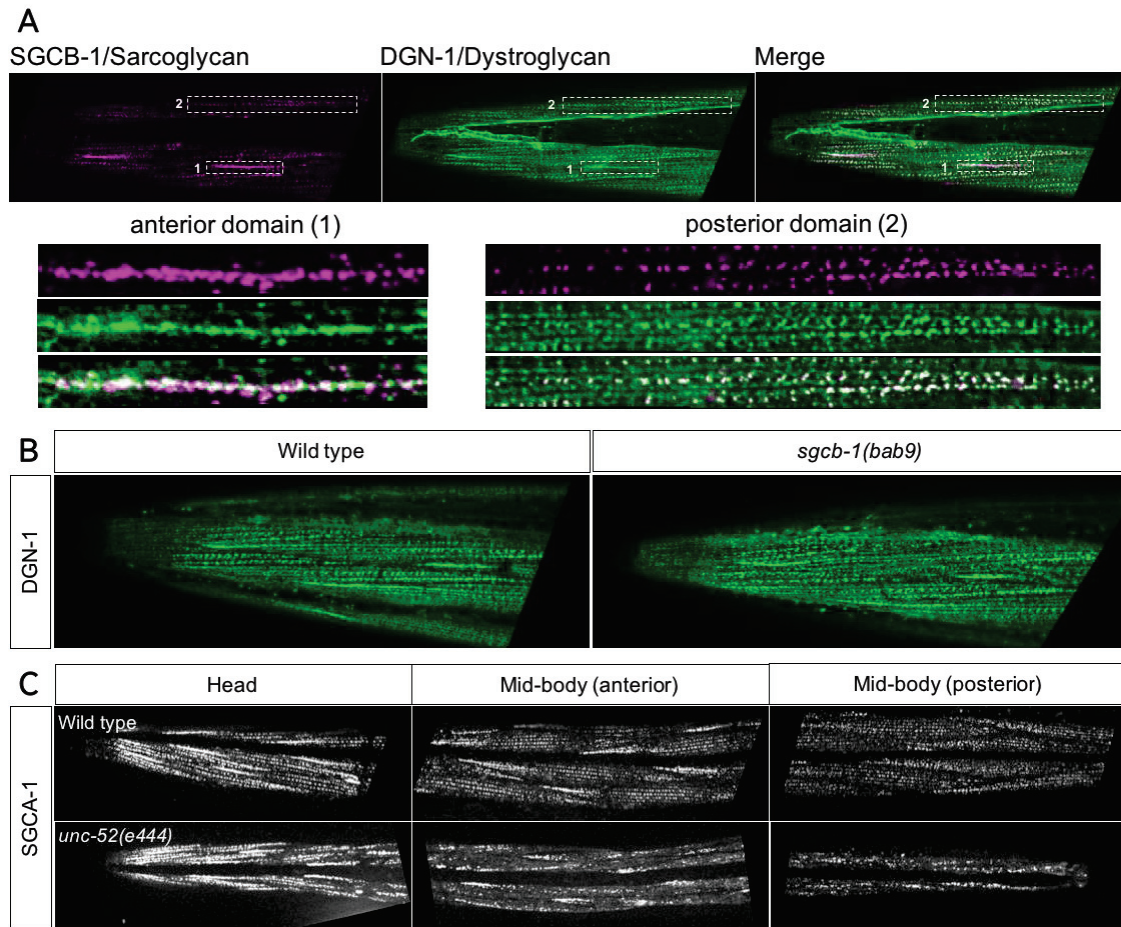
### 3. Interdependence of DG and SG in *C. elegans* muscle

Sarcoglycans are known to interact with dystroglycans during their trafficking to the muscle cell membrane (Noguchi *et al.*, 2000). Sarcoglycans may have an additional role in stabilizing the interaction that takes place between  $\alpha$ -dystroglycan subunit and the sarcolemma (Duclos *et al.*, 1998; Straub *et al.*, 1998).

In worm muscles, DGN-1/Dystroglycan and sarcoglycan localization patterns appeared different at first glance. For example, while DGN-1 was present all along the surface of the cell, SGCB-1 was only found in the tip and the posterior part of each cell. Furthermore, DGN-1 fluorescence appeared broad and generally uniform, while sarcoglycans formed either dense (anterior) or punctate (posterior) patterns. However, more detailed analyses revealed partial colocalization, in particular in the anterior tips of muscles cells, and also in the posterior section (Figure 3 A). In the tip, sarcoglycans fully co-localized with DGN-1, but DGN-1 puncta devoid of sarcoglycan were also visible. In the posterior domain, the clearly distinguishable sarcoglycan microdomains co-localized with puncta that were enriched in DGN-1, as compared to the remaining DGN-1 signal outside of sarcoglycan-containing microdomains. These patterns suggest an interesting interplay between dystroglycan and sarcoglycan domains and further illustrate the complexity of the worm's muscle plasma membrane.

Given the association of dystro- and sarcoglycans in vertebrates (Chan *et al.*, 1998; Noguchi *et al.*, 2000), we asked whether this was also the case in *C. elegans*. To this end, we compared the localization of DGN-1 in wild-type and *sgcb-1* null mutant backgrounds. We observed no clear differences between both genotypes (Figure 3 B), indicating that SGCB-1 is likely not needed to localize DGN-1 at the plasma membrane. However, we cannot rule out that this could result from the presence of SGN-1 proteins in this genetic background.

Conversely, we tested whether DGN-1 depletion altered sarcoglycan localization. Given the strong disruption of DGN-1 surface expression in *unc-52*/perlecan mutants (Figure 1 D), we used this mutant background as a proxy to test the impact of loss of DGN-1. Disruption of perlecan lead to an overall alteration of SGCA-1 localization which was more prominent in the posterior portion of muscle cells. The precise effects of DGN-1 depletion will need to be further investigated in the future using targeted tissue-specific degradation strategies, since null mutants of *dgn-1* are sterile (Johnson *et al.*, 2006).



Results Fig. 3 Partial overlap of dystroglycan and sarcoglycan membrane domains

**A:** DGN-1 and SGCB-1 patterns partly coincide in the anterior and posterior regions of muscle cells. Numbered dashed white boxes indicate corresponding regions of interest. **B:** DGN-1 localization is similar in wild type and *sgcb-1(bab9)* null mutants. **C:** SGCA-1 localization is partly disrupted in *unc-52(e444)* perlecan mutants. SGCA-1 localization appears wild-type in head muscles likely because of incomplete depletion of perlecan in *e444*, an isoform-specific nonsense mutant.

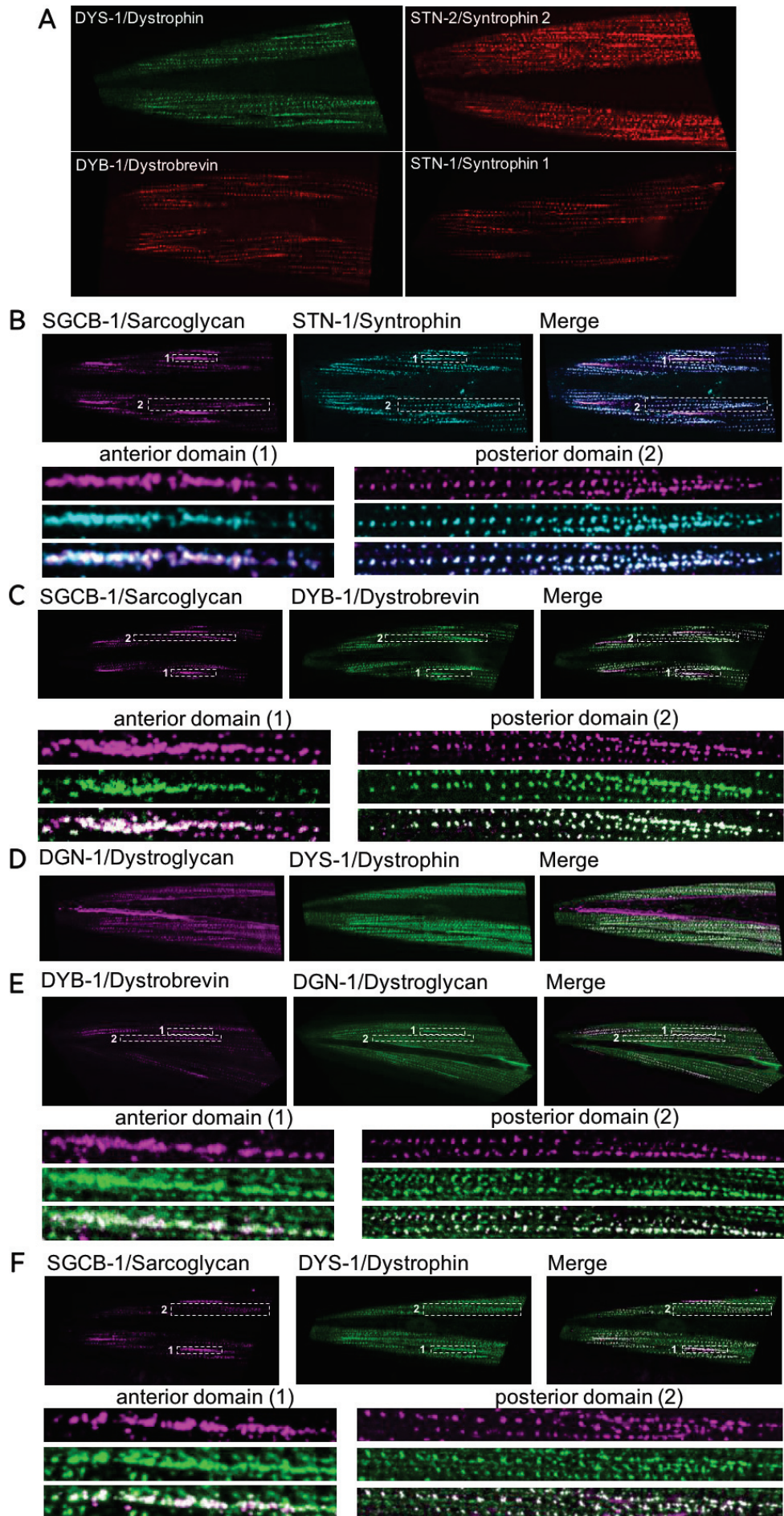
#### 4. DAPC components partition to DGN-1 or Sarcoglycan-containing domains



Cytoplasmic components of the dystrophin-associated protein complex are conserved in *C. elegans* ([Grisoni et al., 2002](#)). However, the subcellular localization of Dystrophin/DYS-1, Dystrobrevin/DYB-1, and the syntrophins STN-1 and STN-2 has not been compared to that of DGN-1 and sarcoglycans so far. We determined where each component was localized and whether they displayed distinct sub-cellular distributions in muscle cells by labeling them with fluorescent protein using CRISPR/*Cas9* gene editing ([Figure 4 A](#)).

All protein fusions were clearly visible in muscle cells and the *wrmScarlet* or *mNeonGreen* fluorophores did not alter protein function since we did not observe characteristic loss-of-function phenotypes ([Grisoni et al., 2002](#); [Gieseler et al., 1999b](#)). As for DGN-1 and sarcoglycans, DAPC components displayed two distinct and clearly recognizable localization patterns. DYS-1 and STN-2 were visible along the muscle surface in a pattern that was highly reminiscent of DGN-1 ([Figure 4 A](#)). In contrast, DYB-1 and STN-1 reproduced the characteristic pattern of sarcoglycans with three sub-compartments: a dense anterior domain, followed by a section without detectable fluorescence that transitioned into a posterior domain made of small punctate clusters ([Figure 4 A](#)).

A detailed analysis of the colocalization of these proteins confirmed the clear correspondence between sarcoglycans and DYB-1/STN-1 ([Figure 4 B and C](#)) on the one hand, and DGN-1 and DYS-1 on the other ([Figure 4 D](#)). Furthermore, cross-comparison of DGN-1 with DYB-1, and SGCB-1 with DYS-1 revealed the same type of partial colocalization patterns as for DGN-1 and SGCB-1 ([Figure 3 A](#) and [Figure 4 E and F](#)). Thus, DAPC components appear to mainly partition into two, partly overlapping, but distinct groups.



#### Results Fig. 4 DAPC components partition to DGN-1 or Sarcoglycan-containing domains

A: DYS-1, STN-2, DYB-1, and STN-1 display two distinct localization patterns. B, C: SGCB-1 co-localizes precisely with STN-1 and DYB-1. D: DGN-1 and DYS-1 co-localize precisely in muscle cells. E, F: Partial overlap of DGN-1/DYB-1 and SGCB-1/DYS-1. Numbered dashed white boxes indicate corresponding regions of interest.

### 5. Interdependence of DG/SG and individual DAPC components

While surface expression of dystroglycans is clearly dependent on interactions with extracellular matrix proteins such as perlecan ([Talts et al., 1999](#)), agrin ([Bowe et al., 1994](#)) or laminins ([Ervasti et al., 1993](#)), it also requires dystrophin ([Ishikawa-Sakurai et al., 2004](#)) and dystrobrevin ([Chung and Campanelli, 1999](#)). We thus tested whether this was also the case in *C. elegans* muscle.

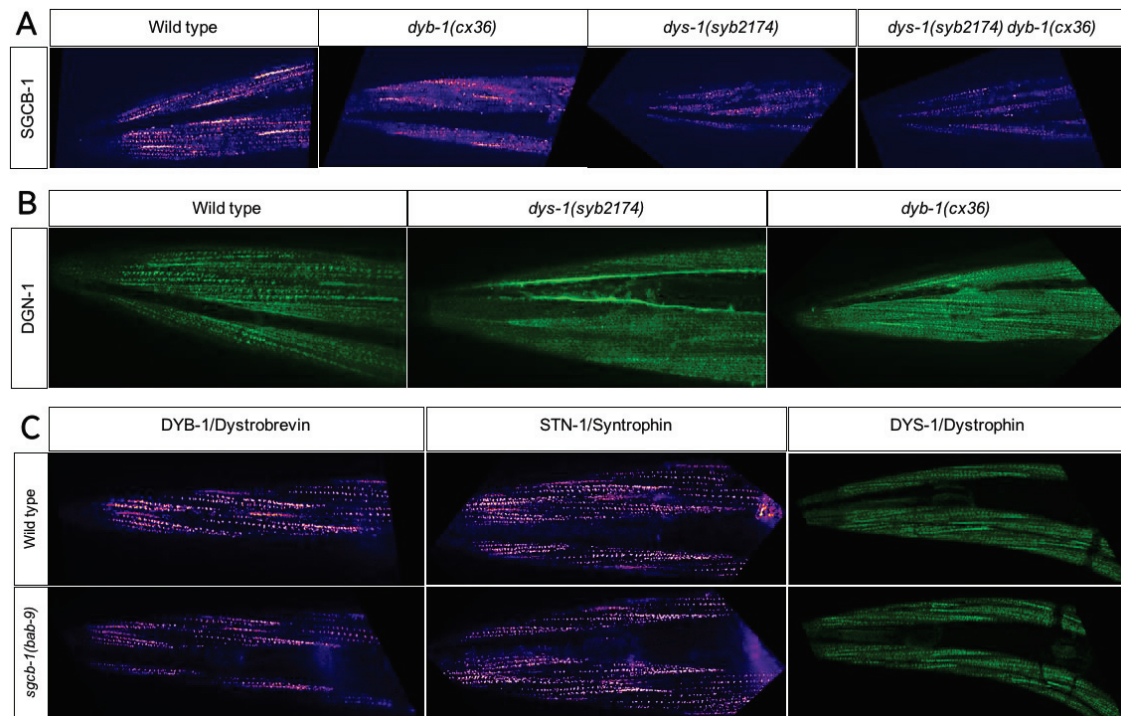
Indeed, we found alterations in SGCB-1 surface expression by depleting dystrobrevin and dystrophin, either individually or together ([Figure 5 A](#)). In *dyb-1* mutants, SGCB-1 surface expression was partly reduced in the anterior domain and essentially undetectable in the posterior punctate domain. Using a novel *knock-out* allele of *dys-1* that deletes the entire dystrophin locus (*syb2174*), we found that complete loss of dystrophin produced an even stronger reduction of SGCB-1 and modified the overall structure of the anterior domain, rendering it more diffuse. This pattern was also observed in the double mutant, suggesting a dominant role of DYS-1 over DYB-1.

Next, we repeated the same analysis for DGN-1. We did not observe any obvious modification of the dystroglycan pattern in dystrobrevin/*dyb-1* mutants. However, complete loss of *dys-1* reduced overall surface expression, disrupted the dense anterior domain, and rendered DGN-1 more diffuse ([Figure 5 C](#)).

Conversely, given their strict colocalization, we wondered whether loss of SGCB-1 would alter the localization of DYB-1 and STN-1, but observed no effect ([Figure 5 D](#)). The latter result was surprising given the known physical association of sarcoglycans and dystrobrevin, but could be due to the remaining presence of SGN-1, for which we don't have a reporter strain. Similarly, dystrophin localization did not appear to be affected by the loss of SGCB-1.

These results confirm the conserved links in *C. elegans* muscle between dystroglycan/DGN-1 and dystrophin/DYS-1 on the one hand, and sarcoglycan and dystrobrevin on the other. In the case of DGN-1/DYS-1, our results challenge previous

reports that suggested a lack of conserved protein-protein interaction motifs in DGN-1 (Johnson *et al.*, 2006).



Results Fig. 5 Sarcoglycan and Dystroglycan localization is dependent by the intracellular DAPC component

A: Loss of DYB-1 and DYS-1 differentially disrupts SGCB-1 localization. B: Loss of DYS-1, but not DYB-1, leads to reduced overall surface expression, disruption of the dense anterior domain, and diffuse DGN-1 localization through the muscle surface. C: Loss of SGCB-1 does not affect DYB-1, STN-1, or DYS-1 localization and expression levels.

## 6. Intricate localization of ion channels reveals a remarkably complex organization of worm muscle membranes

The striking asymmetric distribution patterns of DAPC proteins prompted us to revisit the exact localization of membrane proteins that have been previously associated with the DAPC.

The BK potassium channel SLO-1 was the first ion channel to be associated with the DAPC in *C. elegans* muscle (Carre-Pierrat *et al.*, 2006). A *knock-in* line expressing GFP-tagged SLO-1 (Oh *et al.*, 2017) revealed a remarkably asymmetric localization pattern. Indeed, SLO-1 channels formed a punctate pattern in the posterior half of each muscle cell that coincided with Sarcoglycans/SGCB-1 (Figure 6 A). However, SLO-1 was undetectable in the anterior tip of the cell which concentrates SGCB-1.



Next, we analyzed the localization of ISLO-1, an integral membrane protein that has been linked to the DAPC and binds SLO-1 ([Kim et al., 2009](#)). While ISLO-1's subcellular distribution indeed coincided with SLO-1 in the posterior part of the cell ([Figure 6 B](#)), ISLO-1 was also clearly enriched at the anterior tip ([Figure 6 F](#)), likely in the same pattern as DYB-1 and STN-1. Consistently, ISLO-1 has been shown to interact directly with STN-1 ([Kim et al., 2009](#)).

These observations encouraged us to investigate the distribution of ion channels in *C. elegans* muscle more systematically. We focused our attention on two-pore domain potassium (K2P) channels, the largest family of ion channels present in the *C. elegans* genome. Single-cell RNAseq data indicated that up to 12 different K2P channel subunits could be expressed in body wall muscle ([Cao et al., 2017](#)). We used previously published reporter strains (TWK-18; [El Mouridi et al., 2017](#)) and engineered additional knockin strains for 9 K2P channels (TWK-8, TWK-12, TWK-24, TWK-28, TWK-31, TWK-42, TWK-43, UNC-58, SUP-9) using CRISPR/*Cas9* genome engineering.

Careful analysis of these fluorescent reporters revealed a surprising diversity of situations. First, we confirmed that all of these channels were indeed expressed in body wall muscles, and that their relative fluorescence levels were generally consistent with transcriptomic data. Furthermore, the subcellular distribution patterns of these 10 channels were so characteristic that each channel could be unambiguously recognized by a naïve observer.

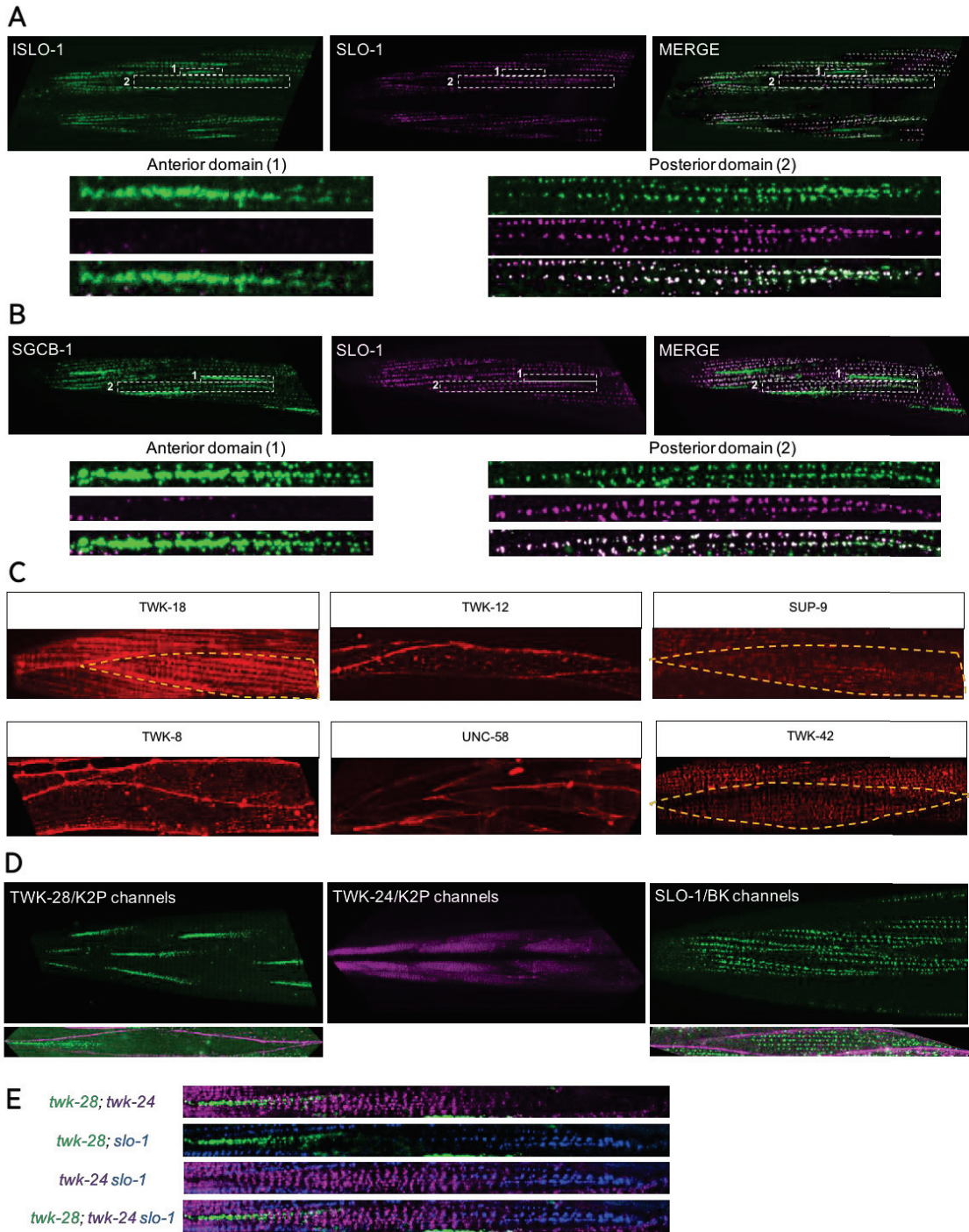
TWK-31 was only visible in unidentified intracellular compartments. TWK-8, TWK-43, and UNC-58 were uniformly distributed at the cell surface and in muscle arms. In contrast, TWK-12 was only found in muscle arms and on the lateral sides of body wall muscle cells, but not on the outer surface that is facing the hypodermis. Most other channels were enriched on this outer face. TWK-18, TWK-42, and SUP-9 showed distinct subcellular distribution patterns on the outer face, which were either diffuse (TWK-18) or punctate (TWK-42, SUP-9). Finally, TWK-24 and TWK-28 localizations were the most remarkable. Indeed, TWK-28 accumulated most prominently at the anterior tip of each muscle cell, forming a dense, “comet-like” structure ([Figure 6 C](#)). Furthermore, while TWK-24 channels initially appeared to be uniformly distributed, comparisons with TWK-28 and SLO-1 revealed that it was in fact absent from the extremities of the cell and enriched around its center ([Figure 6 C](#)). By combining reporter lines labeling SLO-1, TWK-24, and TWK-28, we found that these three potassium channels occupy almost perfectly distinct membrane domains on the outer face of muscle cells. These domains

could be clearly separated even using diffraction-limited confocal microscopy, arguing that the channels are all part of distinct protein complexes.

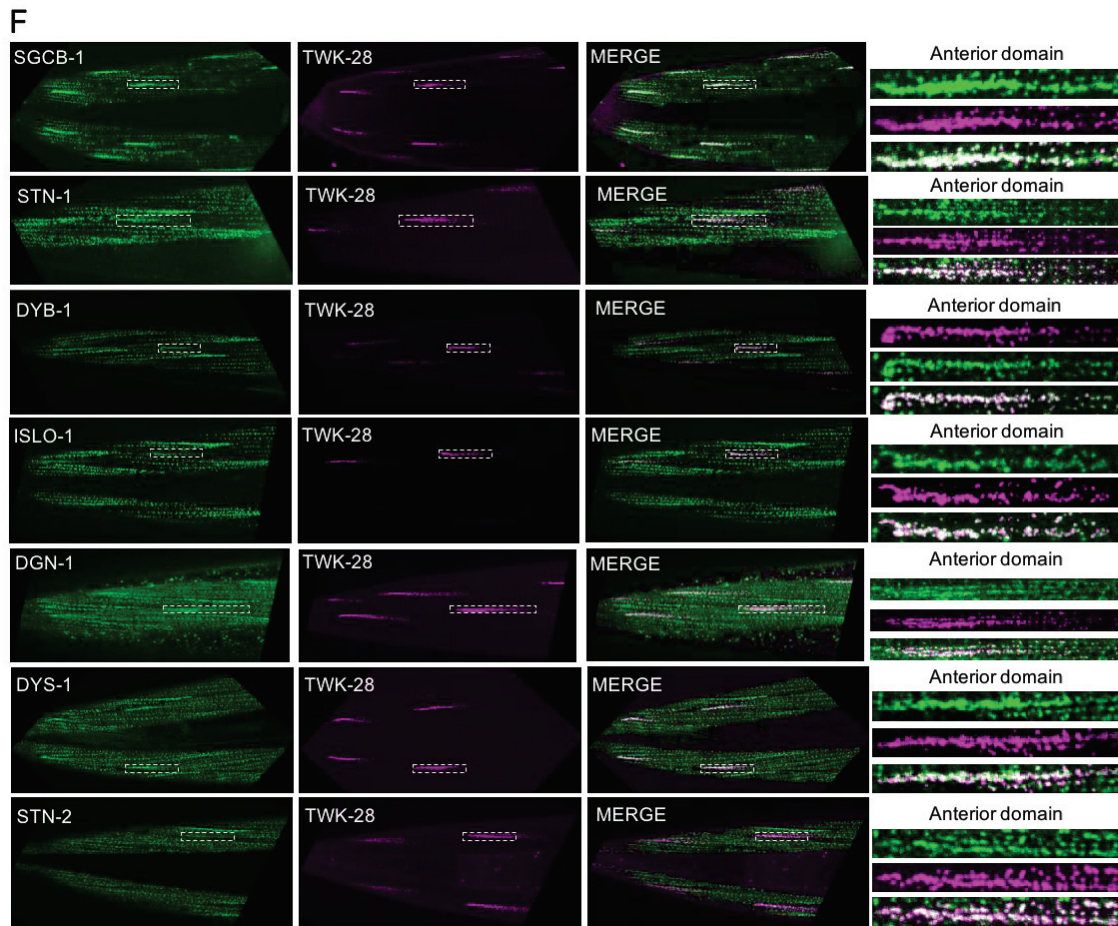
Taken together these results reveal the remarkably complex and an entirely unsuspected, three-dimensional, asymmetric makeup of the plasma membrane of *C. elegans* muscle cells.

The asymmetric pattern TWK-28 was immediately evocative of those of sarcoglycans, STN-1, DYB-1, and ISLO-1. Indeed, when we compared TWK-28 channels to these proteins, we found them to be perfectly co-localized in the anterior part of the cell ([Figure 6 E](#)). Furthermore, TWK-28 also coincided with the anterior domain of DGN-1, DYS-1, and STN-2, in a similar fashion to the colocalization of dystroglycan and sarcoglycan ([Figure 3 A](#)). As for SGCB-1, TWK-28 fluorescence was always contained within DGN-1, DYS-1, and STN-2 domains.

Based on their remarkable overlap, we hypothesized that sarcoglycans could be responsible for determining the localization of TWK-28 and SLO-1 channels. We therefore tested the effect of the single mutant of *sgcb-1* and *sgn-1* on TWK-28 and SLO-1 localization. We observed that loss of either sarcoglycan did not lead to obvious changes in TWK-28 and SLO-1 fluorescence levels, nor did it affect their asymmetrical localization ([supplement to Figure 6](#)). These results suggest that, at least individually, sarcoglycans SGCB-1 or SGN-1 are not necessary for localization of TWK-28 and SLO-1 potassium channels, despite their very clear colocalization pattern.







Results Fig. 6 Intricate localization of ion channels reveals remarkably complex organization of muscle plasma membranes

A: Asymmetric localization of SLO-1 in posterior part of muscle cells. ISLO-1 localization in anterior tip of muscle cell. Co-localization of SLO-1 and ISLO-1 exclusively in posterior domain. B: Precise co-localization of SGCB-1 and SLO-1 exclusively in posterior domain. C: Distinct distribution patterns of two-pore domain potassium channels TWK-18, TWK-42, TWK-8, TWK-12, SUP-9, and UNC-58. Translational knockin reporter lines. D: Asymmetric localization of TWK-28 (anterior) and TWK-24 (central), relative to SLO-1 (posterior). E: Distinct membrane localization patterns of TWK-28-mNeonGreen, TWK-24-wrmScarlet and SLO-1-TagBFP revealed using spectrally-distinct fluorophores. Numbered dashed white boxes indicate corresponding regions of interest. F: Colocalization pattern analysis of TWK-28 with SGCB-1, STN-1, DYB-1, ISLO-1, DGN-1, DYS-1, and STN-2.

## 7. DAPC is required for TWK-28 surface expression

To better understand the molecular and cellular machinery that recruits TWK-28 channels to the anterior tip of muscle cells, we performed an unbiased forward genetic screen. The rationale for this screen is based on the principle that disruption of factors that are required

to address TWK-28 channels to the cell surface would suppress the phenotypes caused by a hyperactive TWK-28 channel.

We recently demonstrated that the activity of vertebrate and invertebrate two-pore domain potassium channels can be tuned by mutating a single residue in the second transmembrane domain, named TM2.6 ([Ben Soussia et al., 2019](#)). We thus used CRISPR/*Cas9* gene editing to engineer a TWK-28 TM2.6 mutant with an L210T substitution. These mutants displayed strongly reduced locomotion, as expected for a mutation that would hyperactive a potassium channel and strongly decrease the excitability of muscle cells. This mutant served as an ideal starting point for our genetic suppression screen.

After screening over 15.000 mutagenized haploid genomes of TWK-28 L210T, we obtained 182 suppressors that had regained a near wild-type ability to move. Among these, 102 were extragenic revertants based on genetic segregation. Using whole genome sequencing for 25 of these 102 mutants. Remarkably, 14 out of these 25 extragenic suppressors affected *dys-1*. One mutant was an allele of *islo-1* ([Figure 7 A and B](#)).

To understand their impact on the surface expression of TWK-28, we combined *loss-of-function* mutations of these genes, in addition to *dyb-1* and *stn-1*, with the fluorescently-labeled TWK-28 reporter. In all cases we observed a marked reduction in the amount of TWK-28 channel. Fluorescence quantification demonstrated that *dys-1* mutants showed the strongest decrease, reducing fluorescence by  $\approx 80\%$ , followed by *islo-1* mutants ( $\approx 70\%$ ), *dyb-1* and *stn-1* mutants ( $\approx 55\%$  and  $\approx 53\%$ , respectively) ([Figure 7 C](#)).

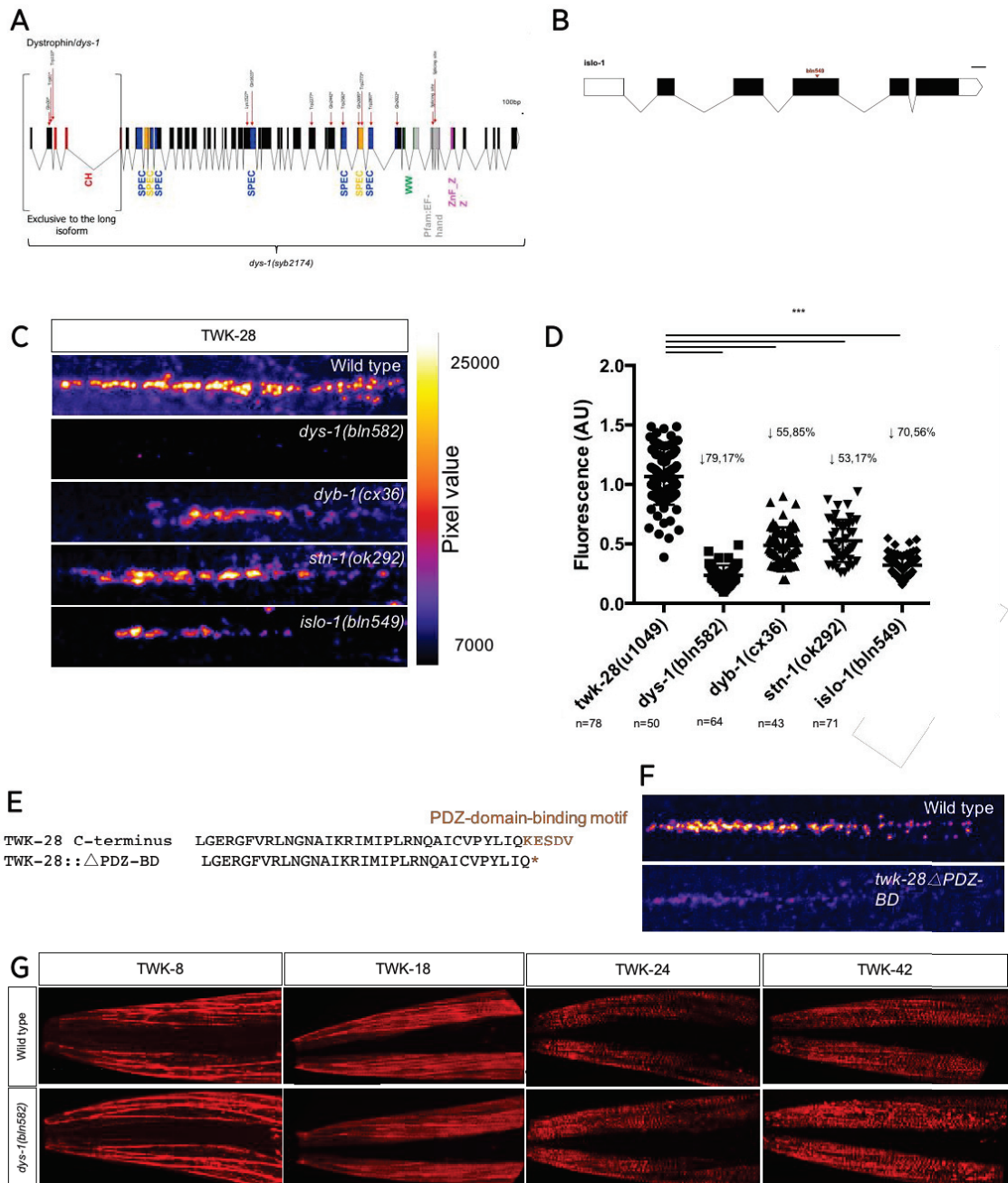
However, in all cases, remaining TWK-28 channels were still restricted to the anterior tip of muscle cells. One interpretation could be that TWK-28 channels were no longer tethered to the DAPC membrane scaffold and could now freely diffuse within the plane of the membrane. We considered this unlikely because it would in theory not reduce the total number of TWK-28 channels at the cell surface, yet, functional suppression of the TWK-28 *gain-of-function* phenotype argued for a reduction in the number of channels at the cell surface. Unless the localization of TWK-28 in its anterior position is necessary for its physiological effect.

Nevertheless, these results suggested that TWK-28 somehow interacted with the DAPC to be stabilized at the cell surface. Recruitment of voltage-gated sodium channels and inwardly-rectifying potassium channels by the DAPC are well-described example of the molecular interactions involved in ion channel regulation by the DAPC ([Connors et al., 2004](#); [Gavillet et al., 2006](#)). A short amino acid sequence in the cytoplasmic C-terminus

of Nav1.5 and Kir4.1 channels is recognized by the PDZ domain of syntrophin, which is itself bound to dystrophin and thus stabilizes these ion channels at the plasma membrane. Using PDZ domain-binding prediction algorithms, we identified such an amino acid sequence in the TWK-28 C-terminus ([Figure 7 E](#)). When we deleted these five amino acids by gene editing in the context of the TWK-28 fluorescent-reporter strain, we observed a dramatic reduction in the number of TWK-28 channels at the cell surface ([Figure 7 F](#)). This result argues for a model in which TWK-28 is directly recognized by one or both *C. elegans* syntrophins and is then stabilized at the plasma membrane by the dystrophin-associated protein complex.

To assess the specificity of the functional regulation of TWK-28 by the DAPC, we tested whether other muscle-expressed K2P channels would also be affected by loss of *dys-1*. None of the four channels we tested were, whether they were uniformly distributed (TWK-8, TWK-18, TWK-42), or asymmetrically localized (TWK-24). This result was further consistent with a lack of predicted PDZ-binding motifs in these for proteins ([Figure 7 G](#)).

Interestingly, in the case of SLO-1 channels, it is thought that ISLO-1 serves an adaptor to recruit SLO-1 to the DAPC, via its interaction with STN-1 ([Kim et al., 2009](#)). However, this model would also predict that SLO-1 should be present in the anterior tip of muscle cells, where ISLO-1 and STN-1 are found. Therefore, a specific factor or cellular mechanism remains to be identified that would prevent SLO-1 from accumulating there.



Results Fig. 7 TWK-28 localization is dependent by DAPC component

**A:** Dystrophin/*dys-1* gene structure. Mutant alleles isolated in TWK-28 *gain-of-function* genetic suppression screen are indicated above (red arrows). Protein domains are indicated below. *dys-1(syb2174)*, molecular null allele; 34-kbase deletion generated by CRISPR/Cas9 gene editing. **B:** *iso-1* gene structure and position of *bln549* allele in exon 3. **C:** Representative images of mNeonGreen-TWK-28 fluorescence in wild type, *dys-1(bln582)*, *dyb-1(cx36)*, *stn-1(ok292)* and *iso-1(bln549)*. **D:** Quantification of TWK-28-mNeonGreen fluorescence by confocal microscopy. **E:** Truncation of the PDZ-domain-binding motif at the TWK-28 C-terminus. **F:** Representative images of mNeonGreen-TWK-28 and mNeonGreen-TWK-28 $\Delta$ PDZ-BD. **G:** Uniformly distributed (TWK-8, TWK-18, TWK-42), or asymmetrically localized (TWK-24) K2P do not require DYS-1 (long-isoform) for surface expression and membrane localization.

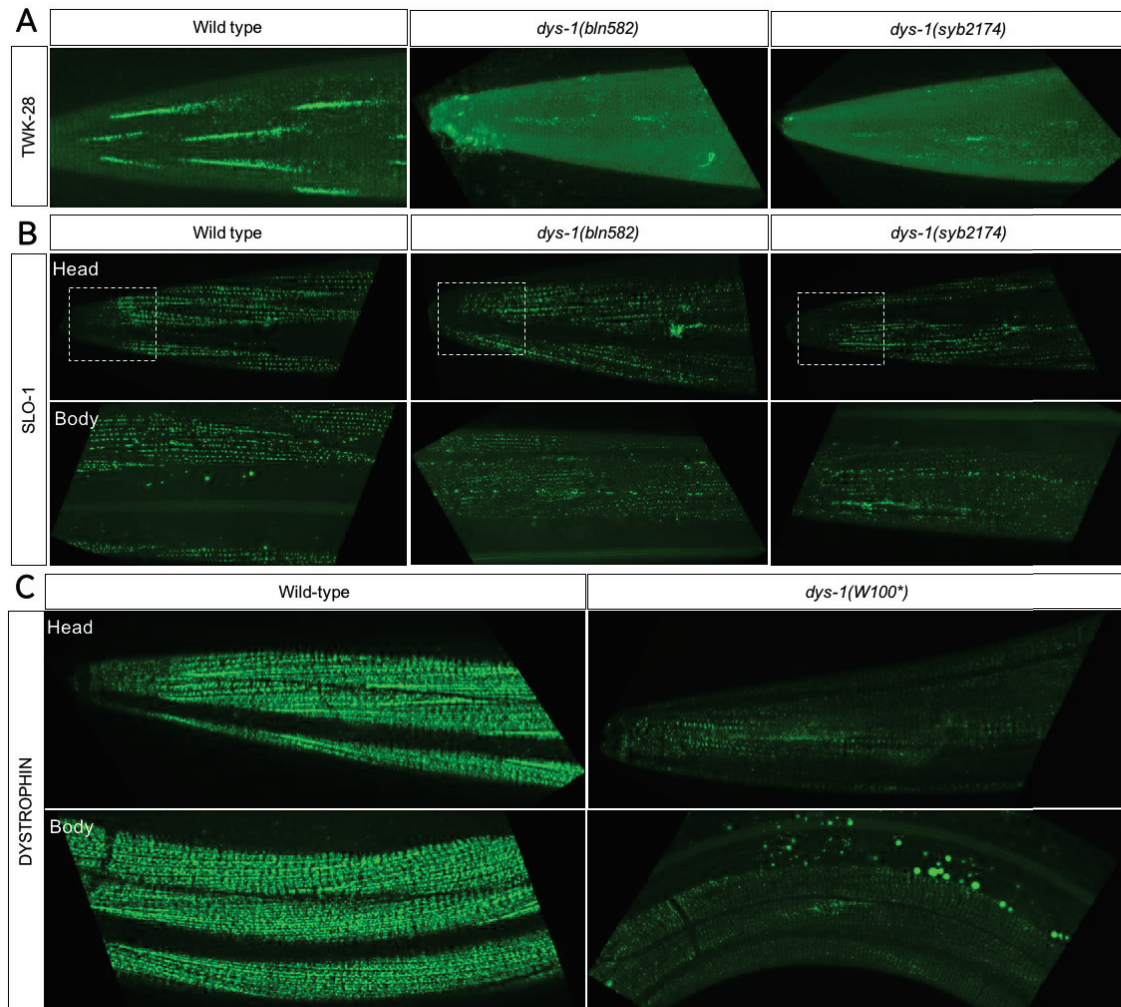
## 8. Differential roles of *dys-1* isoforms

The dystrophin locus of vertebrates and invertebrates encode multiple splice variants. Only the longest dystrophin isoforms contain the N-terminal domain that is thought to interact with the actin cytoskeleton (Figure 8 A). In our genetic screen, we obtained N alleles of *dys-1* with early stop codons within this domain (Figure 8 A). This argued that the long isoform is necessary for TWK-28 surface expression. Indeed, we observed an identical effect when the complete *dys-1(syb2174)* locus was deleted by CRISPR/Cas9 genome editing (Figure 7 A and Figure 8 B).

In contrast, for SLO-1 channels, the long-isoform mutants showed qualitatively different phenotypes compared to the molecular null. While both alleles, lead to a clear reduction in SLO-1 fluorescence in muscles all along the body of the worm (Figure 8 C, *Body*), SLO-1 was differentially affected in the most anterior muscle cells. These muscles have a characteristic cell shape, as they do not have an anterior tapered tip, but rather a straight edge, that abuts the most anterior hypodermal cells. In these most anterior head muscles, SLO-1 is nevertheless located in the posterior half of the cell, leaving a clear anterior void (Figure 8 C, *head, dashed box*). In long-isoform mutants, SLO-1 was displaced more anteriorly, closer to the tip of the nose. While it such a displacement was not obvious in the null mutant. This argued that different DYS-1 isoforms may have distinct roles in some *C. elegans* muscle cells to regulate the precise distribution of SLO-1 channels.

To investigate this question further, we engineered an early stop codon into the translational DYS-1 reporter gene. This mutation strongly reduced DYS-1 fluorescence but did not completely abolish it, arguing that the long isoform represents a major part of DYS-1 proteins in muscle (Figure 8 D). However, we could also observe a residual punctate pattern in the head muscles, which may indicate that shorter DYS-1 isoforms are expressed in these cells and may account for the displaced SLO-1 channels in long-isoform mutants.





Results Fig. 8 Different functions of *dys-1* isoforms for potassium channel localization

A: TWK-28 localization is equally affected in long-isoform-specific (*bln582*) or molecular null (*syb2174*) alleles. B: SLO-1 localization is differentially affected in the most anterior muscle cells in long-isoform-specific (*bln582*) versus molecular null (*syb2174*) alleles. Dashed boxes indicate region of interest. SLO-1 is equally disrupted by both mutant alleles in more posterior muscle cells. C: Differential expression and localization of full-length DYS-1 (*Wild-type*) and non-full-length isoforms (*W100\**)

## 9. A WNT pathway controls the asymmetric organization of TWK-28 channels

While our genetic screen allowed us to demonstrate a selective requirement of DAPC proteins for the surface expression of TWK-28 channels, it did not provide insights into the mechanisms that underlie the striking asymmetric distribution of the channel within each muscle cells. We thus considered a candidate gene approach to address this question.



The 95 *C. elegans* body wall muscle cells are organized into four symmetric muscle quadrants. Each quadrant, is composed of two rows of diamond-shaped muscle cells that line almost the entire length of the animal. These cell mono-layers are conceptually similar to the cellular structure of epithelia. Different molecular pathways generate tissue polarity in different cellular contexts. Generally, these involve Wnt ligand/receptor systems and specific proteins belonging to the core planar cell polarity (PCP) pathway. These mechanisms play a central role in orienting cells within epithelia, allowing them to generate repetitive asymmetric structures, such as in the bristled-wing of *Drosophila* ([Yang and Mlodzik, 2015](#)).

By analogy, we hypothesized that the polarized organization of TWK-28 could also result from the activity of such tissue polarity pathway. We therefore systematically tested available mutants for Wnt and planar cell polarity genes that are conserved in *C. elegans* ([Cravo and Heuvel, 2020](#)).

The intracellular effector protein *Disheveled* is a central player in these molecular cascades as it intervenes in canonical and non-canonical Wnt/b-catenin signaling, in addition to planar polarity pathways ([Mlodzik, 2016](#)). The *C. elegans* genome codes for three *Disheveled* orthologs: *dsh-1*, *dsh-2*, and *mig-5*. Based on single-cell RNASeq data, *mig-5* and *dsh-2* show little to almost undetectable expression in muscle cells, respectively, while *dsh-1* is strongly expressed ([Cao et al., 2017](#)). When we combined a *dsh-1* null mutant with the fluorescent TWK-28 knockin line, we observed a striking reorganization of the channels within muscle cells. Indeed, not only could we detect TWK-28 in the anterior tip of muscle cells, TWK-28 was now also present at the posterior end, in a perfectly symmetrical pattern ([Figure 9 A](#)). Indeed, Juxtaposed comets could be seen in a heads-to-tail orientation throughout the worm, except for the most anterior muscle cells.

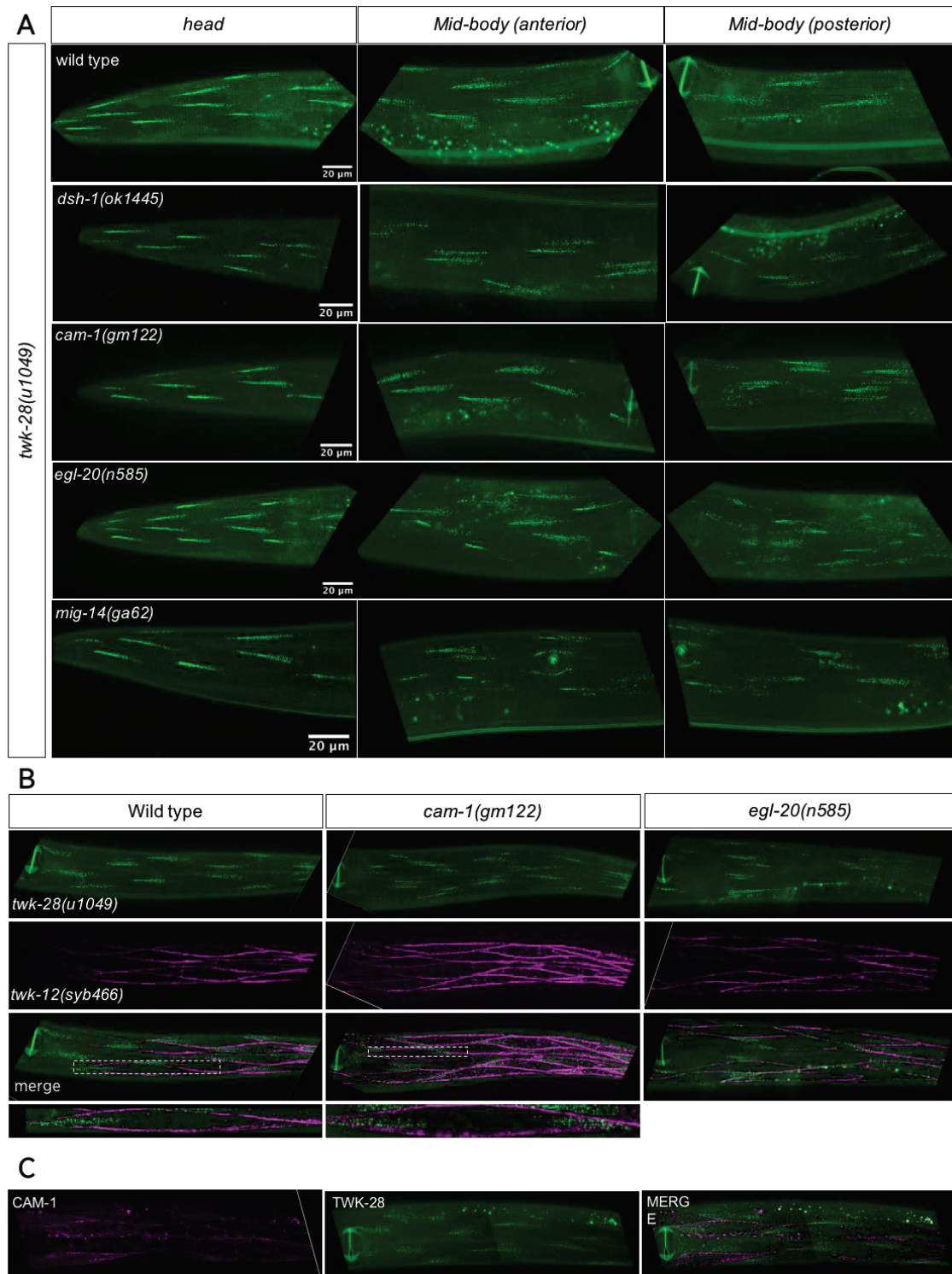
Next, we proceed to test the impact of the core PCP proteins, FMI-1/Stan/Flamingo and PRKL-1/Prickle. We observed no alterations comparable to *dsh-1/Dishevelled* in these mutants, except for rare instances of head-to-tail comets in the *prkl-1* mutant, which we did however not observe in a *fmi-1; prkl-1* double mutant ([supplement to Figure 9](#)). We could not test *vang-1* due to genetic linkage with *twk-28*.

We then tested three genes that belong to the less-well characterized Fat/Dachsous PCP pathway. As for the core PCP components, we saw no clear phenotypes with *cdh-1*, *cdh-3* and *cdh-4* mutants ([supplement to Figure 9](#)).

Given these results, we proceed to further explore the involvement of Wnt-dependent pathways. We first tested a viable *mig-14*/Wntless mutant to reduce secretion of all Wnt ligand at once. This mutation disrupted TWK-28 localization in a similar manner to *dsh-1* (Figure 9 A). We then proceeded to test available null mutants for four Wnt ligands. Among these, only loss of *egl-20* altered TWK-28 localization (Figure 9 A and B). This effect was restricted to cells that are present posteriorly to the vulva, which could be consistent with the graded distribution of EGL-20 from the tail to the mid-body of the worm (Pani and Goldstein, 2018). Mutants of *cwn-1*, *cwn-2*, and *lin-44* had no effect (Supplement to Figure 9).

Finally, we tested two transmembrane proteins that bind Wnt ligands: the frizzled receptor LIN-17, and the tyrosine kinase CAM-1/Ror. LIN-17 (in combination with a mutant of the the *lin-44* Wnt ligand) had no effect (Supplement to Figure 9), while the canonical *cam-1* allele *gm122* clearly altered the subcellular localization of TWK-28 (Figure 9 A and B). Interestingly, *cam-1* mutants phenocopy *egl-20*/Wnt mutant as they only alter TWK-28 comets in the posterior half of the animal. To confirm this result, we tested two additional *cam-1* alleles that showed an identical phenotype to *gm122* (supplement to Figure 9 B). As for Wnt ligands, the remaining Frizzled orthologs and Wnt receptors, MOM-5, MIG-1, CFZ-2, and LIN-18/Ryk, could be involved in controlling TWK-28 distribution in the anterior part of the body.

Taken together, these results reveal a series of factors that intervene in complex, and not fully resolved cellular mechanism to control the asymmetric distribution of TWK-28 in *C. elegans* body wall muscle cell. Further experiments will be needed to (i) test the possible implication of the core PCP component VANG-1/ Van Gogh/Strabismus, (ii) identify the ligands and receptors that control TWK-28 asymmetry in the muscle cells of the anterior half of the worm, (iii) determine the output of the EGL-20/CAM-1/DSH-1 signaling cascade, in particular whether it acts through a canonical Wnt/ $\beta$ -catenin pathway. Given the uniform localization of CAM-1 at cell surface (Figure 9 C), we will also determine the subcellular localization of DSH-1, as it may be the asymmetric component in this context.



**Results Fig. 9 A Wnt pathway controls the asymmetric organization of TWK-28 channels**

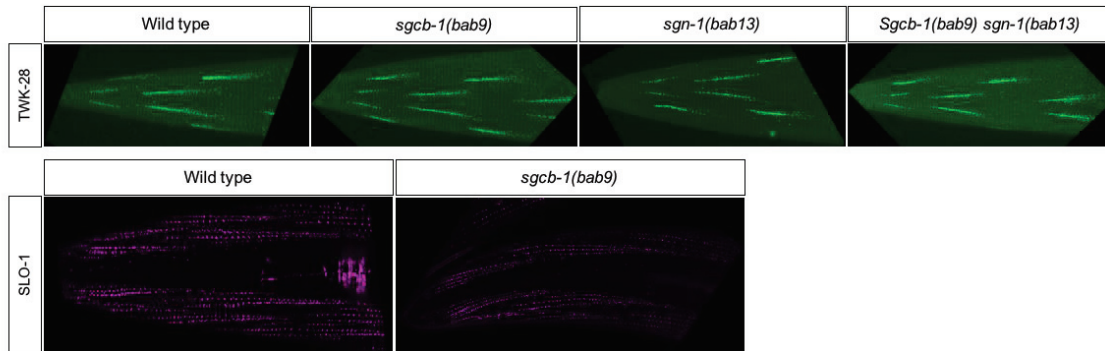
A: Representative images of mNeonGreen-TWK-28 (*u1049*) localization in muscles of the head, and anterior and posterior mid-body of wild type, Dishevelled *dsh-1(ok1445)*, ROR *cam-1(gm122)*, Wnt *egl-20(n585)* and Wntless *mig-14(ga62)*. Juxtaposed TWK-28 containing domains are visible along the body of worm in *dsh-1(ok1445)* and *mig-14(ga62)* mutants, but only in the posterior mid-body of *cam-1(gm122)* and *egl-20(n585)*. B: Muscle contours labeled by TWK-12-wrmScarlet translation fusion knockin strain.

Dashed white boxes indicate corresponding regions of interest magnified below. **C**: Uniform, non-symmetric distribution of CAM-1/ROR at the surface of muscle cells.

# ANNEXES

Supplement figures:

## Supplement to fig. 6

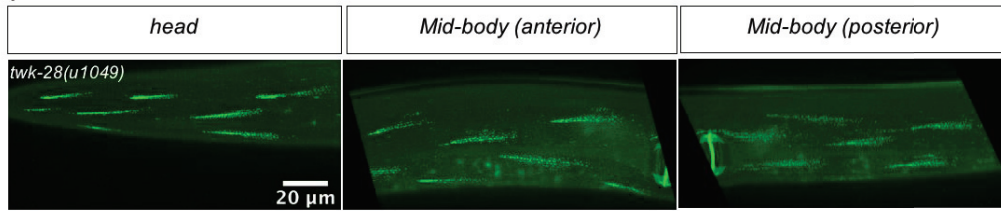


Supp. Fig. 1 Loss of SGCB-1 and/or SGN-1 are not required for TWK-28 or SLO-1 surface expression.

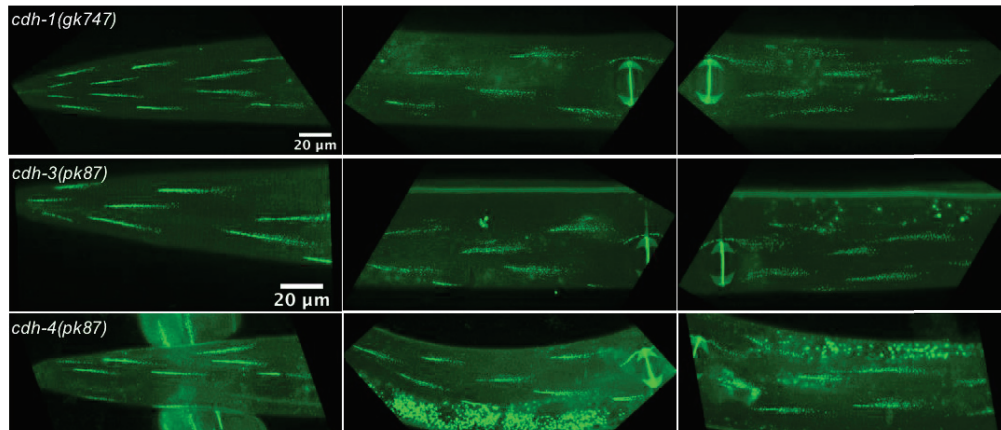


Supplement to fig. 9

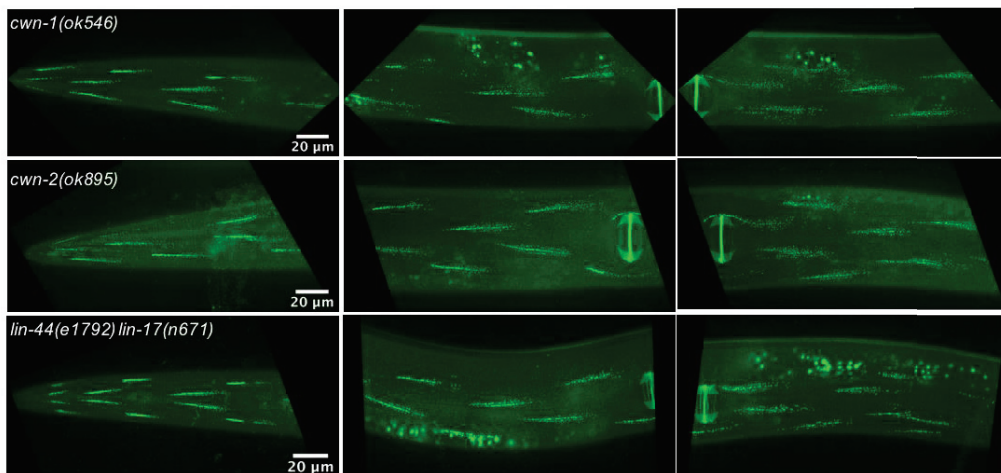
A



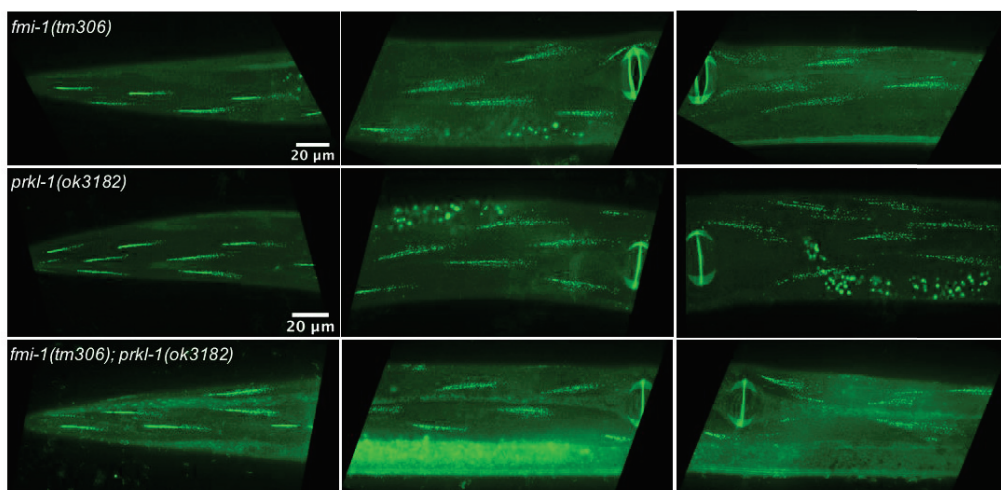
**CADHERIN, THE FAT/DACHSOUS PATHWAY**



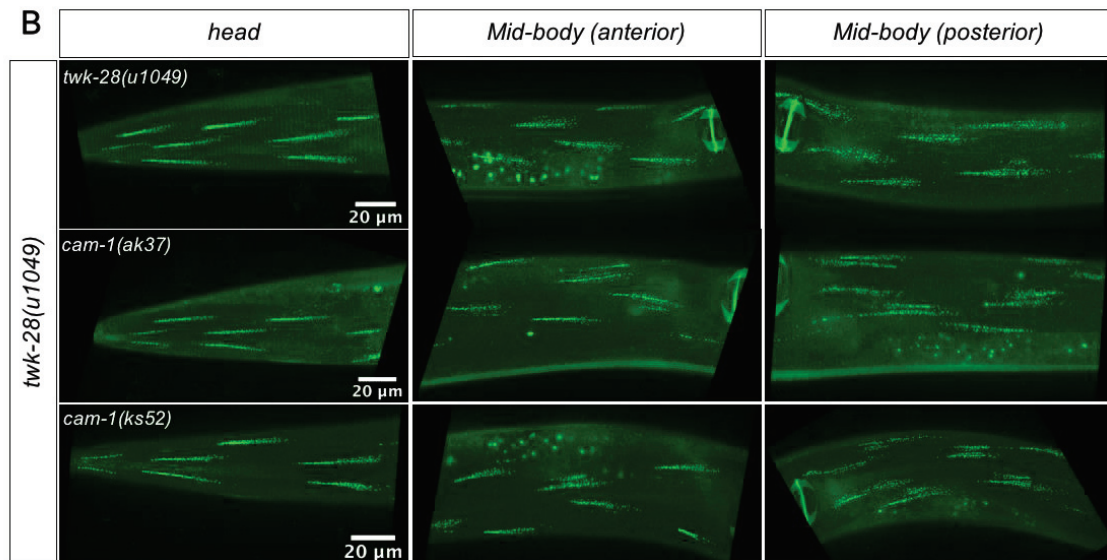
**WNT LIGANDS**



**PLANAR CELL POLARITY COMPONENTS**







Sup Fig. 2 Wnt ligands, a Wnt receptor and planar cell polarity pathway components are not required for asymmetric localization of TWK-28 in muscle cells

A: Representative images of muscles of the head, and the anterior and posterior mid-body showing wild type mNeonGreen-TWK-28 localization in mutants of *C. elegans* orthologs of Cadherin/Fat/Dachsous pathway components (*cdh-1*, *cdh-3*, *cdh-4*), Wnt ligands (*cwn-1*, *cwn-2*, *lin-44*), a Wnt receptor (*lin-17*), and planar cell polarity core components (*fmi-1*, *prkl-1*). B: *cam-1(ak37)* and *cam-1(ks52)* disrupt TWK-28 localisation in muscles of the posterior mid-body.

**Part II: Mutation of a single residue promotes gating of  
vertebrate and invertebrate two-pore domain potassium  
channels**

ARTICLE

<https://doi.org/10.1038/s41467-019-08710-3>

OPEN

# Mutation of a single residue promotes gating of vertebrate and invertebrate two-pore domain potassium channels

Ismail Ben Soussia<sup>1</sup>, Sonia El Mouridi<sup>1</sup>, Dawon Kang<sup>2</sup>, Alice Leclercq-Blondel<sup>1</sup>, Lamyaa Khoubza<sup>3</sup>, Philippe Tardy<sup>1</sup>, Nora Zariohi<sup>1</sup>, Marie Gendrel<sup>1</sup>, Florian Lesage<sup>3</sup>, Eun-Jin Kim<sup>2</sup>, Delphine Bichet<sup>3</sup>, Olga Andrini<sup>1</sup> & Thomas Boulin<sup>1</sup>

Mutations that modulate the activity of ion channels are essential tools to understand the biophysical determinants that control their gating. Here, we reveal the conserved role played by a single amino acid position (TM2.6) located in the second transmembrane domain of two-pore domain potassium (K2P) channels. Mutations of TM2.6 to aspartate or asparagine increase channel activity for all vertebrate K2P channels. Using two-electrode voltage-clamp and single-channel recording techniques, we find that mutation of TM2.6 promotes channel gating via the selectivity filter gate and increases single channel open probability. Furthermore, channel gating can be progressively tuned by using different amino acid substitutions. Finally, we show that the role of TM2.6 was conserved during evolution by rationally designing gain-of-function mutations in four *Caenorhabditis elegans* K2P channels using CRISPR/Cas9 gene editing. This study thus describes a simple and powerful strategy to systematically manipulate the activity of an entire family of potassium channels.

<sup>1</sup>Institut NeuroMyoGène, Univ Lyon, Université Claude Bernard Lyon 1, CNRS UMR 5310, INSERM U1217, Lyon 69008, France. <sup>2</sup>Department of Physiology, College of Medicine and Institute of Health Sciences, Gyeongsang National University, Jinju 52727, South Korea. <sup>3</sup>Institut de Pharmacologie Moléculaire et Cellulaire, LabEx ICST, CNRS UMR 7275, Université de Nice Sophia Antipolis, Valbonne 06560, France. These authors contributed equally: Ismail Ben Soussia, Sonia El Mouridi. Correspondence and requests for materials should be addressed to O.A. (email: [olga.andrini@univ-lyon1.fr](mailto:olga.andrini@univ-lyon1.fr)) or to T.B. (email: [thomas.boulin@univ-lyon1.fr](mailto:thomas.boulin@univ-lyon1.fr))

Two-pore domain potassium (K2P) channels play a central role in the regulation of cellular excitability and the establishment of the membrane potential in excitable and non-excitable cells<sup>1</sup>. This ancient ion channel family has been widely conserved during evolution. Genes encoding K2P channel subunits are found in the genomes of yeast, plants, vertebrates, and invertebrates. Fifteen and eleven genes encoding channel subunits are found in the human and *Drosophila melanogaster* genomes, respectively<sup>2</sup>. Strikingly, a large expansion of the K2P channel gene family has occurred in the model nematode *Caenorhabditis elegans*<sup>3</sup>. While the overall number of genes encoding potassium channel subunits does not differ significantly (approx. 80 in man vs. 70 in *C. elegans*), more than half of these genes (47) encode two-pore domain potassium channel subunits. Interestingly, while all K2P channels share a characteristic topology and domain structure, sequence conservation at the amino acid level is generally low except for closely-related paralogs. Therefore, analyzing sequence diversity in vertebrate and invertebrate K2P channels can offer interesting insights into the key molecular determinants that make up the functional core of this large ion channel family.

Studies aiming to dissect the gating mechanisms of K2P channels have relied on the identification of residues that modify channel activity when mutated. Yeast selection assays<sup>4</sup>, targeted mutagenesis<sup>5–11</sup>, and genetic screens<sup>5,6</sup> have highlighted different amino acid positions that increase channel activity for various K2P channels. Pathogenic mutations have also revealed residues such as the TALK2 G88R mutation which increases channel function and causes a severe and progressive cardiac conduction disorder<sup>7</sup>. Unfortunately, since these mutations affect residues situated in very different parts of the channel (transmembrane domains, pore loops, extracellular, and cytoplasmic regions) and are rarely conserved in all K2P channels, no single residue has so far emerged that could play a conserved role in the control of K2P channel gating.

Interestingly though, we and others have shown that mutations in one position of the second transmembrane segment (further referred to as TM2.6, see results below) have consistent effects in three vertebrate and one invertebrate channel. First, mutation of a glycine residue in *Drosophila* KCNK0/ORK1 was serendipitously found to maximize channel open probability<sup>8</sup>. Next, mutation of a leucine residue at the equivalent position was shown to increase the activity of TWIK1<sup>9</sup>. Finally, mutation of isoleucine in THIK1 and THIK2 similarly increased whole-cell current levels<sup>10</sup>. Based on crystal structures and sequence alignments, these four residues are positioned on the intracellular face of the second transmembrane domain, exposed to the cytoplasmic vestibule, and in close proximity with the intracellular part of the selectivity filter<sup>12–15</sup>. Although the exact mechanism by which these mutations increase channel activity remains to be fully understood, this position nevertheless appeared as a promising candidate for a residue that could play a conserved role in most if not all K2P channels.

In this study, we have combined two-electrode voltage-clamp electrophysiology in *Xenopus* oocytes, single-channel recording in cultured cells, and CRISPR/Cas9 gene editing in *C. elegans* to demonstrate the functional conservation of TM2.6 in vertebrate and invertebrate two-pore domain potassium channels. We show that all vertebrate K2Ps can be activated by mutating TM2.6. These mutations dramatically increase channel activity and in particular single-channel open probability. Consistently, mutating the homologous residue in four *C. elegans* K2P channels elicited behavioral phenotypes that were comparable to those of known gain-of-function mutants. Finally, by building allelic series in *C. elegans* and for channels expressed in *Xenopus* oocytes, we could further demonstrate that channel activity can be progressively

tuned by using different TM2.6 amino acid substitutions. Taken together, these results demonstrate that the TM2.6 position plays an important and well-conserved role in the gating of many if not all two-pore domain potassium channels.

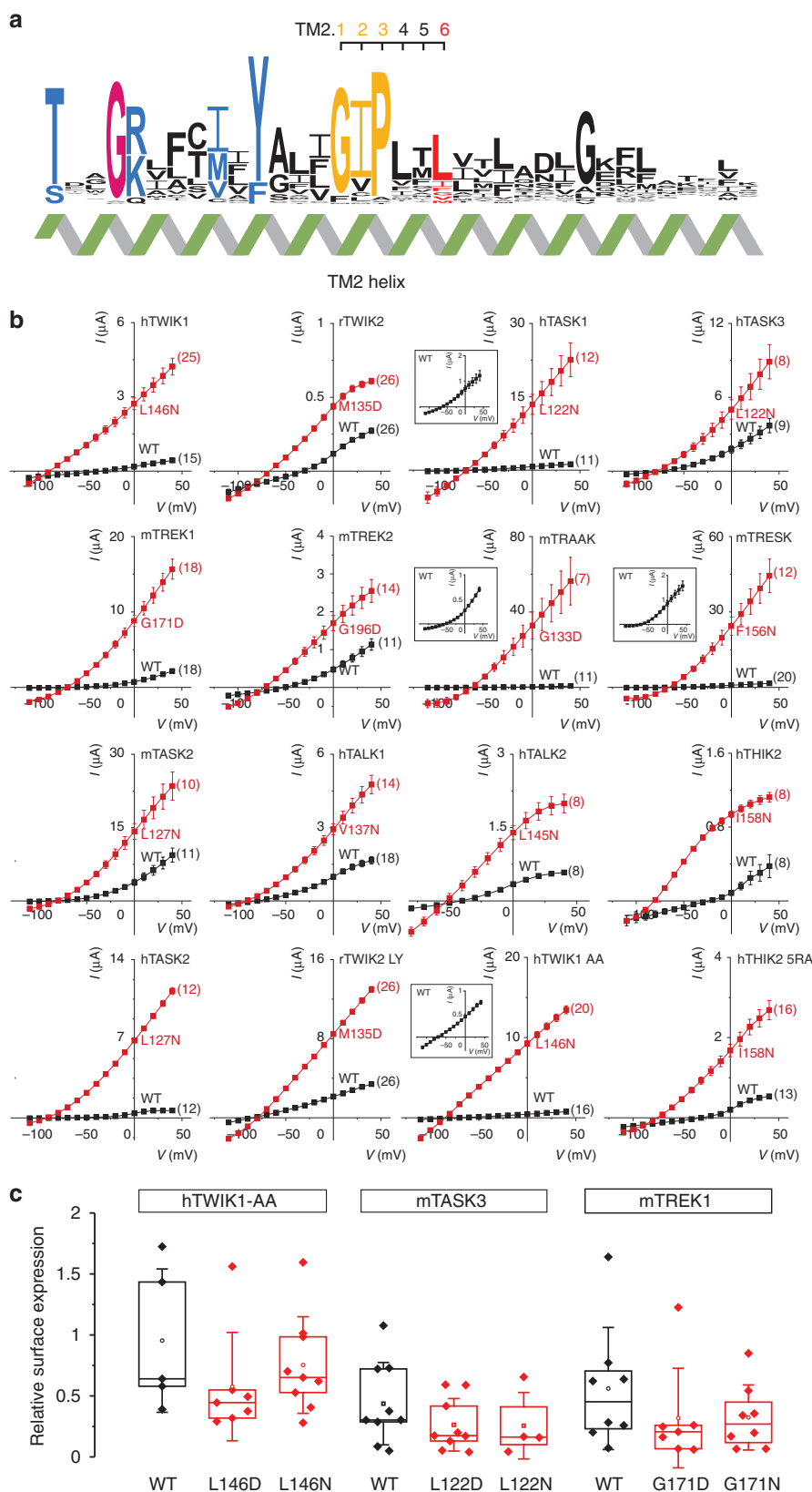
## Results

**Sequence conservation in distantly-related K2P channels.** Two-pore domain potassium (K2P) channels were first identified in the genomes of yeast and *C. elegans* based on their characteristic structure as tandems of pore-forming domains<sup>11</sup>. Interestingly, while all K2P channels share this basic topology, their amino acid sequences have diverged markedly. Vertebrate K2P channels have been classified in 6 families based on their peptide sequences and functional properties. Only members of a given class share high levels of homology (Supplementary Fig. 1). Sequence variation is even more striking for *C. elegans* K2P channels. Within the 47 genes encoding subunits of K2P channels, sequence conservation is generally low except for close relatives. Only five *C. elegans* channels exhibit significant sequence identity with vertebrate orthologs. SUP-9 and TWK-20 are most similar to TASK1/3/5, TWK-14 is a clear ortholog of THIK1/2, and TWK-46 and TWK-48 resemble TWIK1/2 and TRESK, respectively (Supplementary Fig. 1). For most other nematode K2Ps, on average 25% of amino acids are identical to the closest vertebrate relative, even when only the core portion of the channel—from the first to the fourth transmembrane segment—is considered, and variable N- and C-terminal cytoplasmic regions are omitted. For a few *C. elegans* K2P channels, conservation with vertebrate channels is even lower, ranging from 16% to 25% (*twk-6*, *twk-29*, *twk-32*, *twk-47*), although bioinformatic analyses suggest that they retain the characteristic domain organization.

We took advantage of this long evolutionary history to identify residues that could be important for the structure and function of K2P channels. Using an alignment of 66 vertebrate and invertebrate channels, we identified highly conserved residues in three transmembrane helices (TM1, TM2, TM4), two pore helices (Ph1, Ph2), and the selectivity filter (SF1, SF2) sequences (Fig. 1a, Supplementary Fig. 2). In contrast, the sequence of the third transmembrane helix (TM3) did not appear to be under selective pressure.

We next focused on the second transmembrane domain (TM2), and in particular on its central region because it contains the leucine and glycine residues which activate TWIK1, THIK1/2, and ORK1/KCNK0 channels when mutated<sup>8–10</sup>. As in other potassium channel families, conserved glycine residues are found at the center of TM2 in almost all K2Ps (Supplementary Fig. 2). They provide flexibility to these large membrane-spanning helices allowing for the conformational changes thought to be involved in channel gating<sup>16–18</sup>. In addition, the central region of TM2 presented remarkable sequence conservation in distant K2P channels (Fig. 1a). In 48 of 66 channels, this glycine hinge is followed by isoleucine and proline residues (further referred to as the GIP motif). In TWIK2, TASK2, *Drosophila* CG1688, and three *C. elegans* channels (TWK-9, TWK-20, and TWK-40), the isoleucine is replaced by a valine. Mammalian THIK1/2 and *C. elegans* TWK-14 channels have a different motif in which isoleucine is replaced by cysteine, and proline by one of three amino acids (serine, alanine or threonine). Further degenerate motifs are found in *Drosophila* *Sandman* (GMP), nine *C. elegans* channels (MIP, FVP, GIA, GLP, GAP), and the silent channel KCNK7 (GLP).

Sequence conservation of the residues following the GIP motif (and its derivatives) is less obvious in vertebrates. However, a common theme can be observed when 8 *Drosophila* and 43 *C. elegans* channels are included in the analysis. In particular, the



third residue following the GIP motif is generally a leucine (44/66) or an isoleucine (6/66), and more rarely, a glycine (TREK1, TREK2, TRAAK, KCNK0/ORK1), a phenylalanine (TRESK, TWK-17, TWK-24, UNC-58), a valine (TALK1, TWK-14, TWK-18, TWK-29), a methionine (TWIK2, TWK-16, TWK-43), or an alanine (TWK-25). To facilitate the identification of

homologous residues in distantly-related K2P channels, we introduce a nomenclature to identify residues in TM2 by using the conserved glycine hinges as reference positions. This glycine is labeled TM2.1 and the subsequent isoleucine and proline residues of the GIP motif are referred to as TM2.2 and TM2.3. The next three residues are labeled TM2.4, TM2.5, and TM2.6 (Fig. 1a).

**Fig. 1** Mutation of a single residue in TM2 systematically increases K2P channel activity. **a** Sequence conservation along transmembrane helix 2 (TM2 helix) computed from 66 vertebrate, insect, and nematode K2P channels, represented using WebLogo 3<sup>53</sup>. **b** Current-voltage relationships obtained at pH 7.4 in *X. laevis* oocytes by injection of cRNA encoding wild-type (black squares) and TM2.6 mutant channels (red squares). TM2.6 mutations are indicated in red next to corresponding current traces. Insets for hTASK1, mTRAAK, mTRESK, and hTWIK1 AA represent wild-type channel currents at a reduced scale. rTWIK2 LY and hTHIK2 5RA harbor additional mutations in intracellular trafficking signals that allow increased surface expression<sup>10,52</sup>. Each point represents the mean  $\pm$  standard error of the mean, numbers in parentheses represent the number of oocytes tested for each condition. Injected cRNA amounts and incubation times are reported in Supplementary Table 1. **c** Relative surface expression for wild-type and TM2.6 mutant channels using flow cytometry. HA/GFP-tagged wild-type (black) and mutant K2P channels (red) were expressed in HEK cells. Relative surface expression was determined by measuring the median fluorescence intensity of HA-positive cells (labeled in non-permeabilizing conditions) relative to the median fluorescence intensity of the GFP signal (total channel content). Center lines, medians; open circles, means; box limits, 25th and 75th percentiles; whiskers, standard deviation. Kruskal-Wallis, Dunn's multiple comparison test,  $p > 0.05$

The remainder of this study will describe the conserved role played by TM2.6 in the control of K2P channel gating.

### TM2.6 mutation increases activity of vertebrate K2P channels.

To test whether TM2.6 mutation could systematically increase the activity of vertebrate K2Ps, we generated point mutations of TM2.6 to asparagine or aspartate in 16 different rodent (r, *Rattus norvegicus*; m, *Mus musculus*) and human K2P channels (Fig. 1b). We then used two-electrode voltage-clamp recording in *Xenopus* oocytes to compare the total current elicited by wild-type and mutant channels. We found that in all cases, currents were markedly increased for TM2.6 mutants and their selectivity for potassium was maintained as indicated by marked hyperpolarization of reversal potentials (Supplementary Table 1). Depending on the channel, we observed 3- to more than 100-fold increases in total current.

To test whether this increase in current could be simply explained by an increase in surface expression of the channels, we generated hTWIK1-AA, mTASK3, and mTREK1 channels harboring HA-epitope tags in their extracellular Ph2 to M4 loops, and C-terminal GFP fluorescent proteins. We then used immunofluorescence in non-permeabilizing conditions combined with flow cytometry to compare levels of surface expression. In brief, HEK-293 cells were transfected with HA/GFP-tagged wild-type or TM2.6 mutant channels, labeled with primary anti-HA and secondary Alexa594-conjugated antibodies in non-permeabilizing conditions, and sorted by flow cytometry based on two-color fluorescence. Median fluorescence intensity (MFI) was determined for HA and GFP signals and used to determine the relative surface expression. These flow cytometry experiments did not show increased expression of TM2.6 mutant vs. wild-type channels (Fig. 1c), therefore demonstrating that the current increase observed for TM2.6 mutants did not simply result from increased surface expression, but more likely resulted from direct effects on the intrinsic activity of K2P channels.

Taken together, these experiments provide evidence for the consistent role played by TM2.6 in the modulation of channel activity for all vertebrate two-pore domain potassium channels.

### TM2.6 mutation promotes gating of pH-sensitive K2P channels.

To characterize the impact of TM2.6 mutations on channel function, we analyzed the responses of TASK1 and TASK2 channels to changes in extracellular pH. Indeed, alkalinization of the extracellular medium increases the activity of these channels via a direct effect on the selectivity filter (or C-type) gate. Specifically, raising extracellular pH promotes the open state of TASK1<sup>12</sup>, and increases the opening frequency of TASK2<sup>13-15</sup>. We reasoned that if mutant channels were already highly active at physiological pH, they should be less sensitive to stimulation by extracellular alkalinization. Indeed, raising extracellular pH from 7.4 to 9.4 only increased whole-cell currents of TASK1 L122N by

a factor of 1.4, while wild-type currents increased 2.8-fold (Fig. 2a). Similarly, TASK2 L127N currents were only increased by a factor of 2, while pH challenge led to a 10-fold increase in total current for wild-type TASK2 (Fig. 2b).

Furthermore, we found that the activation kinetics of TASK2 channels were markedly affected. Expression of wild-type TASK2 in *Xenopus laevis* oocytes gives rise to a slowly activating outward current in response to depolarizing voltage steps at physiological pH<sup>13,19</sup>. The activation kinetics of wild-type TASK2 increase sharply when TASK2 is stimulated by alkaline pH. Consistent with high basal activity, TASK2 L127N no longer showed the slow time-dependent outward current at neutral pH (Fig. 2b, inset).

Taken together, these experiments suggest that TM2.6 mutants of TASK1 and TASK2 are significantly more active in physiological conditions, likely due to increased activation of the selectivity filter gate.

**TM2.6 mutation increases activity of mechano-gated K2Ps.** To characterize the effect of TM2.6 mutations on the gating of mechano-sensitive K2P channels, we first measured the relative increase in inward current when extracellular potassium is replaced by rubidium. Indeed, substitution of potassium by rubidium in TREK1 induces the stabilization of the selectivity filter gate, for example making it more difficult to close the channel by reducing the internal pH<sup>20</sup>. We found that the current increase induced by ion substitution was strongly affected in TREK1 and TREK2 mutant channels. While wild-type currents increased 5 and 4.2-fold in TREK1 and TREK2, respectively, we only observed 1.6 and 1.2-fold increases for TREK1 G171D and TREK2 G196D, respectively (Fig. 3a, b), which is consistent with a positive effect of TM2.6 mutations on the selectivity filter gate.

Next, we analyzed the response of TREK1, TREK2, and TRAAK channels to open channel block by divalent barium ions. Ba<sup>2+</sup> inhibits these channels in a concentration and time-dependent fashion by competing for the S4 potassium binding site in the selectivity filter. In turn, when channel activity is increased by raising extracellular potassium concentrations or pH (inducing C-type gate stabilization), the magnitude of Ba<sup>2+</sup> inhibition is reduced because occupancy of S4 by potassium is increased<sup>21-23</sup>. Consistent with an increased basal activity, we found that Ba<sup>2+</sup> block was indeed significantly reduced in TM2.6 mutants of TREK1, TREK2, and TRAAK (Fig. 3c).

We then tested the dependence of Ba<sup>2+</sup> inhibition to extracellular potassium ( $[K^+]_o$ ) for TREK1. We again observed that TREK1 G171D was less sensitive to Ba<sup>2+</sup> inhibition, and hence intrinsically more active (Fig. 3d). Ba<sup>2+</sup> block was less pronounced at 5, 20, and 40 mM  $[K^+]_o$  when we compared wild-type to mutant TREK1. And while the magnitude of inhibition further increased between 20 and 40 mM  $[K^+]_o$  for wild-type channels, TREK1 G171D inhibition reached a plateau at 20 mM extracellular potassium, likely reflecting maximal opening of the



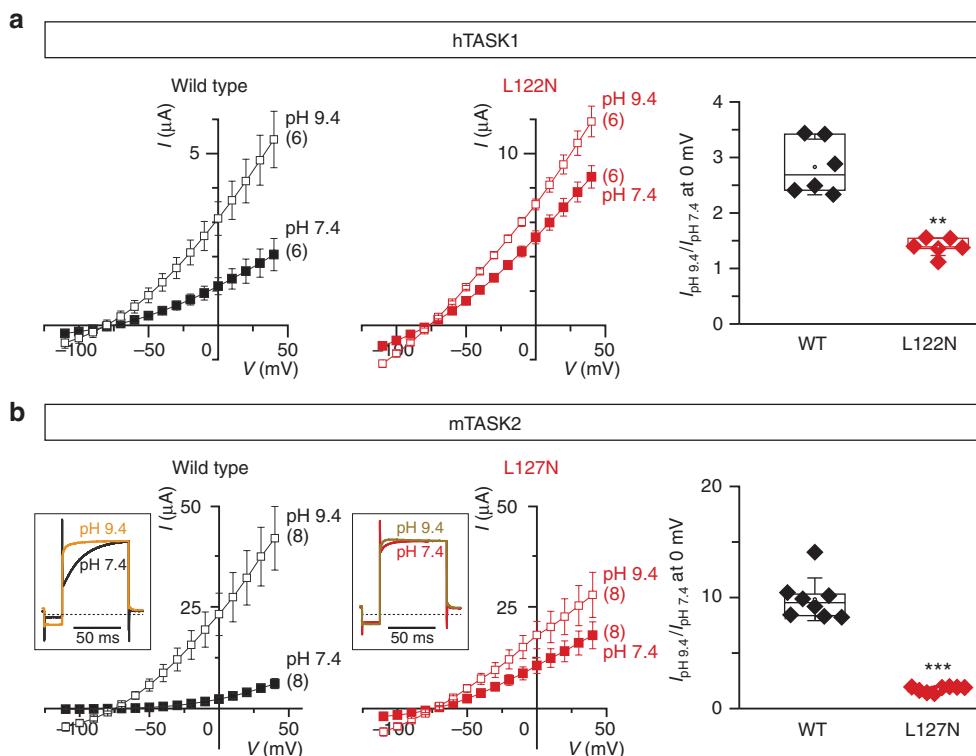


**Fig. 2** TM2.6 mutation increases the basal activity of pH-sensitive K2P channels. Current-voltage relationships of **a** hTASK1 and **b** mTASK2 channels; wild-type (black) and TM2.6 mutant (red) at extracellular pH 7.4 (filled squares) and pH 9.4 (open squares). Each data point represents the mean  $\pm$  standard error of the mean, numbers in parentheses represent the number of oocytes tested for each condition. In **(b)**, insets represent normalized current traces recorded at 0 mV. mTASK2 activation time was  $91.07 \pm 2.27$  ms ( $n = 8$ ) at pH 7.4 (black trace) and  $44.98 \pm 4.96$  ms ( $n = 8$ ) at pH 9.4 (orange trace). mTASK2 L127N activation time was  $39.51 \pm 2.25$  ms ( $n = 8$ ) at pH 7.4 (red trace) and  $29.41 \pm 5.35$  ms ( $n = 5$ ) at pH 9.4 (brown trace). Rightmost panels represent relative current increases, corresponding to the ratio between currents under pH 9.4 perfusion and currents under pH 7.4 perfusion at 0 mV. Mean relative current increases at 0 mV from pH 7.4 to 9.4 were  $2.8 \pm 0.2$  and  $1.4 \pm 0.1$  for wild-type and mutant hTASK1, respectively. Mean relative current increases were  $9.8 \pm 0.7$  and  $1.8 \pm 0.1$  for wild-type and mutant mTASK2, respectively. Currents were recorded 24 h after injection of cRNA (mTASK2 and mTASK2 L127N, 5 ng/oocyte; hTASK1, 2.28 ng/oocyte; hTASK1 L122N, 0.38 ng/oocyte). Each data point represents one oocyte; center lines, medians; open circles, means; box limits, 25th and 75th percentiles; whiskers, standard deviation. Mann-Whitney, \*\* $p < 0.01$ , \*\*\* $p < 0.001$

mutant channel at this concentration (Fig. 3d). In addition, while wild-type channels were inhibited in the same fashion at 0 and 5 mM  $[K^+]_o$ , the level of  $Ba^{2+}$  inhibition was significantly different between the two concentrations in TREK1 G171D. Taken together, these results strongly suggest that TM2.6 mutations promote the gating of mechano-gated K2P channels via the selectivity filter gate.

**TM2.6 mutation increases TRAAK/TREK1 single-channel activity.** To analyze in more detail how mutations of TM2.6 affect channel activity, we performed single-channel recording experiments for TRAAK and TREK1 channels.

First, we transfected TRAAK, TRAAK G133D, TREK1, and TREK1 G171D into HEK-293 cells and compared channel activity in cell-attached patch recordings. We found that TRAAK G133D and TREK1 G171D activity rose approximately 10-fold compared to wild-type channels in this context. While wild-type TRAAK and TREK1 channel activity was slightly increased at depolarized membrane potentials, TM2.6 mutants were consistently more active for all membrane potentials compared to wild-type (Fig. 4a, b).

Next, we analyzed single-channel properties of wild-type and mutant channels. In both mutants, we could observe flickering behavior and long bursts of channel openings consistent with increased channel activity (Fig. 4c, d). In addition, mean open

times were significantly increased compared to wild-type. For example, mean open times of TRAAK channels saw a 2-fold increase from  $0.41 \pm 0.01$  to  $0.81 \pm 0.13$  ms at  $-80$  mV, while TREK1 channel mean open times rose from  $0.56 \pm 0.09$  to  $0.68 \pm 0.08$  ms at  $-80$  mV (Fig. 4e, f).

In contrast, unitary conductance was only modestly affected by TM2.6 mutations in TRAAK and TREK1, and would not explain the dramatic increase in whole-cell current observed in our two-electrode voltage-clamp experiments. We observed differences between wild-type and mutant channels depending on the imposed membrane potential. TRAAK conductance was unchanged by TM2.6 mutation at  $-80$  mV but showed a significant decrease compared to wild-type at  $+80$  mV. TREK1 G171D unitary conductance was significantly higher than wild type at  $-80$  mV, and slightly decreased at  $+80$  mV (Fig. 4e, f). Consistently, the current-voltage relationships of TRAAK and TREK1 (obtained from single-level openings in symmetrical KCl, 150 mM) was also modified. The  $I-V$  relationship of TRAAK G133D showed a slight inward rectification at positive potentials similar to that of TREK2<sup>24</sup> (Fig. 4g, h). TREK1 produced a clear outward rectification at negative potentials, while TREK1 G171D did not.

Taken together, these results provide direct evidence that introducing an aspartate in TM2.6 of TRAAK and TREK1 dramatically affects single-channel open probability and strongly potentiates the channels' activity. Our data are consistent with the

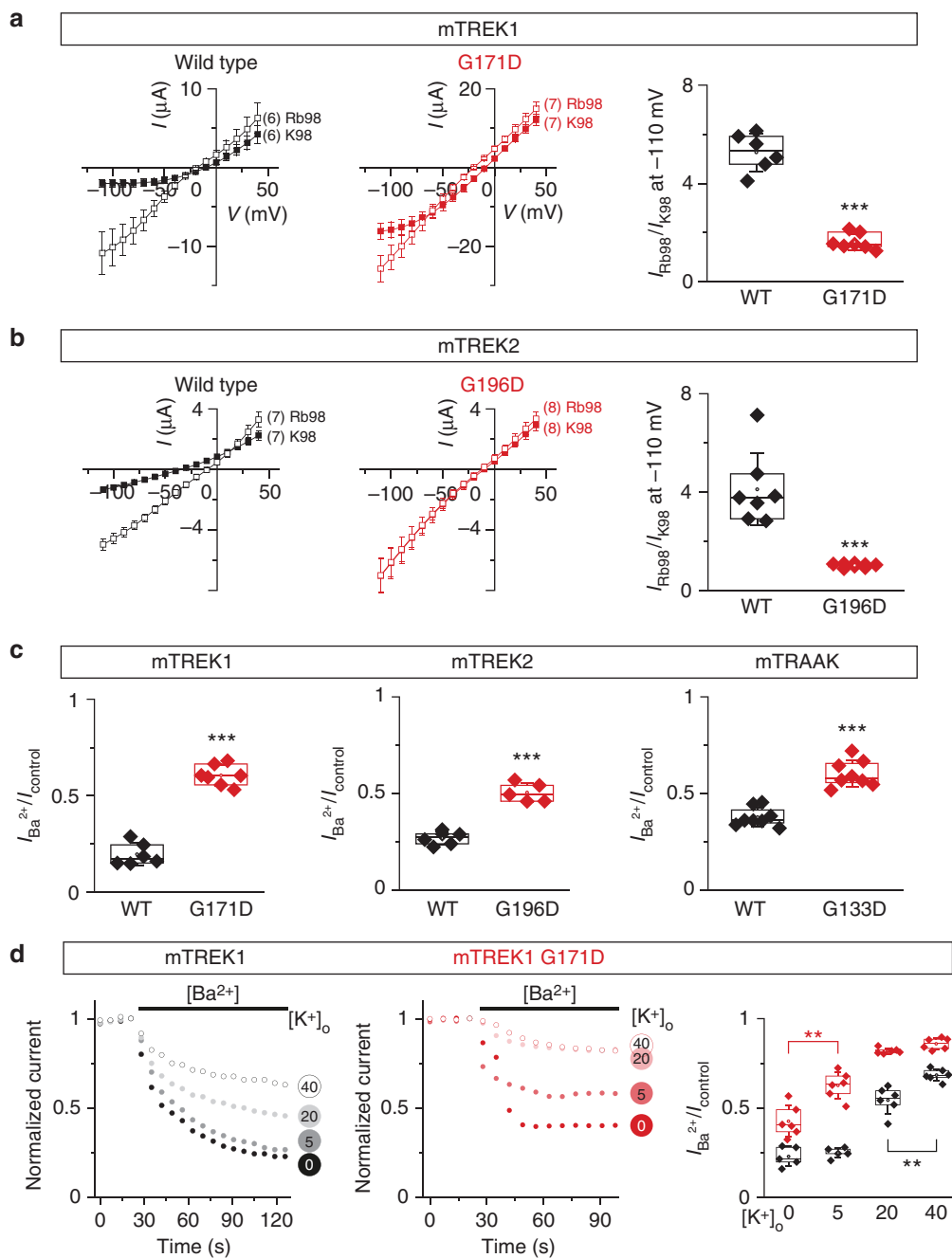


**Fig. 3** TM2.6 mutations promote gating of mechano-gated K2P channels. **a, b** TM2.6 mutation affects TREK1 and TREK2 current increase induced by substituting potassium with rubidium. Current-voltage relationships of mTREK1 and mTREK2 channels; wild-type (black) and TM2.6 mutant (red) at 98 mM extracellular potassium (filled squares) and 98 mM extracellular rubidium (open squares). Each data point represents the mean  $\pm$  standard error of mean, numbers in parentheses represent the number of oocytes tested for each condition. Rightmost panels: mean relative current increases were  $5.3 \pm 0.3$  and  $1.6 \pm 0.1$  for wild-type and mutant mTREK1, respectively, and  $4.1 \pm 0.6$  and  $1.01 \pm 0.02$  for wild-type and mutant mTREK2, respectively. Currents were recorded 24 h after injection of cRNA at 1 ng/oocyte. **c** Magnitude of Ba<sup>2+</sup> inhibition is reduced in TM2.6 mutants of mechano-gated K2P channels. Ratios between currents under barium perfusion and currents under control perfusion at 0 mV, were significantly different for wild-type (black) and mutant channels (red). Mean ratios increased from  $0.19 \pm 0.02$  (mTREK1) to  $0.6 \pm 0.02$  (mTREK1 G171D), from  $0.26 \pm 0.01$  (mTREK2) to  $0.5 \pm 0.01$  (mTREK2 G196D), and from  $0.37 \pm 0.01$  (mTRAAK) to  $0.6 \pm 0.02$  (mTRAAK G133D). Currents were recorded 24 h after injection of cRNA at the following concentrations (in ng/oocyte): mTREK1 wild-type, 5; mTREK1 G171D, 1; mTREK2 wild-type, 3; mTREK2 G196D, 1; mTRAAK wild-type, 10; mTRAAK G133D, 0.1. **d** Inhibition of mTREK1 by 6 mM extracellular Ba<sup>2+</sup> in the presence of increasing concentrations of extracellular K<sup>+</sup> ([K<sup>+</sup>]<sub>o</sub>). Currents were recorded 24 h after injection of cRNA (mTREK1, black, 5 ng/oocyte; mTREK1 G171D, red, 1 ng/oocyte). Left and middle panels show normalized responses of one representative oocyte to barium challenge in the presence of [K<sup>+</sup>]<sub>o</sub> (0, 5, 20, and 40 mM). Right panel: ratio between currents under barium perfusion and currents under control perfusion at 0 mV. Each data point represents one oocyte; center lines, medians; open circles, means; box limits, 25th and 75th percentiles; whiskers, standard deviation. Student's unpaired *t*-test (except **(b)**, Mann-Whitney), \*\**p* < 0.01, \*\*\**p* < 0.001

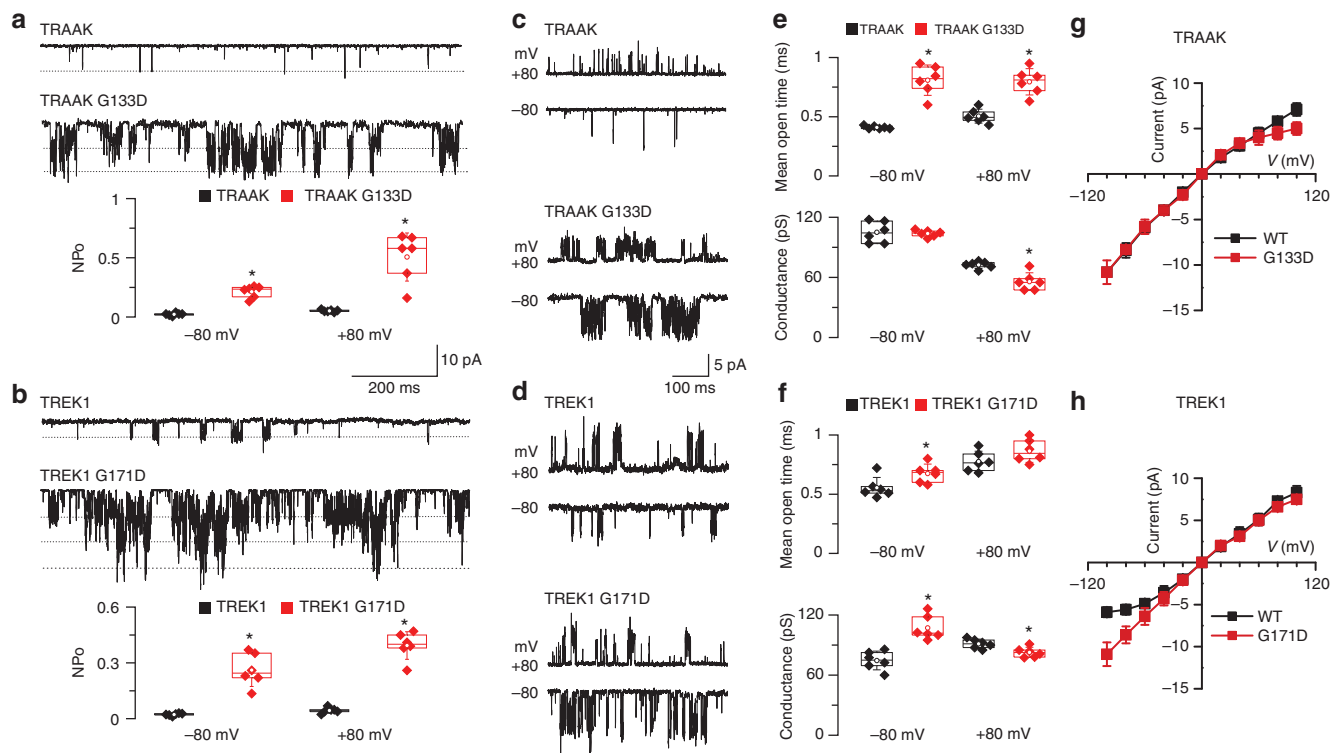


**Fig. 4** TM2.6 mutations in TRAAK and TREK1 increase single-channel open probability. **a, b** Channel opening of TRAAK, TRAAK G133D, TREK1, and TREK1 G171D at  $-80$  mV. Channel activity was determined by NPo analyzed at  $-80$  and  $+80$  mV. **c, d** Single-channel openings of TRAAK, TRAAK G133D, TREK1 and TREK1 G171D at two membrane potentials. Currents were recorded in cell-attached patches held at pipette potentials of  $+80$  and  $-80$  mV. Pipette and bath solutions contained  $150$  mM KCl. **e, f** Mean open time for TRAAK, TRAAK G133D, TREK1, and TREK1 G171D. Average unitary conductance for TRAAK, TRAAK G133D, TREK1, and TREK1 G171D. **g, h** Current-voltage relationships of single channels. Mean  $\pm$  standard deviation. Source data are provided as a Source Data file. Each data point represents one recording; center lines, medians; open circles, means; box limits, 25th and 75th percentiles; whiskers, standard deviation. Mann-Whitney,  $n = 6$ ,  $*p < 0.05$

effect of the TM2.6 G134D mutation reported for *Drosophila* KCNK0/ORK1<sup>8</sup>, which was found to increase single-channel open probability. This congruence is striking given the low levels of sequence identity between KCNK0 and TRAAK/TREK1 channels (Supplementary Table 1). We therefore propose that increased channel open probability most likely explains the consistent increase in activity of TM2.6 mutants.

**Gradual activation of TREK1 and TASK2.** Given the drastic effect of asparagine and aspartate mutations, we wondered whether we could also achieve intermediate levels of channel activation by using different amino acid substitutions at the TM2.6 position. Such allelic series have been reported for TWIK1<sup>25</sup> and TALK2<sup>27</sup>, but also for members of other ion channel families such as large conductance mechanosensitive channels (MscL) of *Escherichia coli*<sup>26</sup>, voltage-dependent Shaker potassium channels, or the ligand-gated K<sup>+</sup> channel Gsuk<sup>27</sup>.

To test this hypothesis, we generated a series of TM2.6 mutants of the TREK1 and TASK2 channels and compared their biophysical properties with those of wild type channels. First, we used the potassium-rubidium ion substitution assay to compare four TREK1 mutants (G171T, G171S, G171D, G171N). We observed significant differences for S, D, and N mutants compared to wild-type TREK1, and between T and S, or S and D mutants (Fig. 5a). This strongly suggests that these mutants achieve distinct levels of channel function.

Next, we analyzed six different TASK2 mutants (L127V, L127G, L127T, L127S, L127D, L127N) and found gradual effects for activation kinetics and pH-sensitivity. At physiological pH,

valine and glycine substitution had intermediate kinetics, while the remaining mutants had comparable, likely maximal, activation kinetics (Fig. 5b, leftmost and middle panel). Using the same mutants, we then compared the stimulating effect of external alkalization. We found consistent results for the six mutants (Fig. 5b, rightmost panel): L127V and L127G showed intermediate phenotypes, while L127T/S/D/N mutants were indistinguishable.

Finally, we investigated the effect of serine substitution on the single-channel properties of TRAAK and TREK1 channels (Supplementary Fig. 3). Similar to G133D, G133S strongly increased NPo of TRAAK at  $-80$  mV and  $+80$  mV, but did not cause a significant increase in mean open time at  $+80$  mV. For TREK1, while NPo, mean open time, and conductance, were significantly increased by G171D at  $-80$  mV, only mean open time was significantly increased in G171S mutants compared to wild-type.

Taken together these results show that different levels of channel activity can indeed be achieved by engineering different amino acid substitutions in TM2.6, further illustrating the pivotal role played by this residue.

**Gradual activation of the nematode K2P channel TWK-18.** Since TM2.6 mutations increase channel gating for all vertebrate channels (Fig. 1b) and for *Drosophila* KCNK0/ORK1<sup>8</sup>, we wondered whether the function of this residue had been further conserved during evolution. We therefore targeted the diverse family of K2P channels expressed in *C. elegans*.

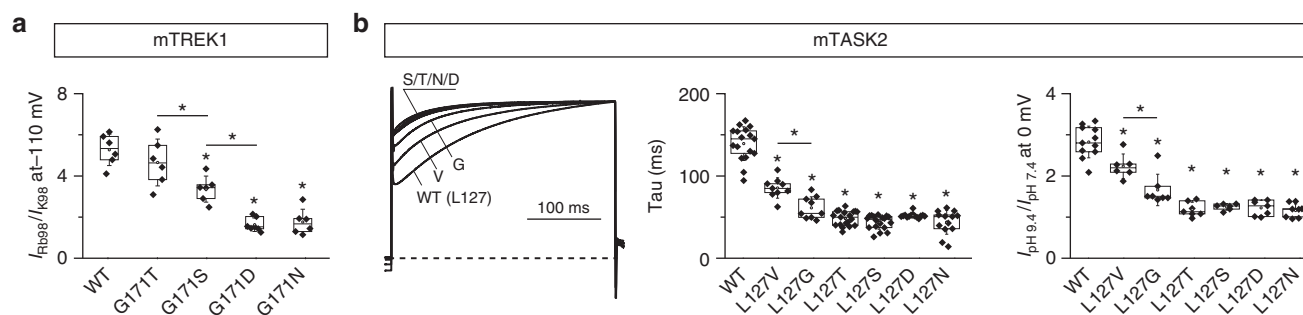


**Fig. 5** Gradual activation of TREK1 and TASK2 by a series of TM2.6 mutations. **a** Response of different TREK1 TM2.6 mutants to rubidium/potassium ion substitution. Ratios of whole-cell currents recorded at  $-110$  mV for  $[Rb^+]_o$  98 mM and  $[K^+]_o$  98 mM. **b** Gradual increase of TASK2 activation kinetics and response to pH challenge for different TM2.6 mutants. Normalized current traces recorded at  $+40$  mV (left panel) and corresponding activation constants (Tau (ms), middle panel). Ratios of whole-cell current recorded at 0 mV with extracellular pH 9.4 and pH 7.4 (right panel). Currents were recorded 24 h after injection of crRNA at 1 ng/oocyte. Each data point represents one oocyte; center lines, medians; open circles, means; box limits, 25th and 75th percentiles; whiskers, standard deviation. ANOVA, Tukey's multiple comparison test,  $*p < 0.05$

To date, only the TWK-18 channel has been functionally characterized using heterologous expression systems<sup>5</sup>. TWK-18 is a potassium-selective outwardly-rectifying channel with a steep temperature-dependence between 25 and 35 °C. To test whether TM2.6 mutation could also increase TWK-18 activity, we compared the TM2.6 mutant TWK-18 V158D with wild-type TWK-18 and the previously described gain-of-function mutant TWK-18 M280I (*cn110*). Consistent with our previous results, we found that TWK-18 V158D was significantly more active than wild-type and M280I mutants at 22 °C when expressed in *Xenopus* oocytes (Fig. 6a, left panel). We then generated additional TM2.6 amino acid substitutions in TWK-18 to test whether we could also achieve gradual activation. Indeed, we found that different residues lead to different levels of whole-cell current, consistent with progressive activation of the TWK-18 channel (Fig. 6a, right panel).

### Rational design of gain-of-function mutants in *C. elegans*.

Despite the fundamental role of K2P channels in cellular physiology<sup>1,28,29</sup>, some basic questions about their biology are still largely unexplored. In particular, comparatively little is known about the precise molecular and cellular processes that determine the number of active channels and their distribution at the cell surface in vivo. Unbiased forward genetic screens in model organisms are well suited to dissect such complex cellular processes and gene regulatory networks in vivo, and gain-of-function mutants of potassium channels are ideal starting points for such screens. For example, genetic modifier screens targeting the SUP-9 channel have identified a diverse set of proteins that are required for trafficking and function of this TASK-related K2P channel<sup>6,30,31</sup>.

We hypothesized that TM2.6 mutation could be a powerful strategy to rationally design hyperactive K2P channel mutants that would open the way for genetic screens. As a proof of principle, we used CRISPR/*Cas9*-based gene editing to target four channels (*twk-18*, *unc-58*, *egl-23*, and *sup-9*) for which gain-of-function mutants with severe and easily observable phenotypes had been reported in the literature.

*twk-18* is exclusively expressed in *C. elegans* body wall muscles<sup>32</sup>. Hyperactivation of TWK-18 by two different point mutations (*cn110*/M280I and *e1913*/G165D) leads to flaccid paralysis that can be rapidly induced and reverted in temperature-shift experiments<sup>5</sup>. *unc-58*(*e665*) (L428F) mutants are short and essentially unable to move forward or backward on solid media<sup>33</sup>. They display a straight body posture accompanied

by a rapid rotation around their anteroposterior axis. *egl-23*(*n601*) (A383V) mutants are unable to lay embryos likely due to the hyperpolarization of vulval muscles (SEM and TB, unpublished). Finally, gain-of-function mutants in which SUP-9 is hyperactive display a characteristic rubberband phenotype in which worms first contract and then rapidly relax their body when prodded on the head<sup>6</sup>.

We engineered asparagine mutations in TM2.6 for *twk-18*, *unc-58*, *egl-23*, and *sup-9*. Except for *sup-9*, mutant worms harboring the desired point mutations could be readily identified in the F1 progeny of injected worms owing to the dominant effect of these mutations (Fig. 6b, d). First, we found that TWK-18 V158N mutant worms showed the same flaccid paralysis as canonical M280I gain-of-function mutants. Second, UNC-58 F294N mutants were severely paralyzed and short but differed qualitatively from the canonical UNC-58 L428F mutant. Indeed, they did not produce the characteristic shaking behavior, and had increased body curvature on agar plates. Third, egg-laying was strongly impaired in EGL-23 L229N mutants (Fig. 6d, e). As expected, fertilized embryos quickly accumulated within the parent, eventually leading to the formation of a bag-of-worms once these animals had completed their embryonic development. Finally, despite multiple attempts, we failed to obtain the SUP-9 L122N mutant. This may be explained by the fact that even moderate gain-of-function mutations of *sup-9* can only be maintained as heterozygous strains<sup>6</sup>, and homozygous animals fail to develop during embryogenesis.

### Allelic series produce gradual phenotypes in *C. elegans*.

In heterologous expression systems such as *Xenopus* oocytes, it is possible to control the level of ion channel expression by titrating the amount of injected cRNA. This is no longer possible when mutations are introduced into the genome by gene editing. As we found for SUP-9, asparagine mutations in TM2.6 may sometimes interfere with normal development or limit viability. We thus wondered whether we could generate weak or intermediate gain-of-function mutants in vivo by using different amino acid substitutions.

We again used CRISPR/*Cas9* gene editing to introduce different TM2.6 mutations in *twk-18*, *unc-58*, *egl-23*, and *sup-9*. In each case, we could identify CRISPR/*Cas9*-edited animals based on the characteristic locomotor (*twk-18*, *unc-58*), egg-laying (*egl-23*) or developmental phenotypes (*sup-9*). First, we were able to generate homozygous SUP-9 L122S mutants, contrary to our previous attempts with the L122N mutation.

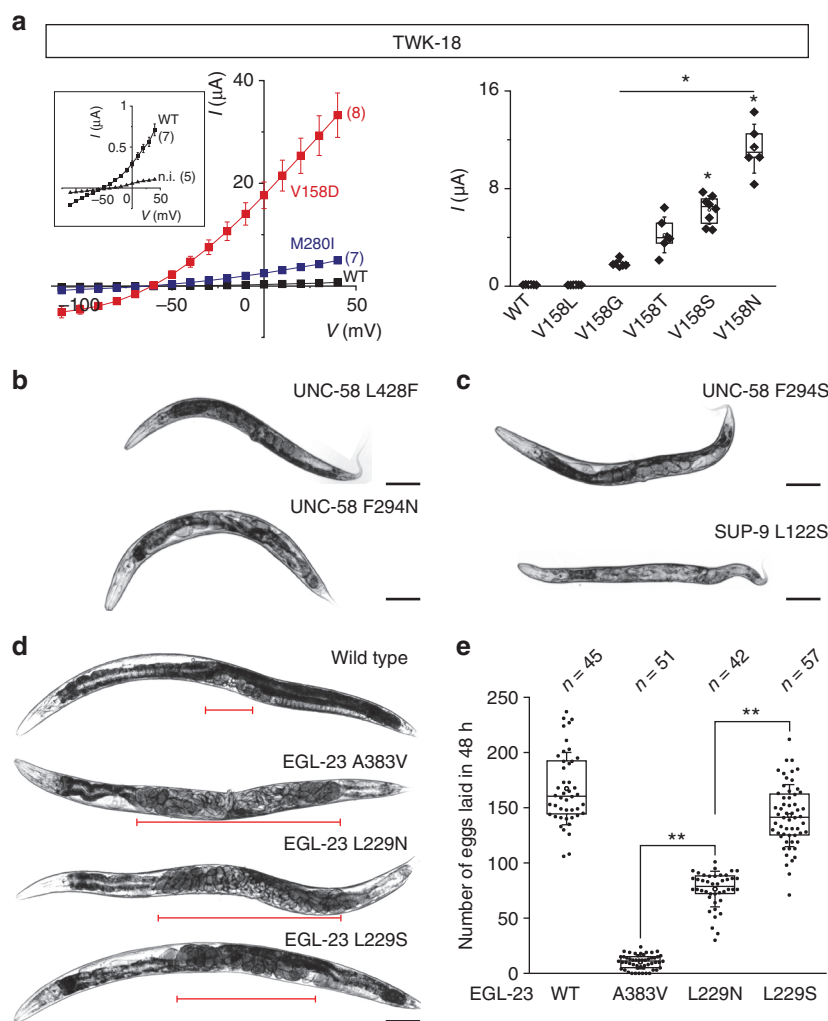


**Fig. 6** Tuning K2P channel activity in vivo using CRISPR/Cas9 gene editing in *C. elegans*. **a** (left panel) Current-voltage relationships obtained at pH 7.4 in *X. laevis* oocytes for TWK-18 wild-type (black squares), TWK-18 M260I (blue squares), and TWK-18 V158D mutant channels (red squares). Inset, current-voltage relationship for wild-type channel and non-injected oocytes at a reduced scale. **a** (right panel) Gradual increase of TWK-18 whole-cell current in a series of TM2.6 mutants. Currents at 0 mV were recorded 24 h after injection of cRNA at 30 ng/oocyte. Each data point represents one oocyte. **b** Representative micrographs of 1-day old adult UNC-58 L428F, UNC-58 F294N, UNC-58 F294S, **c** SUP-9 L122S, and **d** wild type, EGL-23 A383V, EGL-23 L229N, and EGL-23 L229S worms. Red brackets mark the central section of each animal where embryos accumulate. Scale bars, 10  $\mu$ m. **e** Comparison of egg-laying rates of wild-type worms and *egl-23* gain-of-function alleles. Each data point represents the number of embryos laid by a single animal over a 48-h period. *n*, number of animals tested. Center lines, medians; open circles, means; box limits, 25th and 75th percentiles; whiskers, standard deviation. Kruskal-Wallis, Dunn’s multiple comparison test, \**p* < 0.01

These worms however grew very slowly and had strong morphological defects (Fig. 6c). Since they were nevertheless viable, we concluded that SUP-9 L122S is likely a weaker gain-of-function allele than L122N and that channel activity can indeed be set to different levels using serine vs. asparagine substitutions.

Next, we built serine and threonine mutants for *twk-18*, *unc-58*, and *egl-23* to test whether we could detect gradual channel activation using behavioral variation as a proxy. In the case of the temperature-sensitive TWK-18 channel, we could define a clear allelic series by comparing the level of paralysis of *twk-18* mutants at different temperatures. At extreme temperatures, all alleles behaved similarly, i.e., they remained mobile at 15 °C and were paralyzed at 25 and 30 °C. We could however observe clear differences at 20 °C when we measured the proportion of animals that were able to crawl out of a 1 cm-wide circle within a two-and-a-half-hour timespan. At 20 °C, 95% of M280I (*n* = 40), 73% of V158S (*n* = 40), and 63% of V158T (*n* = 40) had crossed this

limit. In contrast, only 22% of the V158N mutants (*n* = 40) had moved significantly over this time period. Using a similar behavioral test for UNC-58, we could also observe progressive phenotypes. 87% of F294S (*n* = 45) and 49% of F294N (*n* = 45) had crossed the perimeter of the circle after an 8 h, compared to 9% of L428F (*n* = 45) mutants.

In the case of *egl-23*, we monitored the rate of egg-laying in the first 48 h after the L4 to adult molt (Fig. 6e). We compared the canonical *n601* (A383V) mutant, and the TM2.6 mutants L229N and L229S. The A383V mutation had the strongest effect on the egg-laying rate. L229N resulted in slightly higher egg-laying rates (i.e., a less pronounced egg-laying defect), while L229S mutants were able to lay eggs at a rate slightly lower than wild-type. This gradual effect was also clearly visible in 1-day old adult animals (Fig. 6d, e). Indeed, wild-type worms carry only a limited number of fertilized eggs at this time point since they lay embryos soon after fertilization. In contrast, A383V and L229N mutants rapidly



accumulate fertilized embryos which eventually leads to death by matricide after 48 h. L229S mutants had an intermediate phenotype consistent with their ability to lay eggs and increased survival time. Eventually, all mutant worms however died due to the accumulation and hatching of their progeny within the parent.

These experiments further validate the notion that TM2.6 is a crucial residue that controls the gating of most, if not all K2P channels. They also demonstrate that channels can be activated progressively *in vivo* using various TM2.6 substitutions, highlighting the versatility of our strategy.

## Discussion

We report here that a single conserved residue in the second transmembrane segment of vertebrate and invertebrate two-pore domain potassium channels plays a key role in the control of K2P channel gating. Mutating this residue (TM2.6) results in higher channel activity in heterologous expression systems and *in vivo* in *C. elegans*. Higher channel activity results from a dramatic increase of channel open probability, and not from a change in surface expression nor unitary conductance. Furthermore, it is possible to engineer gain-of-function mutants with different levels of activity by replacing TM2.6 with a series of amino acids, progressively tuning the activity of K2P channels. TM2.6 systematically increases channel activity in most if not all K2Ps. This universality is remarkable given the low sequence conservation between the vertebrate and invertebrate channels we have tested and raises the question of the mechanism of action of these mutations.

Available crystal structures position TM2.6 on the intracellular side of the second transmembrane domain, exposed to a large cytoplasmic vestibule, and in close proximity to the intracellular part of the selectivity filter<sup>16–18,34</sup>. This location suggests that TM2.6 residues could affect three previously-described gating mechanisms.

Contrary to other potassium channels, K2P channels do not possess a clear bundle-crossing gate or inner gate. Their principal gate is therefore situated at or close to the selectivity filter, also known as a C-type gate because it resembles the C-type inactivation gate of voltage-gated potassium channels<sup>4,18,20,35–38</sup>. In most K2Ps, this C-type gate is regulated by variations in pH and is stabilized by increasing extracellular potassium concentrations<sup>39,40</sup>. Mutations and small molecules have been shown to stabilize this filter gate in different K2P channels<sup>4,18</sup>. Our data are consistent with an effect of TM2.6 mutations on the selectivity filter gate.

Interestingly, a novel type of inner gating mechanism has been proposed recently for TWIK1. Molecular dynamics simulations tracking the movements of water molecules within the intracellular vestibule of the channel found that stochastic de-wetting close to the TM2.6 leucine residue creates a hydrophobic barrier opposing efficient ion passage through the conduction pathway<sup>25,41</sup>. Disrupting this hydrophobic barrier by replacing the leucine with a polar or negatively-charged residue maintained water occupancy within the inner pore and dramatically increased whole-cell currents<sup>25</sup>. Similar hydrophobic barriers have emerged from the study of model nanopores and have been shown to limit ion conduction in ligand-gated neurotransmitter receptors and ion channels<sup>41,42</sup>. For example, mutations disrupting hydrophobic barriers affect current flow through two prokaryotic potassium channels (GsuK, ligand-gated K<sup>+</sup> channel from *Geobacter sulfurreducens*; MthK, Ca<sup>2+</sup>-gated K<sup>+</sup> channel from *Methanobacterium thermoautotrophicum*) and increase open probabilities<sup>29,43</sup>.

A third gating mechanism has been proposed for mechanosensitive channels of the TREK/TRAAK family in which lateral

fenestrations close to the selectivity filter allow the passage of acyl chains belonging to fatty acids of the upper membrane leaflet. Access of lipids to the conduction pathway relies on conformational changes of TM4<sup>34,44,45</sup>. In K2Ps, TM2 of one subunit is opposed to TM4 of the second subunit thereby creating two fenestrations possibly accessible by lipids. Given the central position of TM2.6 within the second transmembrane domain, amino acid substitutions (either charged, hydrophilic, and/or bulky) of TM2.6 could also alter this proposed lipid gating mechanism.

We have found that the majority of K2P channels possess hydrophobic residues at the TM2.6 position (Fig. 1a, Supplementary Fig. 2). Therefore, disruption of a hydrophobic gate is an attractive model that would explain how K2P channels with very different overall primary sequences could all be similarly activated. Furthermore, simulations of model nanopores have demonstrated that hydrophobic barriers can be disrupted by modulating the hydrophobicity of the pore<sup>42</sup>. Consistent with this idea, we found that different hydrophilic or hydrophobic residues produced different levels of channel activity, both *in vitro* and *in vivo*. A few K2P channels do not have hydrophobic TM2.6 residues. Notably, a glycine residue is found in *Drosophila* KCNK0/ORK1 and vertebrate TREK1, TREK2, and TRAAK channels. Molecular dynamics simulations of TREK2 have failed to detect significant de-wetting<sup>46</sup>. Rather different lines of evidence suggest that mutating this glycine residue to an aspartate increases channel gating via the selectivity filter gate<sup>8</sup>.

In conclusion, the exact mechanisms by which TM2.6 mutations promote channel activation remain to be fully elucidated and may vary depending on the channel. Furthermore, it may be difficult to dissociate hydrophobic and C-type gating since TM2.6 is close to the selectivity filter. Depending on the channel, TM2.6 mutation may thus differentially affect the selectivity filter gate, the inner hydrophobic gate, and gating by membrane lipids.

Given the striking phenotypes of the TM2.6 mutants in *C. elegans*, it could appear surprising that they had not been identified in forward genetic screens. A likely explanation is that two or even three base changes are required to introduce these amino acid substitutions. Concomitant mutation of two DNA bases is highly unlikely when using chemical mutagens such as EMS or ENU. Consistently, preliminary experiments targeting other *C. elegans* K2P channels have yielded additional mutants with very strong behavioral defects akin to the phenotypes of classical *uncoordinated* mutants (unpublished). Such gain-of-function mutants will be ideal starting points for forward genetic screens aiming to identify genes that are required for channel expression, trafficking and functional modulation *in vivo*.

In the future, TM2.6 mutations could also be used to identify pharmacological compounds targeting K2P channels. In particular, yeast-based screening strategies have proven to be successful for the discovery of new ion channel modulators<sup>47</sup> and for the identification of specific blocker sites<sup>48</sup>. By using TM2.6 mutants described here, this approach can now be envisioned for K2P channels beyond the highly active TREK1 channel (keeping in mind that TM2.6 mutations may not always fully mirror the pharmacology of wild-type channels). Indeed, specific compounds targeting K2P channels are of great interest, since K2Ps represent important targets for neurological, cardiovascular, and endocrine disorders. For example, gain-of-function mutations in human TALK2 have been shown to cause severe cardiac conduction disorder<sup>7</sup>. A polymorphism in the pancreatic channel TALK1 causes a reduction in  $\beta$ -cell excitability and glucose-stimulated insulin secretion, which could explain increased type 2 diabetes susceptibility<sup>49</sup>. And a mutation increasing TRAAK activity has been linked to a novel neurodevelopmental syndrome known as FHEIG, for facial dysmorphism, hypertrichosis,



epilepsy, intellectual disability/developmental delay, and gingival overgrowth<sup>50</sup>.

Presently, there are no indications about the possible effects of increased channel activity for other human K2P channels. By introducing TM2.6 mutations using CRISPR/Cas9-based gene editing, it will be possible to create well-defined cellular systems or model organisms that could help to predict the functional consequences of increased activity for any K2P channel, while circumventing the pitfalls of standard overexpression strategies. In turn, these model systems could then be used to identify and validate pharmacological agents that modulate the activity of K2P channels.

## Methods

**Expression plasmids.** cDNA sequences were amplified using Phusion high-fidelity DNA polymerase (ThermoFisher Scientific) and assembled into the *Xenopus* oocyte expression vector pTB207<sup>51</sup> by 2- or 3-fragment Isothermal Ligation using the primer combinations indicated in Supplementary Table 5. PCR-amplified sequences were validated by Sanger sequencing.

The resulting vectors used in this study are:

pOA23 hTASK1, pOA24 hTASK1 L122N, pOA21 hTASK3, pOA22 hTASK3 L122N, pOA25 mTASK2 WT, pNZ20 mTASK2 L127N, pIBS25 mTASK2 L127D, pIBS26 mTASK2 L127S, pIBS27 mTASK2 L127T, pIBS28 mTASK2 L127V, pIBS29 mTASK2 L127G, pIBS18 mTREK1 WT, pIBS19 mTREK1 G171D, pIBS20 mTREK1 G171N, pIBS21 mTREK1 G171S, pIBS22 mTREK1 G171T, pIBS23 mTREK1 G171L, pIBS24 mTREK1 G171V, pOA26 mTREK2, pOA27 mTREK2 G196D, pOA28 mTRAAK, pOA29 mTRAAK G133D, pOA30 mTRESK, pOA31 mTRESK F156N, pTB301 TWK-18, pTB314 TWK-18 M280I, pNZ19 TWK-18 V158D, pIBS30 TWK-18 V158N, pIBS31 TWK-18 V158S, pIBS32 TWK-18 V158T, pIBS33 TWK-18 V158L, pIBS34 TWK-18 V158G. hTWIK1, rTWIK2, hTALK1, hTALK2 and hTHIK2 are inserted into the pLIN oocyte expression vector. Additional mutations were introduced by PCR using Pfu Turbo DNA polymerase (Agilent Technologies). hTWIK1-AA was previously described in ref.<sup>9</sup>, hTHIK2-5RA in ref.<sup>10</sup>, and rTWIK2-LY in ref.<sup>52</sup>. For mammalian cell electrophysiology, K2P channel cDNA sequences were inserted into the pIRES2-EGFP vector. For FACS analysis, hTWIK1 AA, mTASK3, and mTREK1 were tagged with HA and GFP, and cloned into a pcDNA3 vector. One or two copies of the hemagglutinin (HA) epitope (YPYDVPDYA) were inserted into the extracellular domain connecting the second pore helix (Ph2) and TM4 transmembrane segment. The GFP coding sequence was added at the cytoplasmic C-terminus of each channel.

**Oocyte electrophysiology.** Capped RNAs were synthesized in vitro from linearized expression vectors using the T7 mMessage mMachine kit (Ambion, Austin, TX, USA).

Defolliculated *X. laevis* oocytes (Ecocyte Bioscience, Dortmund, Germany) were injected with 50 nL containing between 50 pg and 50 ng of cRNA depending on the K2P expression rate (concentrations are indicated in Supplementary Table 1). Oocytes were kept at 18 °C in ORII Calcium solution containing (in millimolar): 82.5 NaCl, 2 KCl, 1 MgCl<sub>2</sub>, 0.7 CaCl<sub>2</sub>, 5 HEPES, gentamicin (25 µg/mL), pH 7.5 (with TRIZMA-Base).

Two-electrode voltage-clamp (TEVC) experiments were performed 24–72 h after the microinjection. Oocytes were mounted in a small home-made recording chamber and continuously superfused with the ND96 standard solution containing (in millimolar): 96 NaCl, 5 KCl, 1.8 CaCl<sub>2</sub>, 2 MgCl<sub>2</sub>, 5 HEPES. pH 7.4 was adjusted with Trizma base. High potassium and high rubidium external solutions (in millimolar): 98 KCl or 98 RbCl, 1.8 CaCl<sub>2</sub>, 2 MgCl<sub>2</sub>, 5 HEPES. pH 7.4 was adjusted with Trizma base. For pH challenge experiments, Trizma base was used to buffer the solution for pH values over 8.0. Barium chloride (Sigma-Aldrich) was prepared as 1 M stock solution in H<sub>2</sub>O and used at 6 mM final concentration in ND96 solution.

Macroscopic currents were recorded using a Warner Instrument OC-725 amplifier, filtered at 10 kHz, digitized using a Digidata-1322 (Axon Instrument). For current visualization and stimulation protocol application, we used Axon pClamp 9 software (Molecular Devices, Sunnyvale, CA). Recording electrodes were pulled to 0.2–1.0 MΩ by using a horizontal puller (Sutter Instrument, Model P-97, USA) and filled with 3 M KCl. Currents were recorded in response to two recording protocols. The first was a voltage-step protocol consisting of a pre-pulse of –80 mV (80 ms duration) from a holding potential of –60 mV, followed by steps (300 ms duration) from –110 to 40 mV, and return to a –60 mV holding potential. Current–voltage curves were obtained by plotting the steady-state currents at the end of each voltage step. The second protocol was a ramp protocol used for time course manipulations, consisting on a pre-pulse of –110 mV (100 ms duration), from a holding potential of –60 mV, followed by a ramp from –110 to 40 mV over 3.5 s. This protocol was automatically repeated every 7 s. The time course of the activation for mTASK-2 channels ( $\tau$ , ms) was calculated by fitting the current trace obtained at 0 mV with a single exponential suite of pClamp 9.

**Flow cytometry.** HEK-293 cells were grown in 60 mm dishes and transiently transfected with HA/GFP-tagged K2P vectors using JetPEI (Polyplus transfection). 24 h after transfection, cells were gently harvested by using PBS, 10 mM EDTA, then centrifuged for 5 min at 350 g and resuspended in PBS, 5% horse serum incubation solution at  $5 \times 10^6$  cells per mL. 100 µL of the cells were then incubated for 2 h on ice with anti-HA antibody (Sigma-Aldrich, HA-7 clone, 1/1000), followed by 1 h with Alexa594-conjugated anti-mouse antibody (Molecular Probes, 1/1000). Cells were washed once with incubation solution and resuspended in PBS. Quantification was performed on a BD LSR2 Fortessa using 525/50 bandpass (excitation GFP 488 nm), 605/40 bandpass (excitation Alexa594 561 nm) and 450/50 (excitation Dapi 405 nm) filter sets. Live single cells were identified as DAPI-negative and based on forward scatter/side scatter profiles. The GFP-positive gate (GFP+) and red-positive gate (Alexa594+ or HA+) were set manually using the following control conditions: (c1) the background level of red fluorescence was determined by measuring fluorescence intensity of empty vector transfected cells incubated with antibodies (c2) the GFP-positive window was estimated from unlabeled transfected cells and (c3) the HA-positive window with cells transfected with an HA-tagged construct incubated with antibodies. Cytometry data were analyzed using the BD CellQuest Pro software (BD Biosciences).

**Single-channel analysis.** HEK-293 cells (obtained from the Korean Cell Line Bank) were seeded at a density of  $2 \times 10^5$  cells per 35 mm dish 24 h prior to transfection in Dulbecco's modified Eagle's medium (DMEM) containing 10% FBS. HEK-293 cells were transfected with mTREK1, mTREK1 G171S, mTREK1 G171D, mTRAAK, mTRAAK G133S, or mTRAAK G133D in pIRES-eGFP DNA using LipofectAMINE2000 and OPTI-MEM 1 Reduced Serum Medium (Life technologies, Grand Island, NY, USA). Cells expressing green fluorescence were detected with the aid of a Nikon microscope equipped with a mercury lamp light source. Cells were used 1–3 days after transfection.

All recordings were performed using a patch clamp amplifier (Axopatch 200, Axon Instruments, Union City, CA, USA). Single-channel currents were filtered at 2 kHz using an 8-pole Bessel filter (–3 dB; Frequency Devices, Haverhill, MA) and transferred to a computer using the Digidata 1320 interface (Axon) at a sampling rate of 20 kHz. Threshold detection of channel openings was set at 50%. Single-channel currents were analyzed with the pCLAMP program (version 10, Axon). The filter dead time was 100 µs (0.3/cutoff frequency) for single-channel analysis, therefore, events lasting less than 50 µs were not detected. Channel activity ( $NP_o$ , where N is the number of channels in the patch and  $P_o$  is the probability of a channel being open) was determined from ~1–2 min of current recording. In experiments using cell-attached patches, the pipette and bath solutions contained (mM): 150 KCl, 1 MgCl<sub>2</sub>, 5 EGTA, and 10 HEPES (pH 7.3). All experiments were performed at ~25 °C.

**C. elegans experiments.** All strains described in this study were built using N2 (obtained from the CGC) as a wild-type starting strain. Strains were fed OP50 and grown at 20 °C unless otherwise noted. Strains generated for this study are listed in Supplementary Table 2.

All TM2.6 mutants were generated using CRISPR/Cas9-based homologous recombination by injecting Cas9 ribonucleoprotein complexes into the syncytial gonad of 1-day old N2 hermaphrodites alongside single-strand DNA oligonucleotide repair templates. First, guide RNA duplexes were formed in vitro by incubating 3 µL of crRNA with 3 µL of tracrRNA (100 µM stock solution each, in Nuclease-Free Water, IDT) in Nuclease-Free Duplex Buffer (IDT) in a final volume of 10 µL. RNA duplexes were then incubated at 95 °C for 5 min, followed by 5 min incubation at room temperature. Next, 1.5 µL of crRNA:tracrRNA duplex was added to 15 µg of recombinant Cas9 protein (Alt-R S. p. Cas9 Nuclease 3NLS, IDT), followed by 125 pmol of single-strand DNA repair template and nuclease-free water up to a final volume of 10 µL. This mix was injected into adult hermaphrodites after centrifugation (10 min, 10,000g, 4 °C). Injected worms were raised at 25 °C for 2–3 days, after which mutant worms were identified in the F1 progeny based on expected phenotypes of known gain-of-function mutants. CRISPR/Cas9-induced molecular lesions were confirmed by Sanger sequencing for all alleles generated in this study. Genome engineering reagents are listed in Supplementary Table 3 and 4.

**Microscopy.** *C. elegans* images were acquired using brightfield illumination on a Zeiss Z1 AxioImager at  $\times 5$  magnification. Worms were immobilized using M9 buffer supplemented with 50 mM sodium azide.

**Reporting summary.** Further information on experimental design is available in the Nature Research Reporting Summary linked to this article.

## Data availability

Data supporting the findings of this manuscript are available from the corresponding authors upon reasonable request. A reporting summary for this article is available as a Supplementary Information file. The source data underlying Figs. 1c, 2a, b, 3a–d, 4a, b, e, f, 5a, b, 6a, e, and Supplementary Fig. 3 are provided as a Source Data file.

Received: 16 July 2018 Accepted: 23 January 2019

Published online: 15 February 2019

## References

- Enyedi, P. & Czirják, G. Molecular background of leak K<sup>+</sup> currents: two-pore domain potassium channels. *Physiol. Rev.* **90**, 559–605 (2010).
- Buckingham, S. D., Kidd, J. F., Law, R. J., Franks, C. J. & Sattelle, D. B. Structure and function of two-pore-domain K<sup>+</sup> channels: contributions from genetic model organisms. *Trends Pharmacol. Sci.* **26**, 361–367 (2005).
- Hobert, O. The neuronal genome of *Caenorhabditis elegans*. *WormBook* 1–106. <https://doi.org/10.1895/wormbook.1.161.1> (2013).
- Bagriantsev, S. N., Peyronnet, R., Clark, K. A., Honoré, E. & Minor, D. L. Multiple modalities converge on a common gate to control K2P channel function. *EMBO J.* **30**, 3594–3606 (2011).
- Kunkel, M. T., Johnston, D. B., Thomas, J. H. & Salkoff, L. Mutants of a temperature-sensitive two-P domain potassium channel. *J. Neurosci.* **20**, 7517–7524 (2000).
- de la Cruz, I. P., Levin, J. Z., Cummins, C., Anderson, P. & Horvitz, H. R. sup-9, sup-10, and unc-93 may encode components of a two-pore K<sup>+</sup> channel that coordinates muscle contraction in *Caenorhabditis elegans*. *J. Neurosci.* **23**, 9133–9145 (2003).
- Friedrich, C. et al. Gain-of-function mutation in TASK-4 channels and severe cardiac conduction disorder. *EMBO Mol. Med.* **6**, 937–951 (2014).
- Ben-Abu, Y., Zhou, Y., Zilberberg, N. & Yifrach, O. Inverse coupling in leak and voltage-activated K<sup>+</sup> channel gates underlies distinct roles in electrical signaling. *Nat. Struct. Mol. Biol.* **16**, 71–79 (2009).
- Chatelain, F. C. et al. TWIK1, a unique background channel with variable ion selectivity. *Proc. Natl Acad. Sci. USA* **109**, 5499–5504 (2012).
- Chatelain, F. C. et al. Silencing of the tandem pore domain halothane-inhibited K<sup>+</sup> channel 2 (THIK2) relies on combined intracellular retention and low intrinsic activity at the plasma membrane. *J. Biol. Chem.* **288**, 35081–35092 (2013).
- Ketchum, K. A., Joiner, W. J., Sellers, A. J., Kaczmarek, L. K. & Goldstein, S. A. A new family of outwardly rectifying potassium channel proteins with two pore domains in tandem. *Nature* **376**, 690–695 (1995).
- Lotshaw, D. P. Biophysical and pharmacological characteristics of native two-pore domain TASK channels in rat adrenal glomerulosa cells. *J. Membr. Biol.* **210**, 51–70 (2006).
- Reyes, R. et al. Cloning and expression of a novel pH-sensitive two pore domain K<sup>+</sup> channel from human kidney. *J. Biol. Chem.* **273**, 30863–30869 (1998).
- Kang, D., Han, J., Talley, E. M., Bayliss, D. A. & Kim, D. Functional expression of TASK-1/TASK-3 heteromers in cerebellar granule cells. *J. Physiol.* **554**, 64–77 (2004).
- Niemeyer, M. I. et al. Neutralization of a single arginine residue gates open a two-pore domain, alkali-activated K<sup>+</sup> channel. *Proc. Natl Acad. Sci. USA* **104**, 666–671 (2007).
- Miller, A. N. & Long, S. B. Crystal structure of the human two-pore domain potassium channel K2P1. *Science* **335**, 432–436 (2012).
- Brohawn, S. G., del Mármol, J. & MacKinnon, R. Crystal structure of the human K2P TRAAK, a lipid- and mechano-sensitive K<sup>+</sup> ion channel. *Science* **335**, 436–441 (2012).
- Lolicato, M. et al. K2P2.1 (TREK-1)-activator complexes reveal a cryptic selectivity filter binding site. *Nature* **547**, 364–368 (2017).
- Kindler, C. H. et al. Amide local anesthetics potently inhibit the human tandem pore domain background K<sup>+</sup> channel TASK-2 (KCNK5). *J. Pharmacol. Exp. Ther.* **306**, 84–92 (2003).
- Piechotta, P. L. et al. The pore structure and gating mechanism of K2P channels. *EMBO J.* **30**, 3607–3619 (2011).
- Ma, X.-Y. et al. External Ba<sup>2+</sup> block of the two-pore domain potassium channel TREK-1 defines conformational transition in its selectivity filter. *J. Biol. Chem.* **286**, 39813–39822 (2011).
- Zhuo, R.-G. et al. The isoforms generated by alternative translation initiation adopt similar conformation in the selectivity filter in TREK-2. *J. Physiol. Biochem.* **71**, 601–610 (2015).
- Fink, M. et al. A neuronal two P domain K<sup>+</sup> channel stimulated by arachidonic acid and polyunsaturated fatty acids. *EMBO J.* **17**, 3297–3308 (1998).
- Kang, D., Choe, C., Cavanaugh, E. & Kim, D. Properties of single two-pore domain TREK-2 channels expressed in mammalian cells. *J. Physiol.* **583**, 57–69 (2007).
- Aryal, P., Abd-Wahab, F., Bucci, G., Sansom, M. S. P. & Tucker, S. J. A hydrophobic barrier deep within the inner pore of the TWIK-1 K2P potassium channel. *Nat. Commun.* **5**, 4377 (2014).
- Yoshimura, K., Batiza, A., Schroeder, M., Blount, P. & Kung, C. Hydrophilicity of a single residue within MscL correlates with increased channel mechanosensitivity. *Biophys. J.* **77**, 1960–1972 (1999).
- Shi, N., Zeng, W., Ye, S., Li, Y. & Jiang, Y. Crucial points within the pore as determinants of K<sup>+</sup> channel conductance and gating. *J. Mol. Biol.* **411**, 27–35 (2011).
- Honoré, E. The neuronal background K2P channels: focus on TREK1. *Nat. Rev. Neurosci.* **8**, 251–261 (2007).
- Lesage, F. & Barhanin, J. Molecular physiology of pH-sensitive background K (2P) channels. *Physiology* **26**, 424–437 (2011).
- de la Cruz, I. P., Ma, L. & Horvitz, H. R. The *Caenorhabditis elegans* Iodotyrosine deiodinase ortholog SUP-18 functions through a conserved channel SC-Box to regulate the muscle two-pore domain potassium channel SUP-9. *PLoS Genet.* **10**, e1004175–16 (2014).
- Greenwald, I. S. & Horvitz, H. R. Dominant suppressors of a muscle mutant define an essential gene of *Caenorhabditis elegans*. *Genetics* **101**, 211–225 (1982).
- El Mouridi, S. et al. Reliable CRISPR/Cas9 genome engineering in *Caenorhabditis elegans* using a single efficient sgRNA and an easily recognizable phenotype. *G3 (Bethesda)* **7**, 1429–1437 (2017).
- Brenner, S. The genetics of *Caenorhabditis elegans*. *Genetics* **77**, 71–94 (1974).
- Dong, Y. Y. et al. K2P channel gating mechanisms revealed by structures of TREK-2 and a complex with Prozac. *Science* **347**, 1256–1259 (2015).
- Bagriantsev, S. N., Clark, K. A. & Minor, D. L. Metabolic and thermal stimuli control K(2P)2.1 (TREK-1) through modular sensory and gating domains. *EMBO J.* **31**, 3297–3308 (2012).
- Schewe, M. et al. A non-canonical voltage-sensing mechanism controls gating in K2P K(+) channels. *Cell* **164**, 937–949 (2016).
- Zilberberg, N., Ilan, N. & Goldstein, S. A. KCNK0: opening and closing the 2-P-domain potassium leak channel entails ‘C-type’ gating of the outer pore. *Neuron* **32**, 635–648 (2001).
- Schneider, E. R., Anderson, E. O., Gracheva, E. O. & Bagriantsev, S. N. Temperature sensitivity of two-pore (K2P) potassium channels. *Curr. Top. Membr.* **74**, 113–133 (2014).
- Cohen, A., Ben-Abu, Y., Hen, S. & Zilberberg, N. A novel mechanism for human K2P2.1 channel gating. Facilitation of C-type gating by protonation of extracellular histidine residues. *J. Biol. Chem.* **283**, 19448–19455 (2008).
- Sandoz, G., Douguet, D., Chatelain, F., Lazdunski, M. & Lesage, F. Extracellular acidification exerts opposite actions on TREK1 and TREK2 potassium channels via a single conserved histidine residue. *Proc. Natl Acad. Sci. USA* **106**, 14628–14633 (2009).
- Aryal, P., Sansom, M. S. P. & Tucker, S. J. Hydrophobic gating in ion channels. *J. Mol. Biol.* **427**, 121–130 (2015).
- Beckstein, O. & Sansom, M. S. P. Liquid-vapor oscillations of water in hydrophobic nanopores. *Proc. Natl Acad. Sci. USA* **100**, 7063–7068 (2003).
- Kong, C. et al. Distinct gating mechanisms revealed by the structures of a multi-ligand gated K(+) channel. *eLife* **1**, e00184 (2012).
- Brohawn, S. G., Campbell, E. B. & MacKinnon, R. Physical mechanism for gating and mechanosensitivity of the human TRAAK K<sup>+</sup> channel. *Nature* **516**, 126–130 (2014).
- Lolicato, M., Riegelhaupt, P. M., Arrigoni, C., Clark, K. A. & Minor, D. L. Transmembrane helix straightening and buckling underlies activation of mechanosensitive and thermosensitive K(2P) channels. *Neuron* **84**, 1198–1212 (2014).
- Aryal, P. et al. Bilayer-mediated structural transitions control mechanosensitivity of the TREK-2 K2P channel. *Structure* **25**, 708–718 (2017).
- Bagriantsev, S. N. et al. A high-throughput functional screen identifies small molecule regulators of temperature- and mechano-sensitive K2P channels. *ACS Chem. Biol.* **8**, 1841–1851 (2013).
- Chatelain, F. C. et al. The pore helix dipole has a minor role in inward rectifier channel function. *Neuron* **47**, 833–843 (2005).
- Vierra, N. C. et al. Type 2 diabetes-associated K<sup>+</sup> channel TALK-1 modulates  $\beta$ -cell electrical excitability, second-phase insulin secretion, and glucose homeostasis. *Diabetes* **64**, 3818–3828 (2015).
- Bauer, C. K. et al. Mutations in KCNK4 that affect gating cause a recognizable neurodevelopmental syndrome. *Am. J. Hum. Genet.* **103**, 621–630 (2018).
- Boulin, T., Gielen, M., Williams, D. C., Paoletti, P. & Bessereau, J.-L. Eight genes are required for functional reconstitution of the *Caenorhabditis elegans* levamisole-sensitive acetylcholine receptor. *Proc. Natl Acad. Sci. USA* **105**, 18590–18595 (2008).
- Bobak, N. et al. Recombinant tandem of pore-domains in a weakly inward rectifying K<sup>+</sup> channel 2 (TWIK2) forms active lysosomal channels. *Sci. Rep.* **7**, 649 (2017).
- Crooks, G. E., Hon, G., Chandonia, J.-M. & Brenner, S. E. WebLogo: a sequence logo generator. *Genome Res.* **14**, 1188–1190 (2004).

## Acknowledgements

The authors are grateful to F. Sepúlveda, V. Renigunta, N. Bobak, S. Feliciangeli, F. Chatelain, and M. Jodar for providing plasmids. The authors thank M. Jospin and M. Gielen for critical reading of the manuscript. Some strains were provided by the CGC, which is funded by NIH Office of Research Infrastructure Programs (P40 OD010440). I. B.S. was supported by AFM Téléthon (Alliance MyoNeurALP). This work was funded by a grant from the European Research Council (T.B., *Kelegans*), Bourse Qualité Recherche from Université Claude Bernard (O.A.), the Korean Government (NRF-2015R1A-5A2-008833), and the Agence Nationale de la Recherche (Laboratory of Excellence “Ion Channel Science and Therapeutics”, grant ANR-11-LABX-0015-01 to F.L., D.B., and L.K.; ANR blanche Dynaselect, grant ANR-14-CE13-0010 to F.L. and D.B.).

## Author contributions

I.B.S., L.K., and O.A. performed two-electrode voltage-clamp experiments. D.K. performed single-channel analyses. D.B. performed FACS analyses. S.E.M., A.L.-B., P.T., N. Z., and M.G. performed experiments in *C. elegans*. All authors were involved in the analysis of the experimental data. The manuscript was written by T.B. with contributions from all other authors.

## Additional information

**Supplementary Information** accompanies this paper at <https://doi.org/10.1038/s41467-019-08710-3>.

**Competing interests:** The authors declare no competing interests.

**Reprints and permission** information is available online at <http://npg.nature.com/reprintsandpermissions/>

**Journal peer review information:** *Nature Communications* thanks Alistair Mathie and the other anonymous reviewer(s) for their contribution to the peer review of this work. Peer reviewer reports are available.

**Publisher's note:** Springer Nature remains neutral with regard to jurisdictional claims in published maps and institutional affiliations.



**Open Access** This article is licensed under a Creative Commons Attribution 4.0 International License, which permits use, sharing, adaptation, distribution and reproduction in any medium or format, as long as you give appropriate credit to the original author(s) and the source, provide a link to the Creative Commons license, and indicate if changes were made. The images or other third party material in this article are included in the article's Creative Commons license, unless indicated otherwise in a credit line to the material. If material is not included in the article's Creative Commons license and your intended use is not permitted by statutory regulation or exceeds the permitted use, you will need to obtain permission directly from the copyright holder. To view a copy of this license, visit <http://creativecommons.org/licenses/by/4.0/>.

© The Author(s) 2019

Supplementary Information

**Mutation of a single residue promotes gating of vertebrate and invertebrate two-pore domain potassium channels**

Ben Soussia\*, El Mouridi\*, *et al.*

*Nature Communications* (2019)

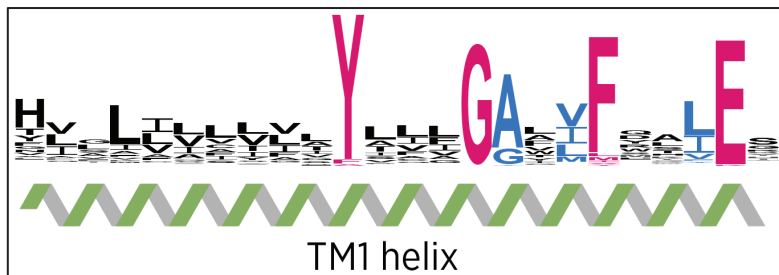
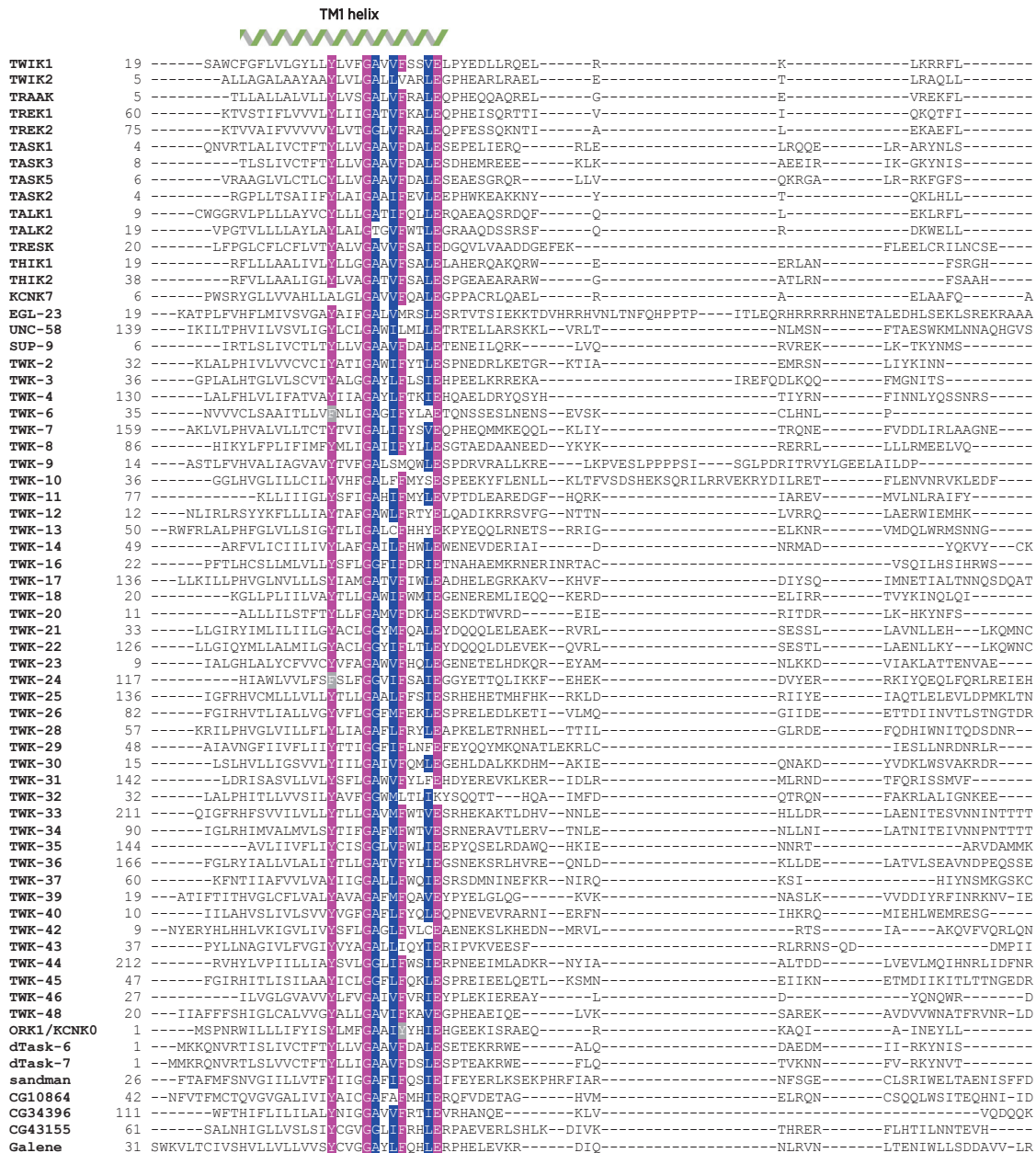








## Supplementary Figure 2

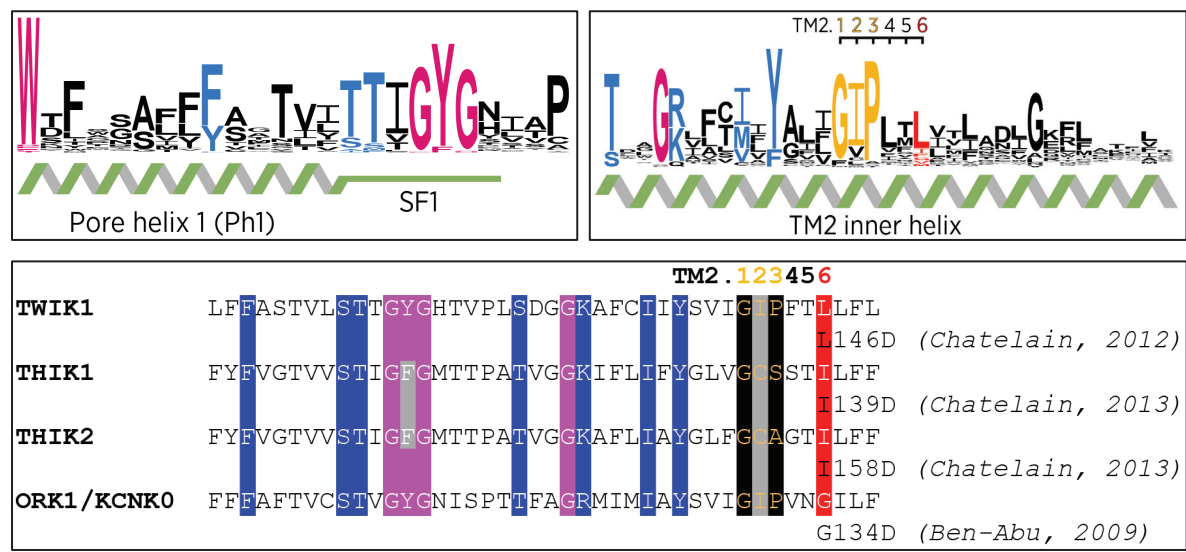
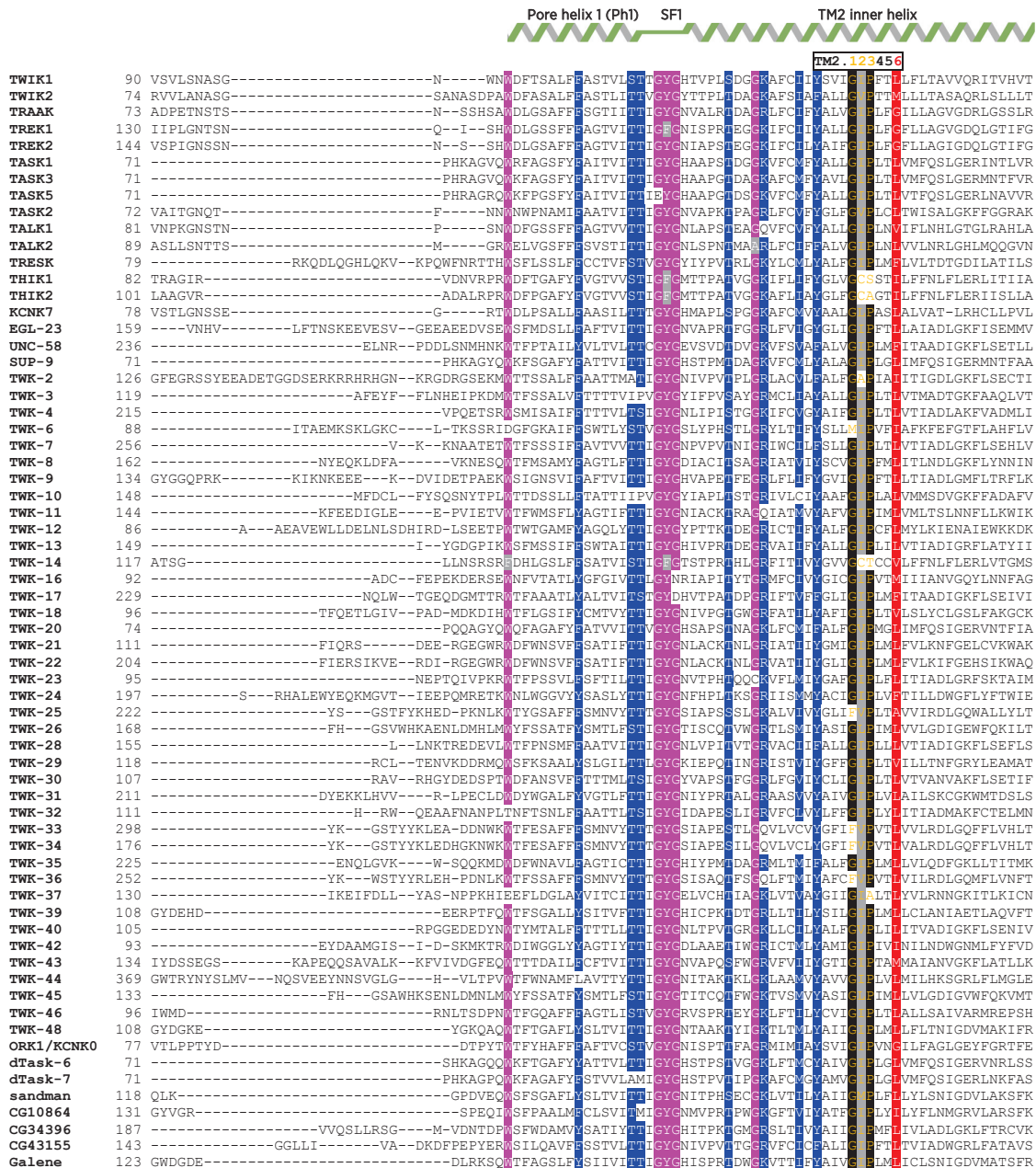


Supplementary Figure 2 - Clustal Omega alignment of human, *C. elegans*, and *D. melanogaster* two-pore domain potassium channel sequences.

Genbank identifiers for aligned sequences are listed below. N- and C-terminal cytoplasmic portions were truncated before alignment. Cartoon representations on top mark the four transmembrane helix regions (TM1, TM2, TM3, and TM4), two pore helix domains (Ph1 and Ph2), and two selectivity filters (SFI and SF2). Sequence logos were generated using WebLogo 3 (Crooks et al., 2004). Highly conserved residues are indicated in *hotpink* and well conserved residues in *maroon*, as in Figure 1.


TWIK1, NP\_002236 ; TWIK2, NP\_004814 ; TRAAK, NP\_201567 ; TREK1, NP\_001017425 ; TREK2, NP\_612190 ; TASK1, NP\_002237 ;  
 TASK3, NP\_001269463 ; TASK5, NP\_071753 ; TASK2, NP\_003731 ; TALK1, NP\_001128578 ; TALK2, AAH25726 ; TRESK, NP\_862823 ;  
 THIK1, NP\_071337 ; THIK2, NP\_071338 ; KCNK7, NP\_203133 ; EGL-23, NP\_001255776 ; UNC-58, NP\_741880 ; SUP-9, NP\_494333 ;  
 TWK-2, NP\_494786 ; TWK-3, NP\_495727 ; TWK-4, NP\_001343566 ; TWK-6, NP\_497973 ; TWK-7, NP\_498903 ; TWK-8, NP\_001023596  
 ; TWK-9, NP\_501724 ; TWK-10, NP\_001300134 ; TWK-11, NP\_001343632 ; TWK-12, NP\_505731 ; TWK-13, NP\_506091 ; TWK-14,  
 NP\_001256414 ; TWK-16, NP\_508526 ; TWK-17, NP\_001024466 ; TWK-18, NP\_509516 ; TWK-20, NP\_510284 ; TWK-21, NP\_510654 ;  
 TWK-22, NP\_510655 ; TWK-23, NP\_001257229 ; TWK-24, AAC32865 ; TWK-25, NP\_502170 ; TWK-26, NP\_508522 ; TWK-28, NP\_508732  
 ; TWK-29, NP\_001021467 ; TWK-30, NP\_492381 ; TWK-31, NP\_001022883 ; TWK-32, NP\_506416 ; TWK-33, NP\_001309463 ; TWK-34,  
 NP\_506906 ; TWK-35, NP\_508031 ; TWK-36, NP\_507485 ; TWK-37, NP\_491810 ; TWK-39, NP\_001076639 ; TWK-40, NP\_001255207 ;  
 TWK-42, NP\_507483 ; TWK-43, NP\_872137 ; TWK-44, NP\_509942 ; TWK-45, NP\_001122742 ; TWK-46, NP\_741678 ; TWK-48,  
 NP\_001022681 ; ORK1/KCNK0, NP\_511112 ; dTask-6, NP\_001262539 ; dTask-7, NP\_649891 ; sandman, NP\_610349 ; CG10864,  
 NP\_650726 ; CG34396, NP\_001097392 ; CG43155, NP\_572720 ; Galene, NP\_612084.

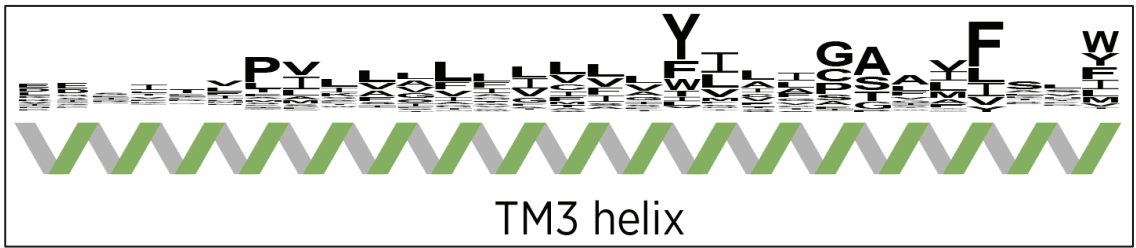
# Supplementary Figure 2



Previously published gain-of-function mutants of TM2.6 (see manuscript for references).

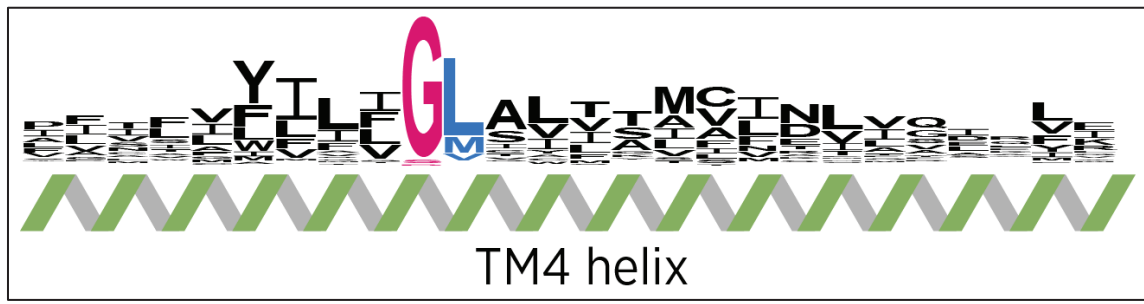
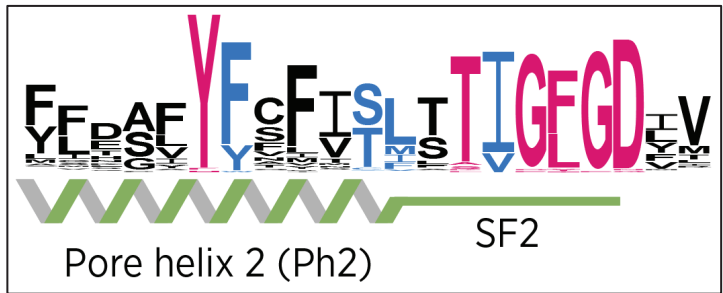
# Supplementary Figure 2

			TM3 helix
			
TWIK1	179	-----	---VAIVHAVLLGFVTVSCFFFIIPAAVFSVLED---
TWIK2	168	-----	---AACWHLVALLGVVTVCFVLPVAVIFAHLEE---
TAAK	167	-----	---VRVLSAMFLFLIGCLLFLVLTPTTFVFCYME---
TREK1	221	-----	---IRIISTIIFFILFGCVLFLVALPAIIFKHIE---
TREK2	236	-----	---TRVISTILFIIAGCIVFVVIIPAVIFKYIE---
TASK1	155	-----	---SMANMVLIGFFSCISTLTCIGAAAFSHYE---
TASK3	155	-----	---SMENMVTVGFSCMGTLTCIGAAAFSQCE---
TASK5	155	-----	---STENLVVAGLLACAATLALGAVAFSHFE---
TASK2	158	-----	---AQITCTVIFIVMGVLVHLVIPPVFMVTE---
TALK1	167	-----	---LQVLGLALFLTLGLTVLILIPPVFMVSHVE---
TALK2	179	-----	---LA---GSCALLSCILLFLLLPFLFSHME---
TRESK	268	-----	---N-LDEVGQQVERLDIPLPIIALIVFAYISCAAAILPFWET---
THIK1	182	-----	---CEVDSLAEVDSLA---GWKPSVYVVMILICTA-SILISCCASAMYTPIE---
THIK2	201	-----	---SEADSLA---GWKPSVYHVLLILGLF-AVLLSCCASAMYTSVE---
KCNK7	166	-----	---AALLQAVALLGLLVASSFVLLPALVWGLQG---
EGL-23	294	-----	---E-VSEEDDLTETEATSLFIFLVYIAFGFMMAAYEP---
UNC-58	348	-----	---D-ILGVDGTEEKLWFPIGAYVSCICICYSIGSAMFITWER---
SUP-9	155	-----	---SSDLII FCTGWG-GLLIFGGAFMSSSYE---
TWK-2	265	-----	---I-LDMMDDEIDKSEVPVLMVPTIILLYI-APGGILFSPILE---
TWK-3	205	-----	---AAIFVCLLFAYPLVVGFIICLST-S---
TWK-4	285	-----	---TEDPKTGRQLLVFLVFLGMYTISACVYTIIEP---
TWK-6	191	-----	---E-TPSNSL--QHDYLIFLSLLLCISLSSSALFSSIE---
TWK-7	356	-----	---H-GMGHDMNIEEKRIIPFLVLAAILVYI-APFGVLMKLE---
TWK-8	302	-----	---E-DIEDEEERSMPPMSVKVALGITVWGFPCALFKLWE---
TWK-9	302	-----	---E-E-EPENNEPRKTEESIALGITFTCYLVAGAKILSVYEP---
TWK-10	240	-----	---KIQNTAFMVLVLLVAVSYVIGGIAYSKI-V---
TWK-11	288	-----	---E-DDE-EEEEIHQDPPVLTSLIATVAVIILSAAVCLFE---
TWK-12	228	-----	---E-DPEAAEERKKKFFPIPIAIIIMLIWIICFSASMFICWED---
TWK-13	325	-----	---E-QIQFDPNSHEKRVSVLFIILLIMLGYV-AGGAYIVRWWE---
TWK-14	225	-----	---SCGGHMD---NWRPSVYKVFVFLFSM-CLVLTITASAGIYSVVE---
TWK-16	188	-----	---IYKESSIQVTSALLCVFLIYVAVGALLPLLNG---
TWK-17	351	-----	---D-DEECEDEEDRLQLPIASYPFTLIIGYCCVGSLLFNTFEK---
TWK-18	213	-----	---E-KTE-NNDDLLSFPISGLLLITVIVWIFCAVLFTFLE---
TWK-20	162	-----	---TPHLLMVSLLTIGFMVIVSGTYMFTIE---
TWK-21	220	-----	---F-FEVPEDDKEDTTFQLRWGLLVIVLVVLCSEFVVSFWE---
TWK-22	300	-----	---E-SGISEDEEQITTFPVKRALFIVFFMVCCLIVSFWE---
TWK-23	176	-----	---KQSDHLLREIAEVLVAGLFVVFIAIGSAVILWEN---
TWK-24	348	-----	---L-DVDVPMGEQVQVPIKSAIIFFFLWIMIISAFIVRLWEY---
TWK-25	312	-----	---G-FVDKLDDEIITLPIKFSVSMILYLLSATMFIPEYDELS---
TWK-26	259	-----	---K-QPVNRKKN-EILLPMLALFLVLAAILICTLTIKMPDHNE---
TWK-28	275	-----	---D-SDSEDSAGDELRIIPVFMVLLVLLAYT-AIGGFLFQSWE---
TWK-29	205	-----	---EDENVSGSTLFFIVLVYLLIGATMIPMLSG---
TWK-30	215	-----	---EEEILDRVLRVFPPLTVFFVFFVYG-CIAAWVVRYWE---
TWK-31	327	-----	---A-DPEKKPEVESRTIPIWLALLICVYVYVAGCSSLFLWET---
TWK-32	230	-----	---F-LWTHLEHAQFVEVFFLVIGILLLYI-GLSSWISWVE---
TWK-33	388	-----	---G-N-KHVDEDEIISLPKAKALLLASYLGACTIFIFYDELS---
TWK-34	267	-----	---G-D-TSIDVNEIIPKIPKACLLALLALYLAFACTIFIHVFDLS---
TWK-35	327	-----	---ERQERHLDIDFDLPLVPGIALIVTWIFICSFVLSVWDH---
TWK-36	342	-----	---G-K-REVDEDEIQLPIKFCMTILIAVLLCTTFVYLVDAVM---
TWK-37	226	-----	---YKMTVLKAFILLVTFWCFGALAIAYVE---
TWK-39	427	SA-RELR---	---EKEMMMNLSNHKQPSMDSSTSRRLRIDIGRSYRSDRSERSDEMSSLHSLRRNRGHRNQEKMPV--SVGICIVFAPISGGAWLFSWWE---
TWK-40	207	-----	---LNLDHLENYISIPFIVVAILLSYI-TFGAVVLSMWE---
TWK-42	213	-----	---P-SP--QNFNGTRPIPLLVLVLFVPMIQCVAYFAYFE---
TWK-43	277	-----	---E-E-AEEVEESDVTEITVLFVAVLVYIIAGSLLMSYEE---
TWK-44	482	-----	---RNTGEDRISEMPLLAI GVAFGWMLCAIIFLRFK---
TWK-45	241	-----	---K-QSIEIKRK-ETLLPMLLAMLVFTYIIICTLTIILFDNE---
TWK-46	186	-----	---IQLIHGVVVFASLLLVFAIPAMVFSIET---
TWK-48	247	M-----	---EQL---EVRETAQAQLESMTVPIISLVVFTMLGVLGVGTTFIKVWE---
ORK1/KCNK0	172	-----	---GLITTVVIALIPGIALFLLLPWVFTYFE---
dTask-6	155	-----	---SEVDLICVVTLSLTIAGGAAAFSKFE---
dTask-7	156	-----	---TEMNMLATGMLSSIIITGAAVFSRYE---
sandman	264	-----	---QYTESDS---DIEREIRGSTDEITVPVTVCFVVMVGYILWGALLFGRWE---
CG10864	221	-----	---ALEGGVGMTRKKVLPSTACLWLIFFYVLTGTVMFANWE---
CG34396	340	-----	---P-YPETFEVDDEFNLPVSVASLLIITYILLGSFGFLMMEF---
CG43155	234	-----	---FICKTWFYAILAVGFLGVYLAAGALLLWED---
Galene	552	SRSREPKNRRRRAERLPPSPRIMSPMGFPVQRQIRRRPSYDYDDD---	---SMYGDEYGDYDGLLPKDRPVPVWLCVFLVVSYILGGAVLFAWYE---

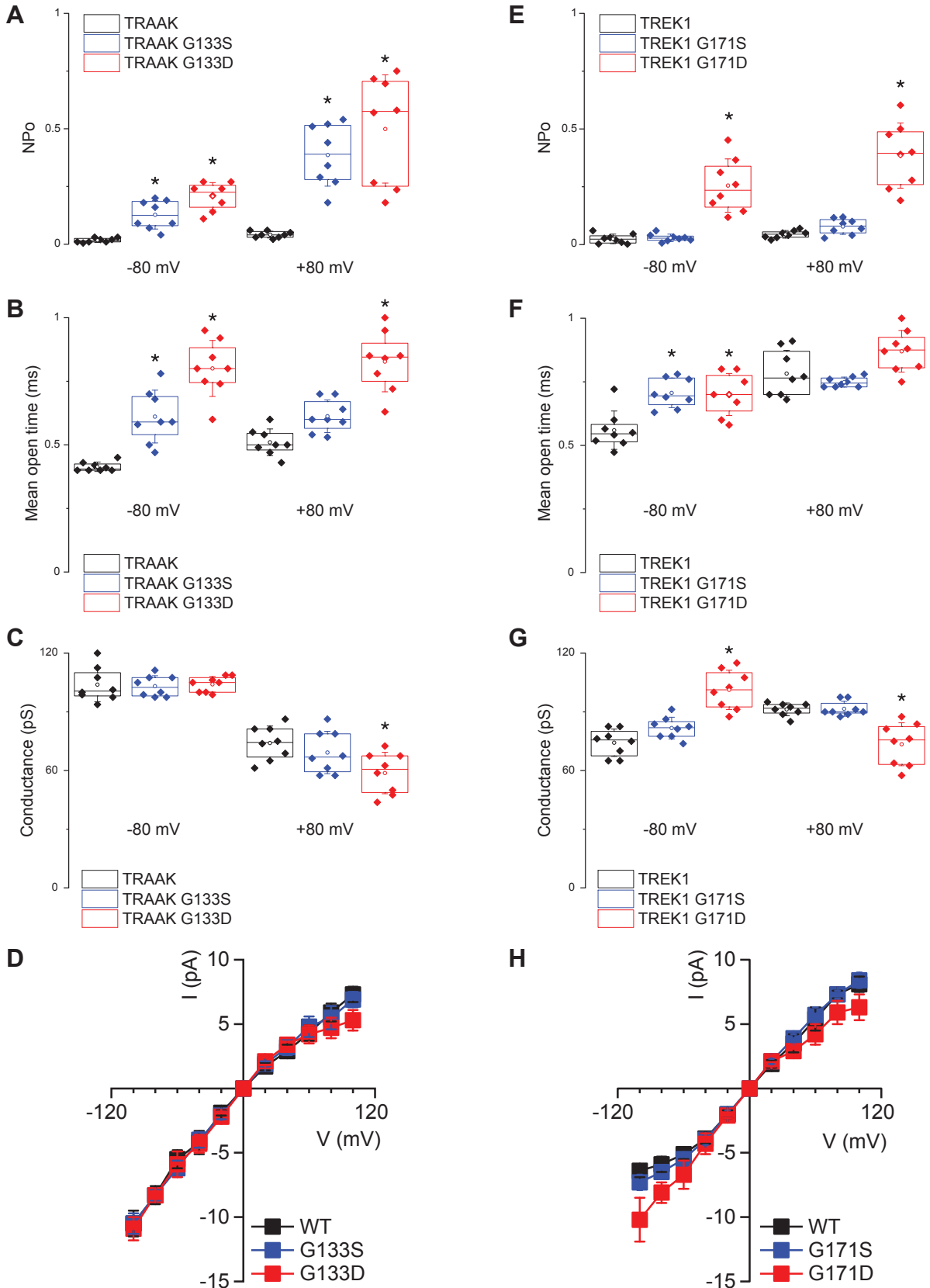


# Supplementary Figure 2

	Pore helix 2 (Ph2) SF2	TM4 inner helix
209	-----DWNFLESFYFCFISLSTIG:GDYVPGEGYNQK-----	F---RELYKIGITCYLLLSLITAMLVVLETFCELHE
198	-----AWSFLDARFYFCFISLSTIG:GDYVPGEAPQP-----	Y---RALYKVLVTYVLFSLIVAMVVLVQTFRHVSD
196	-----DMSKLEAIYFVIVTITTVG:GDYVAGAD--PRQ-----	D---SPAYQPLVWVWILLGLAYFASVLTITGNWLR
250	-----GWSALDAIYFVVITITTVG:GDYVAGGS--DIE-----	Y---LDFYKPVVWFVILVGLAYFAVLSMIGDWLR
265	-----GWTALESIYFVVVITITTVG:GDYVAGGN--AGIN-----	Y---REWYKPLVWFVILVGLAYFAVLSMIGDWLR
183	-----HWTFFQAYYFCFISLSTIG:GDYVALQKQDAL-----	QTKQYVAFSFFVYLLTGLTVIGAPLNLVLRFM
183	-----EWSFFHAYYFCFISLSTIG:GDYVALQKQDAL-----	QKPLVAFSFFVYLLTGLTVIGAPLNLVLRFM
183	-----GWTFFHAYYFCFISLSTIG:GDYVALQKQDAL-----	QKPLVAFSFFVYLLTGLTVIGAPLNLVLRFM
187	-----GWNYLEGLYFSPITLSTIG:GDYVAGVN--PSAN-----	Y---HALYRYFVFLVYLLGLAWLSLFFVNWKVSMEFV
196	-----GWSFSEGFYFCFISLSTIG:GDYVVGTD--PSKH-----	Y---ISVYRSLAAIWIILLGLAWLALILPLGLLLH
205	-----GWSYTEGRYFCFISLSTIG:GDYVIGMN--PSQR-----	Y---PLWYKMNVSLLVLFGLAWLALILKLLSQLE
307	-----QLDFENAFYFCFVITITTVG:GDYVLEH--PN-----	-----FFLFFSYIIVGMEIVFIAFKLVQNRLLI
221	-----GWSYFDSLFCFVAFSTIG:GDYVSSQNAH--YES-----	-----QGLYRFANFVFIIMGVCCYISLFFVISILIK-----
240	-----GWDYVDSLFCFVAFSTIG:GDYVSSQNAH--YRN-----	-----QGLYRLGNFLFILLGVCCYISLFFVISILIK-----
196	-----DCSLLGAVYFCFISLSTIG:EDLLPGRGRSLHPV-----	I---YHLGQALLGLYLLSGLLAMLAVETFSLELQ
331	-----DMDFFKAVYFNFTITTVG:GDYVPRRS--ET-----	-----YMLTIIVYIAISLALTTIAIEIAADALK
187	-----TWSFIIAFHFGFNLHVTVG:GDYVVTDD--YI-----	-----FLSLIVAFVIVGLSVVTCVLDASTHLK
382	-----NWTYFDVAVYFCFVITITTVG:GDYVALQKRGSL-----	QTKQYVAFSFFVYLLTGLTVISAMNLLVLRFL
303	-----DWSYMDARFYFCFISLSTIG:GDYVLPEN--HD-----	-----YIAMLILYLVGLSVTITMCDLAGIQYI
228	-----NITYLDSVYFSLTSTIG:GDYVTPDM--NV-----	-----IHMVLFVAVVILVITITLIDVAAEMI
317	-----MWSFLDSVYFCFVSLTVG:GDYVLPVGTVE-----	-----YMLCSIVFIFIHLITFLAVDVSGSVGI
227	-----NISYLSVSVYFCFISLSTIG:GDYVPTN--LV-----	-----WFSGYCMLFLISDVLNQCIFYFCQARVR
394	-----PWSFFTSFYFCFISLSTIG:GDYVMPRR--DG-----	-----YMYIILLYIILGLAITTMCIDLGVQYI
340	-----DWSYGQSCYFCFISLSTIG:GDYVSVQR--RD-----	-----MMVLCFVYVIVGLSVLSMTINVIQVALE
340	-----EMDFFKALYFNFTITTVG:GDYVFKPS--FD-----	-----LILLTILYIGIISLALTTMAIEIAADLTK
271	-----GVPMIEGVYFCFISLSTIG:GDYVTPGI--PV-----	-----YVIIIFIVFVAVIVTIAIDVVAANI
325	-----DWTFFTSFYFCFISLSTIG:GDYVTPAN--PE-----	-----YMIATFGVVIVGLSMLTVCIDVLQEKLA
267	-----TWVSSAVYFCFISLSTIG:GDYVLPFR--PD-----	-----MMVFNFLILVGLALLSMCFELITDRVA
363	-----EWTFFEARFYFCFVITITTVG:GDYVTPAN--VD-----	-----WLPLATLAYIVFGLIITITMCDLVGSEYI
264	-----NWNYIDSLYFCFISLSTIG:GDYVSNQDVTFRMS-----	-----PDLYRFVNFCLLIGACFFYCLSSASSIVVR-----
222	-----ELDFENGLYFNFLCSTIG:GDYVLPVIR--VE-----	-----LLPITFLYVICISLAIITIAINIGSEYMK
390	-----GPVWSFIHGVYFCFISLSTIG:GDYVLPVIR--VE-----	-----YLAASVYIISLAVITASLDCSSTLTK
250	-----EWDGFTSLYFTLISLSTIG:GDYVLPVIR--VE-----	-----FMPVGVLLIISLAVITASLDCSSTLTK
190	-----KWSIFDAYYFCFISLSTIG:GDYVLPVIR--VE-----	-----QDQPLVYFATIMFLLIISLAVTSACNLLVLRGM
258	-----NWDFLTAIYFCFISLSTIG:GDYVLPVIR--VE-----	-----TACALFVLYFISLALFAMVYAILQERVE
338	-----KWDFLTAIYFCFISLSTIG:GDYVLPVIR--VE-----	-----TACALFVLYFISLALFAMVYAILQERVE
214	-----QLTYFDSVYFCFISLSTIG:GDYVLPVIR--VE-----	-----FLLPITLYITISLAVITASLDCSSTLTK
387	-----EWTYFTAFYFCFISLSTIG:GDYVLPVIR--VE-----	-----FIIINLMTLISLAVITASLDCSSTLTK
353	-----PDSGISFFHAFYFCFISLSTIG:GDYVLPVIR--VE-----	-----FSPITIMFFFGMPILKVVNRVTYIKVC
299	-----GNKPF--GLGFFDARFYFCFISLSTIG:GDYVLPVIR--VE-----	-----YSPFLAAAPLLGLALISIVNTSIYAQLY
313	-----HLEYFEAFYFCFISLSTIG:GDYVLPVIR--VE-----	-----YVFTMAAIIIFSLATMCIIDLAGEYI
235	-----QDFENGLYFCFISLSTIG:GDYVLPVIR--VE-----	-----FLPISVYFMCITLAIITIALDIGSIYVR
252	-----TWTYVESLYFCFISLSTIG:GDYVLPVIR--VE-----	-----IHWTLAFVYVGLITITMCDVVGRRMYL
366	-----RWTFFTSLYFCFISLSTIG:GDYVLPVIR--VE-----	-----MFIYVNFVIVGLSIVSMFISVYVQIKIE
268	-----NWNMMDFGYFCFISLSTIG:GDYVLPVIR--VE-----	-----FAVPIFLIISLAVITASLDCSSTLTK
428	-----GPEPGTGMDMFLCFYFCFISLSTIG:GDYVLPVIR--VE-----	-----NIYENKIKFAPISIIIFFGMAVTKVVNRVTYIKVC
307	-----GDESIGSVMFLCFYFCFISLSTIG:GDYVLPVIR--VE-----	-----FSPITIMFFFGMPILKVVNRVTYIKVC
365	-----NWTLLESFYFCFISLSTIG:GDYVLPVIR--VE-----	-----LITIMFGFLLVGLSIVSMVNLQAKMK
382	-----GPEWDDGLPYFTAFYFCFISLSTIG:GDYVLPVIR--VE-----	-----YAPVPMIFFIEMAVTKVVNRVTYIKVC
253	-----EFVYDAILYFCFISLSTIG:GDYVLPVIR--VE-----	-----SCTIICVLHFIDLSISMLVLRVHHSME
517	-----NWNDFDGAAYFCFISLSTIG:GDYVLPVIR--VE-----	-----GSQELIVCALYLLFGLALIAMCFKLMQDDVV
243	-----GWDFFSGFYFCFISLSTIG:GDYVLPVIR--VE-----	-----YVILDLVYIISLITITMCDLVGVIQYI
249	-----NWTLEFESVYFCFISLSTIG:GDYVLPVIR--VE-----	-----AV--GGIVFVILGLSIVSMVNLQAKMK
315	-----GMTFLGAIYFCFISLSTIG:GDYVLPVIR--VE-----	-----WLFVTLVYCAISLALTTIAIEIAADLTK
518	-----DWDYFKSFYFCFISLSTIG:GDYVLPVIR--VE-----	-----DMFIIFGLIISLIVSMVNLQAKMK
281	-----GDEP--GWNFFDARFYFCFISLSTIG:GDYVLPVIR--VE-----	-----YSPFLAAAPLLGLALISIVNTSIYAQLY
216	-----DWSYLDARFYFCFISLSTIG:GDYVLPVIR--VE-----	F---RELYKIGATVYLLMGLCCMMLFLATLYDIQ
290	-----GWTFLSFYFCFISLSTIG:GDYVLPVIR--VE-----	-----DEAQEKLVITSIYLLFGLALIAMCFKLMQDDVV
201	-----NWPYSISLYFCFISLSTIG:GDYVLPVIR--VE-----	-----FGGWVYVYQIFVIVWFIFSLGLVLMIMFTITRGLQ
183	-----GWSYFDSVYFCFISLSTIG:GDYVLPVIR--VE-----	-----NRKPEYVMPALIFILFGLAIVAASLNLVLRFM
184	-----GWSYFDSVYFCFISLSTIG:GDYVLPVIR--VE-----	-----TNKPGYVLSLVVILFGLAVVAASLNLVLRFM
310	-----DWNYLDSVYFCFISLSTIG:GDYVLPVIR--VE-----	-----DKVEVVFALCAIYLLGLAVIAMCFKLMQDDVV
260	-----KWSLLNSFYFCFISLSTIG:GDYVLPVIR--VE-----	-----ELAQLQSVAAADQHSKLAIFVYMLLGLAVIAMCFKLMQDDVV
379	-----SWTPLDARFYFCFISLSTIG:GDYVLPVIR--VE-----	-----YVMYSMIYLMFGLALTSMTINVLVQKLS
266	-----DWTFFDGFYFCFISLSTIG:GDYVLPVIR--VE-----	-----YMLLCTIYLLIISLALTSMTINVLVQKLS
644	-----NWSFLDARFYFCFISLSTIG:GDYVLPVIR--VE-----	-----ESEQSIAYCSLYLLFGLIALLAMSFNLVQEEFI



### Supplementary Figure 3



#### Single channel properties of TRAAK and TREK1 TM2.6 mutants

(A) TRAAK, TRAAK G133S, TRAAK G133D, (E) TREK1, TREK1 G171S, and TREK1 G171D channel activity determined by NPo analysis at -80 and +80 mV.

(B), (F) Mean open times were obtained from channel openings recorded at -80 mV and +80 mV.

(C), (G) Unitary conductances obtained from channel openings recorded at -80 mV and +80 mV.

(D), (H) Current-voltage relationships of single channels.

Center lines, medians; open circles, means; box limits, 25th and 75th percentiles; whiskers, standard deviation. Kruskal-Wallis, Dunn's multiple comparison test, \*  $p < 0.05$ .

**Supplementary Table 1: Two-electrode voltage-clamp experiments (Figure 1B)**

Channel	TM2.6	cRNA	Day	$E_{rev}$ (mV)	$I$ ( $\mu$ A) at 0 mV
hTWIK1	WT	10 ng	1	$-38.1 \pm 2.4$	0.2
	L146N			$-88.4 \pm 1$	$2.7 \pm 0.2$
rTWIK2	WT	10 ng	1	$-33.1 \pm 1.1$	0.1
	M135D			$-66.4 \pm 2.2$	0.4
hTASK1	WT	0.8 ng	3	$-63.4 \pm 2.5$	$0.7 \pm 0.1$
	L122N			$-71.0 \pm 1.1$	$13.4 \pm 2$
hTASK3	WT	50 pg	1	$-73.4 \pm 4.3$	$1.8 \pm 0.3$
	L122N			$-77.6 \pm 2.5$	$5 \pm 0.8$
mTREK1	WT	1 ng	1	$-66.1 \pm 1.5$	$0.7 \pm 0.1$
	G171D			$-72.0 \pm 0.6$	$8.8 \pm 0.8$
mTREK2	WT	1 ng	2	$-52.5 \pm 2$	$0.5 \pm 0.1$
	G196D			$-72.1 \pm 0.9$	$1.7 \pm 0.2$
mTRAAK	WT	1 ng	2	$-55.6 \pm 1.5$	0.3
	G133D			$-65.8 \pm 0.8$	$32.9 \pm 7.2$
mTRESK	WT	1 ng	1	$-70.8 \pm 1.1$	$0.9 \pm 0.1$
	F156N			$-68.9 \pm 2$	$24.3 \pm 3.6$
mTASK2	WT	5 ng	1	$-87.5 \pm 2.8$	$3.8 \pm 0.6$
	L127N			$-90.3 \pm 6.6$	$14.2 \pm 1.6$
hTALK1	WT	20 ng	1	$-80.5 \pm 3.9$	$1 \pm 0.1$
	V137N			$-93.6 \pm 2.2$	$2.9 \pm 0.2$
hTALK2	WT	20 ng	1	$-42.4 \pm 2.1$	0.3
	L145N			$-51.4 \pm 3.5$	$1.4 \pm 0.1$
hTHIK2	WT	50 ng	2	$-31.1 \pm 5.1$	0.1
	I158D			$-83.3 \pm 0.9$	1
hTASK2	WT	10 ng	1	$-77.4 \pm 2.7$	0.4
	L127N			$-93.4 \pm 0.6$	$6.8 \pm 0.2$
rTWIK2 LY	WT	10 ng	1	$-84.3 \pm 0.8$	$2.2 \pm 0.1$
	M135D			$-79.9 \pm 0.8$	$8.5 \pm 0.2$
hTWIK1 AA	WT	10 ng	1	$-71.7 \pm 4$	0.4
	L146N			$-85.1 \pm 0.9$	$9.3 \pm 0.4$
hTHIK2 5RA	WT	15 ng	1	$-31.2 \pm 1.4$	0.2
	I158N			$-76.5 \pm 1$	$1.7 \pm 0.2$



**Supplementary Table 2: Strain list**

<b>Strain</b>	<b>Genotype</b>	<b>Description</b>
JIP1658	<i>egl-23(bln309) V</i>	EGL-23-wrmScarlet
JIP1506	<i>egl-23(bln309bln334) V</i>	EGL-23(L229N)-wrmScarlet
JIP1559	<i>egl-23(bln309bln359) V</i>	EGL-23(L229S)-wrmScarlet
JIP1620	<i>unc-58(bln448) X</i>	UNC-58(F294S)
JIP1621	<i>unc-58(bln449) X</i>	UNC-58(F294T)
JIP1622	<i>unc-58(bln450) X</i>	UNC-58(F294N)
JIP1623	<i>twk-18(bln451) X</i>	TWK-18(V158N)
JIP1636	<i>twk-18(bln458) X</i>	TWK-18(V158S)
JIP1706	<i>twk-18(bln491) X</i>	TWK-18(V158T)
JIP1677	<i>sup-9(bln476) II</i>	SUP-9(L122S)

**Supplementary Table 3: List of single strand oligonucleotides (DNA and RNA) for CRISPR/Cas9 genome engineering**

	<b>Sequence (5' to 3')</b>	<b>Description</b>
<b>crRNA</b> <b><i>unc-58</i></b>	gcggcagugauagacauuag	Use to generate UNC-58 (F294x)
oPT271	cggaaagggttttctcagtagcattcgcgcttggttggtataccactAatgtCTatCacTgcCgccgatattggtaaa tttttatctgaaacattactccagtttgtgagct	Repair template (Ultramer) for UNC-58 (F294S)
oPT273	tcggaaagggttttctcagtagcattcgcgcttggttggtataccactAatgACAATacTgcCgccgatattggtaa atttttatctgaaacattactccagtttgtgagctt	Repair template (Ultramer) for UNC-58 (F294T)
oPT275	tcggaaagggttttctcagtagcattcgcgcttggttggtataccactAatgAAATacTgcCgccgatattggtaa atttttatctgaaacattactccagtttgtgagctt	Repair template (Ultramer) for UNC-58 (F294N)
<b>crRNA</b> <b><i>egl-23</i></b>	ugguauuccguuacacugc	Use to generate EGL-23 (L229x)
oSEM402	ttcgcctccaccatcatttctgatatgaattttccgagatctgcaattgcTagACTtgtaaacggaataccaatta gaccataaccaatgacaaatagacggccac	Repair template (Ultramer) for EGL-23 (L229S)
oSEM356	ttcgcctccaccatcatttctgatatgaattttccgagatctgcaattgcTagGTTtgtaaacggaataccaatta gaccataaccaatgacaaatagacggccac	Repair template (Ultramer) for EGL-23 (L229N)
<b>crRNA</b> <b><i>twk-18</i></b>	uaaagacugagcacugugag	Use to generate TWK-18 (V158x)
oSEM435	ctggatggggtcgttttgctactatcctttacgcattcattggaattccaTtGacaAACTTtAagtTtGtactgtct tggtagtctttttgccaagggatg	Repair template (Ultramer) for TWK-18 (V158N)
oSEM436	ctggatggggtcgttttgctactatcctttacgcattcattggaattccaTtGacaAGTTtAagtTtGtactgtct tggtagtctttttgccaagggatg	Repair template (Ultramer) for TWK-18 (V158S)
oSEM437	ctggatggggtcgttttgctactatcctttacgcattcattggaattccaTtGacaACTTtAagtTtGtactgtct tggtagtctttttgccaagggatg	Repair template (Ultramer) for TWK-18 (V158T)
<b>crRNA</b> <b><i>sup-9</i></b>	cgcacuggcgggaauuccau	Use to generate SUP-9 (L122x)
oNZ161	tggaactcctggaaaattttcagcaactcaccaatactctgaaacatgataTTtccTaGtggaaattcccgccagtg cgtagagcatgcagaaaacttttccgg	Repair template (Ultramer) for SUP-9 (L122N)
oMG798	tggaactcctggaaaattttcagcaactcaccaatactctgaaacatgatGCTGccTaGtggaaattcccgccagtg cgtagagcatgcagaaaacttttccgg	Repair template (Ultramer) for SUP-9 (L122S)

**Supplementary Table 4: Genotyping primer combinations for *C. elegans* mutants**

<b>Allele</b>	<b>Primer</b>	<b>Sequence (5' to 3')</b>	<b>Description</b>
<i>unc-58</i> F294X	oTB522	cgggggtagtaatatggatgaagg	338bp PCR product; verify by sequencing.
	oTB508	ggaccacccggttgattgtaa	
<i>egl-23</i> L229X	oSEM357	cccaccattaaccgagtttg	487bp PCR product digested by FspBI; WT: 134/353bp Mutant: 104/134/249bp
	oSEM358	tcccagattataagcaggcaat	
<i>twk-18</i> V158X	oSEM430	tgcggcgcttaagtatttg	673bp PCR product digested by RsaI; WT: 673bp Mutant: 384/289bp
	oSEM431	ggagatggggaaagacaaca	
<i>sup-9</i> L122X	oMG850	caactgtgataacgacgatcgg	PCR oMG850-852-856: WT: 986/324bp L122N&L122S: 986bp PCR oMG850-852-855 WT: 986bp L122N: 986/324bp PCR oMG850-852-853 WT: 986bp L122S: 986/324bp
	oMG852	caccgcgtcgaaatatgtcc	
	oMG853	cgggaattccaCtAggCAGC	
	oMG855	gcgggaattccaCtAggaAA	
	oMG856	gcgggaattccaTtGggACT	

**Supplementary Table 5: List of plasmids**

Plasmid/ gene	Primer	Sequence (5' to 3')	Isothermal Ligation with EcoRV digested pTB207 and			
pTB301/ <i>TWK-18</i> <i>WT</i>	oTB553	ccactagtaacggccgcccagtggtgctggaa ttctgcagatatggcgattggtgcaag	oTB553- 554	from pOX twk -18 <sup>1</sup>		
	oTB554	cgggccccccctcgagcggccgcccagtggtg atggatctagatgtcatgctctagat				
pNZ19/ <i>TWK-18</i> (V158D)	oNZ52	tgtgagtggaaattccaatga	oTB553- oNZ52 oTB554- oNZ53			
	oNZ53	tgctactatcctttacgcattcattggaat tccactcacaGACctcagtccttactgtct tgg				
pTB314/ <i>TWK-18</i> (M280I)	oTB571	actccaacaattggGATgaaatcgtaatcc	oTB553- oTB571 oTB554- oTB572			
	oTB572	catattgataggactcgtgtattctccac ttgtgtcaat				
pOA23/ <i>hTASK1</i> <i>WT</i>	oOA21	ccactagtaacggccgcccagtggtgctggaa ttctgcagatatgaagcggcagaacgtgcg	oOA21-22		from hTASK- 1-pSGEM <sup>2</sup>	
	oOA22	agctcgggccccccctcgagcggccgcccag tgtgatggattcacacggagctcctgcgct				
pOA24/ <i>hTASK1</i> (L122N)	oOA23	ctggaacatgacATTcgtgagcgggatgcc	oOA21-23 oOA24-22			
	oOA24	ggcatcccgctcacgAATgtcatgttccag				
pOA21/ <i>hTASK3</i> <i>WT</i>	oOA18	ccactagtaacggccgcccagtggtgctggaa ttctgcagatatgaagaggcagaacgtgcg	oOA18- oIS17	from hTASK- 3-pSGEM <sup>2</sup>		
	oIS17	agctcgggccccccctcgagcggccgcccag tgtgatggatctaaacggacttccggcggt				
pOA22/ <i>hTASK3</i> (L122N)	oOA26	gctctggaacatgacATTtgtcagcgggat	oOA18-26 oIS17- oOA25			
	oOA25	atcccgctgacaAATgtcatgttccagagc				
pOA25/ <i>mTASK2</i> <i>WT</i>	oNZ56	ccactagtaacggccgcccagtggtgctggaa ttctgcagatatggtggaccggggtccttt	oNZ56-57			from pTLN mTASK-2 <sup>3</sup>
	oNZ57	agctcgggccccccctcgagcggccgcccag tgtgatggattcacgtgcccctgggggta				
pNZ20/ <i>mTASK2</i> (L127N)	oNZ55	gcacagcggcaccgccgaaga	oNZ56-55 oNZ54-57			
	oNZ54	ctgtgtcttctacggcctcttcgggggtgcc gctgtgcAACacatggatcagtgccctggg				
pOA26/ <i>mTREK2</i> <i>WT</i>	oOA30	ccactagtaacggccgcccagtggtgctggaa ttctgcagatatgaaatttccaatcgagac	oOA30-31		from mTREK2c -pEXO	
	oOA31	agctcgggccccccctcgagcggccgcccag tgtgatggatttagtttctgtcttcaagta				
pOA27/ <i>mTREK2</i> (G196D)	oOA43	tccagccaataagaaATCaaaaagcgggat	oOA30-43 oOA42-31			
	oOA42	atcccgctttttGATttcttattggctgga				
pOA28/ <i>mTRAAK</i> <i>WT</i>	oOA34	ccactagtaacggccgcccagtggtgctggaa ttctgcagatatgcgagcaccacactcct	oOA34-35	from mTRAAK- pEXO		
	oOA35	agctcgggccccccctcgagcggccgcccag tgtgatggatctacaccggcacggccttgt				
pOA29/ <i>mTRAAK</i> (G133D)	oOA45	tcccggcagcagcatATCgaacagtgggat	oOA34-45 oOA44-35			
	oOA44	atcccactgttcGATatgctgctggcggga				

pOA30/ <i>mTRESK</i> <i>WT</i>	oOA38	ccactagtaacggccgcccagtgctgctggaa ttctgcagatatggaggctgaggagccacc	oOA38-39	from <i>mTRESK</i> - pEXO
	oOA39	agctcgggccccccctcgagcggccgcccag tgtgatggatttaccaggtagcgaaactt		
pOA31/ <i>mTRESK</i> ( <i>F156N</i> )	oOA41	gtctgtgaggaccagATTcattagagggat	oOA38-41 oOA40-39	
	oOA40	atccctctaataatgAATctggtcctcacagac		
	oTB			

<sup>1</sup> purchased from addgene

<sup>2</sup> kindly provided by V.K. Renigunta

<sup>3</sup> kindly provided by F.V. Sepúlveda

**Part III: Reliable CRISPR/Cas9 Genome Engineering in  
*Caenorhabditis elegans* Using a Single Efficient sgRNA and an  
Easily Recognizable Phenotype**



# Reliable CRISPR/Cas9 Genome Engineering in *Caenorhabditis elegans* Using a Single Efficient sgRNA and an Easily Recognizable Phenotype

Sonia El Mouridi, Claire Lecroisey, Philippe Tardy, Marine Mercier, Alice Leclercq-Blondel, Nora Zariohi, and Thomas Boulin<sup>1</sup>

Univ Lyon, Université Claude Bernard Lyon 1, CNRS UMR-5310, INSERM U-1217, Institut NeuroMyoGène, F-69622 Villeurbanne, France

ORCID IDs: 0000-0002-3674-3151 (S.E.M.); 0000-0002-4313-2527 (P.T.); 0000-0003-1508-8845 (M.M.); 0000-0002-1734-1915 (T.B.)

**ABSTRACT** CRISPR/Cas9 genome engineering strategies allow the directed modification of the *Caenorhabditis elegans* genome to introduce point mutations, generate knock-out mutants, and insert coding sequences for epitope or fluorescent tags. Three practical aspects, however, complicate such experiments. First, the efficiency and specificity of single-guide RNAs (sgRNA) cannot be reliably predicted. Second, the detection of animals carrying genome edits can be challenging in the absence of clearly visible or selectable phenotypes. Third, the sgRNA target site must be inactivated after editing to avoid further double-strand break events. We describe here a strategy that addresses these complications by transplanting the protospacer of a highly efficient sgRNA into a gene of interest to render it amenable to genome engineering. This sgRNA targeting the *dpy-10* gene generates genome edits at comparatively high frequency. We demonstrate that the transplanted protospacer is cleaved at the same time as the *dpy-10* gene. Our strategy generates scarless genome edits because it no longer requires the introduction of mutations in endogenous sgRNA target sites. Modified progeny can be easily identified in the F1 generation, which drastically reduces the number of animals to be tested by PCR or phenotypic analysis. Using this strategy, we reliably generated precise deletion mutants, transcriptional reporters, and translational fusions with epitope tags and fluorescent reporter genes. In particular, we report here the first use of the new red fluorescent protein mScarlet in a multicellular organism. wrmScarlet, a *C. elegans*-optimized version, dramatically surpassed TagRFP-T by showing an eightfold increase in fluorescence in a direct comparison.

## KEYWORDS

CRISPR/Cas9  
genome  
engineering  
*Caenorhabditis  
elegans*  
mScarlet  
*dpy-10*  
coconversion

The pace of technical developments allowing the direct manipulation of genome sequences has seen a marked acceleration in recent years with the emergence of RNA-targeted nucleases derived from bacterial immune systems (Doudna and Charpentier 2014; Zetsche *et al.* 2015). In particular, the binary system relying on the *Streptococcus pyogenes* Cas9

endonuclease targeted by CRISPR (clustered, regularly interspaced, short, palindromic repeat) RNAs has been successfully used to generate point mutations, deletion, or DNA insertions in an ever-growing number of experimental systems. *S. pyogenes* CRISPR/Cas9 has been adapted early on in the model nematode *Caenorhabditis elegans* (Friedland *et al.* 2013; Dickinson *et al.* 2013; Chen *et al.* 2013; Frøkjær-Jensen 2013; Dickinson and Goldstein 2016). Previously, heritable genome engineering could only be achieved in *C. elegans* by remobilizing a *Drosophila Mos1* transposon, which could be inserted and excised in the germline (Robert and Bessereau 2007; Frøkjær-Jensen *et al.* 2010).

Despite great promise and early success, day-to-day CRISPR experiments are often not straightforward. Different factors might explain variability and inefficiency of CRISPR/Cas9 genome engineering in *C. elegans*. One specific reason could be the limited expression of heterologous genes in the germline due to dedicated cosuppression mechanisms (Kelly and Fire 1998). One approach to circumvent this problem has been to inject preassembled ribonucleoprotein (RNP) complexes of

Copyright © 2017 El Mouridi *et al.*

doi: <https://doi.org/10.1534/g3.117.040824>

Manuscript received February 3, 2017; accepted for publication March 2, 2017; published Early Online March 7, 2017.

This is an open-access article distributed under the terms of the Creative Commons Attribution 4.0 International License (<http://creativecommons.org/licenses/by/4.0/>), which permits unrestricted use, distribution, and reproduction in any medium, provided the original work is properly cited.

Supplemental material is available online at [www.g3journal.org/lookup/suppl/doi:10.1534/g3.117.040824/-/DC1](http://www.g3journal.org/lookup/suppl/doi:10.1534/g3.117.040824/-/DC1).

<sup>1</sup>Corresponding author: Institut NeuroMyoGène, Université Claude Bernard Lyon 1, CNRS UMR 5310, INSERM U1217, 8 Rue Raphael Dubois, 69100 Villeurbanne, France. E-mail: [thomas.boulin@univ-lyon1.fr](mailto:thomas.boulin@univ-lyon1.fr)

SpCas9 and CRISPR RNAs (crRNA – tracrRNA duplexes) directly into the germline (Cho *et al.* 2013; Paix *et al.* 2015).

Another general reason for CRISPR failure is that efficacy and specificity vary greatly between different single-guide RNAs (sgRNA). Systematic analyses in different systems have led to the prediction that protospacers terminating by a single guanosine (GNGG) or ideally a double guanosine motif (GGNGG) are generally more effective (Doench *et al.* 2014; Farboud and Meyer 2015). To estimate the prevalence of such sites, we selected a set of 22 genes coding for two-pore domain potassium channel subunits and collected the sequences of all sgRNA target sites in and close to exons of these genes. On average, these 22 loci contained  $138 \pm 40$  protospacers. We found that  $20 \pm 5\%$  of these matched the GNGG motif, and only  $5 \pm 2\%$  matched the GGNGG motif (Supplemental Material, Table S1 in File S1). Since, the proximity of an sgRNA to the target site has a positive impact on the likelihood to generate gene edits (Paix *et al.* 2014), it is therefore likely that few or no high-efficiency sgRNAs will be situated close to a given target region.

One approach to compensate for low CRISPR/Cas9 activity has been to use selection strategies to increase the number of tested progeny. Antibiotic and phenotypic selection protocols have been adapted in *C. elegans* (Ward 2015; Dickinson *et al.* 2015; Norris *et al.* 2015; Dickinson and Goldstein 2016; Schwartz and Jorgensen 2016). They have the further advantage of reducing hands-on time and facilitate the detection of successful genome editing events. When phenotypic or antibiotic selection is not applicable, Co-CRISPR strategies can be used to increase the likelihood of identifying individuals with genome edits. These coconversion approaches consist of injecting the sgRNA targeting a locus of interest together with a second sgRNA that targets a “marker gene” (Kim *et al.* 2014; Arribere *et al.* 2014). Progeny that carry a modification in the “marker” locus are then more likely to carry edits in the locus of interest. However, since two distinct sgRNAs do not necessarily cut with the same efficiency or in the same germ cell, effectiveness of traditional Co-CRISPR coconversion is variable and mostly indicates a successful injection and expression of Cas9 and sgRNA.

In addition, all available strategies require the protospacer sequence to be disrupted once the edit is generated to prevent further CRISPR/Cas9 cutting/activity. This almost always requires the introduction of point mutations in the protospacer adjacent motif (PAM) or in multiple bases of the protospacer. The consequences of such mutations in introns and up- or downstream regulatory regions are difficult, if not impossible, to predict. Similarly, silent mutations in exons can have unfavorable effects due to codon usage bias. Therefore, it would be ideal if genome edits, in particular insertions or point mutations, could be generated without modification of the surrounding original genomic sequence.

Finally, since CRISPR/Cas9 guide RNAs are short 19- to 20-bp-long sequences, there are often multiple closely matching sites (*i.e.*, differing only by a few base pairs) in the genome that could be targeted, albeit at lower frequency. While algorithms have been developed to easily predict such potential off-target sites (Hsu *et al.* 2013; Doench *et al.* 2016), the prevalence of undesired CRISPR events has not been systematically analyzed in *C. elegans* and would require *ad hoc* experiments for each sgRNA.

We describe here a two-step strategy for reliable and scarless modification of the *C. elegans* genome using a single-guide RNA that facilitates the detection of genome engineering events based on an easily recognizable phenotype. Indeed, we reasoned that it should be possible to circumvent many practical hurdles described above if we transplanted the protospacer for a highly efficient sgRNA into a genomic locus of interest to create an “entry strain” that would be more amenable to genome engineering. Specifically, we inserted a protospacer and PAM from the *dpy-10* gene (Arribere *et al.* 2014) – further referred

to as the “*d10* site” or “*d10* sequence” – close to the targeted genomic region. In this “*d10*-entry strain,” we could then induce double-strand breaks at both the transplanted *d10* site and the endogenous *dpy-10* locus using a single sgRNA. We demonstrated that the *d10* site and the *dpy-10* locus were efficiently cut within the same nucleus. Finally, we found that coconversion events (insertions of fluorescent reporter genes and epitope tags) occurred on average in 8% (*i.e.*, 1 in 12 animals) of F1 progeny that also carried mutations in the marker gene *dpy-10*, revealing a high incidence of coconversion events. Since this coconversion step no longer relied on an endogenous protospacer from the targeted locus, we did not need to introduce mutations in PAM or protospacer sequences and could generate perfectly accurate and scarless genome edits. Although our strategy is especially suited to insert sequences into the genome, we could also obtain large, precisely targeted gene deletions.

## MATERIALS AND METHODS

### Strains generated in this study

N2 Bristol was used as a wild-type starting strain for transgenic lines generated in this study. Worms were raised at 20° on nematode growth medium and fed *Escherichia coli* OP50. Worms were grown at 25° after injection. Table S2 in File S1 provides a comprehensive list of the strains constructed for this study.

### Molecular biology

Single-guide RNA expression vectors (see Supplementary Methods in File S1) and plasmid repair templates were constructed using standard molecular biology techniques and Gibson assembly (Gibson 2011). They were systematically validated by Sanger sequencing before injection. Tables S3 and S4 in File S1, respectively, list the oligonucleotides and vectors used in this study. The Cas9-expression vector pDD162 was obtained from Addgene (Dickinson *et al.* 2013). Vectors generated for this study are available upon request.

### DNA preparation and microinjection

The pDD162, pMD8, and pPT53 plasmids were purified using the Qiagen EndoFree Plasmid Mega Kit (Qiagen). All other vectors were prepared using Invitrogen PureLink HQ Mini Plasmid Purification Kit (ThermoFisher Scientific). Single-strand DNA repair templates were synthesized and PAGE-purified by Integrated DNA Technologies (IDT). These single-strand DNA oligonucleotides were aliquoted and stored at –80° upon resuspension in IDTE (10 mM Tris, pH = 7.5, 0.1 mM EDTA, IDT). Except specified otherwise, plasmid vectors and ssDNA were diluted in water and injected at a final concentration of 50 ng/μl; co-injection markers were injected at 5 ng/μl. DNA mixes were injected into a single gonad of 1-d-old adult hermaphrodites raised at 20°. They were then cloned onto individual plates after overnight incubation at 25°.

### PCR screening

PCR DNA amplification was performed on crude worm extracts. In brief, worms were collected in ice-cold 1× M9 buffer, and 5 μl of packed worms were lysed by freeze thaw lysis in 14 μl of Worm Lysis Buffer [50 mM KCl, 10 mM Tris-HCl (pH = 8.3), 2.5 mM MgCl<sub>2</sub>, 0.45% Nonidet P-40, 0.45% Tween 20, 0.01% (w/v) Gelatin], to which 1 μl of proteinase K was added (1 mg/ml final concentration). After freezing at –80°, lysates were incubated for 1 hr at 65°, and proteinase K was inactivated by further incubation at 95° for 20 min.

High-fidelity DNA polymerases (Q5 High-Fidelity DNA Polymerase, New England Biolabs; Phusion High-Fidelity PCR Kit, Thermo

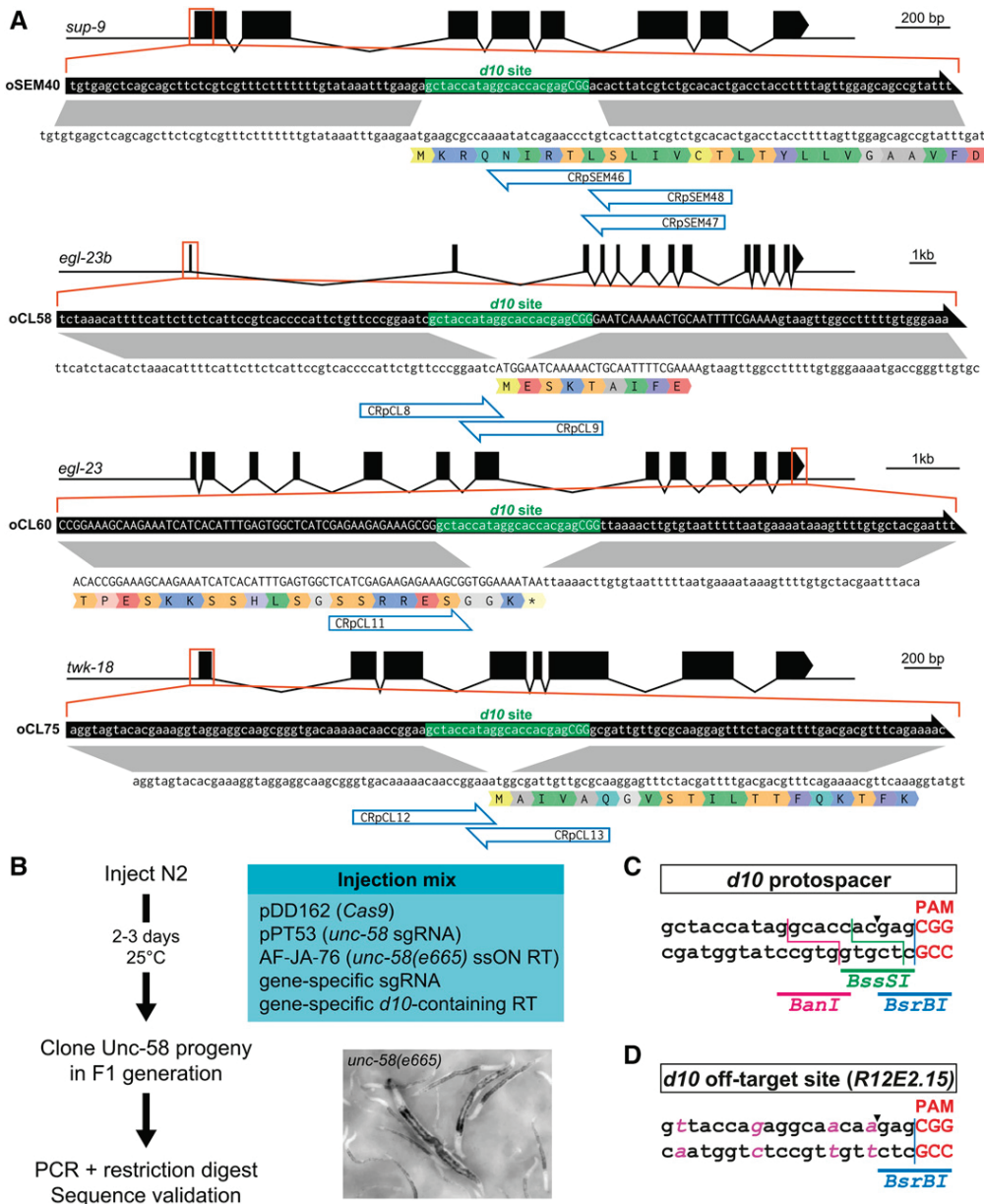


**Figure 1** Generation of *d10*-entry strains. (A) Insertion of the *d10* sequence into *sup-9*, *egl-23b*, *egl-23* (C-terminus), and *twk-18* using a single-strand oligonucleotide repair template compatible with multiple sgRNAs. Genes and their intron/exon structure are displayed in the 5′–3′ orientation. The ssON repair templates are represented by black arrows (containing the *d10* sequence in green) above the coding strand and translation of the target gene. Correspondence of homology regions between the ssON repair template and genomic locus is indicated in gray. sgRNA binding sites are indicated by blue open arrows. (B) *unc-58* coconversion is used to detect the insertion of *d10* sequences into a gene of interest. *unc-58(e665)* mutants are easily identified in the F1 progeny of injected P0 animals based on their straight body posture, lack of mobility, and characteristic rotation around the antero-posterior body axis. RT, repair template. (C) *BanI*, *BssSI*, and *BsrBI* restriction sites are present in the *d10* protospacer sequence and are used for RFLP analysis. The *Cas9* double-strand break site is indicated by an arrowhead. (D) *R12E2.15* contains the only predicted off-target site of the *d10* sgRNA. Four base changes (in pink) distinguish both sites. A *BsrBI* site follows the *Cas9* double-strand break site (indicated by an arrowhead), between the –3 and –4 bases relative to the protospacer adjacent motif (PAM).

Fisher Scientific) were used for PCR amplification to maximize the chances of recovery of desired modifications. Indeed, when we generated the *TagRFP-T::twk-18* knock-in strain, we initially screened 77 F1 clones using a low-fidelity DNA Polymerase (TaqOzyme, Ozyme) and found no edits. When we immediately rescreened the same worm lysates with a more processive, high-fidelity DNA polymerase (Phusion, ThermoFisher Scientific) we identified five positive clones. PCR primers used for this study are listed in Table S3 in File S1.

### Generation of sgRNA expression vector by single-strand DNA isothermal ligation

All sgRNA expression vectors were built using the novel pPT2 vector (see Supplementary Methods in File S1). In brief, pPT2 was linearized by *PmeI*/*SexAI* double digestion. The protospacer sequence was then inserted by isothermal ligation using a single-strand oligonucleotide

containing the protospacer sequence flanked by 20-bp-long homology arms corresponding to the sequences upstream of *PmeI* and downstream of *SexAI*. If it was not already present in the sequence, a guanine residue was manually added 5′ to the protospacer sequence to optimize U6 promoter activity. A unique identifier was given to each sgRNA using the following nomenclature: CRpXYn, where “CR” stands for “CRISPR/Cas9 recognition site” and pXYn is the name of the corresponding sgRNA expression plasmid.

### Codon-optimization of mScarlet

wrmScarlet was generated by gene synthesis (Gblock, IDT) based on the mScarlet sequence (Genbank KY021423; Bindels *et al.* 2017; Figure S3 in File S1). Codon-optimization was performed using the “*C. elegans* codon adapter” service (Redemann *et al.* 2011) with the following parameters: “0 introns,” “optimize for weak mRNA structure at ribosome



■ **Table 1** Insertion of *d10* protospacer at four genomic loci

Gene (WormBase ID)	Proportion of Unc-58-Marked Progeny with <i>d10</i> Site	Proportion of Wild-Type Siblings with <i>d10</i> Site (%)
<i>sup-9</i> II (WBGene00006318)	14/39 (35%)	3/14 (21)
<i>egl-23b</i> IV (WBGene00001190)	9/13 (69%)	6/108 (6)
<i>egl-23</i> IV (WBGene00001190)	8/8 (100%)	
<i>twk-14</i> V (WBGene00006669)	0/13	
<i>twk-18</i> X (WBGene00006672)	0/1	7/93 (7)

binding site,” and “avoid splice sites in coding region.” The Gblock fragment library was combined by isothermal ligation with left and right homology regions flanking the *d10* sequence in *twk-18(bln213)* to generate the repair template pSEM87. The wrmScarlet cDNA sequence is available upon request.

### Microscopy and fluorescence quantification

Freely moving worms were observed on nematode growth media (NGM) plates using an AZ100 microscope (Nikon) equipped with a Flash 4.0 CMOS camera (Hamamatsu Photonics).

Confocal imaging was performed using an inverted confocal microscope (Olympus IX83) equipped with a confocal scanner unit spinning-disk scan head (Yogokawa) and an electron multiplying charge-coupled device camera (iXon Ultra 888). Worms were imaged on 2% fresh agar pads mounted in M9 solution containing 50 mM NaN<sub>3</sub>.

Comparison of wrmScarlet and TagRFP-T fluorescence was performed as follows: (1) confocal stacks of the head region were acquired for TagRFP-T and wrmScarlet knock-in strains on the same day, using identical settings, and NaN<sub>3</sub> immobilization; (2) the same number of confocal slices was selected from each stack; (3) stacks were projected by summing fluorescence at each pixel position in the stack; (4) total fluorescence was measured in areas of identical size and position relative to the anterior tip of the worm and pharynx; and (5) total fluorescence was corrected by subtracting equipment noise, *i.e.*, fluorescence measured in an area of the same size outside of the sample.

### Data availability

All *C. elegans* strains and plasmids described in this study are available upon request.

## RESULTS

### Generation of *d10*-entry strains as a starting point for robust and precise gene modification

Our strategy starts with the insertion of the *d10* sequence (*i.e.*, *dpy-10* protospacer + PAM) into the locus of interest (Figure 1A). First, we targeted three positions in two genes coding for two-pore domain potassium channel subunits: (1) the ATG start site of *sup-9*, (2) the ATG of the *egl-23b* isoform, and (3) the common stop codon of all *egl-23* isoforms (Figure 1A). Next, we predicted all possible sgRNA sequences within a 50-base window around these positions, and selected sgRNAs close to the ATG or stop codons. Using multiple sgRNAs increases the chances of finding at least one sgRNA that cuts efficiently enough to insert the *d10* site at the desired location. We then defined the portion of the gene to be replaced by the *d10* site, based on the positions of the most upstream and most downstream PAM sequences. Finally, we designed a single-strand oligonucleotide sequence (ssON) containing the *d10* sequence flanked by up- and downstream homology regions of ~50 bases (Figure 1A). This ssON could serve as a

repair template with all selected sgRNAs since it did not contain their protospacer or PAM sequences.

Next, we built the necessary sgRNA expression constructs using a novel vector and assembly strategy. This vector (pPT2) is composed of an RNA Polymerase III U6 promoter from *K09B11.12* (Friedland *et al.* 2013; Katic *et al.* 2015) followed by two restriction sites (PmeI and SexAI), followed by the sgRNA portion corresponding to the CRISPR tracrRNA and 3' UTR of *K09B11.12*. This vector was linearized by restriction digest with PmeI and SexAI, and the crRNA sequence was incorporated by isothermal ligation (Gibson assembly; Gibson 2011) using a single single-strand DNA oligonucleotide (see *Materials and Methods* and Supplementary Methods in File S1). These sgRNA expression vectors were systematically validated using Sanger sequencing.

Since it is not possible to predict the efficiency of an sgRNA *a priori*, we reasoned that we could increase the likelihood of finding a *d10* insertion at the locus of interest by using a moderately efficient Co-CRISPR. We chose a previously described reagent combination that introduces a mutation in the two-pore domain potassium channel *unc-58* and replicates the L428F amino acid change found in the *unc-58(e665)* reference allele (Arribere *et al.* 2014). *unc-58(e665)* produces a dominant and easily recognizable phenotype. Worms have a straight body posture and are essentially unable to move on solid NGM medium throughout their postembryonic development (Figure 1B). However, they are viable and fertile. *unc-58(e665)*-like progeny can be detected 2–3 d postinjection and individual F1 worms can be cloned right away to ensure that independent events are selected.

To generate *d10*-entry strains for *sup-9* and *egl-23*, we injected wild-type N2 worms with a mix of plasmid DNA and ssON repair templates (Figure 1B). In each case, the mix was composed of (i) a Cas9 expression vector (pDD162), (ii) the sgRNA expression vector targeting *unc-58* (pPT53), (iii) one gene-specific sgRNA expression vector, (iv) the ssON to introduce the *e665* mutation AF-JA-76 (Arribere *et al.* 2014), and (v) the ssON required to introduce the *d10* site (Figure 1A and Table S3 in File S1). After 3–4 d, we cloned Unc-58-marked F1 worms to single plates. We then detected the presence of the *d10* site in the F2 population by PCR amplification and restriction digest. The *d10* sequence contains sites for three restriction enzymes (*Ban*I, *Bsr*BI, and *Bss*I) that can be used for restriction fragment length polymorphism analysis (RFLP) (Figure 1C). In each case, we designed a PCR primer pair that produced a fragment of 500–600 bp, centered on the *d10* site. In this way, we were able to generate multiple independent *d10*-entry strains for each of the targeted loci (Table 1 and Table S2 in File S1). In each case, we selected homozygous clones for the *d10* insertion that lacked the *unc-58* gain-of-function mutation, and validated them by Sanger sequencing around the *d10* sites.

Next, we targeted the two-pore domain potassium channel subunits *twk-14* and *twk-18*. We obtained 13 Unc-58-marked progeny in the *twk-14* experiment, none of which contained the *d10* sequence, and did not pursue this experiment further. In the *twk-18* experiment (Figure 1Ad), only one of 41 injected P0 worms gave a single Unc-58 worm (Table 1). Since this marked F1 worm did not incorporate the *d10* site in *twk-18*, we decided to screen its unmarked siblings. Doing so, we found seven independent insertion events out of 93 tested clones. Similarly, we found three additional *d10* insertion events in 14 unmarked siblings of the *sup-9* experiment, and six additional *d10* insertions in 108 unmarked siblings of the experiment targeting the ATG of the *egl-23b* splice variant (Table 1).

In conclusion, screening for Unc-58-marked F1 progeny allowed us to rapidly identify P0 individuals for which the injection was successful and CRISPR/Cas9 activity was present in the germline. Cloning Unc-58 worms at the F1 generation ensured that we selected independent edits

■ **Table 2 High CRISPR/Cas9 activity at transplanted *d10* site**

Gene (WormBase ID)	Number of Marked F1 Progeny	Number of Clones Lacking <i>BanI</i> Site (%)	Number of Clones Lacking <i>BsrBI</i> [+ <i>BssSI</i> ] Site (%)	Combined Number of Clones Lacking Restriction Sites (%)
<i>tag-68 I</i> (WBGene00006445)	45	11 (24%)	10 (22)	21 (47)
<i>egl-23 IV</i> (WBGene00001190)	43	7 (16%)		
<i>twk-18 X</i> (WBGene00006672)	36	5 (14%)	4 [+3] (19)	12 (33)
<i>unc-58 X</i> (WBGene00006792)	42	11 (26%)	11 (26)	22 (52)

and decreased the number of animals to clone and analyze by PCR. In three cases, we also found *d10* protospacer insertions in nonmarked siblings, although at lower frequencies than in *Unc-58*-marked F1 progeny. In total, we successfully targeted five different sites in the genome using this protocol (Table S2 in File S1).

### Efficient and specific cutting of transplanted *d10* sites

Different laboratories have independently reported that the sgRNA targeting the *d10* site is among the most efficient ones currently known (I. Katic, M. Boxem, C. Gally, J.-L. Bessereau, personal communication). The reasons for this high efficacy are unclear. For example, the site matches the GNGG motif and not GGNGG (Farboud and Meyer 2015). A more favorable chromatin organization or the sequence of the *dpy-10* locus itself might explain high CRISPR activity in this gene. Since we transplanted only the protospacer and PAM sequences of the *d10* site, we decided to estimate the frequency of cuts in transplanted *d10* sites before attempting to engineer these loci by homologous recombination.

DNA double-strand breaks can be repaired by homologous recombination using the sister chromatid to restore a wild-type sequence or by nonhomologous end joining (NHEJ), which results in small indels close to the cut site. We reasoned that we could therefore estimate the double-strand break frequency by looking for the destruction of the restriction sites present in and around the  $-3/-4$  position relative to the NGG, *i.e.*, the Cas9 cut site (Figure 1C). Note that only catastrophic events that result in sufficiently modified *d10* sites that could no longer be targeted by the Cas9/*d10*-sgRNA duplex would be detected in this way. This experiment therefore underestimates the double-strand break frequency since precise repair events using the sister chromatid would not be detected.

We selected four *d10*-entry strains on three different chromosomes (*tag-68 I*, *egl-23 IV*, *twk-18 X*, and *unc-58 X*). Each strain was injected with a DNA mixture containing (i) a Cas9 expression vector (pDD162), (ii) an sgRNA expression vector targeting *dpy-10* (pMD8), and (iii) a ssON to introduce the *cn64* mutation (AF-ZF-827) in *dpy-10* (Arribere *et al.* 2014). Next, we singled F1 progeny showing a Dpy-10 phenotype, *i.e.*, Rol (*cn64/+*), Dpy ( $-/-$ ), or DpyRol (*cn64/-*) (Levy *et al.* 1993; Arribere *et al.* 2014). Finally, we tested all clones that segregated the Dpy-10 phenotype in their progeny and observed the loss of the *BanI* site in 14–26% of them (Table 2). Since *BanI* is located 5' to the cut site (Figure 1C), we tested the remaining *BanI*-positive clones (*i.e.*, lacking mutations in *BanI*) with *BsrBI* and *BssSI*. This led us to identify additional events, likely affecting the bases closest to the  $-3/-4$  cut site. In total, we found that between 33 and 52% of Dpy-10-marked F1 worms had lost at least one restriction site, which demonstrates that heterologous *d10* sites can be cut at high frequency and are present in Co-CRISPR-marked F1 progeny.

Bioinformatic analysis predicts a single, low scoring, off-target site for the *d10* sgRNA, situated in the uncharacterized gene *R12E2.15* (Figure 1D). We investigated potential off-target cutting of the *d10* sgRNA by

analyzing the *R12E2.15* locus in 32 independent F1 worms that segregated the Dpy-10 phenotypes. None of these 32 lines showed scars around the potential off-target cut site of the *d10* sgRNA.

Given the high correlation between worms displaying Dpy-10 phenotypes and double-strand break events in the transplanted *d10*-site, and given the high selectivity of the *d10* sgRNA for the endogenous and transplanted sites, we chose to focus only on Dpy-10-marked Co-CRISPR individuals in our coconversion experiments.

### Generation of multiple knock-in lines using a single *d10*-entry strain

As a proof of principle for our strategy, we targeted the *twk-18* locus. TWK-18 is one of 47 two-pore domain potassium channels in the *C. elegans* genome. Its expression pattern and localization in body wall muscle cells has been reported previously (Kunkel *et al.* 2000). We decided to generate two N-terminal fusions (1) with the red fluorescent protein TagRFP-T (Shaner *et al.* 2008) and (2) with the blue fluorescent protein TagBFP (Chai *et al.* 2012). As a repair template, we constructed two vectors with left and right homology regions of 2073 and 1993 bp (Figure 2A). We injected each repair template separately into the *twk-18 d10*-entry strain (JIP1143) with (i) a Cas9 expression vector (pDD162), (ii) the sgRNA expression vector targeting *dpy-10* (pMD8), (iii) the ssON to introduce the *cn64* mutation in *dpy-10* (AF-ZF-827), and (iv) the fluorescent reporter pCFJ90 as a co-injection marker to identify transgenic animals based on mCherry fluorescence in the pharynx (Figure 2B). We selected 77 (TagBFP) and 98 (TagRFP-T) Dpy-10-marked F1 progeny. Finally, we used PCR screening to identify five and six clones respectively, which had integrated the TagRFP-T and TagBFP sequences in the *twk-18* locus, corresponding to a recombination frequency of 6% of Dpy-10-marked F1 progeny (Table 3).

When we prepared these knock-in lines for observation by confocal fluorescence microscopy, we noted that TWK-18-TagBFP had a very reproducible subcellular distribution at the exterior surface of body wall muscle cells (Figure 3B). The highly repetitive grid-like pattern was very different from the one reported previously since it appeared to show a strong green fluorescent protein signal in the endoplasmic reticulum (Kunkel *et al.* 2000). This intracellular localization was not consistent with the electrophysiological effect of TWK-18 gain-of-function mutants, in which TWK-18 most likely exerts its hyperpolarizing role at the plasma membrane. We believe these differences probably resulted from a strong overexpression of TWK-18 in this study compared to our knock-in strain, highlighting the importance of physiological expression levels when observing the distribution of cell surface-targeted channels and receptors (Gendrel *et al.* 2009). When comparing the TagRFP-T and TagBFP knock-in strains, we noticed not only a marked difference in brightness but also in the apparent resolution (Figure 3B). The overall pattern of TagRFP-T was similar to TagBFP but the longer emission wavelength of TagRFP-T (emission maximum, 584 nm) did not afford the same resolution as the much shorter emission wavelength of TagBFP (emission maximum, 457 nm). This is in part explained by the

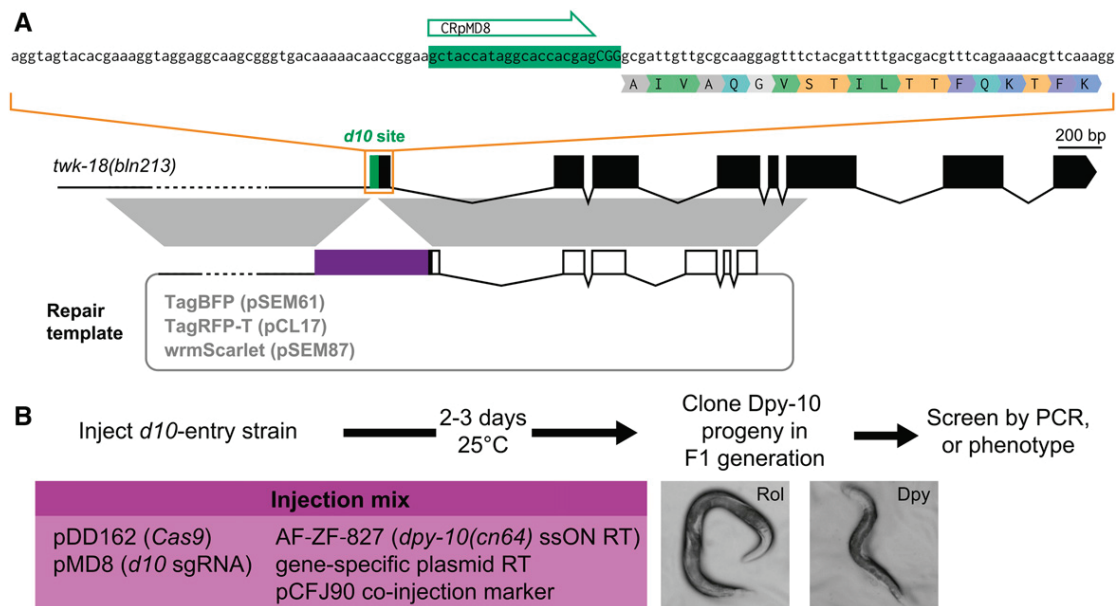


**Figure 2** Generation of multiple knock-in lines using a single *d10*-entry strain. (A) A single *d10*-entry strain is used to engineer N-terminal TagBFP, TagRFP-T, and wrmScarlet fusions in the *twk-18* locus. Correspondence of homology regions between the plasmid repair template and *twk-18* genomic locus is indicated in gray. RT, repair template. (B) Two to 3 days following injection of a *d10*-entry strain with a CRISPR/Cas9 mix, F1 progeny with Dpy-10 phenotypes (Rol or Dpy) can be easily recovered, and further screened in the F2 generation to identify the desired genome edits by PCR or phenotype.

fact that resolution is proportional to the emission wavelength, making TagBFP an interesting alternative to increase imaging resolution without changing imaging hardware.

Next, we targeted three additional loci on different chromosomes (*sup-9 II*, *twk-40 III*, and *egl-23 IV*) and generated seven different edits with a variety of insert types (TagRFP-T, TagRFP-T::ZF1, SL2::TagRFP-T, and TagBFP) (Table 3 and Table S2 in File S1). We found that we could reliably edit these different loci. Indeed, edit frequencies in Dpy-10-marked F1 worms ranged from 3 to 19% (average 8%). Taken together, these experiments demonstrate that it is possible to take advantage of the high CRISPR activity of the *d10* sgRNA to robustly engineer the genome of *C. elegans*. This strategy significantly reduces hands-on work by focusing only on the animals that most likely carry genome edits. It generates scarless edits since it does not require the introduction of mutations in endogenous protospacer sequences.

### wrmScarlet, a brighter red fluorescent protein

The development of improved blue (TagBFP; Chai *et al.* 2012), cyan (mTurquoise2; Goedhart *et al.* 2012), green (mNeonGreen; Shaner *et al.* 2013), and red fluorescent proteins (TagRFP-T; Shaner *et al.* 2008) has greatly increased our capacity to detect proteins expressed at physiological levels. However, the properties of these new fluorophores are generally characterized in bacteria or cell culture systems, and are not always retained in *C. elegans* cells or in specific subcellular compartments (Heppert *et al.* 2016).

In an effort to improve the detection of fusion proteins *in vivo*, we have investigated the behavior of the recently described red fluorescent protein mScarlet (Bindels *et al.* 2017). mScarlet has currently the highest reported brightness, quantum yield, and fluorescence lifetime of any red fluorescent protein. We synthesized a *C. elegans* codon-optimized cDNA (Redemann *et al.* 2011) of mScarlet, which we named wrmScarlet (Figure S3 in File S1). We combined this cDNA with homology arms flanking the *d10* site in *twk-18* to generate a *wrmScarlet::twk-18* repair

plasmid (pSEM87, Figure 2A, and Figure S3 in File S1). Following the same strategy as before, we injected 29 P0 worms (*twk-18 d10*-entry strain, JIP1440) with an injection mix containing (i) pDD162 (*Cas9*), (ii) the ssON to introduce the *cn64* mutation in *dpy-10* (AF-ZF-827), (iii) the sgRNA expression vector targeting *dpy-10* (pMD8), and (iv) *wrmScarlet::twk-18* repair plasmid (pSEM87). Out of 29 injected P0 worms, 11 produced Dpy-10 F1 progeny. In total, we analyzed 123 Dpy-10-marked F1 worms that segregated Dpy-10 progeny and found six clones incorporating the wrmScarlet sequence (Table 3).

While undetectable by eye, specific fluorescence can be observed on NGM plates in *TagRFP-T::twk-18* worms with a macroscope (Nikon AZ100) coupled to a CMOS camera (Flash 4, Hamamatsu Photonics). Using the same macroscope, acquisition parameters and filter sets, wrmScarlet-TWK-18 was significantly brighter than the TagRFP-T fusion, so much so that it became visible to the naked eye (Figure 3A). We next compared the subcellular distribution and brightness of these two translational fusions using spinning-disk confocal imaging. Both protein fusions had grossly identical distribution patterns (Figure 3B). However, the wrmScarlet fusion was ~8 times brighter than the TagRFP-T fusion in this assay (Figure 3C). In fact, the distribution of the wrmScarlet::TWK-18 fusion protein appeared more uniform than TagRFP-T::TWK-18, possibly due to the increased fluorescent signal, which compensated for the reduced resolution when compared to TagBFP (Figure 3B). These properties make wrmScarlet a very convincing replacement for TagRFP-T and should greatly facilitate the detection of protein fusions expressed at low, physiological expression levels.

### Generation of an epitope-tagged knock-in using a long single-strand oligonucleotide

For short edits, single-strand DNA oligonucleotides can be very efficient repair templates (Zhao *et al.* 2014; Arribere *et al.* 2014; Katic *et al.* 2015). We tested if a large ssON could be used as a repair template to integrate



■ Table 3 Summary of genome editing experiments

Gene (WormBase ID)	Inserted Sequence	Proportion of P0 with Dpy-10 Progeny	Proportion of Dpy-10-Marked F1 Progeny with Edits	Percentage Edits per Dpy-10-Marked F1 Progeny (%)
<i>sup-9 II</i> (WBGene00006318)	TagRFP-T	11/42	4/142	3
<i>twk-40 III</i> (WBGene00006691)	TagRFP-T::ZF1	16/35	3/45	7
<i>egl-23 IV</i> (WBGene00001190)	TagRFP-T	12/60	5/79	6
	SL2::TagRFP-T	9/63	3/37	8
	TagBFP	10/24	5/27	19
	TagBFP2	10/33	7/68	10
	wrmScarlet	19/35	14/190	7
	2xMyc	8/30	9/67	14
<i>twk-18 X</i> (WBGene00006672)	TagRFP-T	5/27	5/77	6
	TagBFP	4/20	6/98	6
	wrmScarlet	11/29	6/123	5

two repeats of the Myc tag sequence into the *egl-23* locus (Figure S2 in File S1). We synthesized a 182-nucleotide-long ssDNA fragment containing part of the last exon of *egl-23* to restore the full-length C-terminal sequence, followed by 75 nt encoding two Myc tag sequences (2xMyc), and the original stop codon and 3' UTR region of the *egl-23* gene (Table S3 in File S1). In theory, each strand could serve as a template for recombination, but we selected the strand complementary to the sgRNA following the observations of Katic *et al.* (2015). We injected 30 P0 worms (JIP1150) with a DNA mixture containing (i) a Cas9 expression vector (pDD162), (ii) the expression vector for the *d10* sgRNA (pMD8), (iii) the ssON that introduces the *cn64* mutation in *dpy-10* (AF-ZF-827), (iv) ssON containing the 2xMyc tag sequence (oSEM158), and (v) pCFJ90 as a co-injection marker to identify transgenic animals based on mCherry fluorescence in the pharynx. We selected 67 Dpy-10-marked F1 progeny and among these, nine carried the 2xMyc tag. This 14% edit frequency was comparable, yet slightly higher than the average efficiency of longer inserts using double-strand DNA repair templates (Table 3).

The high edit efficiency observed in this experiment shows that our strategy is very effective to tag proteins of interest for immunohistochemical or protein biochemistry experiments. Generating this epitope-tagged strain required <2 wk, with no additional cloning steps and could be repeated easily to integrate a variety of epitope tags, opening the way for different downstream applications.

### Generation of a large, targeted deletion using a *d10*-entry strain

One starting point for many CRISPR experiments is the desire to engineer loss-of-function mutations in a gene of interest. Previously, researchers relied on random mutagenesis with chemical mutagens or ionizing radiation followed by fastidious screening and extensive backcrossing to wild-type strains to eliminate background mutations (Boulin and Hobert 2012). CRISPR/Cas9 engineering offers the possibility to generate gene deletions with minimal background mutations. A simple approach relies on the repair of double-strand breaks by NHEJ pathways (Friedland *et al.* 2013; Chen *et al.* 2013; Katic and Großhans 2013; Waaijers *et al.* 2013; Dickinson and Goldstein 2016). One, two, or more sgRNAs are injected together and phenotypic or PCR screening strategies are used to retrieve deletion mutants by PCR amplification. However, the exact breakpoints of these deletions are not controllable in this scheme and there is always the potential for undesired edits due to off-target effects for each sgRNA.

*d10*-entry strains can also serve as a starting point to generate precisely defined gene deletions. As a proof of principle, we targeted the *egl-23* locus. *egl-23* is a large locus comprising 12 exons, and removal of

the entire *egl-23a* splice isoform required an 8-kb deletion (Figure S2 in File S1). Our goal was to replace the complete *egl-23a* locus by a transgene expressing the red fluorescent protein mCherry in the pharynx which could be used as a genetic balancer and knock-out mutant of *egl-23*. We therefore constructed a repair template composed of two homology regions of 2 kb, which flanked the transcriptional reporter unit (*Pmyo-2::mCherry::unc-54 3' UTR*). This construct was then injected into the appropriate *egl-23 d10*-entry strain (JIP1150) along with (i) a Cas9 expression vector (pDD162), (ii) the expression vector for the *d10* sgRNA (pMD8), and (iii) the ssON that introduces the *cn64* mutation in *dpy-10* (AF-ZF-827). Out of 40 Dpy-10 progeny, we identified one knock-out line (JIP1253). We validated that the genome edit was accurate by Sanger sequencing. We further verified that the possible off-target site of the *d10* sgRNA was unaffected (Figure 1D). While this particular trial was less efficient than smaller insertions, it confirmed that *d10*-entry strains can be used to generate large deletion and gene replacements, in addition to being ideally suited for the insertion of kilobase-sized inserts or epitope tags.

### DISCUSSION

The major conceptual innovation of our strategy is to render genes highly susceptible to CRISPR/Cas9 engineering by transplanting the *d10* sequence. As we have described above, highly effective sgRNAs matching the GGNGG motif are underrepresented in the genome, and are therefore rarely found in close proximity to the region of interest. While editing frequency is highly variable between sgRNAs at different loci or even within the same locus, we found that editing using our *d10* strategy was robust at different loci, with edit frequencies averaging 8%, *i.e.*, 1 in 12 F1 progeny. In addition, editing was also robust at a single locus. This is particularly valuable and time-saving when multiple edits need to be generated in the same locus, as is usually the case when a gene is being characterized in depth. For example, we took advantage of this high editing frequency to rapidly generate multiple chromatic variants in the *twk-18* locus. This allowed us for the first time to precisely compare the resolution and fluorescence intensity of TagBFP, TagRFP-T, and the recently published mScarlet. Based on the highly stereotypical distribution pattern of TWK-18 at the muscle surface, we could show that (1) TagBFP fusions provided the best apparent resolution, (2) a codon-optimized wrmScarlet was ~8 times brighter than TagRFP-T, and (3) the increased signal of wrmScarlet partly compensated for the lesser resolution of red vs. blue fluorescent proteins.

One unique feature of our strategy is that edits can be designed so that all original genomic sequences are perfectly preserved. Indeed, by using the transplanted *d10* sgRNA instead of sgRNAs from the targeted locus, no

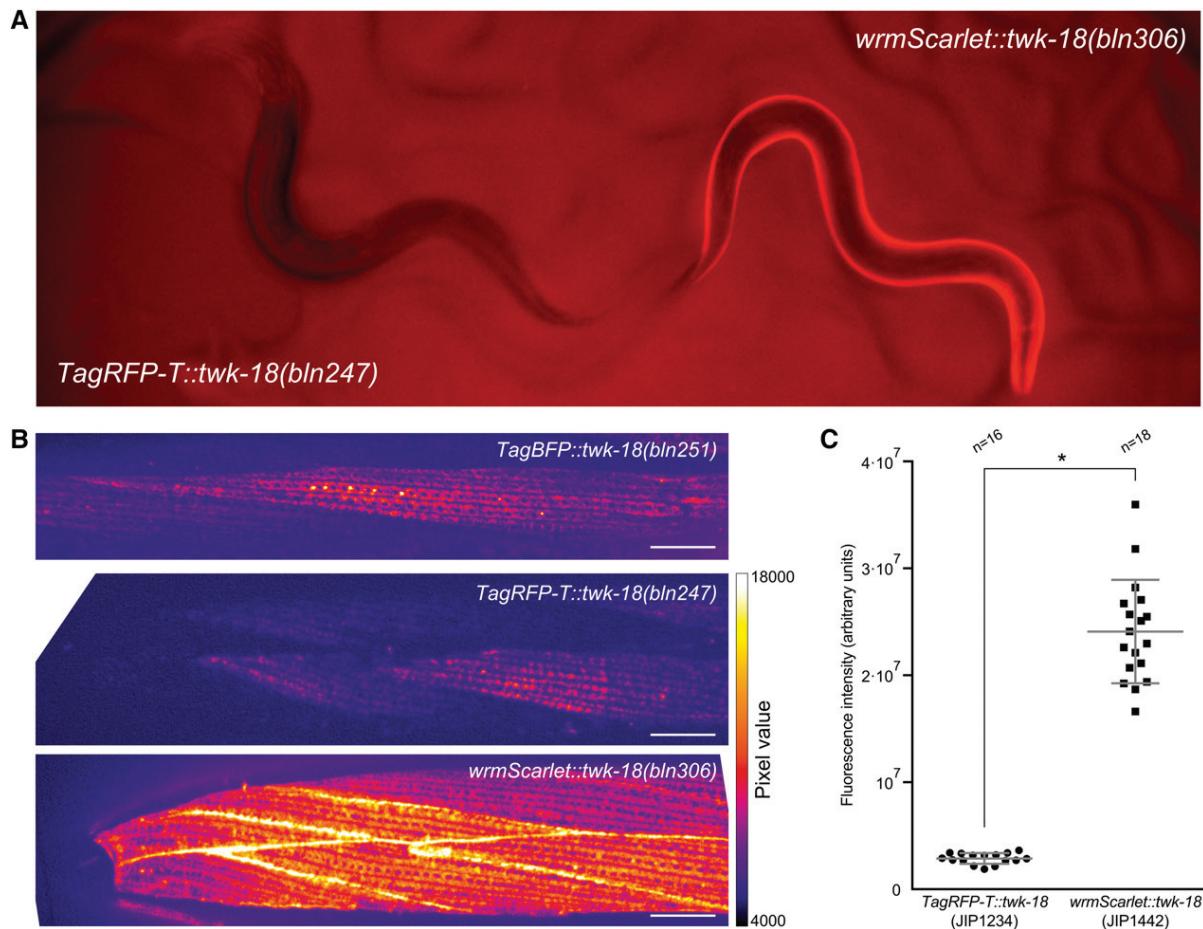


**Figure 3** Comparison of TagBFP, TagRFP-T, and wrmScarlet using reliable editing of the *twk-18* locus. (A) wrmScarlet::TWK-18 is visibly brighter than TagRFP-T::TWK-18. Side-by-side comparison of two young adult hermaphrodites. wrmScarlet-associated fluorescence is visible by eye in freely moving worms on NGM plates, while TagRFP-T is not detectable by eye in this context. (B) The two-pore domain potassium channel TWK-18 decorates the plasma membrane of body wall muscle cells. Representative images of head muscle cells labeled with N-terminal fusions of TWK-18 to TagBFP, TagRFP-T, and wrmScarlet. Head is left. Bar, 10  $\mu$ m. (C) Quantification of fluorescence intensity shows an eightfold increase in fluorescence between TagRFP-T and wrmScarlet. Mean  $\pm$  SD. Student's *t*-test, \**P* < 0.0001.

mutations need to be introduced to avoid continued CRISPR/Cas9 activity once the edit is performed. This facilitates and accelerates experimental design, because only one repair template is designed instead of specific repair constructs for each endogenous sgRNA that would be considered for an edit.

Another benefit of our strategy is that we could retrieve multiple independent lines from the same injected animal by cloning animals in the F1 generation, which is not possible in strategies that rely on the screening of mixed populations of F2 progeny, *e.g.*, with antibiotic selection strategies. Therefore, since we could focus on relatively few F1 clones, multiple methods could be used to detect the desired genome edit such as direct observation, phenotypic screening, or PCR detection. Limiting the number of animals that need to be analyzed could also mitigate PCR detection issues (see *PCR screening*).

From a practical perspective, our strategy provides multiple layers of quality control. Based on the easily recognizable Dpy-10 Co-CRISPR phenotype, we could directly monitor the success of injections and assess the general efficiency of the experiment over time and between experimenters. We could determine if an experiment would likely be successful within 3 d postinjection by monitoring the number of marked F1 progeny. Finally, all steps of our protocol are only limited by the generation time of *C. elegans*, making it particularly time-efficient.

Obtaining the *d10*-entry strain is the major bottleneck of our strategy. This step, like every CRISPR/Cas9 experiment, relies (1) on the ability to find an endogenous sgRNA that cuts efficiently and (2) on the rate of homology directed repair at the cut site, which could be influenced by the local genomic context or specific sequence features of the homology arms. During this study, we were unable to recover *d10* insertions in some of our target loci despite testing multiple sgRNAs. For some genes, we eventually succeeded by using double-stranded DNA repair templates with long homology arms instead of single-strand oligonucleotides.

Another practical concern appears when targeting loci that are closely linked to *unc-58* (to build *d10*-entry strains) or *dpy-10* (to engineer *d10* loci), which are situated at the center of chromosome II and X, respectively. Since we select F1 progeny based on mutation of *dpy-10* or *unc-58*, it is likely that genome edits will be linked to these marker mutations. In that case, one should consider the wild-type siblings in the progeny of an injected P0 individual that produced a significant fraction of marked progeny.

So far, we have tested this strategy only with the *d10* sequence, but in principle, any highly effective sgRNA that targets a gene producing a dominant Co-CRISPR phenotype could be used. Conceptually, our strategy could also be extended to other genetic model organisms. In

particular, a Co-CRISPR strategy based on the *white* locus has been recently published, and could be a starting point to adapt this strategy to engineer the *Drosophila* genome (Ge *et al.* 2016).

## ACKNOWLEDGMENTS

We thank J.-L. Bessereau, I. Katic, and members of the Bessereau team for helpful discussion, M. Jospin for comments on the manuscript, and M. D'Alessandro for constructing pMD8. pCFJ90 was a gift of C. Frøkjær-Jensen. We thank Wormbase, which is supported by National Institutes of Health grant U41 HG002223. This work was supported by a research grant from Fondation Fyssen (T.B.) and an European Research Council Starting Grant (Project *Kelegans*) (T.B.). This work is dedicated to the memory of Christian Boulin.

## LITERATURE CITED

- Arribere, J. A., R. T. Bell, B. X. H. Fu, K. L. Artiles, P. S. Hartman *et al.*, 2014 Efficient marker-free recovery of custom genetic modifications with CRISPR/Cas9 in *Caenorhabditis elegans*. *Genetics* 198: 837–846.
- Bindels, D. S., L. Haarbosch, L. van Weeren, M. Postma, K. E. Wiese *et al.*, 2017 mScarlet: a bright monomeric red fluorescent protein for cellular imaging. *Nat. Methods* 14: 53–56.
- Boulin, T., and O. Hobert, 2012 From genes to function: the *C. elegans* genetic toolbox. *WIREs Dev Biol* 1: 114–137.
- Chai, Y., W. Li, G. Feng, Y. Yang, X. Wang *et al.*, 2012 Live imaging of cellular dynamics during *Caenorhabditis elegans* postembryonic development. *Nat. Protoc.* 7: 2090–2102.
- Chen, C., L. A. Fenk, and M. De Bono, 2013 Efficient genome editing in *Caenorhabditis elegans* by CRISPR-targeted homologous recombination. *Nucleic Acids Res.* 41: e193.
- Cho, S. W., J. Lee, D. Carroll, J.-S. Kim, and J. Lee, 2013 Heritable gene knockout in *Caenorhabditis elegans* by direct injection of Cas9-sgRNA ribonucleoproteins. *Genetics* 195: 1177–1180.
- Dickinson, D. J., and B. Goldstein, 2016 CRISPR-based methods for *Caenorhabditis elegans* genome engineering. *Genetics* 202: 885–901.
- Dickinson, D. J., J. D. Ward, D. J. Reiner, and B. Goldstein, 2013 Engineering the *Caenorhabditis elegans* genome using Cas9-triggered homologous recombination. *Nat. Methods* 10: 1028–1034.
- Dickinson, D. J., A. M. Pani, J. K. Heppert, C. D. Higgins, and B. Goldstein, 2015 Streamlined genome engineering with a self-excising drug selection cassette. *Genetics* 200: 1035–1049.
- Doench, J. G., E. Hartenian, D. B. Graham, Z. Tothova, M. Hegde *et al.*, 2014 Rational design of highly active sgRNAs for CRISPR-Cas9-mediated gene inactivation. *Nat. Biotechnol.* 32: 1262–1267.
- Doench, J. G., N. Fusi, M. Sullender, M. Hegde, E. W. Vaimberg *et al.*, 2016 Optimized sgRNA design to maximize activity and minimize off-target effects of CRISPR-Cas9. *Nat. Biotechnol.* 34: 184–191.
- Doudna, J. A., and E. Charpentier, 2014 The new frontier of genome engineering with CRISPR-Cas9. *Science* 346: 1258096.
- Farboud, B., and B. J. Meyer, 2015 Dramatic enhancement of genome editing by CRISPR/Cas9 through improved guide RNA design. *Genetics* 199: 959–971.
- Friedland, A. E., Y. B. Tzur, K. M. Esvelt, M. P. Colaiacovo, G. M. Church *et al.*, 2013 Heritable genome editing in *C. elegans* via a CRISPR-Cas9 system. *Nat. Methods* 10: 741–743.
- Frøkjær-Jensen, C., 2013 Exciting prospects for precise engineering of *Caenorhabditis elegans* genomes with CRISPR/Cas9. *Genetics* 195: 635–642.
- Frøkjær-Jensen, C., M. W. Davis, J. Taylor, T. W. Harris, D. G. Moerman *et al.*, 2010 Targeted gene deletions in *C. elegans* using transposon excision. *Nat. Methods* 7: 451–453.
- Ge, D. T., C. Tipping, M. H. Brodsky, and P. D. Zamore, 2016 Rapid screening for CRISPR-directed editing of the *Drosophila* genome using *white* coconversion. *G3* 6: 3197–3206.
- Gendrel, M., G. Rapti, J. E. Richmond, and J.-L. Bessereau, 2009 A secreted complement-control-related protein ensures acetylcholine receptor clustering. *Nature* 461: 992–996.
- Gibson, D. G., 2011 Enzymatic assembly of overlapping DNA fragments. *Methods Enzymol.* 498: 349–361.
- Goedhart, J., D. Stetten von, M. Noirclerc-Savoye, M. Lelimousin, L. Joosen *et al.*, 2012 Structure-guided evolution of cyan fluorescent proteins towards a quantum yield of 93%. *Nat. Commun.* 3: 751.
- Heppert, J. K., D. J. Dickinson, A. M. Pani, C. D. Higgins, A. Steward *et al.*, 2016 Comparative assessment of fluorescent proteins for in vivo imaging in an animal model system. *Mol. Biol. Cell* 27: 3385–3394.
- Hsu, P. D., D. A. Scott, J. A. Weinstein, F. A. Ran, S. Konermann *et al.*, 2013 DNA targeting specificity of RNA-guided Cas9 nucleases. *Nat. Biotechnol.* 31: 827–832.
- Katic, I., and H. Großhans, 2013 Targeted heritable mutation and gene conversion by Cas9-CRISPR in *Caenorhabditis elegans*. *Genetics* 195: 1173–1176.
- Katic, I., L. Xu, and R. Ciosk, 2015 CRISPR/Cas9 genome editing in *Caenorhabditis elegans*: evaluation of templates for homology-mediated repair and knock-ins by homology-independent DNA repair. *G3* 5: 1649–1656.
- Kelly, W. G., and A. Fire, 1998 Chromatin silencing and the maintenance of a functional germline in *Caenorhabditis elegans*. *Development* 125: 2451–2456.
- Kim, H., T. Ishidate, K. S. Ghanta, M. Seth, D. Conte *et al.*, 2014 A co-CRISPR strategy for efficient genome editing in *Caenorhabditis elegans*. *Genetics* 197: 1069–1080.
- Kunkel, M. T., D. B. Johnstone, J. H. Thomas, and L. Salkoff, 2000 Mutants of a temperature-sensitive two-P domain potassium channel. *J. Neurosci.* 20: 7517–7524.
- Levy, A. D., J. Yang, and J. M. Kramer, 1993 Molecular and genetic analyses of the *Caenorhabditis elegans* *dpy-2* and *dpy-10* collagen genes: a variety of molecular alterations affect organismal morphology. *Mol. Biol. Cell* 4: 803–817.
- Norris, A. D., H.-M. Kim, M. P. Colaiacovo, and J. A. Calarco, 2015 Efficient genome editing in *Caenorhabditis elegans* with a toolkit of dual-marker selection cassettes. *Genetics* 201: 449–458.
- Paix, A., Y. Wang, H. E. Smith, C.-Y. S. Lee, D. Calidas *et al.*, 2014 Scalable and versatile genome editing using linear DNAs with microhomology to Cas9 sites in *Caenorhabditis elegans*. *Genetics* 198: 1347–1356.
- Paix, A., A. Folkmann, D. Rasoloson, and G. Seydoux, 2015 High efficiency, homology-directed genome editing in *Caenorhabditis elegans* using CRISPR-Cas9 ribonucleoprotein complexes. *Genetics* 201: 47–54.
- Redemann, S., S. Schloissnig, S. Ernst, A. Pozniakowsky, S. Ayloo *et al.*, 2011 Codon adaptation-based control of protein expression in *C. elegans*. *Nat. Methods* 8: 250–252.
- Robert, V., and J.-L. Bessereau, 2007 Targeted engineering of the *Caenorhabditis elegans* genome following *Mos1*-triggered chromosomal breaks. *EMBO J.* 26: 170–183.
- Schwartz, M. L., and E. M. Jorgensen, 2016 SapTrap, a toolkit for high-throughput CRISPR/Cas9 gene modification in *Caenorhabditis elegans*. *Genetics* 202: 1277–1288.
- Shaner, N. C., M. Z. Lin, M. R. McKeown, P. A. Steinbach, K. L. Hazelwood *et al.*, 2008 Improving the photostability of bright monomeric orange and red fluorescent proteins. *Nat. Methods* 5: 545–551.
- Shaner, N. C., G. G. Lambert, A. Chammas, Y. Ni, P. J. Cranfill *et al.*, 2013 A bright monomeric green fluorescent protein derived from *Branchiostoma lanceolatum*. *Nat. Methods* 10: 407–409.
- Waaajers, S., V. Portegijs, J. Kerver, B. B. L. G. Lemmens, M. Tijsterman *et al.*, 2013 CRISPR/Cas9-targeted mutagenesis in *Caenorhabditis elegans*. *Genetics* 195: 1187–1191.
- Ward, J. D., 2015 Rapid and precise engineering of the *Caenorhabditis elegans* genome with lethal mutation co-conversion and inactivation of NHEJ repair. *Genetics* 199: 363–377.
- Zetsche, B., J. S. Gootenberg, O. O. Abudayyeh, I. M. Slaymaker, K. S. Makarova *et al.*, 2015 Cpf1 is a single RNA-guided endonuclease of a class 2 CRISPR-Cas system. *Cell* 163: 759–771.
- Zhao, P., Z. Zhang, H. Ke, Y. Yue, and D. Xue, 2014 Oligonucleotide-based targeted gene editing in *C. elegans* via the CRISPR/Cas9 system. *Nature Publishing Group* 24: 247–250.

Communicating editor: B. J. Andrews

**Supplementary information for**

**Reliable CRISPR/Cas9 genome engineering in *Caenorhabditis elegans* using  
a single efficient sgRNA and an easily recognizable phenotype**

Sonia El Mouridi, Claire Lecroisey, Philippe Tardy, Marine Mercier,  
Alice Leclercq-Blondel, Nora Zariohi, Thomas Boulin<sup>§</sup>

Institut NeuroMyoGène  
Univ Lyon, Université Claude Bernard Lyon 1  
CNRS UMR 5310, INSERM U1217  
8 Rue Raphaël Dubois  
69100, Villeurbanne, France

<sup>§</sup> Corresponding author: [thomas.boulin@univ-lyon1.fr](mailto:thomas.boulin@univ-lyon1.fr)



Figure 2 Supplement 1

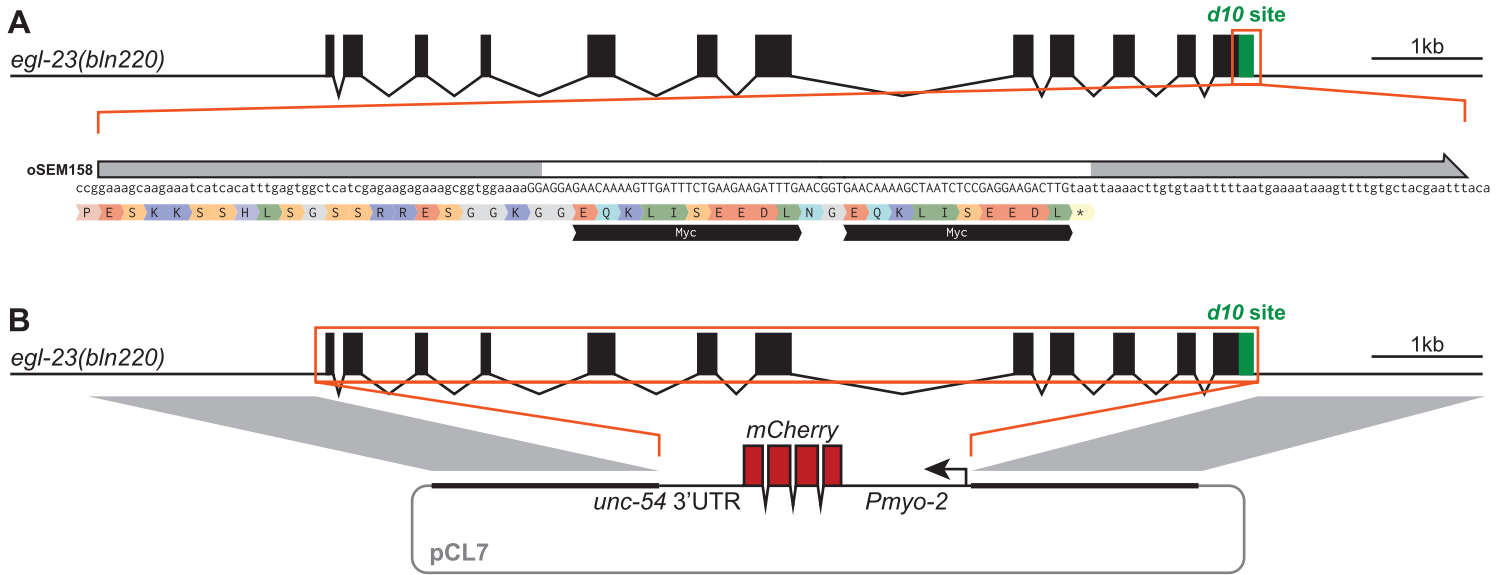


Figure 2 Supplement 1

**A** Insertion of a 2xMyc tag into the *egl-23* locus using a single-strand DNA template. Correspondence of homology regions between the ssON repair template and genomic locus is indicated in gray. The sequence of the resulting fusion protein is indicated below the DNA sequence with single-letter amino acid code. Black bars labeled “Myc” indicate the position of the *myc* tag sequences.

**B** Deletion and replacement of the *egl-23a* locus by a *Pmyo-2::mCherry* reporter transgene. Correspondence of homology regions between the plasmid repair template (pCL7) and genomic locus is indicated in gray. The *Pmyo-2::mCherry::unc-54 3'UTR* transgene is inserted in the reverse orientation relative to the *egl-23* gene.





**Supplementary Tables****Supplementary Table 1:** Prevalence of GNNG and GGNGG protospacers in and close to exons of two-pore domain potassium channel genes.

<b>Gene</b>	<b>NGG</b>	<b>GNNG</b>	<b>GGNGG</b>	<b>GNNG/NGG</b>	<b>GGNGG/NGG</b>
<i>egl-23</i>	226	59	23	0.26	0.10
<i>sup-9</i>	115	27	10	0.23	0.09
<i>unc-58</i>	181	33	9	0.18	0.05
<i>twk-3</i>	85	8	2	0.09	0.02
<i>twk-6</i>	70	10	2	0.14	0.03
<i>twk-8</i>	70	10	2	0.14	0.03
<i>twk-12</i>	134	26	6	0.19	0.04
<i>twk-13</i>	190	49	19	0.26	0.10
<i>twk-14</i>	122	23	8	0.19	0.07
<i>twk-16</i>	146	34	10	0.23	0.07
<i>twk-17</i>	185	40	13	0.22	0.07
<i>twk-18</i>	121	18	6	0.15	0.05
<i>twk-20</i>	108	17	5	0.16	0.05
<i>twk-23</i>	118	29	7	0.25	0.06
<i>twk-24</i>	102	25	5	0.25	0.05
<i>twk-25</i>	166	25	6	0.15	0.04
<i>twk-28</i>	132	22	5	0.17	0.04
<i>twk-30</i>	139	25	7	0.18	0.05
<i>twk-32</i>	148	33	8	0.22	0.05
<i>twk-40</i>	148	33	8	0.22	0.05
<i>twk-44</i>	195	43	6	0.22	0.03
<i>twk-46</i>	132	31	5	0.23	0.04
<b>Average ratios</b>				<b>0.20</b>	<b>0.05</b>

**Supplementary Table 2: Strain list**

<b>Strain</b>	<b>Genotype</b>	<b>Description</b>
JIP1141-2	<i>tag-68(bln209) I</i> <i>tag-68(bln212) I</i>	Insertion of <i>d10</i> site in 5' of <i>tag-68</i>
JIP1155-7	<i>sup-9(bln224) II</i> <i>sup-9(bln225) II</i> <i>sup-9(bln226) II</i>	Insertion of <i>d10</i> site in 5' of <i>sup-9</i>
JIP1127, JIP1129	<i>egl-23(bln172) IV</i> <i>egl-23(bln179) IV</i>	Insertion of <i>d10</i> site in 5' of <i>egl-23b</i>
JIP1149-50	<i>egl-23(bln219) IV</i> <i>egl-23(bln220) IV</i>	Insertion of <i>d10</i> site in 3' of <i>egl-23</i>
JIP1143	<i>twk-18(bln213) X</i>	Insertion of <i>d10</i> site in 5' of <i>twk-18</i>
JIP1152	<i>tag-68(bln222) I</i>	Insertion of TagRFP-T in <i>tag-68</i> at 5'
JIP1224-6	<i>sup-9(bln236) II</i> <i>sup-9(bln237) II</i> <i>sup-9(bln238) II</i>	Insertion of TagRFP-T in <i>sup-9</i> at 5'
JIP1368-70	<i>twk-40(bln282) III</i> <i>twk-40(bln283) III</i> <i>twk-40(bln284) III</i>	Insertion of TagRFP-T::ZF1 in <i>twk-40</i> at 3'
JIP1171-5	<i>egl-23(bln227) IV</i> <i>egl-23(bln228) IV</i> <i>egl-23(bln229) IV</i> <i>egl-23(bln230) IV</i> <i>egl-23(bln231) IV</i>	Insertion of TagRFP-T in <i>egl-23</i> at 3'
JIP1221-3	<i>egl-23(bln233) IV</i> <i>egl-23(bln234) IV</i> <i>egl-23(bln235) IV</i>	Insertion of SL2::TagRFP-T in <i>egl-23</i> at 3'
JIP1336	<i>egl-23(bln277) IV</i>	Insertion of TagBFP in <i>egl-23</i> at 3'
JIP1448-50	<i>egl-23(bln309) IV</i> <i>egl-23(bln310) IV</i> <i>egl-23(bln311) IV</i>	Insertion of wrmScarlet in <i>egl-23</i> at 3'
JIP1233-5	<i>twk-18(bln246) X</i> <i>twk-18(bln247) X</i> <i>twk-18(bln248) X</i>	Insertion of TagRFP-T in <i>twk-18</i> at 5'
JIP1236, JIP1251-2	<i>twk-18(bln249) X</i> <i>twk-18(bln250) X</i> <i>twk-18(bln251) X</i>	Insertion of TagBFP in <i>twk-18</i> at 5'
JIP1440-42	<i>twk-18(bln304) X</i> <i>twk-18(bln305) X</i> <i>twk-18(bln306) X</i>	Insertion of wrmScarlet in <i>twk-18</i> at 5'
JIP1328-9, JIP1331	<i>egl-23(bln269) IV</i> <i>egl-23(bln270) IV</i> <i>egl-23(bln272) IV</i>	Insertion of 2xMyc sequence in <i>egl-23</i> at 3'
JIP1253	<i>egl-23(bln252[Pmyo-2::mCherry::3'UTR unc-54])IV</i>	Deletion and replacement of <i>egl-23a</i> by <i>Pmyo-2::mCherry::3' UTR unc-54</i>

**Supplementary Table 3: List of single strand oligonucleotides**

Primer	Sequence (5' to 3')	Description
AF-ZF-827	CACTTGAACCTTCAATACGGCAAGATGAGAATGA CTGGAACCGTACCGCATGCGGTGCCTATGGTAG CGGAGCTTCACATGGCTTCAGACCAACAGCCTAT	ssDNA repair template; <i>dpy-10(cn64)</i>
AF-JA-76	ATTTTGTGGTATAAAATAGCCGAGTTAGGAAAC AAATTTTCTTTTCAGGTTTCTCAGTAGTGACCA TGTGCGTGGATCTTGCCTCCACACATCTCAAGG CGTACTT	ssDNA repair template; <i>unc-58(e665)</i>
oSEM158	Gaaagcaagaaatcatcacatttgagtggctcat cgagaagagaaagcgggtggaaaaGGAGGAGAACAA AAAGTTGATTTCTGAAGAAGATTTGAACGGTGAA CAAAAGCTAATCTCCGAGGAAGACTTGtaattaa Aacttggtgaatttttaataaaaataaagttttg tgctacgaattt	ssDNA repair template; insertion of 2xMyc sequence in <i>egl-23</i> at 3' <i>d10</i> site
oPT85	AACTACAGTATCCCAACTGATTGTGGTAACACATC ACGGCATGCACCACGGCTACCATAGGCACCACGAG CGGGATTGTGGCATGTGGTGTGTGTTACGCGAGAG GCGGCGACACGTCGAGAG	ssDNA repair template; insertion of <i>d10</i> sequence in <i>tag-68</i>
oSEM40	TGTGAGCTCAGCAGCTTCTCGTCGTTTCTTTTTT GTATAAATTTGAAGAGCTACCATAGGCACCACGAG CGGACACTTATCGTCTGCACACTGACCTACCTTTT AGTTGGAGCAGCCGATTT	ssDNA repair template; insertion of <i>d10</i> sequence in <i>sup-9</i>
oCL60	CCGAAAGCAAGAAATCATCACATTTGAGTGGCTC ATCGAGAAGAGAAAGCGGGCTACCATAGGCACCAC GAGCGGTTAAAACCTGTGTAATTTTTAATGAAAT AAAGTTTTGTGCTACGAATTT	ssDNA repair template; insertion of <i>d10</i> sequence in <i>egl-23</i> at 3' <i>d10</i> site
oCL58	TCTAAACATTTTTCATTCTTCTCATTCCGTCACCCC ATTCTGTTCCCGAATCGCTACCATAGGCACCACG AGCGGGAATCAAAAACGCAATTTTCGAAAAGTAA GTTGGCCTTTTTGTGGGAAA	ssDNA repair template; insertion of <i>d10</i> sequence in <i>egl-23b</i>
oCL75	AGGTAGTACACGAAAGGTAGGAGGCAAGCGGTGA CAAAAACAACCGGAAGCTACCATAGGCACCACGAG CGGGCGATTGTTGCGCAAGGAGTTTCTACGATTTT GACGACGTTTCAGAAAAC	ssDNA repair template; insertion of <i>d10</i> sequence in <i>twk-18</i>
oNZ7	caagagttggaccaatgggaatattggatgaagct tttgagatgagcctTACCGCTCGTGGTGCCTATG GTAGCgtcgatTTTTgattatctttagaatgctc gtgcaaattgtataattagt	ssDNA repair template; insertion of <i>d10</i> sequence in <i>twk-14</i>
oSEM171	gtgaatgatcacgcacgata	Primer pair for amplification of <i>d10</i> off-target site in <i>R12E2.15</i>
oSEM172	gtactgtggtggtggtggtg	
oCL77	CCAACCCCTCTCATCCTTTT	Primer pair for amplification of <i>d10</i> site in <i>twk-18(bln213)</i>
oCL78	TTTCATAGTCGATTTTCATTCAGA	
oPT95	GAAAATTTGGAACCGGCTA	Primer pair for amplification of <i>d10</i> site in <i>tag-68(bln212)</i>
oTB586	CAACGTCTTCTGCATCGAAA	
oSEM31	ATGAACCTCCTAGTGCTCCG	Primer pair for amplification of <i>d10</i> site in <i>sup-9(bln226)</i>
oSEM32	GGAAATGGGCTCTCGTTGTG	
oCL44	AAAGCGTACAGCGAAGAAGC	Primer pair for amplification of <i>d10</i> site in <i>egl-23(bln220)</i>
oCL34	TTCCAAGCATATTTGTGATCG	
oCL45	CGATTGTGAGCCAATGAGAA	Primer pair for amplification of <i>d10</i> site in <i>egl-23b(bln172)</i>
oCL46	CGCTTTTCAATTTTCCATGC	

oSEM140	GCCAAAAGAAGACCCATGAC	Primer pair for amplification of <i>d10</i> site in <i>twk-40(b1n271)</i>
oSEM141	AAAAATCGCTCTAAATTTCCAGTT	

**Supplementary Table 4: List of plasmids**

Plasmid/ locus	Primer	Sequence (5' to 3')	Description
pSEM91/ <i>egl-23</i>	oCL101	ActcactatagggggcgcGcctcgacctgcaggtcgagctGGCTA TATGGTTTGGAGGAA	LHR amplification
	oSEM275	TTTTCCACCGCTTTCTCTTC	
	oSEM276	AcatttgagtggctcatcgaGaagagaaaagcgggtggaaaaATGGT CAGCAAGGGAGAGGC	wrmScarlet amplification
	oSEM277	AaaactttattttcattaaaAattacacaagttttaattaCTTGT AGAGCTCGTCCATTC	
	oSEM278	TTAAAACCTTGTGAATTTTT	RHR amplification
	oCL106	TtcttggccttttgctggccttttgctcacatggcagCATGCAGT CGAGACATTTACATC	
pCL16/ <i>egl-23</i>	oCL101	ActcactatagggggcgcgacctcgacctgcaggtcgagctGGCTA TATGGTTTGGAGGAA	LHR amplification
	oCL102	GcatgttctccttaatacagctcttcgcccttagacacccatTTTTC CACCGCTTTCTCTTC	
	oCL103	AcatttgagtggctcatcgaagaagagaaaagcgggtggaaaaATGGT GTCTAAGGGCGAAGA	TagRFP-T amplification
	oCL104	CacaaaactttattttcattaaaattacacaagttttaTTAAT TAAGTTTGTGCCCCA	
	oCL105	CtgcgacctccctagcaaaactggggcacaacttaattaaTTAAA ACTTGTGTAATTTTAAATGAAAATAAAGTTTTGTGCTACGA	RHR amplification
	oCL106	ttccttggccttttgctggccttttgctcacatggcagCATGCAGT CGAGACATTTACATC	
pCL22/ <i>egl-23</i>	oCL101	ActcactatagggggcgcgacctcgacctgcaggtcgagctGGCTA TATGGTTTGGAGGAA	LHR amplification
	oCL127	acaagcagttaactaggtgaaagtaggatgagacagcTTATTTTC CACCGCTTTCTCTTC	
	oCL128	tgagtggctcatcgaagaagagaaaagcgggtggaaaaataGCTGTCT CATCCTACTTTACCC	SL2::TagRFP-T amplification
	oCL104	CacaaaactttattttcattaaaattacacaagttttaTTAAT TAAGTTTGTGCCCCA	
	oCL105	CtgcgacctccctagcaaaactggggcacaacttaattaaTTAAA ACTTGTGTAATTTTAAATGAAAATAAAGTTTTGTGCTACGA	RHR amplification
	oCL106	ttccttggccttttgctggccttttgctcacatggcagCATGCAGT CGAGACATTTACATC	
pSEM67/ <i>egl-23</i>	oCL101	actcactatagggggcgcgacctcgacctgcaggtcgagctGGCTA TATGGTTTGGAGGAA	LHR amplification
	oSEM142	tgtacagtttcatatgcatattctccttaataagctctgatTTTC CACCGCTTTCTCTTC	
	oSEM143	TCAGAGCTTATTAAGGAGAA	TagBFP amplification
	oSEM146	aaaactttattttcattaaaattacacaagttttaattaATTAA GCTTGTGACCCAGTT	
	oSEM145	CGCAAACGCCAAGACCACATATAGATCCAAGAAACCG	TagBFP2 point mutation
	oSEM144	TTTCTTGGATCTATATGTGGTCTTGGCGTTTGCATGAGATGGCT ACCGC	
	oSEM147	CtgcgacctcccagcaaaactgggtcacaagcttaattaaTAAA ACTTGTGTAATTTTT	RHR amplification
	oCL106	TtcttggccttttgctggccttttgctcacatggcagCATGCAGT CGAGACATTTACATC	

pSEM69/ <i>egl-23</i>	oCL101	actcactatagggggcgcgccctgacctgcaggtcgagctGGCTA TATGGTTTGGAGGAA	LHR amplification
	oSEM142	tgtacagtttcatatgcatattctccttaataagctctgaTTTTC CACCGCTTTCTCTTC	
	oSEM143	TCAGAGCTTATTAAGGAGAA	TagBFP amplification
	oSEM146	aaaacttttattttcattaaaaattacacaagttttaattaATTAA GCTTGTGACCCAGTT	
	oSEM147	ctgcgacctcccagcaaaactgggtcacaagcttaattaatTAAA ACTTGTGTAATTTTT	RHR amplification
	oCL106	ttcctggccttttctggccttttctcacatggcagCATGCAGT CGAGACATTTACATC	
pSEM55/ <i>sup-9</i>	oSEM75	gactcactatagggggcgcgccctgacctgcaggtcgagcGTGCA GCAGGAAGTGATGGA	LHR amplification
	oSEM74	TCTTCAAATTTATACAAAAAAGAAACGACGAGAAGCTGCTGA	
	oSEM63	gcagcttctcgtcgttttcttttttgtataaatttgaagaATGGT GTCTAAGGGCGAAGA	TagRFP-T amplification
	oSEM72	tgcagacgataagtgcagggttctgatatttggcgcttATTAA GTTTGTGCCCCAGTT	
	oSEM77	AAGCGCCAAAATATCAGAACCC	RHR amplification
	oSEM76	cggttcttgcccttttctggccttttctcacatggcagTAGTC ATCCCGAAAACGTC	
pSEM61/ <i>twk-18</i>	oCL117	gactcactatagggggcgcgccctgacctgcaggtcgagcATGGG AATTGGTGCATTTTC	LHR amplification
	oSEM123	TTCCGTTGTTTTTGTCAACC	
	oSEM125	aaggtaggaggcaagcgggtgacaaaaacaaccgaaatgTCAGA GCTTATTAAGGAGAA	TagBFP amplification
	oSEM128	acgtcgtcaaaatcgtagaaactccttgcgcaacaatcgCATTA GCTTGTGACCCAGTT	
	oSEM127	GCGATTGTTGCGCAAGGAGT	RHR amplification
	oCL120	cggttcttgcccttttctggccttttctcacatggcagGTGAA CAAGACCGCACAGAA	
pCL17/ <i>twk-18</i>	oCL117	gactcactatagggggcgcgccctgacctgcaggtcgagcATGGG AATTGGTGCATTTTC	LHR amplification
	oCL118	gcatgttctccttaatcagctcttcgcccttagacacatTTCCG GTTGTTTTTGTCAACC	
	oCL91	cгааaggtaggaggcaagcgggtgacaaaaacaaccgaaATGGT GTCTAAGGGCGAAGA	TagRFP-T amplification
	oCL92	acgtcgtcaaaatcgtagaaactccttgcgcaacaatcgCATTA GTTTGTGCCCCAGTT	
	oCL119	actgcgacctccctagcaaaactggggcacaacttaatgcGATTG TTGCGCAAGGAGTTT	RHR amplification
	oCL120	cggttcttgcccttttctggccttttctcacatggcagGTGAA CAAGACCGCACAGAA	
pSEM87/ <i>twk-18</i>	oCL117	gactcactatagggggcgcgccctgacctgcaggtcgagcATGGG AATTGGTGCATTTTC	LHR amplification
	oSEM123	TTCCGTTGTTTTTGTCAACC	
	oSEM127	GCGATTGTTGCGCAAGGAGT	RHR amplification
	oCL120	cggttcttgcccttttctggccttttctcacatggcagGTGAA CAAGACCGCACAGAA	
pSEM80/ <i>twk-40</i>	oSEM135	ccgccagatcttcggatggctcgagttttcagcaagaTAAGGA CGGTTGCAATTAATC	LHR amplification
	oSEM136	aataagctagcaccgctcgtgggtgcctatggtagcaccgTTCAA TTGAGGCCAATGCTC	
	oSEM137	attgaaccggtgctaccataggcaccagcggtgctagCTTAT TTTTAGATTAATTGT	RHR amplification
	oSEM138	atggcagctgagaatattgtaggatcttctagaaagaTTTTTG	

		GCGAAAAATTCAGGT	
	oMM7	gatttatcgattttggagcattggcctcaattgaaagtggcaat cgctatgggtcaattctcactggaagaactcaagaagttcatgtta tgggtgcttaagggcgaagagctgattaagg	TagRFP-T amplification
	oTB600	acaccggttaaaacaaaaaaaaaacaacacaattaatctaaaaa taaggatccgccactacctccagagccaccATTAAGTTTGTGCC CAGTTTGC	
	oTB601	cacaaacttaatgggtggctctggaggtagtgggcGAACAGAATAC AAAACGCGACTTTGTGATGCGTTCCGCCGTGAAGGATACTGCCCG TACAACGACAATTGCACATATGCTCACGACAAGATGAGCTGAGA GTTCCGTAActtatttttagattaattgtgtttgtttttttttg tttaacgggtg	Integration of ZF1 sequence
pPT46/ <i>tag-68</i>	oPT86	aattgcaaatctaaatgtttCCACATGCCACAATCCATCGgtttt agagctagaaatagc	Forward primer
	oPT87	gctattttctagctctaaaacCGATGGATTGTGGCATGTGGaaaca ttagatttgcaatt	Reverse primer
pPT47/ <i>tag-68</i>	oPT88	gctattttctagctctaaaacCAATCCATCGTGGTGCATGCaaaca ttagatttgcaatt	Forward primer
	oPT89	gctattttctagctctaaaacCAATCCATCGTGGTGCATGCaaaca ttagatttgcaatt	Reverse primer
pSEM46/ <i>sup-9</i>	oSEM27	aatgcaaatctaaatgtttCCACATGCCACAATCCATCGgtttta gagctagaaatagc	Forward primer
	oSEM28	gctattttctagctctaaaacAAATATTAAGAAGAAGCTGCaaaca ttagatttgcaatt	Reverse primer
pSEM48/ <i>sup-9</i>	oSEM43	aatgcaaatctaaatgtttGTGTGCAGACGATAAGTGACgtttt agagctagaaatagc	Forward primer
	oSEM44	gctattttctagctctaaaacGTCACCTATCGTCTGCACACaaaca ttagatttgcaatt	Reverse primer
pSEM50/ <i>sup-9</i>	oSEM47	aatgcaaatctaaatgtttGTGTGCAGACGATAAGTGACgttt tagagctagaaatag	Forward primer
	oSEM48	ctattttctagctctaaaacGTCACCTATCGTCTGCACACaaaca ttagatttgcaatt	Reverse primer
pCL11/ <i>egl-23</i>	oCL67	attgcaaatctaaatgtttGTCATCGAGAAGAGAAAGCGGgtttt agagctagaaatagc	Forward primer
	oCL68	gctattttctagctctaaaacCCGCTTCTCTTCTCGATGACaaac atttagatttgcaat	Reverse primer
pCL8/ <i>egl-23b</i>	oCL61	attgcaaatctaaatgtttGCCATTCTGTTCCCGGAATCagtttt agagctagaaatagc	Forward primer
	oCL62	gctattttctagctctaaaactGATTCCGGGAACAGAATGGcaaac atttagatttgcaat	Reverse primer
pCL9/ <i>egl-23b</i>	oCL63	attgcaaatctaaatgtttGAGTTTTTATTCCATGATTCgtttt agagctagaaatagc	Forward primer
	oCL64	gctattttctagctctaaaacGAATCATGGAATCAAAAACCaac atttagatttgcaat	Reverse primer
pCL12/ <i>twk-18</i>	oCL69	aatgcaaatctaaatgtttGTGACAAAAACAACCGGAAAggtttt agagctagaaatagc	Forward primer
	oCL70	gctattttctagctctaaaacTTCCGGTTGTTTTTGTACaaaca ttagatttgcaatt	Reverse primer
pCL13/ <i>twk-18</i>	oCL71	attgcaaatctaaatgtttGTGCGCAACAATCGCCATTTcgtttt agagctagaaatagc	Forward primer
	oCL72	gctattttctagctctaaaacGAAATGGCGATTGTTGCGCAcaaac atttagatttgcaat	Reverse primer
pMM1/ <i>twk-40</i>	oMM1	AATTGCAAATCTAAATGTTTgcattggcctcaattgaaagtGTTT TAGAGCTAGAAATAGC	Forward primer
	oMM2	GCTATTTCTAGCTCTAAAACACTTTCAATTGAGGCAATGCAAAC ATTTAGATTTGCAATT	Reverse primer
pNZ1/	oNZ1	ATTGCAAATCTAAATGTTTGcctttaatcagagttttactGTTTT	Forward primer



<i>twk-14</i>		AGAGCTAGAAATAGC	
	oNZ2	GCTATTTCTAGCTCTAAAACagtaaaactctgattaaaggCAAAC ATTTAGATTTGCAAT	Reverse primer
pNZ2/ <i>twk-14</i>	oNZ3	ATTGCAAATCTAAATGTTTgaaactctgattaaagggttaGTTTT AGAGCTAGAAATAGC	Forward primer
	oNZ4	GCTATTTCTAGCTCTAAAACtaaacctttaatcagagtttcAAAC ATTTAGATTTGCAAT	Reverse primer
pNZ3/ <i>twk-14</i>	oNZ5	ATTGCAAATCTAAATGTTTgccgagtaaaactctgattaaGTTTT AGAGCTAGAAATAGC	Forward primer
	oNZ6	GCTATTTCTAGCTCTAAAACttaatcagagttttactcggcAAAC ATTTAGATTTGCAAT	Reverse primer

## Supplementary Methods

# Building sgRNA expression vectors using pPT2

This protocol describes the steps and tools used to generate sgRNA expression vectors using the pPT2 vector backbone. See the materials and methods section for the required reagents (e.g. Gibson assembly reagents, sequencing primers).

We recommend the online service benchling.com for sgRNA, oligo and vector design.

## I. Identifying a suitable protospacer motif

- A protospacer is a 19-20 bp sequence flanked at its 3' end by an NGG PAM (protospacer adjacent motif). Different online tools are available to identify possible protospacers in a region of interest (crispr.mit.edu ; tefor.net/crispor/crispor.cgi ; benchling.com).
- When multiple protospacer sequences are possible, select the closest (to the site to engineer) and/or the most specific sequence (use the off-target prediction tool provided by benchling for example). In general, four non-matching bases should be enough to significantly reduce off-target cutting, especially if the mismatches are located in the 3' region of the protospacer (Hsu *et al.* 2013).

## II. Building the sgRNA vector sequence *in silico*

- The pPT2 vector contains the U6 promoter and 3' UTR of *KO9B11.12* (Friedland *et al.* 2013) and two restriction sites (PmeI and SexAI) to linearize the vector, followed by the invariant sgRNA scaffold sequence (see Figure 1A).
- To generate the sgRNA expression vector sequence, insert the protospacer sequence (**without** the PAM, i.e. NGG) between the U6 promoter and the sgRNA scaffold as shown in figure 1B.
- If the selected protospacer sequence does not begin with a guanine residue, add this nucleotide manually to the 5' of the protospacer (i.e. resulting in a "19+1" bp insertion in pPT2, see figure 1B).
- Name this vector pXYn where XY are the initials of the person building the vector and n the number of the vector. Accordingly, the protospacer sequence is then labeled CRpXYn (generate a "feature" with the sequence, excluding the added G, to identify it easily in the genomic sequence).
- Generate one 60 bp oligonucleotide centered on the protospacer sequence as shown in figure 1C (forward or reverse). **Gibson assembly can be performed with a single primer** (see IIIa). Alternatively, generate two complementary 60 bp oligonucleotides centered on the protospacer sequence as shown in figure 1C (see IIIb).

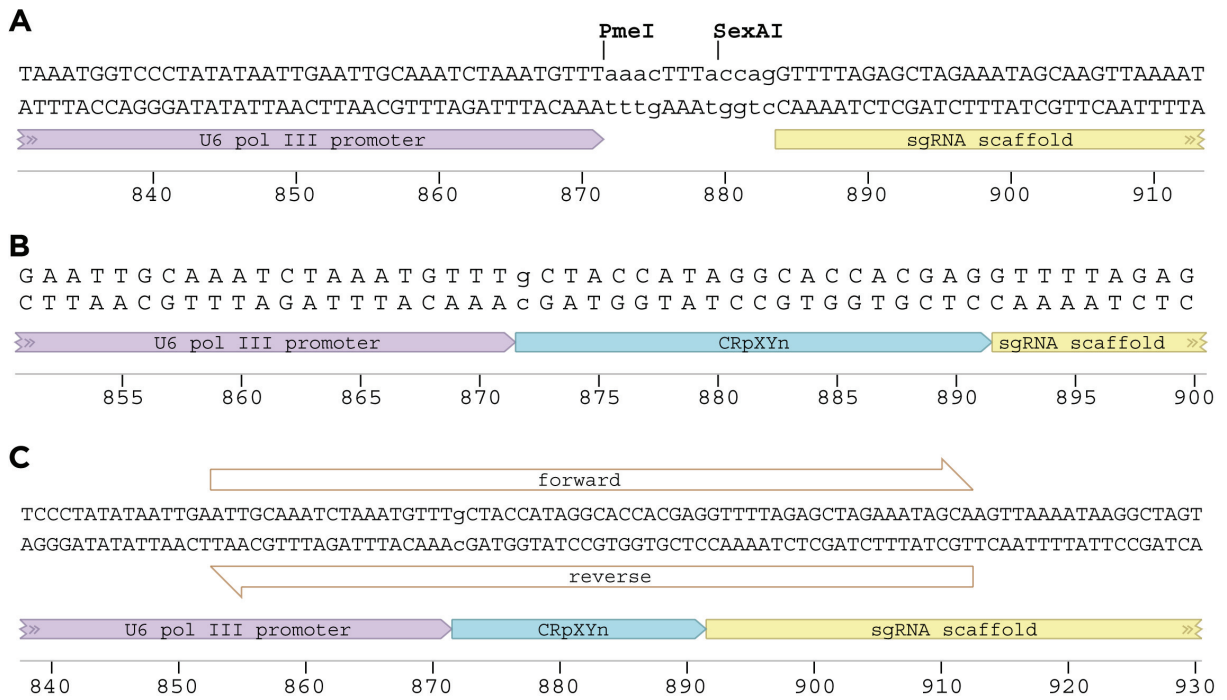


Figure 1 - Insertion of a protospacer sequence into the pPT2 sgRNA expression vector.

### IIIa. Building the sgRNA vector using a single oligonucleotide

The protospacer sequence is incorporated into the pPT2 vector as follows:

- 1 | Linearize pPT2 using the *PmeI* and *SexAI* restriction enzymes.
- 2 | Purify the linearized pPT2 vector using gel extraction.

#### 3 | Gibson assembly

- Thaw an aliquot of Gibson Master Mix and keep on ice.
- Mix 100 ng of linearized pPT2 vector with 1  $\mu$ L of 100  $\mu$ M (or 0.1 nmole) of single strand oligonucleotide and add water up to 5  $\mu$ L if necessary.
- Add 15  $\mu$ L of Gibson Master Mix to the DNA mix.
- Incubate at 50°C for 15 to 60 minutes (60 minutes is optimum).
- Transform 5  $\mu$ L of this reaction, and grow on LB+Ampicilin plates.
- Perform a control experiment (Gibson assembly without oligonucleotide) for each new batch of linearized pPT2 vector.

#### 4 | Sequence validation

- Due to the high efficiency/specificity of Gibson assembly, colony PCR is not required.
- Validate the resulting vector by sequencing with pJET1.2fwd or pJET1.2rev.

### IIIb. Building the sgRNA vector using oligonucleotide dimers

- The protospacer sequence is incorporated into the pPT2 vector as follows.

- 1 | Linearize pPT2 using the *PmeI* and *SexAI* restriction enzymes.

2 | Purify the linearized pPT2 vector using gel extraction.

3 | **Hybridize oligonucleotides** (using a thermocycler)

- Add 1  $\mu\text{L}$  of each oligonucleotide (at 100  $\mu\text{M}$ ) to 18  $\mu\text{L}$  of water.
- Run the program below on a thermal cycler to anneal primers.
- Add 30  $\mu\text{L}$  of water to the resulting sample.

95°C	10 min
95°C to 85°C	[-2.0 °C/s]
85°C	1 min
85°C to 75°C	[-0.3°C/s]
75°C	1 min
75°C to 65°C	[-0.3°C/s]
65°C	1 min
65°C to 55°C	[-0.3°C/s]
55°C	1 min
55°C to 45°C	[-0.3°C/s]
45°C	1 min
45°C to 35°C	[-0.3°C/s]
35°C	1 min
35°C to 25°C	[-0.3°C/s]
25°C	1 min
4°C	Hold.

4 | **Gibson assembly**

- Thaw an aliquot of Gibson Master Mix and keep on ice.
- Mix 100 ng of linearized pPT2 vector with 1  $\mu\text{L}$  of hybridized oligonucleotides and add water up to 5  $\mu\text{L}$  if necessary.
- Add 15  $\mu\text{L}$  of Gibson Master Mix to the DNA mix.
- Incubate at 50°C for 15 to 60 minutes (60 minutes is optimum).
- Transform 5  $\mu\text{L}$  of this reaction, and grow on LB+Ampicilin plates.
- Perform a control experiment (Gibson assembly without oligonucleotide dimer) for each new batch of linearized pPT2 vector.

5 | **Sequence validation**

- Due to the high efficiency/specificity of Gibson assembly, colony PCR is not required.
- Validate the resulting vector by sequencing with pJET1.2fwd or pJET1.2rev.

## Materials and Methods

### pPT2 sequence file

The annotated sequence file for the pPT2 vector can be downloaded as a Genbank format (readable in ApE and benchling.com) at the following link:

<http://www.excitingworms.eu/resources/pPT2.gb>

### Homemade Gibson Assembly Reagents

Based on *Methods in Enzymology, Volume 498*

CHAPTER FIFTEEN part 5: *Enzymatic Assembly of Overlapping DNA Fragments* (Daniel G. Gibson)

#### 5X ISO Buffer, 2 mL (store at -20°C)

Tris-HCl pH=7,5 1M	1 mL
MgCl <sub>2</sub> 2 M	50 µL
dGTP 100 mM	20 µL
dATP 100 mM	20 µL
dTTP 100 mM	20 µL
dCTP 100 mM	20 µL
DTT 1 M	100 µL
NAD <sup>+</sup> 50 mM	200 µL
PEG8000	0.5 g
H <sub>2</sub> O	add up to 2 mL

- Prepare 320 µL aliquots and store at -20°C.

#### Gibson Master Mix, 1.2 mL (store at -20°C)

For the assembly of DNA molecules with overlaps of 20-80 bp.

5X ISO buffer	320 µL
T5 Exonuclease (10 U/µL)	0.64 µL
Phusion (2 U/µL)	20 µL
Taq Ligase (40 U/µL)	160 µL
H <sub>2</sub> O	700 µL

Note: For overlaps that are larger than 80 bp, 3.2 µL exonuclease is used in this mix.

- Separate into 50 µL aliquots. Store at -20°C. The enzymes remain active after 10 cycles of freeze-thaw.

#### Sequencing Primers

pJET1.2fwd 5'-cgactcactatagggagagcggc-3'

pJET1.2rev 5'-aagaacatcgattttccatggcag-3'

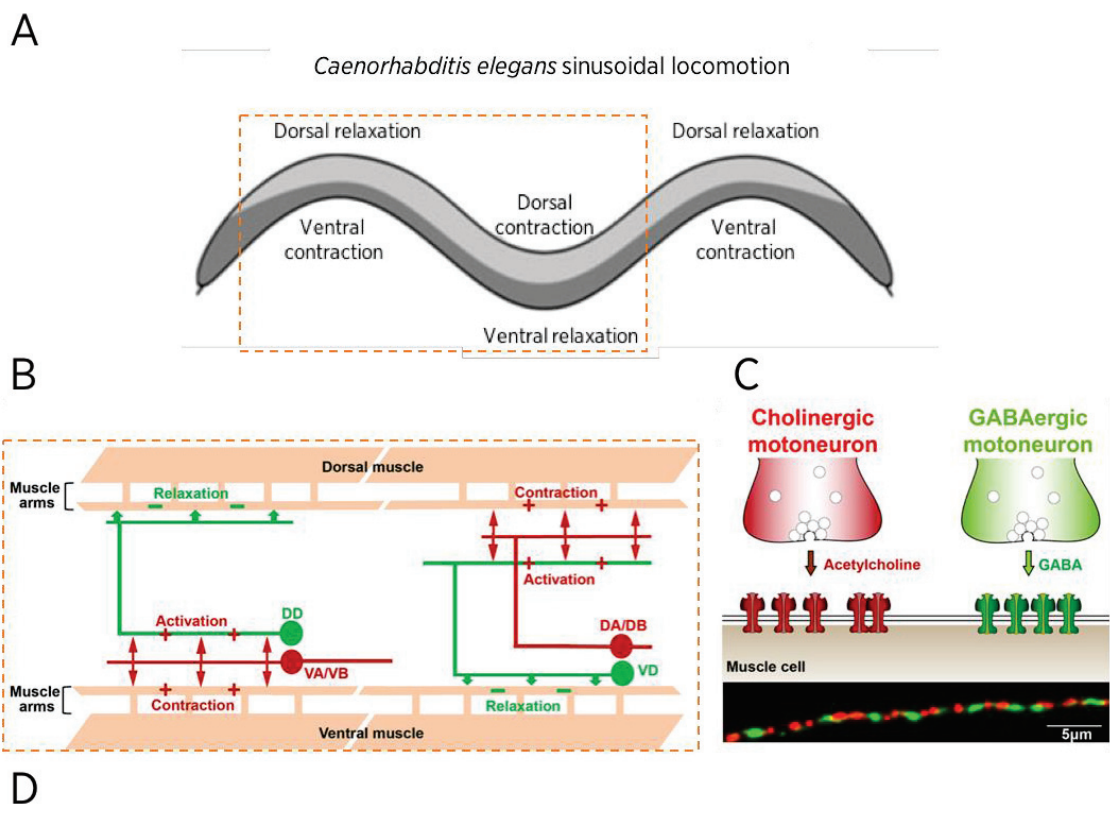
## DISCUSSION AND PERSPECTIVES



## K2P potassium channels in *C. elegans* muscle

1. Why K2P channels are asymmetrically localized in muscle cells?

Worm locomotion consists of cycles of muscle contraction on one side (cholinergic excitation) and relaxation on the opposite side (GABAergic synapses present in the body wall muscle), creating alternating waves ([Thapliyal and Babu, 2018](#)) and, therefore, a typical sinusoidal movement ([Figure 37 A and B](#)). In addition to an excitation/inhibition balance, this movement involves different sensory signals integrated by neurons in the locomotor circuit.



**Cell type consensus expression profiles.** Values listed are transcripts per million.

Gene	Touch receptor neurons	Body wall muscle
<i>twk-28</i>	5,681	44,423

Figure 37 *Caenorhabditis elegans* sinusoidal locomotion

**A:** The contraction and relaxation cycles of opposite body wall muscle cells lead to a sinusoidal movement typical of *C. elegans*. Adapted from [Thapliyal and Babu, 2018](#) **B:** To establish the neuromuscular junction, muscle cells send projections called “muscle arms” to the axon, where they receive either excitatory

cholinergic (red) or inhibitory GABAergic innervation (green). **C**: Each body wall muscle cell contains clusters of receptors for both acetylcholine, which induces its contraction, and GABA, which induces its relaxation. B and C are adapted from [Zhou and Bessereau, 2019](#) D: RNAseq data show the expression of *twk-28* in touch receptor neurons, in addition to body wall muscle. Adapted from [Cao et al., 2017](#).

On the other hand, mechanosensitive ion channels are able to respond to various stimuli featuring physical force, such as vibration, sound waves, stretch or mechanical indentation (reviewed in [Ranade et al., 2015](#)). To date, a clear link between the localization and function of K2P ion channels has not been established. Given the asymmetric distribution of TREK-1 at the intercalated discs of cardiomyocytes ([Hund et al., 2014](#)) (see introduction, [figure 3](#), C), one interesting aspect is whether the TREK-1 K2P channel has any specific purpose in this region. Since the activity of this channel is modulated by mechanical stresses, one can imagine that TREK-1 could serve as a sensor modulating muscle activity according to the tension perceived at the cell-to-cell junctions. Interestingly, we showed that the potassium K2P channel TWK-28 is localized only at the anterior tip of body wall muscle cells. Also, single cell transcriptome data ([Cao et al., 2017](#)) show expression of *twk-28* in touch receptor neurons ([Figure 37 D](#)). So, if, in addition to the GABAergic inhibition, on the post-synaptic side, TWK-28 had mechanosensitivity, being activated by the stretching of the muscle cell membrane, thus, on the relaxed body wall muscle side ([Figure 37 A](#)) there would be an increased hyperpolarization by activating these potassium channels, allowing greater relaxation. This could, perhaps, provide more efficiency and maybe precision in the sinusoidal movement of these animals. The fact that TWK-28 is mostly located in the muscle cell tips, may play an unknown-so far role in the coordination of such movement, by generating a local difference in the membrane potential of these cells participating in the sequence of the contraction/relaxation cycles. Furthermore, it is possible that the "comet-like" distribution of TWK-28 could be linked to interactions with components of the extracellular matrix, unknown to date, that could be mostly present in areas where there are physical contacts between more than two cells. In this case, why is TWK-28 not equally enriched on the posterior tip? Could it be a cell polarization dependent on factors such as the WNT pathways? This is one of the hypotheses we made, which led to another project conducted by Alice Peysson, a PhD student in the lab. Alice revealed that the WNT pathway is involved in the localization of TWK-28 (see Results, part I, [fig. 9](#)), as some mutants such as *Disheveled* could alter this distribution, being able to localize TWK-28 both at the anterior and posterior tip of the muscular cell. It might not be a direct

interaction, but Disheveled could disrupt one or more components of the cell membrane, and this would have an effect on the channel localization. The model of interaction between WNT-pathway proteins and TWK-28, as well as its specificity, is currently being investigated by Alice Peysson.

## 2. Why so many K2P channels in a single cell?

47 K2P channels are co-expressed in different tissues such as neurons or muscle in *C. elegans* ([Figure 38](#)) ([Cao et al., 2017](#)). In addition, we showed that 9 K2P channels are present in a single cell of the body wall muscle of the nematode (see introduction, [figure 6](#)). These channels have different and identifiable distribution patterns, suggesting that their localization probably depends on different cellular and molecular regulatory mechanisms. So far, we do not have any example of a mechanism that could be common to regulate more than one K2P channel.

But, why so many channels from the same family are present in the same cell membrane? Is there functional redundancy? We can imagine that the loss of one channel could be compensated by the other K2P channels co-existing in the same cell, either by an increase in their expression or by a regulation of their electrical activity. It could also be compensated by the negative regulation of channels whose current is "opposite", such as sodium channels. This kind of compensation was already shown by Julio-Kalajzić *et al.* analyzing intestinal Cl<sup>-</sup> and fluid secretion. In the intestine, fluid secretion is associated with an efflux of chloride anions (thanks to CFTR Cl<sup>-</sup> channels) into the lumen of the intestine (reviewed in [Barret and Keely, 2000](#)). For this secretion to occur, the participation of cAMP-dependent K<sup>+</sup> channels, present in the basolateral membrane of enterocytes, is crucial. The transport of K<sup>+</sup> in the basolateral membrane is mainly driven by the potassium channel KCNQ1 and its regulatory subunit KCNE3 ([Schroeder et al., 2000](#)). Julio-Kalajzic *et al.* demonstrated recently that under double *knock-out* mutant conditions of KCNQ1-KCNE3, there is a remaining K<sup>+</sup> current. This current was associated to a K2P potassium channel called TASK-2, which is co-expressed with KCNQ1-KCNE3 in the same cells. Thus, even if the molecular and cellular mechanisms are still unclear, TASK-2 might play an important role in the absence of KCNQ1-KCNE3 by providing an alternative conductance to ensure the continuity of the secretion process in the intestine ([Julio-Kalajzic et al., 2017](#)).

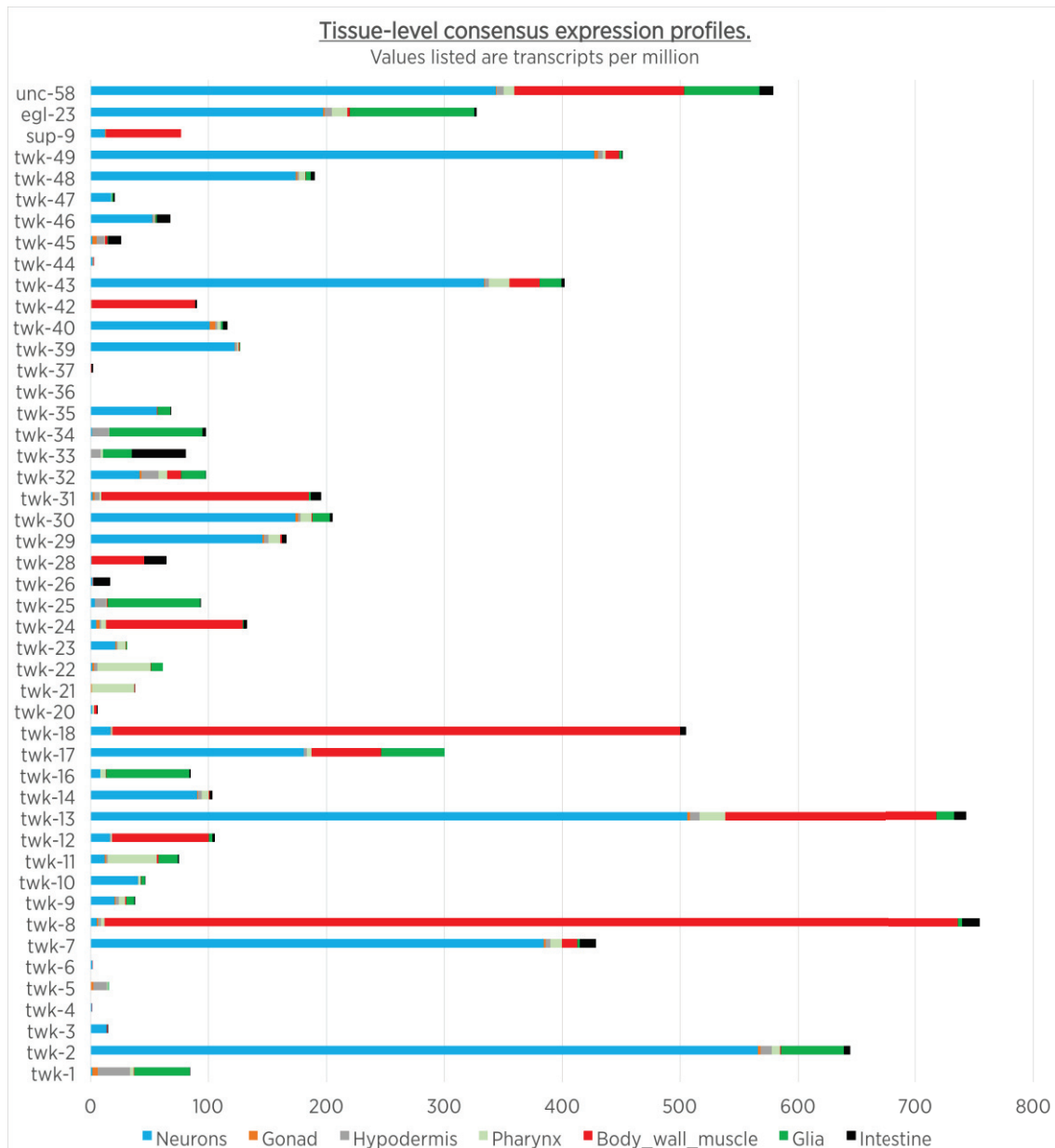


Figure 38 Principal tissues expressing K2P channels in *C.elegans*

As a result, in our case, we could imagine that the loss of a single K2P channel would have no effect on the functioning of the worm body wall muscle, as its role would be immediately compensated. From few examples observed in the laboratory, we can say that although the absence of some K2P channels has no effect, many other muscular *loss-of-function* mutants are able to originate locomotor phenotypes, some of them easily identifiable, as is the case of UNC-58 (*loopy* phenotype). Besides, EGL-23 and TWK-24 are another two K2P channels expressed in the vulval muscles ([figure 38](#)); the loss of only EGL-23 leads to an early egg-laying, where the embryos are still immature. So, the activity of EGL-23 is not compensated by the TWK-24 one.

Finally, for TWK-28, *loss-of-function* mutants exhibit on the worm tracker a subtle defective locomotor phenotype when compared to wild-type animals (Terese Lawry, Chalfie's Lab, unpublished data). All of these findings may indicate that there may not always be functional redundancy between K2P channels. Especially if we consider that the distribution of these channels is characteristic and different from one to another, probably having a direct impact on their not yet known role at the sub-cellular level.

### 3. Potassium channels are present in different sub-complexes in body wall muscle

In *C. elegans* body wall muscle, potassium channels show different localizations. Certain channels are found filling the entire surface of the cell (TWK-42), others are located in sub-compartments, either in the anterior (TWK-28), posterior (SLO-1) or central (TWK-24) tip of the muscle cell. Finally, another class is present in the lateral membrane (TWK-12 or UNC-58) of the body wall muscle cells ([Figure 39 A](#), also see introduction [figure 6](#)). But, what mechanisms are controlling each of these specific locations? The answer remains unknown, but different hypotheses are being considered. Firstly, there could be regulatory sub-units that would retain these channels in the regions to which they belong. For example, a comparable study of cholinergic receptors (AChR) in *C. elegans* revealed the involvement of a transmembrane protein, LEV-10, in the maintenance of clusters of these receptors at neuromuscular junctions, as shown in [figure 39 C](#) ([Gally et al., 2004](#)).

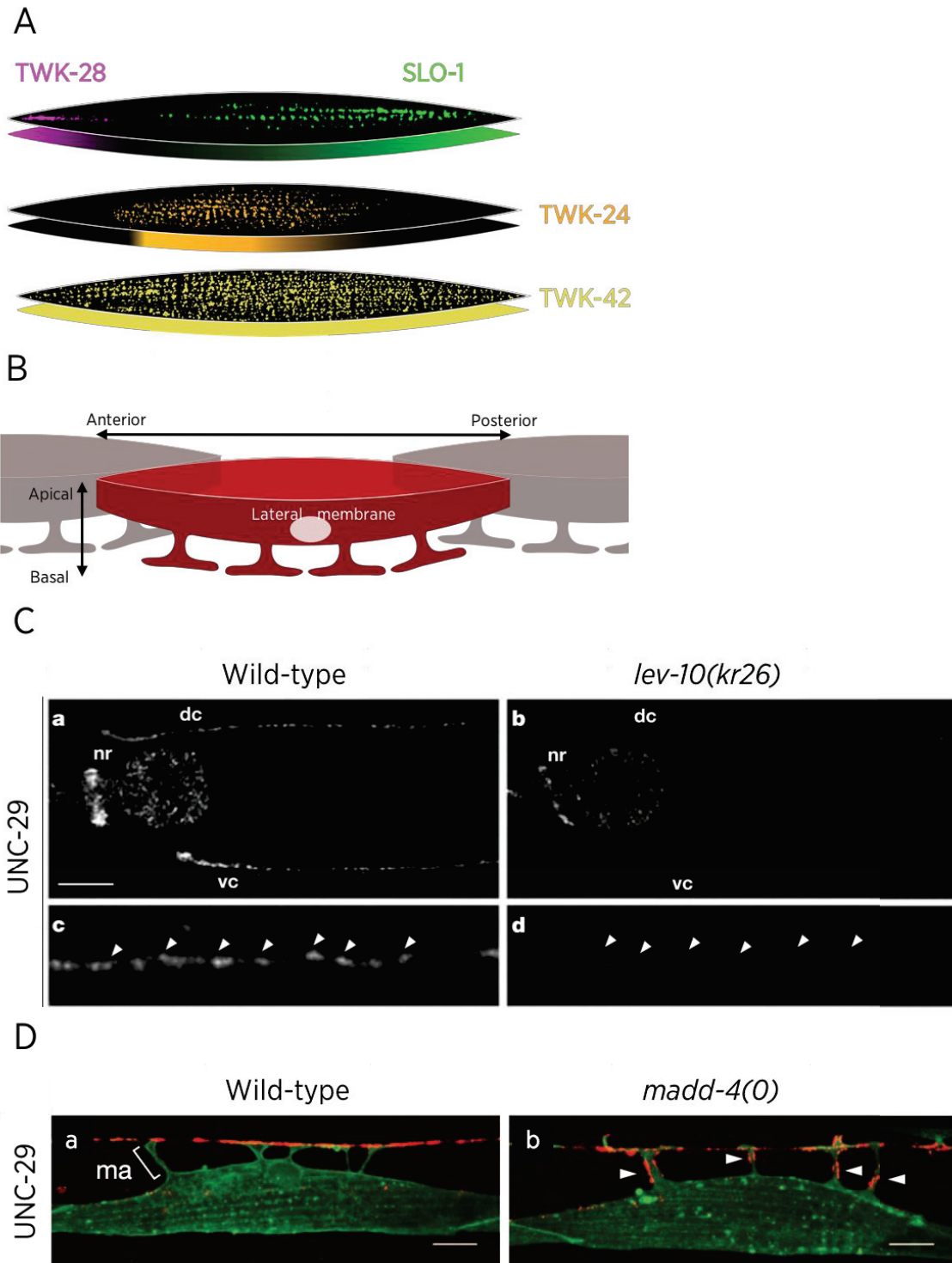


Figure 39 K2P channels distribution pattern in muscle. LEV-10 and MADD-4 are required for the AchRs clustering.

**A:** Schematic representation of K2P channels distribution in body wall muscle. Each “rhomboid” represents a single cell. **B:** Representation of three muscle cells with the apical surface, lateral membrane and muscle arms. **C:** Distribution at the NMJ of the nicotine-sensitive cholinergic receptor subunit UNC-29 in wild-type condition. In absence of LEV-10, a transmembrane regulatory protein, UNC-29 is strongly reduced in the nerve ring (nr) and absent from both dorsal (dc) and ventral (vc) nerve cord. Adapted from [Gally et al.](#)



[2004](#). D: UNC-29 distribution is altered in punctin/madd-4 null mutant, being localized in muscle arms (ma). Adapted from [Pinan-Lucarré et al., 2014](#).

If we consider other K2P channels, such as TWK-12 or UNC-58, which is positioned in the lateral membrane of the muscle cell (see introduction, [Figure 6 B](#)), one relevant question is how is the diffusion of these transmembrane proteins to other regions of the lipid bilayer, such as the muscle arms, prevented? An interesting study on the localization of cholinergic receptors at neuromuscular junctions by Pinan-Lucarré *et al.* described a mechanism that could be analogous to the one sought for K2P. The authors demonstrated that punctin/MADD-4 is required for the clustering of AchR UNC-29 subunit in NMJs ([Pinan-Lucarré et al., 2014](#)). Interestingly, they also revealed that in *madd-4 knock-out* mutants, the amount of UNC-29 is not only reduced at the NMJ, but the channel is dispersed into non-synaptic areas such as the muscle arms, in which in wild-type conditions UNC-29 is not expressed ([Figure 39 D](#)). We believe that an analogous mechanism could exist to maintain the K2P channels located stably in the anterior subdomains where they are found, with no capacity to diffuse through the muscle cell membrane. One way to elucidate some of these mechanisms would be to perform visual genetic screens on these channels and look for mutants where the channel is still expressed but would be localized in regions other than the wild-type ones.

In the case of TWK-28, proteins such as syntrophins, dystrobrevin and sarcoglycans, which present an asymmetric localization with an enrichment at the anterior tip of muscle cell (see results, part I, [fig. 6 F](#)), could be involved in the localization/addressing of the channel. The question that remains to be investigated is how are these asymmetric proteins addressed to the membrane in development and how are themselves kept asymmetrically distributed, since there are no known physical delimitations in the anatomy of the muscle cell that could create these subdomains.

## Novel genetic association between DAPC and K2P channels

### 1. Discovery of new regulatory factors of TWK-28

To identify factors involved in the regulation of TWK-28, we performed a phenotypic genetic screen based on the paralysis of *twk-28* (L210T) *gain-of-function* mutant worms, which served as a starting point. After a random mutagenesis with EMS, we looked for animals that were again mobile. This strategy allowed us to identify several genes, as it is the case of dystrophin, whose absence causes a decrease of TWK-28 from the surface of the muscle cell, thus producing a suppression of the paralysis phenotype present in the *gof* animals before the mutagenesis. Given the disposition of TWK-28 and its enrichment in the anterior cell tip of the body wall muscle, isolating genes that could affect this asymmetric distribution with our approach was not the objective. However, it would be possible and interesting to make a visual genetic screen strategy, where we would also induce a random mutagenesis and look, with the help of a microscope, for animals where the channel distribution is disturbed. Another option would be to perform a candidate gene method, in which genes related to, for example, cell polarity, such as WNT-pathway components, could be tested. The last one gave rise to the project of Alice Peysson, another student in the laboratory, who is currently analyzing the genetic interaction between different WNT proteins with respect to the localization of TWK-28 in body wall muscle.

### 2. Specificity of Dystrophin in the regulation of TWK-28. Could different DSY-1/Dystrophin isoforms have separate functions?

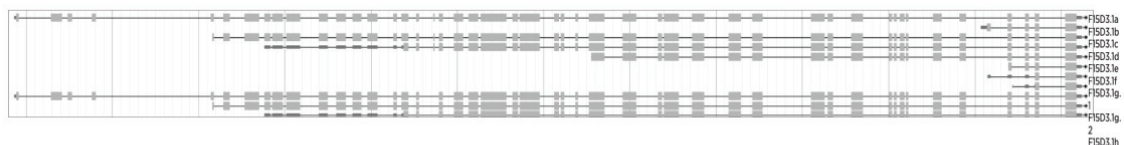
Given the central and structural role of dystrophin in muscle, one can imagine that the absence of this crucial protein could have a large effect on the membrane, which would explain the disruption of TWK-28 and probably other ion channels localization. However, when we observed other muscular K2P channels under *dys-1*/dystrophin mutant conditions, no alteration in their pattern was detected. The specificity of the regulation of the TWK-28 channel by the dystrophin, was striking to us. This type of specific interaction was already observed by another student on the lab, Philippe Tardy. He studied the UNC-58 K2P channel and identified an unusual interaction of this channel with ankyrin, which proved to be necessary for its localization on the muscle membrane. Interestingly, ankyrin is not required for the localization of TWK-28 (data unpublished).

Then, the role in ion channels localization of these two large proteins is specific and selective.

On the other hand, as in vertebrates, in *C. elegans* the dystrophin/*dys-1* gene also codes for multiple isoforms (Figure 40 A). Could these isoforms play different roles in muscle? Interestingly, on the genetic screen of TWK-28 L210T, we were able to isolate 14 alleles with different mutations in the *dys-1* gene, three of them located in the N-terminus part of the longest isoform (Figure 40 B). This is the only isoform that contains the actin interaction domains (calponin homology, CH). Next, we reproduced the same mutation (W110\*) in the transcriptional *knock-in dys-1::degron::mNeonGreen* strain, where the mNeonGreen was inserted at the C-ter end of the gene, i.e. targeting all *dys-1* isoforms. As the long isoform was not present (W110\* mutation), the fluorescent signal we see would correspond to the remaining isoforms. Intriguingly, the distribution of this signal in the cells of the body wall muscle was markedly weaker compared to what was observed in the presence of all dystrophin isoforms. The remaining isoforms localization, compared to the long one, also seemed to be less diffuse, forming small clusters at the cell surface (see results, part I, fig. 8 C). This suggests that there are at least two sub-populations of dystrophin present in the muscle. Do these two protein-populations play different roles in BWM?

A

*dys-1* isoforms



B

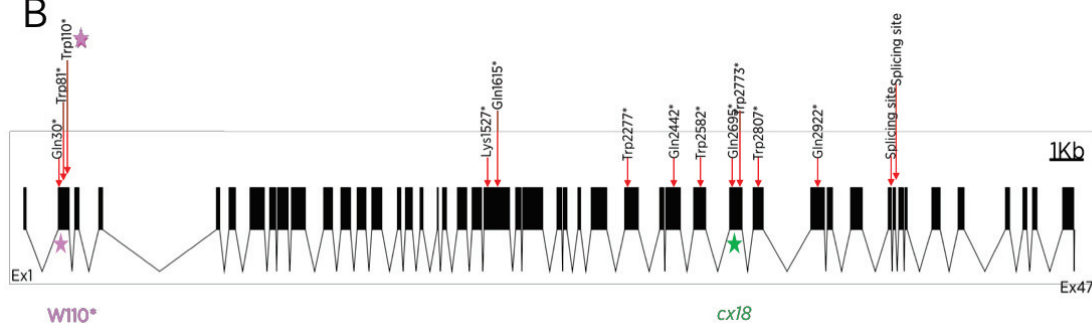


Figure 40 *dys-1* isoforms and genetic screen alleles

A: dystrophin/*dys-1* presents eleven isoforms in *C. elegans*, all of them sharing the C-terminus region (right). B: *dys-1* gene schematic representation. The black boxes represent exons and the lines introns. Red

arrows represent the localizations of the fourteen mutant alleles isolated from the genetic screen on TWK-28, being *dys-1* W110\* the referent long-isoform allele.

Interestingly, studies analyzing the expression of the BK SLO-1 channel in the *dys-1(cx18)* mutant ([Sancar et al., 2011](#)), show a strong reduction of the channel at the cell surface (see introduction, [figure 36](#)). *dys-1(cx18)* induces an early stop that affects all dystrophin isoforms. However, when we use the long isoform mutant *dys-1(bn582)* W110\*, where the other isoforms are present, we see that the SLO-1 channel is altered but not disappeared: in head muscles, we see a delocalization towards regions where SLO-1 is not present in wild-type conditions, such as regions of head muscles near the nose of the worm. In addition, although we continue to see a puncta pattern, in both the body and head muscles we see that the localization is more diffuse. Thus, it is clear that *dys-1(cx18)* and *dys-1(bn582)* do not have the same effect on SLO-1 localization, suggesting that SLO-1 regulation is isoform-dependent. Therefore, we decided to look at SLO-1 in the molecular null of *dys-1*. In this *dys-1(syb2174)* mutant the entire gene locus has been removed, including all the isoforms. We have shown that in the absence of all isoforms, with *dys-1(syb2174)*, the effect on SLO-1 localization looks more like the *dys-1(cx18)* mutant one. In addition, we have consistently shown that the location of the short DYS-1 isoforms resembles the SLO-1 channel puncta pattern in the BWM (see results, part I, [fig. 8](#)).

As a conclusion, we revealed that for the regulation of the SLO-1 localization, the short isoforms of DYS-1 are more relevant, while for TWK-28 the long isoform is critical.

### 3. Is the syntrophin PDZ domain implicated in the regulation of TWK-28?

*stn-1* is the coding gene for the  $\alpha$  and  $\beta$ -syntrophin homologue protein in *C. elegans* ([Grisoni et al., 2002b](#)). We have shown that STN-1 has an asymmetric subcellular localization in body wall muscle of the worm, exhibiting an enrichment that co-localizes with TWK-28 in the anterior tip of the cells. In addition, we have also revealed that in the context of fluorescence-tagged *mNeonGreen::twk-28*, mutations in various components of DAPC, including *stn-1*, lead to a strong decrease of TWK-28-associated fluorescence on the surface of muscle cells.

Interestingly, the STN-1 protein conserves almost all functional domains of vertebrate syntrophins ([Grisoni et al., 2002b](#)). This includes the PDZ domain, which is responsible

for its interaction with numerous transmembrane proteins, such as ion channels. A well-studied example in the literature is the interaction of the PDZ domain of syntrophin with the C-terminus region of the voltage-sensitive sodium channels (Na<sub>v</sub>) in both skeletal ([Gee et al., 1998](#)) and cardiac ([Gavillet et al., 2006](#)) muscles. The interaction of syntrophin through its PDZ domain with the K<sub>ir</sub> family of potassium channels in the heart of mice was also evidenced ([Connors et al., 2004](#)).

These findings, combined with our results, led us to hypothesize a possible interaction between the TWK-28 channel and the PDZ domain of STN-1. Subsequently, we identified on the C-terminus of TWK-28 a PDZ-binding-motif sequence (PDZ-BM) of which the absence causes a strong reduction of the channel on the surface of the muscle cells (see results, part I, [fig. 7](#) A-D). Possibly, by removing this PDZ-BM from TWK-28, the channel is no longer able to interact with syntrophin, thus losing its stability on the cell membrane. But, it also could be independent on syntrophin, thus, a second scenario may involve another unidentified protein with a PDZ domain. One way to verify all these interactions, is to perform *in vitro* biochemical studies such as GST pull down, using the PDZ-domain fragments of STN-1 and the C-ter fragment of TWK-28. Also, although more challenged, co-immunoprecipitation and western blot experiments can be performed.

Finally, a third scenario may envisage that the sequence identified as PDZ-BM in TWK-28 is actually an interaction sequence with intracellular signaling proteins or a sequence involved somehow in the trafficking of the channel to the cell surface or in its maintenance, so that when it is absent, the channel is destabilized or unable to reach the membrane and therefore its quantity is reduced. A regulatory protein called ISLO-1 could be a good candidate. ISLO-1, was identified as a modulatory subunit of the BK potassium SLO-1 channel ([Kim et al., 2009](#)). Interestingly, the *islo-1* gene was also isolated in our genetic screen performed on TWK-28. Also, *islo-1 loss-of-function* mutants are able to produce a strong reduction in the TWK-28 channel-associated fluorescence on the surface of muscle cells. As well, ISLO-1 also co-localizes with TWK-28 in the anterior body wall muscle cell type (see results, [fig. 6](#) F). All these results indicate that ISLO-1 interacts somehow with TWK-28, for which, interaction-experiments will be performed as a next step.

#### 4. Dystroglycan/DGN-1 in body wall muscle of *C. elegans*. Which role does it play?

The principal gene coding for dystroglycan in *C. elegans* is *dgn-1*, which expression has been observed in different tissues but not in muscle ([Johnson et al., 2006](#)). We have shown that DGN-1 is present in muscle tissue of *C. elegans*, including body wall muscle. This is more consistent with the expression of vertebrates dystroglycans, where they form part of the muscular dystrophin-associated proteins complex ([Ervasti and Campbell, 1993](#)). Curiously, we also showed that DGN-1 localization is similar to that of dystrophin in BWM, suggesting that dystroglycan, contrary to what was assumed, might be part of the DAPC in the body wall muscle of worms. Nevertheless, its physical interaction to dystrophin, not yet explored, has probably evolved, since the PPxY sequence present in the C-terminus of the vertebrate  $\beta$ -dystroglycan and necessary for its binding to dystrophin ([Huang et al., 2000](#)), is not conserved in the worm ([Figure 41 A](#)) ([Johnson et al., 2006](#)). However, this does not exclude the existence of a new sequence in DGN-1 (different from the PPxY motif) that would allow the interaction with a different region of DYS-1. Interestingly, in DYS-1, the homologous to the  $\beta$ -dystroglycan-binding region in human dystrophin, is not fully degenerated ([Figure 41 B](#)). Furthermore, we interestingly have shown that the localization of DGN-1 in BWM looks declustered and more diffuse in the *dys-1(bln582)* W110\* mutant (See results, part I, [fig. 5 B](#)), indicating a clear genetic interaction between dystroglycan and dystrophine in *C. elegans* muscle. Complementary coimmunoprecipitation or *in vitro* GST pull-down experiments are planned to be carried out in the future.

To conclude, we have shown that it is likely that dystroglycan forms part of the DAPC in the body wall muscle of *C. elegans*, although the interaction sequences between DGN-1 and DYS-1 are not fully conserved.



A

Human (DAG1) and <i>C. elegans</i> (DGN-1) dystroglycans			
DAG1	LIAGIIAMICYRKKRKGKLTLEDQATFIKKGVPIIFADELDDSKPPSSSMLILQEEKA	824	
DGN-1.1	LIAVAIIIYCACIKKSGKK-KSTSTEYVSKGLPVVFPDEVEENDPHTA-GTPMLAREERP	541	
	*** * : * *:.** . . : :.***:*** * : : : . * : : * : :		
DAG1	PLPPPEYPNQSVPETTPLNQDTMGEYTPLRDEDPNAPPYQPPPPFTAPMEGKGSRPKNMT	884	
DGN-1.1	PL-----KVSQHENPLYKPPPIASNSPRLGHASS-SS	573	
	** : . : : * * : * : * : : : : * . :		
DAG1	PYRSPPYVPP*	895	
DGN-1.1	NQKLQSPFIPP*	584	
	: * : * * *		

B

Human (Dystrophin) and <i>C. elegans</i> (DYS-1.a.1) dystrophins			
Dystrophin	INTRWKLLOVAVEDRVROLHEAHRDFGPASQHFLLSTSVOGPWERAISP-NKVPYYINHET	3078	
DYS-1.a.1	VNKRYSTLKRAIRIRQA AVRNAASDFGPTSEHFLNQSVTLPWQRAISKSNLLPYIEQTS	3071	
	:*.*:. * : * . * : : * * : * : * : * . * * : * * * * * * : * : * : :		
Dystrophin	QTTCWDHPKMTELYQSLADLNNVRFSA YRTAMKLRRLQKALCLDLLSLSAACDALDQHNL	3138	
DYS-1.a.1	EKTQWEHPVWVEIVKELSQFN RVKFLAYRTAMKLRALQKRLCLDLVDLTLLEKAFVRLKG	3131	
	:.* * : * * * . * : : . * : : * . * : * * * * * * * * * * * : . * : : :		

Figure 41 Dystrophin and dystroglycan conservation in *C. elegans*

A: C-terminus cytoplasmic region (blue) of human (DAG-1) and *C. elegans* dystroglycan sequence alignment. In *C. elegans*, the human dystroglycan PPxY binding sequence to dystrophin (red) is not conserved. B: Sequence of the dystroglycan binding-region in dystrophin. Residues required for this interaction are represented in red, of which some are conserved in *C. elegans* (blue) and others not.

On the other hand, one of the roles of dystroglycans is to provide the interface between the extra and intracellular medium at the sarcolemma (Ervasti *et al.*, 1993). Although, the dystroglycan in *C. elegans* does not undergo a cleavage process to give two  $\alpha$  and  $\beta$ -dystroglycan subunits, as occurs in vertebrates (Ibraghimov-Beskrovnya *et al.*, 1992), glycosylation of this protein has been found to take place in the worm (Johnson *et al.*, 2006). Besides,  $\alpha$ -dystroglycan interacts with different proteins of the extracellular matrix, including perlecan (Talts *et al.*, 1999), which led us to wonder if this is also the case in *C. elegans*. Indeed, we have consistently shown that the localization of DGN-1 in the muscle is altered in the absence of perlecan/UNC-52 (see results, part I, fig. 1 D), suggesting a conserved role of DGN-1 in linking the sarcolemma to the extracellular matrix.

Finally, in order to shed some light on the function of DGN-1 in muscle, and since its absence gives rise to sterile mutants (Johnson *et al.*, 2006), we decided to do an auxin-inducible time and tissue-specific degradation (Zhang *et al.*, 2015). The auxin-inducible

degradation of DGN-1 will allow us to: 1) elucidate the role of DGN-1 in the formation of the sarcoglycan sub-complex in muscle. These results would be contrasted to what occurs in vertebrates, where the dystroglycan interacts with the sarcoglycans after assembly for their trafficking from Golgi to the sarcolemma ([Noguchi et al., 2000](#)). Furthermore, data in the literature on the interaction of sarcoglycans and dystroglycans are inconsistent: some studies propose that only the  $\delta$ -sarcoglycan subunit binds to both  $\alpha$  and  $\beta$ -dystroglycan ([Chan et al., 1998](#)), while others indicate that all four subunits of the SG subcomplex bind to  $\beta$ -dystroglycan ([Sakamoto et al., 1997](#)). Given this discrepancy, we could check if this interaction is conserved in *C. elegans* and perform more detailed molecular studies on the interdependence of these two families of proteins, taking advantage of the simplicity of the model. 2) On the other hand, the depletion of DGN-1 would allow us to test whether it is implicated in the stabilization of the rest of the DAPC components, such as dystrophin, syntrophin or dystrobrevin. 3) Finally, we would be able to see whether the absence of DGN-1 has an effect on TWK-28 localization, since both proteins co-localize at muscle cell surface (See results, part I, [fig. 6 F](#)).

#### 5. Do sarcoglycans in *C. elegans* function as in vertebrates?

Sarcoglycans (SG) form a sub-complex of the DAPC and in *C. elegans* they are encoded by three genes: *sgca-1*, *sgcb-1* and *sgn-1*. Only SGCA-1 has been partially characterized, whereas no analysis of the remaining SG has been published. We have demonstrated that both SGCA-1 and SGCB-1 have a similar compartmentalized localization in the body wall muscle of *C. elegans* (see results, part I, [fig. 2 A and B](#)). For SGN-1 we do not have information about its distribution yet (project under investigation). But given the location of SGCA-1 and SGCB-1, our hypothesis holds that the three proteins would form a sub-complex which would interact with the DAPC, as occurs in vertebrates (reviewed in [Tarakci et al., 2016](#)). We have demonstrated that the absence of *sgca-1* causes a drastic decrease on SGCB-1 at the cell surface, and vice versa, the amount of SGCA-1 protein is strongly reduced in the absence of *sgcb-1* (see results, part I, [fig. 2 J](#)). This is also consistent with what occurs in vertebrates, where the correct trafficking of sarcoglycans after synthesis in order to reach the membrane requires the simultaneous presence of all SG subunits ([Holt et al., 1998](#)). Also, the absence of a single subunit causes the loss of the entire subcomplex ([Bonnemann et al., 1995](#); [Noguchi et al., 1995](#); [Nigro et al., 1996b](#)).

Interestingly, our results show that the absence of *sgn-1* affects the distribution of SGCA-1 but not that of SGCB-1 (see results, part I, [fig. 2 J](#)). In the literature, SGN-1 is considered the  $\gamma/\delta$ -sarcoglycan homologue ([Carre-Pierrat et al., 2006](#); [Gieseler et al., 2017](#)). However, in vertebrates  $\gamma$ -SG and  $\delta$ -SG there are many differences as for example in the patterns of expression:  $\gamma$ -SG is expressed exclusively in cardiac and skeletal muscle ([Noguchi et al., 1995](#)) while  $\delta$ -SG is expressed, in addition to striated muscle, in smooth muscle ([Nigro et al., 1996a](#)). In *C. elegans*, the tissues expressing *sgn-1* are not yet defined, although RNAseq data show expression mainly in body wall muscle and slightly in neurons ([Cao et al., 2017](#)). Additionally, in vertebrates, during the synthesis of sarcoglycans,  $\beta$  and  $\delta$ -SG are initially assembled and then,  $\gamma$  and  $\alpha$ -SG are recruited ([Holt et al., 1998](#); [Shi et al., 2004](#)). Let us assume that SGN-1 represents the  $\gamma$ -SG (and not  $\delta$ -SG) subunit in the worm: we can hypothesize that SGCB-1/ $\beta$ -sarcoglycan first binds to SGCA-1/ $\alpha$ -sarcoglycan and then, SGN-1/ $\gamma$ -SG is recruited. So, SGCA-1 and SGCB-1 would interact with each other and SGN-1 would only bind to SGCA-1. This would explain why *sgn-1* mutants would only have an effect on the location of SGCA-1 and not that of SGCB-1. It would also explain how the SGCA-1 and SGCB-1 sub-units depend on each other.

In parallel, given the glycosylation of sarcoglycans, it has been considered that they could act as receptors for extracellular matrix proteins ([Chan et al., 1998](#)). Based on this, we have tested whether there is a genetic interaction between the extracellular matrix component perlecan/UNC-52 and worms  $\beta$ -sarcoglycan. Indeed, we have demonstrated that  $\beta$ -sarcoglycan/SGCB-1 is strongly reduced in body wall muscle cells in *unc-52* mutants (see results, part I, [fig. 3 C](#)), suggesting a possible interaction of sarcoglycans and extracellular matrix in *C. elegans* muscle.

Furthermore, it has been shown that sarcoglycans interact with the C-terminus domain of dystrophin ([Chen et al., 2006](#)). Is this interaction preserved in *C. elegans*? Our results show that a genetic interaction exists between dystrophin and sarcoglycans in worms, since the localization of SGCB-1 is drastically altered showing a strong reduction (see results, part I, [fig. 5 A](#)) in the context of *dys-1(syb2174)* null molecular mutants. This is comparable to what was observed by Oh *et al.* when analyzing the amount of another sarcoglycan, SGCA-1, in the *dys-1(eg33)* mutants by western blot ([Oh et al., 2012](#)), confirming an interaction between dystrophin and the sarcoglycan sub-complex in worms. In addition, in the same figure we also show a genetic interaction between

dystrobrevin/*dyb-1* and *sgcb-1*, which is also conserved in evolution, since  $\alpha$ -dystrobrevin is known to interact with the sarcoglycans subcomplex in vertebrates ([Yoshida et al., 2000](#)). As a consequence, the hypothesis that the interactions in the DAPC of *C. elegans* are similar to those found in the DAPC of vertebrates becomes more plausible.

Finally, in the [fig. 3 B](#) of results part I, we see that the localization of DGN-1 is not altered in the absence of *sgcb-1*. So, although sarcoglycans are known to interact with dystroglycans after their assembly in vertebrates ([Noguchi et al., 2000](#)), we have not been able to see this interdependence in the worm.

Also, even if all DAPC components tested had an effect on TWK-28 localization, our results show that sarcoglycans do not seem to be required (see results, part I, [fig. S6](#)).

So far, we have shown that several DAPC proteins, such as dystrophin and dystrobrevin, are necessary for the correct localization of the sarcoglycans in the BWM cell membrane. However, we have not obtained any effect on the distribution of proteins like dystrophin, dystrobrevin, syntrophin, dystroglycans under sarcoglycan mutant conditions. This could indicate that sarcoglycans, despite their transmembrane location that one could attribute to a central role in DAPC, these proteins do not appear to be essential for the formation of DAPC and the location of most of its intracellular (dystrophin, syntrophin and dystrobrevin) and transmembrane (dystroglycans) proteins.

## General conclusions

In vertebrates, the dystrophin-associated protein complex (DAPC) constitutes a crucial structural element in the muscle costamere, since it establishes a bridge between the cytoskeleton and the extracellular matrix. We have shown that multiple proteins of this complex, such as dystrophin/DYS-1, sarcoglycans (SGCA-1 and SGCB-1), syntrophin/STN-1 and dystrobrevin/DYB-1 have a compartmentalized localization in the body wall muscle of *C. elegans*. We have also revealed that dystroglycan/DGN-1, whose presence in the striated muscle of the worm was excluded until today, also presents an asymmetric and dystrophin-like distribution in the body wall muscle cells. In addition, we have demonstrated that there is a genetic interdependence between *C. elegans* DAPC components, similar to vertebrates. As a complementary study, we plan to carry out soon biochemical interaction analyses of the DAPC proteins, especially of sarcoglycans and dystroglycans, since almost nothing is known in the literature about their role in *C. elegans* muscle.

Furthermore, the dystrophin complex has been involved in the regulation of several transmembrane proteins, including ion channels. In my thesis project, one of the axes consisted in studying the association of worms DAPC and K2P channels family. First, we have shown that the localization of the muscular K2P channel TWK-28 depends on dystrophin and other associated proteins, such as syntrophin/STN-1 or dystrobrevin/DYB-1. We have also shown that this interaction is specific to TWK-28, since dystrophin does not seem to be required for the localization of other K2P channels co-expressed with TWK-28 in the body wall muscle. Finally, preliminary studies indicate that the PDZ-binding motif sequence present in the C-terminus region of TWK-28 is required for the localization of the channel in the sarcolemma. Accordingly, biochemical studies of the interaction of TWK-28 with syntrophin are envisaged in the future, in order to elucidate the molecular mechanisms behind the stabilization of TWK-28 in the body wall muscle cell membrane.

Finally, given the asymmetrical comet-like distribution of TWK-28, which is located exclusively at the anterior tip of each body wall muscle cell, we hypothesized that this pattern could correspond to a novel planar cell polarity example in *C. elegans*. Therefore, in collaboration with Alice Peysson, another PhD student in the team, we have started the analysis of the effect on the compartmentalized distribution of TWK-28 of different

components of the WNT pathway, such as Disheveled/DSH-1, ROR/CAM-1 or WNT ligand/EGL-20. Preliminary results indicate that WNT is involved in establishing the asymmetry observed in TWK-28. This project is currently being investigated by Alice Peysson.



## REFERENCES

- Adams, M.E., Odom, G.L., Kim, M.J., Chamberlain, J.S., Froehner, S.C., 2018. Syntrophin binds directly to multiple spectrin-like repeats in dystrophin and mediates binding of nNOS to repeats 16–17. *Human Molecular Genetics* 27, 2978–2985. <https://doi.org/10.1093/hmg/ddy197>
- Ahn, A.H., Kunkel, L.M., 1995. Syntrophin binds to an alternatively spliced exon of dystrophin. *The Journal of Cell Biology* 128, 363–371. <https://doi.org/10.1083/jcb.128.3.363>
- Aller, M.I., 2005. Modifying the Subunit Composition of TASK Channels Alters the Modulation of a Leak Conductance in Cerebellar Granule Neurons. *Journal of Neuroscience* 25, 11455–11467. <https://doi.org/10.1523/JNEUROSCI.3153-05.2005>
- Anderson, M.S., Kunkel, L.M., 1992. The molecular and biochemical basis of Duchenne muscular dystrophy. *Trends in Biochemical Sciences* 17, 289–292. [https://doi.org/10.1016/0968-0004\(92\)90437-E](https://doi.org/10.1016/0968-0004(92)90437-E)
- Araishi, K., Sasaoka, T., Imamura, M., Noguchi, S., Hama, H., Wakabayashi, E., Yoshida, M., Hori, T., Ozawa, E., 1999. Loss of the Sarcoglycan Complex and Sarcospan Leads to Muscular Dystrophy in  $\beta$ -Sarcoglycan-Deficient Mice. *Human Molecular Genetics* 8, 1589–1598. <https://doi.org/10.1093/hmg/8.9.1589>
- Balasubramanian, S., Fung, E.T., Haganir, R.L., 1998. Characterization of the tyrosine phosphorylation and distribution of dystrobrevin isoforms. *FEBS Letters* 432, 133–140. [https://doi.org/10.1016/S0014-5793\(98\)00804-7](https://doi.org/10.1016/S0014-5793(98)00804-7)
- Barresi, R., Moore, S.A., Stolle, C.A., Mendell, J.R., Campbell, K.P., 2000. Expression of  $\gamma$ -Sarcoglycan in Smooth Muscle and Its Interaction with the Smooth Muscle Sarcoglycan-Sarcospan Complex. *J. Biol. Chem.* 275, 38554–38560. <https://doi.org/10.1074/jbc.M007799200>
- Barrett, K.E., Keely, S.J., 2000. Chloride Secretion by the Intestinal Epithelium: Molecular Basis and Regulatory Aspects. *Annu. Rev. Physiol.* 62, 535–572. <https://doi.org/10.1146/annurev.physiol.62.1.535>
- Ben Soussia, I., El Mouridi, S., Kang, D., Leclercq-Blondel, A., Khoubza, L., Tardy, P., Zariohi, N., Gendrel, M., Lesage, F., Kim, E.-J., Bichet, D., Andriani, O., Boulin, T., 2019. Mutation of a single residue promotes gating of vertebrate and invertebrate two-pore domain potassium channels. *Nat Commun* 10, 787. <https://doi.org/10.1038/s41467-019-08710-3>
- Bessou, C., Giuglia, J.B., Franks, C.J., Holden-Dye, L., Ségalat, L., 1998. Mutations in the *Caenorhabditis elegans* dystrophin-like gene *dys-1* lead to hyperactivity and suggest a link with cholinergic transmission. *Neurogenetics* 2, 61–72. <https://doi.org/10.1007/s100480050053>
- Bhat, S.S., Ali, R., Khanday, F.A., 2019. Syntrophins entangled in cytoskeletal meshwork: Helping to hold it all together. *Cell Prolif* 52, e12562. <https://doi.org/10.1111/cpr.12562>
- Blake, D.J., Nawrotzki, R., Peters, M.F., Froehner, S.C., Davies, K.E., 1996. Isoform Diversity of Dystrobrevin, the Murine 87-kDa Postsynaptic Protein. *J. Biol. Chem.* 271, 7802–7810. <https://doi.org/10.1074/jbc.271.13.7802>
- Blake, D.J., Weir, A., Newey, S.E., Davies, K.E., 2002. Function and Genetics of Dystrophin and Dystrophin-Related Proteins in Muscle. *Physiological Reviews* 82, 291–329. <https://doi.org/10.1152/physrev.00028.2001>
- Bönnemann, C.G., Modi, R., Noguchi, S., Mizuno, Y., Yoshida, M., Gussoni, E., McNally, E.M., Duggan, D.J., Angelini, C., Hoffman, E.P., Ozawa, E., Kunkel, L.M., 1995.  $\beta$ -sarcoglycan (A3b) mutations cause autosomal recessive muscular dystrophy with loss of the sarcoglycan complex. *Nat Genet* 11, 266–273. <https://doi.org/10.1038/ng1195-266>
- Bönnemann, C., 1996. Genomic screening for beta-sarcoglycan gene mutations: missense mutations may cause severe limb-girdle muscular dystrophy type 2E (LGMD 2E). *Human Molecular Genetics* 5, 1953–1961. <https://doi.org/10.1093/hmg/5.12.1953>

- Bowe, M.A., Deyst, K.A., Leszyk, J.D., Fallon, J.R., 1994. Identification and purification of an agrin receptor from torpedo postsynaptic membranes: A heteromeric complex related to the dystroglycans. *Neuron* 12, 1173–1180. [https://doi.org/10.1016/0896-6273\(94\)90324-7](https://doi.org/10.1016/0896-6273(94)90324-7)
- Boyce, F.M., Beggs, A.H., Feener, C., Kunkel, L.M., 1991. Dystrophin is transcribed in brain from a distant upstream promoter. *Proceedings of the National Academy of Sciences* 88, 1276–1280. <https://doi.org/10.1073/pnas.88.4.1276>
- Brancaccio, A., Schulthess, T., Gesemann, M., Engel, J., 1997. The N-terminal Region of alpha-Dystroglycan is an Autonomous Globular Domain. *Eur J Biochem* 246, 166–172. <https://doi.org/10.1111/j.1432-1033.1997.00166.x>
- Brenman, J.E., Chao, D.S., Gee, S.H., McGee, A.W., Craven, S.E., Santillano, D.R., Wu, Z., Huang, F., Xia, H., Peters, M.F., Froehner, S.C., Brecht, D.S., 1996. Interaction of Nitric Oxide Synthase with the Postsynaptic Density Protein PSD-95 and  $\alpha$ 1-Syntrophin Mediated by PDZ Domains. *Cell* 84, 757–767. [https://doi.org/10.1016/S0092-8674\(00\)81053-3](https://doi.org/10.1016/S0092-8674(00)81053-3)
- Brenner, S., 1974. The genetics of *Caenorhabditis elegans*. *Genetics* 77, 71–94.
- Brouilly, N., Lecroisey, C., Martin, E., Pierson, L., Mariol, M.-C., Qadota, H., Labouesse, M., Streichenberger, N., Mounier, N., Gieseler, K., 2015. Ultra-structural time-course study in the *C. elegans* model for Duchenne muscular dystrophy highlights a crucial role for sarcomere-anchoring structures and sarcolemma integrity in the earliest steps of the muscle degeneration process. *Hum. Mol. Genet.* 24, 6428–6445. <https://doi.org/10.1093/hmg/ddv353>
- Cao, J., Packer, J.S., Ramani, V., Cusanovich, D.A., Huynh, C., Daza, R., Qiu, X., Lee, C., Furlan, S.N., Steemers, F.J., Adey, A., Waterston, R.H., Trapnell, C., Shendure, J., 2017. Comprehensive single-cell transcriptional profiling of a multicellular organism. *Science* 357, 661–667. <https://doi.org/10.1126/science.aam8940>
- Carr, C., Fischbach, G.D., Cohen, J.B., 1989. A novel 87,000-Mr protein associated with acetylcholine receptors in Torpedo electric organ and vertebrate skeletal muscle. *The Journal of Cell Biology* 109, 1753–1764. <https://doi.org/10.1083/jcb.109.4.1753>
- Carre-Pierrat, M., Grisoni, K., Gieseler, K., Mariol, M.-C., Martin, E., Jospin, M., Allard, B., Ségalat, L., 2006. The SLO-1 BK Channel of *Caenorhabditis elegans* is Critical for Muscle Function and is Involved in Dystrophin-dependent Muscle Dystrophy. *Journal of Molecular Biology* 358, 387–395. <https://doi.org/10.1016/j.jmb.2006.02.037>
- Chamberlain, J.S., 2000. Muscular Dystrophy Meets the Gene Chip. *The Journal of Cell Biology* 151, F43–F46. <https://doi.org/10.1083/jcb.151.6.F43>
- Chan, Y., Bönnemann, C.G., Lidov, H.G.W., Kunkel, L.M., 1998. Molecular Organization of Sarcoglycan Complex in Mouse Myotubes in Culture. *Journal of Cell Biology* 143, 2033–2044. <https://doi.org/10.1083/jcb.143.7.2033>
- Chatelain, F.C., Bichet, D., Douguet, D., Feliciangeli, S., Bendahhou, S., Reichold, M., Warth, R., Barhanin, J., Lesage, F., 2012. TWIK1, a unique background channel with variable ion selectivity. *Proceedings of the National Academy of Sciences* 109, 5499–5504. <https://doi.org/10.1073/pnas.1201132109>
- Chen, J., Shi, W., Zhang, Y., Sokol, R., Cai, H., Lun, M., Moore, B.F., Farber, M.J., Stepanchick, J.S., Bönnemann, C.G., Chan, Y.M., 2006. Identification of functional domains in sarcoglycans essential for their interaction and plasma membrane targeting. *Experimental Cell Research* 312, 1610–1625. <https://doi.org/10.1016/j.yexcr.2006.01.024>
- Chen, B., Ge, Q., Xia, X.-M., Liu, P., Wang, S.J., Zhan, H., Eipper, B.A., Wang, Z.-W., 2010. A Novel Auxiliary Subunit Critical to BK Channel Function in *Caenorhabditis elegans*. *Journal of Neuroscience* 30, 16651–16661. <https://doi.org/10.1523/JNEUROSCI.3211-10.2010>

- Chen, B., Liu, P., Zhan, H., Wang, Z.-W., 2011. Dystrobrevin Controls Neurotransmitter Release and Muscle Ca<sup>2+</sup> Transients by Localizing BK Channels in *Caenorhabditis elegans*. *Journal of Neuroscience* 31, 17338–17347. <https://doi.org/10.1523/JNEUROSCI.3638-11.2011>
- Chung, W., Campanelli, J.T., 1999. WW and EF Hand Domains of Dystrophin-Family Proteins Mediate Dystroglycan Binding. *Molecular Cell Biology Research Communications* 2, 162–171. <https://doi.org/10.1006/mcbr.1999.0168>
- Connors, N.C., Kofuji, P., 2002. Dystrophin Dp71 Is Critical for the Clustered Localization of Potassium Channels in Retinal Glial Cells. *J. Neurosci.* 22, 4321–4327. <https://doi.org/10.1523/JNEUROSCI.22-11-04321.2002>
- Connors, N.C., Adams, M.E., Froehner, S.C., Kofuji, P., 2004. The Potassium Channel Kir4.1 Associates with the Dystrophin-Glycoprotein Complex via  $\alpha$ -Syntrophin in Glia. *J. Biol. Chem.* 279, 28387–28392. <https://doi.org/10.1074/jbc.M402604200>
- Cox, E.A., 2004. Sticky worms: adhesion complexes in *C. elegans*. *Journal of Cell Science* 117, 1885–1897. <https://doi.org/10.1242/jcs.01176>
- Cravo, J., van den Heuvel, S., 2020. Tissue polarity and PCP protein function: *C. elegans* as an emerging model. *Current Opinion in Cell Biology* 62, 159–167. <https://doi.org/10.1016/j.ceb.2019.11.004>
- Crosbie, R.H., Lebakken, C.S., Holt, K.H., Venzke, D.P., Straub, V., Lee, J.C., Grady, R.M., Chamberlain, J.S., Sanes, J.R., Campbell, K.P., 1999. Membrane Targeting and Stabilization of Sarcospan Is Mediated by the Sarcoglycan Subcomplex. *Journal of Cell Biology* 145, 153–165. <https://doi.org/10.1083/jcb.145.1.153>
- Davies, A.G., Pierce-Shimomura, J.T., Kim, H., VanHoven, M.K., Thiele, T.R., Bonci, A., Bargmann, C.I., McIntire, S.L., 2003. A Central Role of the BK Potassium Channel in Behavioral Responses to Ethanol in *C. elegans*. *Cell* 115, 655–666. [https://doi.org/10.1016/S0092-8674\(03\)00979-6](https://doi.org/10.1016/S0092-8674(03)00979-6)
- Davies, K.E., Nowak, K.J., 2006. Molecular mechanisms of muscular dystrophies: old and new players. *Nat Rev Mol Cell Biol* 7, 762–773. <https://doi.org/10.1038/nrm2024>
- Deconinck, A.E., Rafael, J.A., Skinner, J.A., Brown, S.C., Potter, A.C., Metzinger, L., Watt, D.J., Dickson, J.G., Tinsley, J.M., Davies, K.E., 1997. Utrophin-Dystrophin-Deficient Mice as a Model for Duchenne Muscular Dystrophy. *Cell* 90, 717–727. [https://doi.org/10.1016/S0092-8674\(00\)80532-2](https://doi.org/10.1016/S0092-8674(00)80532-2)
- de la Cruz, I.P., Levin, J.Z., Cummins, C., Anderson, P., Horvitz, H.R., 2003. *sup-9*, *sup-10*, and *unc-93* May Encode Components of a Two-Pore K<sup>+</sup> Channel that Coordinates Muscle Contraction in *Caenorhabditis elegans*. *J. Neurosci.* 23, 9133–9145. <https://doi.org/10.1523/JNEUROSCI.23-27-09133.2003>
- Dey, D., Eckle, V.-S., Vitko, I., Sullivan, K.A., Lasiacka, Z.M., Winckler, B., Stornetta, R.L., Williamson, J.M., Kapur, J., Perez-Reyes, E., 2014. A potassium leak channel silences hyperactive neurons and ameliorates status epilepticus. *Epilepsia* 55, 203–213. <https://doi.org/10.1111/epi.12472>
- Dixon, S.J., 2005. Muscle arm development in *Caenorhabditis elegans*. *Development* 132, 3079–3092. <https://doi.org/10.1242/dev.01883>
- Djillani, A., Mazella, J., Heurteaux, C., Borsotto, M., 2019. Role of TREK-1 in Health and Disease, Focus on the Central Nervous System. *Front. Pharmacol.* 10, 379. <https://doi.org/10.3389/fphar.2019.00379>
- Duclos, F., Straub, V., Moore, S.A., Venzke, D.P., Hrstka, R.F., Crosbie, R.H., Durbeeej, M., Lebakken, C.S., Ettinger, A.J., van der Meulen, J., Holt, K.H., Lim, L.E., Sanes, J.R., Davidson, B.L., Faulkner, J.A., Williamson, R., Campbell, K.P., 1998. Progressive Muscular Dystrophy in  $\alpha$ -Sarcoglycan-deficient Mice. *Journal of Cell Biology* 142, 1461–1471. <https://doi.org/10.1083/jcb.142.6.1461>

- Durbeej, M., Henry, M.D., Campbell, K.P., 1998. Dystroglycan in development and disease. *Current Opinion in Cell Biology* 10, 594–601. [https://doi.org/10.1016/S0955-0674\(98\)80034-3](https://doi.org/10.1016/S0955-0674(98)80034-3)
- Duprat, F., 1997. TASK, a human background K<sup>+</sup> channel to sense external pH variations near physiological pH. *The EMBO Journal* 16, 5464–5471. <https://doi.org/10.1093/emboj/16.17.5464>
- Emery, A.E.H., 1991. Population frequencies of inherited neuromuscular diseases—A world survey. *Neuromuscular Disorders* 1, 19–29. [https://doi.org/10.1016/0960-8966\(91\)90039-U](https://doi.org/10.1016/0960-8966(91)90039-U)
- Ettinger, A.J., Feng, G., Sanes, J.R., 1997. ε-Sarcoglycan, a Broadly Expressed Homologue of the Gene Mutated in Limb-Girdle Muscular Dystrophy 2D. *J. Biol. Chem.* 272, 32534–32538. <https://doi.org/10.1074/jbc.272.51.32534>
- Ervasti, J.M., Ohlendieck, K., Kahl, S.D., Gaver, M.G., Campbell, K.P., 1990. Deficiency of a glycoprotein component of the dystrophin complex in dystrophic muscle. *Nature* 345, 315–319. <https://doi.org/10.1038/345315a0>
- Ervasti, J.M., Campbell, K.P., 1991. Membrane organization of the dystrophin-glycoprotein complex. *Cell* 66, 1121–1131. [https://doi.org/10.1016/0092-8674\(91\)90035-W](https://doi.org/10.1016/0092-8674(91)90035-W)
- Ervasti, J., Campbell, K., 1993. A role for the dystrophin-glycoprotein complex as a transmembrane linker between laminin and actin. *The Journal of Cell Biology* 122, 809–823. <https://doi.org/10.1083/jcb.122.4.809>
- Ervasti, J.M., 2007. Dystrophin, its interactions with other proteins, and implications for muscular dystrophy. *Biochimica et Biophysica Acta (BBA) - Molecular Basis of Disease* 1772, 108–117. <https://doi.org/10.1016/j.bbadis.2006.05.010>
- Francis, G.R., Waterston, R.H., 1985. Muscle organization in *Caenorhabditis elegans*: localization of proteins implicated in thin filament attachment and I-band organization. *The Journal of Cell Biology* 101, 1532–1549. <https://doi.org/10.1083/jcb.101.4.1532>
- Gally, C., Eimer, S., Richmond, J.E., Bessereau, J.-L., 2004. A transmembrane protein required for acetylcholine receptor clustering in *Caenorhabditis elegans*. *Nature* 431, 578–582. <https://doi.org/10.1038/nature02893>
- Gavillet, B., Rougier, J.-S., Domenighetti, A.A., Behar, R., Boixel, C., Ruchat, P., Lehr, H.-A., Pedrazzini, T., Abriel, H., 2006. Cardiac Sodium Channel Na<sub>v</sub>1.5 Is Regulated by a Multiprotein Complex Composed of Syntrophins and Dystrophin. *Circulation Research* 99, 407–414. <https://doi.org/10.1161/01.RES.0000237466.13252.5e>
- Gee, S.H., Blacher, R.W., Douville, P.J., Provost, P.R., Yurchenco, P.D., Carbonetto, S., 1993. Laminin-binding protein 120 from brain is closely related to the dystrophin-associated glycoprotein, dystroglycan, and binds with high affinity to the major heparin binding domain of laminin. *J. Biol. Chem.* 268, 14972–14980.
- Gee, S.H., Madhavan, R., Levinson, S.R., Caldwell, J.H., Sealock, R., Froehner, S.C., 1998. Interaction of Muscle and Brain Sodium Channels with Multiple Members of the Syntrophin Family of Dystrophin-Associated Proteins. *J. Neurosci.* 18, 128–137. <https://doi.org/10.1523/JNEUROSCI.18-01-00128.1998>
- Gieseler, K., Bessou, C., Ségalat, L., 1999a. Dystrobrevin- and dystrophin-like mutants display similar phenotypes in the nematode *Caenorhabditis elegans*. *neurogenetics* 2, 87–90. <https://doi.org/10.1007/s100480050057>
- Gieseler, K., Abdel-Dayem, M., Ségalat, L., 1999b. In vitro interactions of *Caenorhabditis elegans* dystrophin with dystrobrevin and syntrophin. *FEBS Letters* 461, 59–62. [https://doi.org/10.1016/S0014-5793\(99\)01421-0](https://doi.org/10.1016/S0014-5793(99)01421-0)
- Gieseler, K., Grisoni, K., Ségalat, L., 2000. Genetic suppression of phenotypes arising from mutations in dystrophin-related genes in *Caenorhabditis elegans*. *Current Biology* 10, 1092–1097. [https://doi.org/10.1016/S0960-9822\(00\)00691-6](https://doi.org/10.1016/S0960-9822(00)00691-6)



- Gieseler, K., Mariol, M.C., Bessou, C., Migaud, M., Franks, C.J., Holden-Dye, L., Ségalat, L., 2001. Molecular, genetic and physiological characterisation of dystrobrevin-like (*dyb-1*) mutants of *Caenorhabditis elegans*. *J. Mol. Biol.* 307, 107–117. <https://doi.org/10.1006/jmbi.2000.4480>
- Gieseler, K., 2017. Development, structure, and maintenance of *C. elegans* body wall muscle. *WormBook* 1–59. <https://doi.org/10.1895/wormbook.1.81.2>
- Girard, C., 2002. p11, an annexin II subunit, an auxiliary protein associated with the background K<sup>+</sup> channel, TASK-1. *The EMBO Journal* 21, 4439–4448. <https://doi.org/10.1093/emboj/cdf469>
- Grady, R.M., Merlie, J.P., Sanes, J.R., 1997. Subtle Neuromuscular Defects in Utrophin-deficient Mice. *Journal of Cell Biology* 136, 871–882. <https://doi.org/10.1083/jcb.136.4.871>
- Grisoni, K., Gieseler, K., Ségalat, L., 2002a. Dystrobrevin requires a dystrophin-binding domain to function in *Caenorhabditis elegans*: Dystrophin-dystrobrevin interactions in *C. elegans*. *European Journal of Biochemistry* 269, 1607–1612. <https://doi.org/10.1046/j.1432-1327.2002.02780.x>
- Grisoni, K., Martin, E., Gieseler, K., Mariol, M.-C., Ségalat, L., 2002b. Genetic evidence for a dystrophin-glycoprotein complex (DGC) in *Caenorhabditis elegans*. *Gene* 294, 77–86. [https://doi.org/10.1016/S0378-1119\(02\)00762-X](https://doi.org/10.1016/S0378-1119(02)00762-X)
- Grisoni, K., Gieseler, K., Mariol, M.-C., Martin, E., Carre-Pierrat, M., Moulder, G., Barstead, R., Ségalat, L., 2003. The *stn-1* Syntrophin Gene of *C.elegans* is Functionally Related to Dystrophin and Dystrobrevin. *Journal of Molecular Biology* 332, 1037–1046. <https://doi.org/10.1016/j.jmb.2003.08.021>
- Grum, V.L., Li, D., MacDonald, R.I., Mondragón, A., 1999. Structures of Two Repeats of Spectrin Suggest Models of Flexibility. *Cell* 98, 523–535. [https://doi.org/10.1016/S0092-8674\(00\)81980-7](https://doi.org/10.1016/S0092-8674(00)81980-7)
- Górecki, D.C., Monaco, A.P., Derry, J.M.J., Walker, A.P., Barnard, E.A., Barnard, P.J., 1992. Expression of four alternative dystrophin transcripts in brain regions regulated by different promoters. *Hum Mol Genet* 1, 505–510. <https://doi.org/10.1093/hmg/1.7.505>
- Hack, A.A., Groh, M.E., McNally, E.M., 2000. Sarcoglycans in muscular dystrophy. *Microsc. Res. Tech.* 48, 167–180. [https://doi.org/10.1002/\(SICI\)1097-0029\(20000201/15\)48:3/4<167::AID-JEMT5>3.0.CO;2-T](https://doi.org/10.1002/(SICI)1097-0029(20000201/15)48:3/4<167::AID-JEMT5>3.0.CO;2-T)
- Hack, A.A., Lam, M.Y., Cordier, L., Shoturma, D.I., Ly, C.T., Hadhazy, M.A., Hadhazy, M.R., Sweeney, H.L., McNally, E.M., 2000. Differential requirement for individual sarcoglycans and dystrophin in the assembly and function of the dystrophin-glycoprotein complex. *J. Cell. Sci.* 113 (Pt 14), 2535–2544.
- Hall, D.H., Hedgecock, E.M., 1991. Kinesin-related gene *unc-104* is required for axonal transport of synaptic vesicles in *C. elegans*. *Cell* 65, 837–847. [https://doi.org/10.1016/0092-8674\(91\)90391-B](https://doi.org/10.1016/0092-8674(91)90391-B)
- Han, B., Bellemer, A., Koelle, M.R., 2015. An Evolutionarily Conserved Switch in Response to GABA Affects Development and Behavior of the Locomotor Circuit of *Caenorhabditis elegans*. *Genetics* 199, 1159–1172. <https://doi.org/10.1534/genetics.114.173963>
- Hedgecock, E.M., Culotti, J.G., Hall, D.H., 1990. The *unc-5*, *unc-6*, and *unc-40* genes guide circumferential migrations of pioneer axons and mesodermal cells on the epidermis in *C. elegans*. *Neuron* 4, 61–85. [https://doi.org/10.1016/0896-6273\(90\)90444-K](https://doi.org/10.1016/0896-6273(90)90444-K)
- Hemmings, L., Kuhlman, P.A., Critchley, D.R., 1992. Analysis of the actin-binding domain of alpha-actinin by mutagenesis and demonstration that dystrophin contains a functionally homologous domain. *The Journal of Cell Biology* 116, 1369–1380. <https://doi.org/10.1083/jcb.116.6.1369>
- Hervieu, G.J., Cluderay, J.E., Gray, C.W., Green, P.J., Ranson, J.L., Randall, A.D., Meadows, H.J., 2001. Distribution and expression of TREK-1, a two-pore-domain potassium channel, in the adult rat CNS. *Neuroscience* 103, 899–919. [https://doi.org/10.1016/s0306-4522\(01\)00030-6](https://doi.org/10.1016/s0306-4522(01)00030-6)



- Heurteaux, C., Guy, N., Laigle, C., Blondeau, N., Duprat, F., Mazzuca, M., Lang-Lazdunski, L., Widmann, C., Zanzouri, M., Romey, G., Lazdunski, M., 2004. TREK-1, a K<sup>+</sup> channel involved in neuroprotection and general anesthesia. *EMBO J.* 23, 2684–2695. <https://doi.org/10.1038/sj.emboj.7600234>
- Heurteaux, C., Lucas, G., Guy, N., El Yacoubi, M., Thümmler, S., Peng, X.-D., Noble, F., Blondeau, N., Widmann, C., Borsotto, M., Gobbi, G., Vaugeois, J.-M., Debonnel, G., Lazdunski, M., 2006. Deletion of the background potassium channel TREK-1 results in a depression-resistant phenotype. *Nat. Neurosci.* 9, 1134–1141. <https://doi.org/10.1038/nn1749>
- Hibino, H., Fujita, A., Iwai, K., Yamada, M., Kurachi, Y., 2004. Differential Assembly of Inwardly Rectifying K<sup>+</sup> Channel Subunits, Kir4.1 and Kir5.1, in Brain Astrocytes. *J. Biol. Chem.* 279, 44065–44073. <https://doi.org/10.1074/jbc.M405985200>
- Hnia, K., Zouiten, D., Cantel, S., Chazalotte, D., Hugon, G., Fehrentz, J.-A., Masmoudi, A., Diment, A., Bramham, J., Mornet, D., Winder, S.J., 2007. ZZ domain of dystrophin and utrophin: topology and mapping of a  $\beta$ -dystroglycan interaction site. *Biochemical Journal* 401, 667–677. <https://doi.org/10.1042/BJ20061051>
- Hoffman, E.P., Brown, R.H., Kunkel, L.M., 1987. Dystrophin: The protein product of the duchenne muscular dystrophy locus. *Cell* 51, 919–928. [https://doi.org/10.1016/0092-8674\(87\)90579-4](https://doi.org/10.1016/0092-8674(87)90579-4)
- Hoffman, E.P., Fischbeck, K.H., Brown, R.H., Johnson, M., Medori, R., Loire, J.D., Harris, J.B., Waterston, R., Brooke, M., Specht, L., Kupsky, W., Chamberlain, J., Caskey, C.T., Shapiro, F., Kunkel, L.M., 1988. Characterization of Dystrophin in Muscle-Biopsy Specimens from Patients with Duchenne's or Becker's Muscular Dystrophy. *N Engl J Med* 318, 1363–1368. <https://doi.org/10.1056/NEJM198805263182104>
- Hoffman, E.P., Kunkel, L.M., Angelini, C., Clarke, A., Johnson, M., Harris, J.B., 1989. Improved diagnosis of Becker muscular dystrophy by dystrophin testing. *Neurology* 39, 1011–1017. <https://doi.org/10.1212/wnl.39.8.1011>
- Holt, K.H., Campbell, K.P., 1998. Assembly of the Sarcoglycan Complex: INSIGHTS FOR MUSCULAR DYSTROPHY. *J. Biol. Chem.* 273, 34667–34670. <https://doi.org/10.1074/jbc.273.52.34667>
- Honoré, E., 2007. The neuronal background K<sub>2</sub>P channels: focus on TREK1. *Nat Rev Neurosci* 8, 251–261. <https://doi.org/10.1038/nrn2117>
- Horio, Y., Hibino, H., Inanobe, A., Yamada, M., Ishii, M., Tada, Y., Satoh, E., Hata, Y., Takai, Y., Kurachi, Y., 1997. Clustering and Enhanced Activity of an Inwardly Rectifying Potassium Channel, Kir4.1, by an Anchoring Protein, PSD-95/SAP90. *J. Biol. Chem.* 272, 12885–12888. <https://doi.org/10.1074/jbc.272.20.12885>
- Huang, X., Poy, F., Zhang, R., Joachimiak, A., Sudol, M., Eck, M.J., 2000. [No title found]. *Nat. Struct Biol.* 7, 634–638. <https://doi.org/10.1038/77923>
- Hund, T.J., Snyder, J.S., Wu, X., Glynn, P., Koval, O.M., Onal, B., Leymaster, N.D., Unudurthi, S.D., Curran, J., Camardo, C., Wright, P.J., Binkley, P.F., Anderson, M.E., Mohler, P.J., 2014.  $\beta$ IV-Spectrin regulates TREK-1 membrane targeting in the heart. *Cardiovascular Research* 102, 166–175. <https://doi.org/10.1093/cvr/cvu008>
- Ibraghimov-Beskrovnaia, O., Ervasti, J.M., Leveille, C.J., Slaughter, C.A., Sernett, S.W., Campbell, K.P., 1992. Primary structure of dystrophin-associated glycoproteins linking dystrophin to the extracellular matrix. *Nature* 355, 696–702. <https://doi.org/10.1038/355696a0>
- Ishikawa-Sakurai, M., 2004. ZZ domain is essentially required for the physiological binding of dystrophin and utrophin to  $\beta$ -dystroglycan. *Human Molecular Genetics* 13, 693–702. <https://doi.org/10.1093/hmg/ddh087>

- Johnson, R.P., 2006. C. elegans dystroglycan DGN-1 functions in epithelia and neurons, but not muscle, and independently of dystrophin. *Development* 133, 1911–1921. <https://doi.org/10.1242/dev.02363>
- Johnson, R.P., Kramer, J.M., 2012. Neural Maintenance Roles for the Matrix Receptor Dystroglycan and the Nuclear Anchorage Complex in *Caenorhabditis elegans*. *Genetics* 190, 1365–1377. <https://doi.org/10.1534/genetics.111.136184>
- Julio-Kalajzić, F., Villanueva, S., Burgos, J., Ojeda, M., Cid, L.P., Jentsch, T.J., Sepúlveda, F.V., 2018. K<sub>2P</sub> TASK-2 and KCNQ1-KCNE3 K<sup>+</sup> channels are major players contributing to intestinal anion and fluid secretion: TASK-2 and KCNQ1-KCNE3 K<sup>+</sup> channels in intestinal anion secretion. *J Physiol* 596, 393–407. <https://doi.org/10.1113/JP275178>
- Khirani, S., Ramirez, A., Aubertin, G., Boulé, M., Chemouny, C., Forin, V., Fauroux, B., 2014. Respiratory muscle decline in duchenne muscular dystrophy: Respiratory Function in DMD. *Pediatr Pulmonol.* 49, 473–481. <https://doi.org/10.1002/ppul.22847>
- Kim, H., Pierce-Shimomura, J.T., Oh, H.J., Johnson, B.E., Goodman, M.B., McIntire, S.L., 2009. The Dystrophin Complex Controls BK Channel Localization and Muscle Activity in *Caenorhabditis elegans*. *PLoS Genet* 5, e1000780. <https://doi.org/10.1371/journal.pgen.1000780>
- Klamut, H.J., Gangopadhyay, S.B., Worton, R.G., Ray, P.N., 1990. Molecular and functional analysis of the muscle-specific promoter region of the Duchenne muscular dystrophy gene. *Mol. Cell. Biol.* 10, 193–205. <https://doi.org/10.1128/MCB.10.1.193>
- Koenig, M., Hoffman, E.P., Bertelson, C.J., Monaco, A.P., Feener, C., Kunkel, L.M., 1987. Complete cloning of the Duchenne muscular dystrophy (DMD) cDNA and preliminary genomic organization of the DMD gene in normal and affected individuals. *Cell* 50, 509–517. [https://doi.org/10.1016/0092-8674\(87\)90504-6](https://doi.org/10.1016/0092-8674(87)90504-6)
- Koenig, M., Monaco, A.P., Kunkel, L.M., 1988. The complete sequence of dystrophin predicts a rod-shaped cytoskeletal protein. *Cell* 53, 219–228. [https://doi.org/10.1016/0092-8674\(88\)90383-2](https://doi.org/10.1016/0092-8674(88)90383-2)
- Koenig, M., Kunkel, L.M., 1990. Detailed analysis of the repeat domain of dystrophin reveals four potential hinge segments that may confer flexibility. *J. Biol. Chem.* 265, 4560–4566.
- Kunkel, Maya T., Johnstone, D.B., Thomas, J.H., Salkoff, L., 2000. Mutants of a Temperature-Sensitive Two-P Domain Potassium Channel. *J. Neurosci.* 20, 7517–7524. <https://doi.org/10.1523/JNEUROSCI.20-20-07517.2000>
- Lapidos, K.A., Chen, Y.E., Earley, J.U., Heydemann, A., Huber, J.M., Chien, M., Ma, A., McNally, E.M., 2004. Transplanted hematopoietic stem cells demonstrate impaired sarcoglycan expression after engraftment into cardiac and skeletal muscle. *J. Clin. Invest.* 114, 1577–1585. <https://doi.org/10.1172/JCI200423071>
- Lazarenko, R.M., Willcox, S.C., Shu, S., Berg, A.P., Jevtovic-Todorovic, V., Talley, E.M., Chen, X., Bayliss, D.A., 2010. Motoneuronal TASK Channels Contribute to Immobilizing Effects of Inhalational General Anesthetics. *Journal of Neuroscience* 30, 7691–7704. <https://doi.org/10.1523/JNEUROSCI.1655-10.2010>
- Lesage, F., Guillemare, E., Fink, M., Duprat, F., Lazdunski, M., Romey, G., Barhanin, J., 1996. TWIK-1, a ubiquitous human weakly inward rectifying K<sup>+</sup> channel with a novel structure. *EMBO J.* 15, 1004–1011.
- Lesage, F., Lazdunski, M., 2000. Molecular and functional properties of two-pore-domain potassium channels. *Am. J. Physiol. Renal Physiol.* 279, F793–801. <https://doi.org/10.1152/ajprenal.2000.279.5.F793>
- Leyva-Leyva, M., Sandoval, A., Felix, R., González-Ramírez, R., 2018. Biochemical and Functional Interplay Between Ion Channels and the Components of the Dystrophin-Associated Glycoprotein Complex. *J Membrane Biol* 251, 535–550. <https://doi.org/10.1007/s00232-018-0036-9>

- Li, D., Long, C., Yue, Y., Duan, D., 2009. Sub-physiological sarcoglycan expression contributes to compensatory muscle protection in mdx mice. *Human Molecular Genetics* 18, 1209–1220. <https://doi.org/10.1093/hmg/ddp015>
- Lou, Q., Hansen, B.J., Fedorenko, O., Csepe, T.A., Kalyanasundaram, A., Li, N., Hage, L.T., Glukhov, A.V., Billman, G.E., Weiss, R., Mohler, P.J., Györke, S., Biesiadecki, B.J., Carnes, C.A., Fedorov, V.V., 2014. Upregulation of Adenosine A1 Receptors Facilitates Sinoatrial Node Dysfunction in Chronic Canine Heart Failure by Exacerbating Nodal Conduction Abnormalities Revealed by Novel Dual-Sided Intramural Optical Mapping. *Circulation* 130, 315–324. <https://doi.org/10.1161/CIRCULATIONAHA.113.007086>
- Mackinnon, A.C., Qadota, H., Norman, K.R., Moerman, D.G., Williams, B.D., 2002. C. elegans PAT-4/ILK Functions as an Adaptor Protein within Integrin Adhesion Complexes. *Current Biology* 12, 787–797. [https://doi.org/10.1016/S0960-9822\(02\)00810-2](https://doi.org/10.1016/S0960-9822(02)00810-2)
- Maingret, F., Lauritzen, I., Patel, A.J., Heurteaux, C., Reyes, R., Lesage, F., Lazdunski, M., Honoré, E., 2000. TREK-1 is a heat-activated background K(+) channel. *EMBO J.* 19, 2483–2491. <https://doi.org/10.1093/emboj/19.11.2483>
- Mathie, A., A. Rees, K., F. El Hachmane, M., L. Veale, E., 2010. Trafficking of Neuronal Two Pore Domain Potassium Channels. *CN* 8, 276–286. <https://doi.org/10.2174/157015910792246146>
- McClatchey, S.T., Wang, Z., Linden, L.M., Hastie, E.L., Wang, L., Shen, W., Chen, A., Chi, Q., Sherwood, D.R., 2016. Boundary cells restrict dystroglycan trafficking to control basement membrane sliding during tissue remodeling. *eLife* 5, e17218. <https://doi.org/10.7554/eLife.17218>
- McNally, E., 1996. Mutations that disrupt the carboxyl-terminus of gamma-sarcoglycan cause muscular dystrophy. *Human Molecular Genetics* 5, 1841–1847. <https://doi.org/10.1093/hmg/5.11.1841>
- Megeney, L.A., Kablar, B., Garrett, K., Anderson, J.E., Rudnicki, M.A., 1996. MyoD is required for myogenic stem cell function in adult skeletal muscle. *Genes & Development* 10, 1173–1183. <https://doi.org/10.1101/gad.10.10.1173>
- Millar, J.A., Barratt, L., Southan, A.P., Page, K.M., Fyffe, R.E.W., Robertson, B., Mathie, A., 2000. A functional role for the two-pore domain potassium channel TASK-1 in cerebellar granule neurons. *Proceedings of the National Academy of Sciences* 97, 3614–3618. <https://doi.org/10.1073/pnas.97.7.3614>
- Mlodzik, M., 2016. The Dishevelled Protein Family, in: *Current Topics in Developmental Biology*. Elsevier, pp. 75–91. <https://doi.org/10.1016/bs.ctdb.2015.11.027>
- Moerman, D., 2006. Sarcomere assembly in C. elegans muscle. *WormBook*. <https://doi.org/10.1895/wormbook.1.81.1>
- Monaco, A.P., Neve, R.L., Colletti-Feener, C., Bertelson, C.J., Kurnit, D.M., Kunkel, L.M., 1986. Isolation of candidate cDNAs for portions of the Duchenne muscular dystrophy gene. *Nature* 323, 646–650. <https://doi.org/10.1038/323646a0>
- Montanaro, F., Carbonetto, S., Campbell, K.P., Lindenbaum, M., 1995. Dystroglycan expression in the wild type and mdx mouse neural retina: Synaptic colocalization with dystrophin, dystrophin-related protein but not laminin. *J. Neurosci. Res.* 42, 528–538. <https://doi.org/10.1002/jnr.490420411>
- Montanaro, F., Lindenbaum, M., Carbonetto, S., 1999.  $\alpha$ -Dystroglycan Is a Laminin Receptor Involved in Extracellular Matrix Assembly on Myotubes and Muscle Cell Viability. *Journal of Cell Biology* 145, 1325–1340. <https://doi.org/10.1083/jcb.145.6.1325>
- El Mouridi, S., Lecroisey, C., Tardy, P., Mercier, M., Leclercq-Blondel, A., Zariohi, N., Boulin, T., 2017. Reliable CRISPR/Cas9 Genome Engineering in *Caenorhabditis elegans* Using a Single Efficient sgRNA and an Easily Recognizable Phenotype. *G3* 7, 1429–1437. <https://doi.org/10.1534/g3.117.040824>

- Newey, Sarah E., Benson, M.A., Ponting, C.P., Davies, K.E., Blake, D.J., 2000. Alternative splicing of dystrobrevin regulates the stoichiometry of syntrophin binding to the dystrophin protein complex. *Current Biology* 10, 1295–1298. [https://doi.org/10.1016/S0960-9822\(00\)00760-0](https://doi.org/10.1016/S0960-9822(00)00760-0)
- Nigro, V., 1996a. Identification of a novel sarcoglycan gene at 5q33 encoding a sarcolemmal 35 kDa glycoprotein. *Human Molecular Genetics* 5, 1179–1186. <https://doi.org/10.1093/hmg/5.8.1179>
- Nigro, V., Moreira, E. de S., Piluso, G., Vainzof, M., Belsito, A., Politano, L., Puca, A.A., Passos-Bueno, M.R., Zatz, M., 1996b. Autosomal recessive limb-girdle muscular dystrophy, LGMD2F, is caused by a mutation in the  $\delta$ -sarcoglycan gene. *Nat Genet* 14, 195–198. <https://doi.org/10.1038/ng1096-195>
- Nilsson, Johanna, Nilsson, Jonas, Larson, G., Grahn, A., 2010. Characterization of site-specific O-glycan structures within the mucin-like domain of  $\alpha$ -dystroglycan from human skeletal muscle. *Glycobiology* 20, 1160–1169. <https://doi.org/10.1093/glycob/cwq082>
- Noguchi, S., McNally, E.M., Othmane, K.B., Hagiwara, Y., Mizuno, Y., Yoshida, M., Yamamoto, H., B n nemann, C.G., Gussoni, E., Denton, P.H., Kyriakides, T., Middleton, L., Hentati, F., Hamida, M.B., Nonaka, I., Vance, J.M., Kunkel, L.M., Ozawa, E., 1995. Mutations in the Dystrophin-Associated Protein [IMAGE]-Sarcoglycan in Chromosome 13 Muscular Dystrophy. *Science* 270, 819–822. <https://doi.org/10.1126/science.270.5237.819>
- Noguchi, S., Wakabayashi, E., Imamura, M., Yoshida, M., Ozawa, E., 2000. Formation of sarcoglycan complex with differentiation in cultured myocytes: Sarcoglycan complex formation process in cultured myocytes. *European Journal of Biochemistry* 267, 640–648. <https://doi.org/10.1046/j.1432-1327.2000.00998.x>
- Oh, H.J., Abraham, L.S., van Hengel, J., Stove, C., Proszynski, T.J., Gevaert, K., DiMario, J.X., Sanes, J.R., van Roy, F., Kim, H., 2012. Interaction of  $\alpha$ -Catulin with Dystrobrevin Contributes to Integrity of Dystrophin Complex in Muscle. *J. Biol. Chem.* 287, 21717–21728. <https://doi.org/10.1074/jbc.M112.369496>
- Oh, K.H., Haney, J.J., Wang, X., Chuang, C.-F., Richmond, J.E., Kim, H., 2017. ERG-28 controls BK channel trafficking in the ER to regulate synaptic function and alcohol response in *C. elegans*. *eLife* 6, e24733. <https://doi.org/10.7554/eLife.24733>
- Ono, S., 2014. Regulation of Structure and Function of Sarcomeric Actin Filaments in Striated Muscle of the Nematode *Caenorhabditis elegans*: ACTIN REGULATION IN NEMATODE MUSCLE. *Anat. Rec.* 297, 1548–1559. <https://doi.org/10.1002/ar.22965>
- Ozawa, E., Mizuno, Y., Hagiwara, Y., Sasaoka, T., Yoshida, M., 2005. Molecular and cell biology of the sarcoglycan complex. *Muscle Nerve* 32, 563–576. <https://doi.org/10.1002/mus.20349>
- Pani, A.M., Goldstein, B., 2018. Direct visualization of a native Wnt in vivo reveals that a long-range Wnt gradient forms by extracellular dispersal. *eLife* 7, e38325. <https://doi.org/10.7554/eLife.38325>
- Patel, A.J., Honoré, E., Lesage, F., Fink, M., Romey, G., Lazdunski, M., 1999. Inhalational anesthetics activate two-pore-domain background K<sup>+</sup> channels. *Nat. Neurosci.* 2, 422–426. <https://doi.org/10.1038/8084>
- Peters, M.F., Kramarcy, N.R., Sealock, R., Froehner, S.C., 1994. beta 2-Syntrophin: localization at the neuromuscular junction in skeletal muscle. *Neuroreport* 5, 1577–1580.
- Peters, M.F., Sadoulet-Puccio, H.M., Mark Grady, R., Kramarcy, N.R., Kunkel, L.M., Sanes, J.R., Sealock, R., Froehner, S.C., 1998. Differential Membrane Localization and Intermolecular Associations of  $\alpha$ -Dystrobrevin Isoforms in Skeletal Muscle. *Journal of Cell Biology* 142, 1269–1278. <https://doi.org/10.1083/jcb.142.5.1269>
- Petitprez, S., Zmoos, A.-F., Ogrodnik, J., Balse, E., Raad, N., El-Haou, S., Albesa, M., Bittihn, P., Luther, S., Lehnart, S.E., Hatem, S.N., Coulombe, A., Abriel, H., 2011. SAP97 and Dystrophin



Macromolecular Complexes Determine Two Pools of Cardiac Sodium Channels  $Na_v 1.5$  in Cardiomyocytes. *Circ Res* 108, 294–304. <https://doi.org/10.1161/CIRCRESAHA.110.228312>

- Petrof, B.J., Shrager, J.B., Stedman, H.H., Kelly, A.M., Sweeney, H.L., 1993. Dystrophin protects the sarcolemma from stresses developed during muscle contraction. *Proceedings of the National Academy of Sciences* 90, 3710–3714. <https://doi.org/10.1073/pnas.90.8.3710>
- Pinan-Lucarré, B., Tu, H., Pierron, M., Cruceyra, P.I., Zhan, H., Stigloher, C., Richmond, J.E., Bessereau, J.-L., 2014. *C. elegans* Punctin specifies cholinergic versus GABAergic identity of postsynaptic domains. *Nature* 511, 466–470. <https://doi.org/10.1038/nature13313>
- Ranade, S.S., Syeda, R., Patapoutian, A., 2015. Mechanically Activated Ion Channels. *Neuron* 87, 1162–1179. <https://doi.org/10.1016/j.neuron.2015.08.032>
- Rees, M.L.J., Lien, C.-F., Górecki, D.C., 2007. Dystrobrevins in muscle and non-muscle tissues. *Neuromuscular Disorders* 17, 123–134. <https://doi.org/10.1016/j.nmd.2006.11.003>
- Rentschler, S., Linn, H., Deininger, K., Bedford, M.T., Espanel, X., Sudol, M., 1999. The WW Domain of Dystrophin Requires EF-Hands Region to Interact with  $\beta$ -Dystroglycan. *Biological Chemistry* 380. <https://doi.org/10.1515/BC.1999.057>
- Richmond, J.E., Jorgensen, E.M., 1999. One GABA and two acetylcholine receptors function at the *C. elegans* neuromuscular junction. *Nat Neurosci* 2, 791–797. <https://doi.org/10.1038/12160>
- Roberds, S.L., Anderson, R.D., Ibraghimov-Beskrovnaya, O., Campbell, K.P., 1993. Primary structure and muscle-specific expression of the 50-kDa dystrophin-associated glycoprotein (adhalin). *J. Biol. Chem.* 268, 23739–23742.
- Roberds, S.L., Leturcq, F., Allamand, V., Piccolo, F., Jeanpierre, M., Anderson, R.D., Lim, L.E., Lee, J.C., Tomé, F.M.S., Romero, N.B., Fardeau, M., Beckmann, J.S., Kaplan, J.-C., Campbell, K.P., 1994. Missense mutations in the adhalin gene linked to autosomal recessive muscular dystrophy. *Cell* 78, 625–633. [https://doi.org/10.1016/0092-8674\(94\)90527-4](https://doi.org/10.1016/0092-8674(94)90527-4)
- Roberts, R.G., 2001. Dystrophins and dystrobrevins. *Genome Biol* 2, reviews3006.1. <https://doi.org/10.1186/gb-2001-2-4-reviews3006>
- Rougier, J.-S., Gavillet, B., Abriel, H., 2013. Proteasome inhibitor (MG132) rescues Nav1.5 protein content and the cardiac sodium current in dystrophin-deficient mdx5cv mice. *Front. Physiol.* 4. <https://doi.org/10.3389/fphys.2013.00051>
- Rybakova, I.N., Amann, K.J., Ervasti, J.M., 1996. A new model for the interaction of dystrophin with F-actin. *The Journal of Cell Biology* 135, 661–672. <https://doi.org/10.1083/jcb.135.3.661>
- Rybakova, I.N., Patel, J.R., Ervasti, J.M., 2000. The Dystrophin Complex Forms a Mechanically Strong Link between the Sarcolemma and Costameric Actin. *Journal of Cell Biology* 150, 1209–1214. <https://doi.org/10.1083/jcb.150.5.1209>
- Sadoulet-Puccio, H.M., Rajala, M., Kunkel, L.M., 1997. Dystrobrevin and dystrophin: An interaction through coiled-coil motifs. *Proceedings of the National Academy of Sciences* 94, 12413–12418. <https://doi.org/10.1073/pnas.94.23.12413>
- Sakamoto, A., Ono, K., Abe, M., Jasmin, G., Eki, T., Murakami, Y., Masaki, T., Toyooka, T., Hanaoka, F., 1997. Both hypertrophic and dilated cardiomyopathies are caused by mutation of the same gene, -sarcoglycan, in hamster: An animal model of disrupted dystrophin-associated glycoprotein complex. *Proceedings of the National Academy of Sciences* 94, 13873–13878. <https://doi.org/10.1073/pnas.94.25.13873>
- Sancar, F., Touroutine, D., Gao, S., Oh, H.J., Gendrel, M., Bessereau, J.-L., Kim, H., Zhen, M., Richmond, J.E., 2011. The Dystrophin-associated Protein Complex Maintains Muscle Excitability by Regulating  $Ca^{2+}$ -dependent  $K^+$  (BK) Channel Localization. *J. Biol. Chem.* 286, 33501–33510. <https://doi.org/10.1074/jbc.M111.227678>

- Sandonà, D., Gastaldello, S., Martinello, T., Betto, R., 2004. Characterization of the ATP-hydrolysing activity of  $\alpha$ -sarcoglycan. *Biochemical Journal* 381, 105–112. <https://doi.org/10.1042/BJ20031644>
- Sandoz, G., Tardy, M.P., Thummler, S., Feliciangeli, S., Lazdunski, M., Lesage, F., 2008. Mtap2 Is a Constituent of the Protein Network That Regulates Twik-Related K<sup>+</sup> Channel Expression and Trafficking. *Journal of Neuroscience* 28, 8545–8552. <https://doi.org/10.1523/JNEUROSCI.1962-08.2008>
- Schroeder, B.C., Waldegger, S., Fehr, S., Bleich, M., Warth, R., Greger, R., Jentsch, T.J., 2000. A constitutively open potassium channel formed by KCNQ1 and KCNE3. *Nature* 403, 196–199. <https://doi.org/10.1038/35003200>
- Sepúlveda, F.V., Pablo Cid, L., Teulon, J., Niemeyer, M.I., 2015. Molecular Aspects of Structure, Gating, and Physiology of pH-Sensitive Background K<sub>2P</sub> and Kir K<sup>+</sup>-Transport Channels. *Physiological Reviews* 95, 179–217. <https://doi.org/10.1152/physrev.00016.2014>
- Shi, W., Chen, Z., Schottenfeld, J., Stahl, R.C., Kunkel, L.M., Chan, Y.-M., 2004. Specific assembly pathway of sarcoglycans is dependent on beta- and delta-sarcoglycan. *Muscle Nerve* 29, 409–419. <https://doi.org/10.1002/mus.10566>
- Sotgia, F., Lee, H., Bedford, M.T., Petrucci, T., Sudol, M., Lisanti, M.P., 2001. Tyrosine Phosphorylation of  $\beta$ -Dystroglycan at Its WW Domain Binding Motif, PPxY, Recruits SH2 Domain Containing Proteins<sup>†</sup>. *Biochemistry* 40, 14585–14592. <https://doi.org/10.1021/bi011247r>
- Stevenson, S.A., Cullen, M.J., Rothery, S., Coppen, S.R., Severs, N.J., 2005. High-resolution en-face visualization of the cardiomyocyte plasma membrane reveals distinctive distributions of spectrin and dystrophin. *European Journal of Cell Biology* 84, 961–971. <https://doi.org/10.1016/j.ejcb.2005.09.015>
- Straub, V., Duclos, F., Venzke, D.P., Lee, J.C., Cutshall, S., Leveille, C.J., Campbell, K.P., 1998. Molecular Pathogenesis of Muscle Degeneration in the  $\delta$ -Sarcoglycan-Deficient Hamster. *The American Journal of Pathology* 153, 1623–1630. [https://doi.org/10.1016/S0002-9440\(10\)65751-3](https://doi.org/10.1016/S0002-9440(10)65751-3)
- Sulston, J.E., Horvitz, H.R., 1977. Post-embryonic cell lineages of the nematode, *Caenorhabditis elegans*. *Developmental Biology* 56, 110–156. [https://doi.org/10.1016/0012-1606\(77\)90158-0](https://doi.org/10.1016/0012-1606(77)90158-0)
- Sulston, J.E., Schierenberg, E., White, J.G., Thomson, J.N., 1983. The embryonic cell lineage of the nematode *Caenorhabditis elegans*. *Developmental Biology* 100, 64–119. [https://doi.org/10.1016/0012-1606\(83\)90201-4](https://doi.org/10.1016/0012-1606(83)90201-4)
- Suzuki, A., Yoshida, M., Ozawa, E., 1995. Mammalian alpha 1- and beta 1-syntrophin bind to the alternative splice-prone region of the dystrophin COOH terminus. *The Journal of Cell Biology* 128, 373–381. <https://doi.org/10.1083/jcb.128.3.373>
- Talts, J.F., Andac, Z., Göhring, W., Brancaccio, A., Timpl, R., 1999. Binding of the G domains of laminin  $\alpha$ 1 and  $\alpha$ 2 chains and perlecan to heparin, sulfatides,  $\alpha$ -dystroglycan and several extracellular matrix proteins. *EMBO J* 18, 863–870. <https://doi.org/10.1093/emboj/18.4.863>
- Tarakci, Berger, 2016. The sarcoglycan complex in skeletal muscle. *Front Biosci* 21, 744–756. <https://doi.org/10.2741/4418>
- Thapliyal, S., Babu, K., 2018. *C. elegans* Locomotion: Finding Balance in Imbalance, in: Chattopadhyay, K., Basu, S.C. (Eds.), *Biochemical and Biophysical Roles of Cell Surface Molecules*, *Advances in Experimental Medicine and Biology*. Springer Singapore, Singapore, pp. 185–196. [https://doi.org/10.1007/978-981-13-3065-0\\_14](https://doi.org/10.1007/978-981-13-3065-0_14)
- Trzebiatowska, A., Topf, U., Sauder, U., Drabikowski, K., Chiquet-Ehrismann, R., 2008. *Caenorhabditis elegans* Teneurin, *ten-1*, Is Required for Gonadal and Pharyngeal Basement



- Membrane Integrity and Acts Redundantly with Integrin *ina-1* and Dystroglycan *dgn-1*. *MBoC* 19, 3898–3908. <https://doi.org/10.1091/mbc.e08-01-0028>
- Vainzof, M., Moreira, E., Ferraz, G., Passos-Bueno, M., Marie, S., Zatz, M., 1999. Further evidence for the organisation of the four sarcoglycan proteins within the dystrophin–glycoprotein complex. *Eur J Hum Genet* 7, 251–254. <https://doi.org/10.1038/sj.ejhg.5200263>
- Vandebrouck, A., Sabourin, J., Rivet, J., Balghi, H., Sebillé, S., Kitzis, A., Raymond, G., Cognard, C., Bourmeyster, N., Constantin, B., 2007. Regulation of capacitative calcium entries by  $\alpha$ 1-syntrophin: association of TRPC1 with dystrophin complex and the PDZ domain of  $\alpha$ 1-syntrophin. *FASEB j.* 21, 608–617. <https://doi.org/10.1096/fj.06-6683com>
- Wagner, K.R., Cohen, J.B., Haganir, R.L., 1993. The 87K postsynaptic membrane protein from torpedo is a protein-tyrosine kinase substrate homologous to dystrophin. *Neuron* 10, 511–522. [https://doi.org/10.1016/0896-6273\(93\)90338-R](https://doi.org/10.1016/0896-6273(93)90338-R)
- Wang, Z.-W., Saifee, O., Nonet, M.L., Salkoff, L., 2001. SLO-1 Potassium Channels Control Quantal Content of Neurotransmitter Release at the *C. elegans* Neuromuscular Junction. *Neuron* 32, 867–881. [https://doi.org/10.1016/S0896-6273\(01\)00522-0](https://doi.org/10.1016/S0896-6273(01)00522-0)
- Wei, H., Wei, X., Han, R., 1996. Wei *et al.* Reply: *Phys. Rev. Lett.* 77, 1657–1657. <https://doi.org/10.1103/PhysRevLett.77.1657>
- WormBase (*dys-1*): [https://wormbase.org/species/c\\_elegans/gene/WBGene00001131#0-9f-10](https://wormbase.org/species/c_elegans/gene/WBGene00001131#0-9f-10)
- Wes, P.D., Chevesich, J., Jeromin, A., Rosenberg, C., Stetten, G., Montell, C., 1995. TRPC1, a human homolog of a *Drosophila* store-operated channel. *Proceedings of the National Academy of Sciences* 92, 9652–9656. <https://doi.org/10.1073/pnas.92.21.9652>
- White J. G., Southgate E., Thomson J. N. and Brenner S. The structure of the nervous system of the nematode *Caenorhabditis elegans*, 1986. *Phil. Trans. R. Soc. Lond. B* 314, 1–340. <https://doi.org/10.1098/rstb.1986.0056>
- White, J., 2018. Clues to basis of exploratory behaviour of the *C. elegans* snout from head somatotropy. *Phil. Trans. R. Soc. B* 373, 20170367. <https://doi.org/10.1098/rstb.2017.0367>
- Xu, R., Singhal, N., Serinagaoglu, Y., Chandrasekharan, K., Joshi, M., Bauer, J.A., Janssen, P.M.L., Martin, P.T., 2015. Deletion of Galgt2 (B4Galnt2) Reduces Muscle Growth in Response to Acute Injury and Increases Muscle Inflammation and Pathology in Dystrophin-Deficient Mice. *The American Journal of Pathology* 185, 2668–2684. <https://doi.org/10.1016/j.ajpath.2015.06.008>
- Yang, B., Jung, D., Rafael, J.A., Chamberlain, J.S., Campbell, K.P., 1995. Identification of  $\alpha$ -Syntrophin Binding to Syntrophin Triplet, Dystrophin, and Utrophin. *J. Biol. Chem.* 270, 4975–4978. <https://doi.org/10.1074/jbc.270.10.4975>
- Yang, Y., Mlodzik, M., 2015. Wnt-Frizzled/Planar Cell Polarity Signaling: Cellular Orientation by Facing the Wind (Wnt). *Annu. Rev. Cell Dev. Biol.* 31, 623–646. <https://doi.org/10.1146/annurev-cellbio-100814-125315>
- Yoshida, M., 2000. Biochemical evidence for association of dystrobrevin with the sarcoglycan-sarcospan complex as a basis for understanding sarcoglycanopathy. *Human Molecular Genetics* 9, 1033–1040. <https://doi.org/10.1093/hmg/9.7.1033>
- Yoshida-Moriguchi, T., Campbell, K.P., 2015. Matriglycan: a novel polysaccharide that links dystroglycan to the basement membrane. *Glycobiology* 25, 702–713. <https://doi.org/10.1093/glycob/cwv021>
- Zarrinpar, A., Bhattacharyya, R.P., Lim, W.A., 2003. The Structure and Function of Proline Recognition Domains. *Science Signaling* 2003, re8–re8. <https://doi.org/10.1126/stke.2003.179.re8>

- Zerangue, N., Schwappach, B., Jan, Y.N., Jan, L.Y., 1999. A New ER Trafficking Signal Regulates the Subunit Stoichiometry of Plasma Membrane KATP Channels. *Neuron* 22, 537–548. [https://doi.org/10.1016/S0896-6273\(00\)80708-4](https://doi.org/10.1016/S0896-6273(00)80708-4)
- Zhang, L., Ward, J.D., Cheng, Z., Dernburg, A.F., 2015. The auxin-inducible degradation (AID) system enables versatile conditional protein depletion in *C. elegans*. *Development* 142, 4374–4384. <https://doi.org/10.1242/dev.129635>
- Zhou, S., Opperman, K., Wang, X., Chen, L., 2008. *unc-44* Ankyrin and *stn-2*  $\gamma$ -Syntrophin Regulate *sax-7* L1CAM Function in Maintaining Neuronal Positioning in *Caenorhabditis elegans*. *Genetics* 180, 1429–1443. <https://doi.org/10.1534/genetics.108.091272>
- Zhou, X., Bessereau, J.-L., 2019. Molecular Architecture of Genetically-Tractable GABA Synapses in *C. elegans*. *Front. Mol. Neurosci.* 12, 304. <https://doi.org/10.3389/fnmol.2019.00304>